University of South Bohemia in České Budějovice

Faculty of Science

Acid/base properties and reactivity
of square planar complexes

Ph.D. Thesis

Olga Dvořáčková, MSc.

Supervisor: doc. Zdeněk Chval, PhD.

Faculty of Health and Social Sciences

University of South Bohemia in České Budějovice

České Budějovice 2022

Annotation

Complexes of platinum and other transition metals are important compounds with many applications including anticancer treatment. This thesis is based on the computational studies dealing with the properties and reactivity of square planar complexes. We showed that the central metal atom acts as a Lewis acid in standard coordination bonds but is able to interact as a Lewis base when being in contact with a Lewis acid. Substitution(s) of the nonleaving ligand(s) enabled a fine-tuning of the reactivity of Pt(II) compounds.

Declaration

I hereby declare that I am the author of this dissertation and that I have used only those sources and literature detailed in the list of references.

České Budějovice, 15. 2. 2022   ....

                                                                      Olga Dvořáčková

Financial support

Acknowledgements

List of papers and author's contribution

The thesis is based on the following papers:

I. Chval Z., **Dvořáčková O.**, Chvalová D., Burda JV. Square-Planar Pt(II) and Ir(I) Complexes as the Lewis Bases: Donor–Acceptor Adducts with Group 13 Trihalides and Trihydrides. *Inorg Chem* 2019; 58:3616–26. (IF$_{2019}$ = 4.825).

OD participated in QM calculations, data analysis and the paper writing. Approx. contribution 25%.

II. **Dvořáčková O.**, Chval Z. Tuning the Reactivity and Bonding Properties of Metal Square-Planar Complexes by the Substitution(s) on the Trans-Coordinated Pyridine Ring. *ACS Omega* 2020; 5:11768–83. (IF$_{2020}$ = 3.512).

IIa. Correction to **Dvořáčková O.**, Chval Z. Tuning the Reactivity and Bonding Properties of Metal Square-Planar Complexes by the Substitution(s) on the Trans-Coordinated Pyridine Ring. *ACS Omega* 2020; 5:15761. (IF$_{2020}$ = 3.512).

OD performed QM calculations, data analysis and participated in the paper writing. Approx. contribution 70%.

III. **Dvořáčková O.**, Chval Z. Tuning the Reactivity and Bonding Properties of the Pt(II) Complexes by the Substitution(s) on the Trans-Coordinated Non-Aromatic Amine Ligand. *ChemistrySelect* 2021; 6:3162–8. (IF$_{2020}$ = 2.109).

OD performed QM calculations, data analysis and participated in the paper writing. Approx. contribution 70%.

List of other works the author did collaborate on and wishes to mention:

Vágnerová T, Michálková H, Dvořáčková O, Topinková E. Comparison between EWGSOP1 and EWGSOP2 criteria and modelling of diagnostic algorithm for sarcopenic obesity in over 70 years old patients. *Eur Geriatr Med* 2022, doi: 10.1007/s41999-021-00602-4. (IF$_{2020}$ = 1.710)

Kavan Š, Dvořáčková O, Pokorný J, Brumarová L. Long-Term Power Outage and Preparedness of the Population of a Region in the Czech Republic—A Case Study. *Sustainability* 2021, 13(23):13142. (IF$_{2020}$ = 3.251)

Velemínský M. Sr., Dvořáčková O., Samková J., Rost M., Sethi D. Prevalence of adverse childhood experiences (ACE) in the Czech Republic. *Child Abuse Negl* 2020; 102:104249. (IF$_{2020}$ = 3.928)

Chrdle A., Tinavská P., Dvořáčková O., Filipová P., Hnetilová V., Žampach P., Batistová K., Chmelík V., Semper AE., Beeching N. Early Diagnosis of Tularemia by Flow Cytometry, Czech Republic, 2003–2015. *Emerg Infect Dis* 2019; 25:1919–27. (IF$_{2019}$ = 6.259)

Zahálková K., Chrdle A., Dvořáčková O., Kašparová M., Horníková M., Chmelík V. The Scottish model of vancomycin dosing and therapeutic drug monitoring improves both efficacy and safety of vancomycin therapy. *Vnitr lek* 2017; 64:717–24.

Kajanová A., Stránský P., Dvořáčková O. *Metodologie výzkumu v oblasti sociálních věd*. ZSF JU, České Budějovice, 2017. 106 s.

Kočová H., Bartošová B., Dvořáčková O., Farář V., Gaillyová R., Haberlová J., Kohout P., Krawczyk P., Kryski M., Michalík J., Mrázová L., Neumannová K., Nosková P., Ošlejšková H., Repko M., Svatošová M., Šabatová D., Šesták J. *Spinální svalová atrofie v souvislostech*. Grada, Praha, 2017. 352 s.

Co-author agreement

Doc. Zdeněk Chval, PhD., the supervisor of this Ph.D. thesis, the lead author of paper OD1 and co-author of papers OD2 and OD3, fully acknowledges the stated contribution of Olga Dvořáčková to these manuscripts.

………………………………………………

Doc. Zdeněk Chval, PhD.

Table of Contents

List of abbreviations

BAMCB	1,2-bis(aminomethyl)cyclobutane
BE	binding energy
BSSE	basis set superposition error
CASPT	complete active space perturbation theory
CC	coupled clusters
CI	configuration interaction
CyH	cyclohexyl
CyP	cyclopropyl
DACH	bidentate 1,2-diaminocyclohexane
DFT	density functional theory
ECP	effective core potential
ETS–NOCV	extended transition state – natural orbitals for chemical valence
GGA	generalized gradient approximation
GTO	Gaussian type orbital
HF	Hartree-Fock theory
LCAO	linear combination of atomic orbitals
L(S)DA	local (spin) density approximation
M	metal
MO	molecular orbital
NAO	natural atomic orbital
NBO	natural bond orbital
NH_2X	substituted amine
PCM	polarizable continuum model
pyr	pyridine
pyrX	substituted pyridine
SCF	self-consistent field
STO	Slater type orbital
TS	transition state
w	water molecule
X	substituent

1. Introduction

1.1 Platinum

Presented work is based on theoretical studies of platinum complexes. Platinum is one of the rare transition metals. Despite its high melting point (1768 °C), the oldest known uses are reported from Egypt as early as in the 7th century BC. On the Pacific coast of South America the pre-Columbian blacksmiths were able to incorporate platinum into masks and jewelry at least 2000 years ago (possibly as Pt-Au alloy) [1]. Its discovery for the Western science was one of the unexpected results of Spanish exploitation of their South American colonies, bringing it to Europe during the 18th century first as an unknown silvery metal "platina del Pinto" (little silver from the river Pinto). Charles Wood, a metallurgist currently dwelling in Carthagena in New Spain (Cartagena, Colombia), took platinum samples to Jamaica. In 1741 he sent some of it to his relative, English doctor and scientist William Brownrigg, who after a thorough investigation presented his discoveries about this metal to the Royal Society of London in 1750 [2].

The interest of the contemporary European scientists in the "eighth metal" was finally sparked by the publication *Relación histórica del viage a la América Meridional* written by Jorge Juan and Antonio de Ulloa, after their appointment on an 8-year French Geodesic Mission (which main goal was to settle the question of Earth's curvature) to Ecuador [3,4].

During the French Revolution, a Commission of prominent French scientists, including Antione Lavoisiere, was set up to formulate the unified system of weights and measures. Lavoisier himself collaborated on the determination of one cubic centimeter of distilled water. Nevertheless, in 1799 the metric system was officially confirmed during the reign of Napoleon. Platinum was chosen as the stable material for the valid kilogram prototype (*Kilogramme des Archives*) made by the former King's goldsmith with plenty experience in platinum melting, Marc E. Janety, equaling one cubic decimeter of water at 4°C [5]. From 1899 until 2019 the *International Prototype of Kilogram* (a.k.a. *grand K*) was in use, which consisted of platinum alloy Pt-10Ir (10% iridium in mass) and offered even higher hardness than Pt alone (together with the known resistance to oxidation, high density, low magnetic susceptibility etc.) [6]. Since 20th May 2019, the kilogram definition has been based on the Planck's constant [7].

Practical use of platinum, together with other related metals known as Platinum Group Metals, has been on the rise roughly since the middle of the 20th century, thanks to the demands of automobile industry, oil refineries, electronics, special medical alloys, as well

as jewelry. Currently, half of the world's Pt demand is saturated by the mines in South Africa (specifically the Bushveld Igneous Complex near Pretoria), one third comes from Russia, and the rest comes from the USA, Canada and Zimbabwe [8].

A steady rise in the interest of the scientific community in platinum was followed by a steep increase in the publication numbers after the year 1990 (Fig. 1). In the last ten years, the most frequent areas of platinum research are physical, inorganic or multidisciplinary chemistry, material chemistry, electrochemistry, and oncology (Fig. 2).
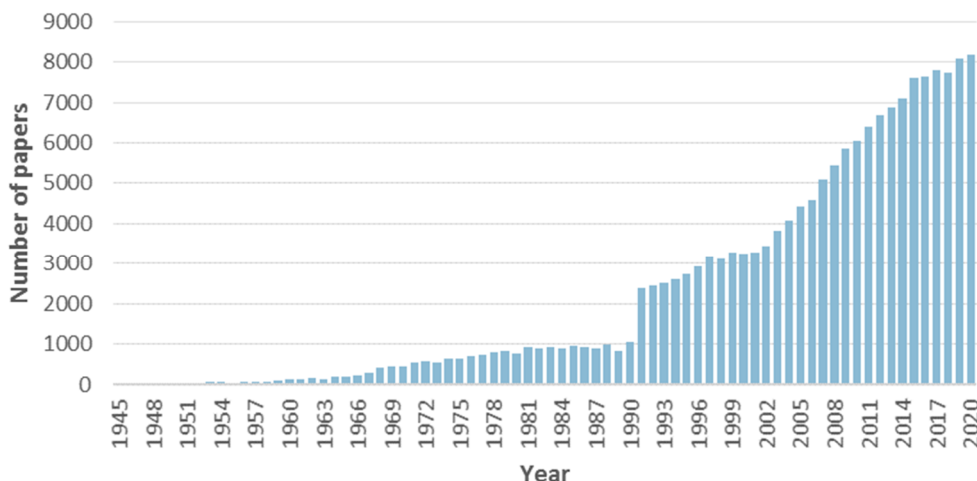

Figure 1. Number of papers in the Web of Science database with the keyword "platinum" in the years 1945–2020.
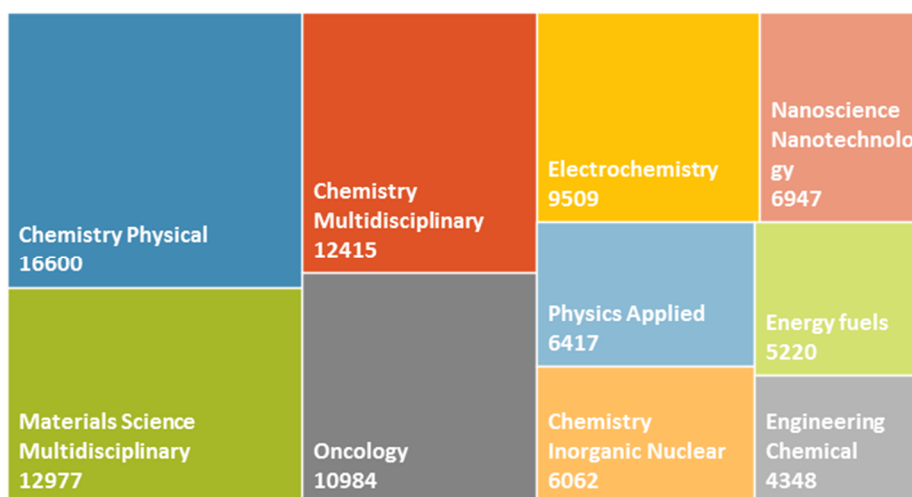

Figure 2. Ten most popular research areas based on platinum referenced in the Web of Science database in the last 10 years, as of April, 2021.

1.2   Platinum complexes and cancer treatment

Treating cancer has been one of the major goals of medicine since the second half of the 20th century. Sadly, this quest still continues, as cancer counts are a leading cause of death worldwide (just second after cardiovascular diseases), with almost 10 million deaths in 2020 and more than 16 million projected in 2040 [9]. Still, cancer is far from being a "modern disease". Bone lesions ascribed to cancer (osteocarcinomas) were identified in human and animal (even dinosaur) fossils [10]. First written information about "a disease that cannot be cured" comes from Egyptian papyri about 5000 years old. The terms carcinos (Greek), cancer (Latin), and oncos (Greek) come from the famous ancient physicians Hippocrates (5th–4th century BC), Celsus and Galen (both 2nd century AD), respectively.

More insights into the mechanism of cancer brought the widespread use of microscope in the 18th and 19th century, leading to the proposition of a cell theory ("Omnis cellula e cellula") by a German scientist Rudolf Virchow in 1858 [11] and the description of the metastasis process by an English surgeon Campbell De Morgan around the year 1874 [12]. In the beginning of the 20th century the hypothesis of the genetic basis of cancer was elaborated by a German scientist Theodor Boveri, namely as the abnormal cell multiplication arising from chromosomal abnormalities, and the disability of cells to control their inherent tendency to divide whenever possible. Boveri even predicted the existence of tumor suppressor mechanisms and is perhaps the first who suggested that hereditary factors (genes) are linearly arranged along chromosomes [13].

The process of cell division became an important target in the cancer treatment. The most clinically successful cytostatic drug still in use against various types of cancer is cisplatin, or cis-diamminedichloroplatinum(II) (Fig. 3).

Figure 3. Chemical structure of cisplatin.

Cisplatin is a very simple planar molecule, which had been known since 1844 as "Peyrone's chloride" [14]. However, its cytostatic properties were first discovered by Rosenberg et al. in 1965 [15]. Interestingly, it happened in an experiment investigating the growth of *E. coli* in the presence of electric field. The microorganisms showed remarkable filamentous nature – the cells were growing without dividing themselves. As it turned out,

the cause of this feature was not the electric field but the dissolved electrode material, platinum, which reacted with the ammonium chloride buffer [16].

It took another almost 15 years to the final approval of cisplatin as the first-line treatment of testicular cancer by the US FDA in 1979 [17]. Its severe nephrotoxicity together with debilitating nausea and vomiting are treated by extensive hydration and administration of serotonin receptor antagonists [18,19]. Still other unwanted side effects remain (ototoxicity, peripheral neuropathy). Nowadays, cisplatin continues to be one of the most used anticancer drugs [20]. This drug started the interest in similar transition metal-based anticancer substances with lesser toxicity and/or activity against more types of cancer and less prone to acquired resistance of some tumors [21].

Of the over 3000 synthesized platinum compounds, about 30+ have entered clinical trials but only three are in everyday clinical use as registered marketed drugs – except cisplatin these are carboplatin {cis-[Pt(1,1-cyclobutanedicarboxylate)(NH$_3$)$_2$]} and oxaliplatin {cis-[Pt(oxalate)(*R,R*-1,2-diaminocyclohexane)]} [22]. Three more, nedaplatin {cis-[Pt(glycolate)(NH$_3$)$_2$]}, lobaplatin [Pt(lactate)(1,2-diamino-methylcyclobutane)] and heptaplatin {Pt(cis-malonatol)[(4R,5R)-4,5-bis(aminomethyl)-2-isopropyl-1,3-dioxolane]} are approved in Japan, China and South Korea, respectively (Fig. 4) [23].

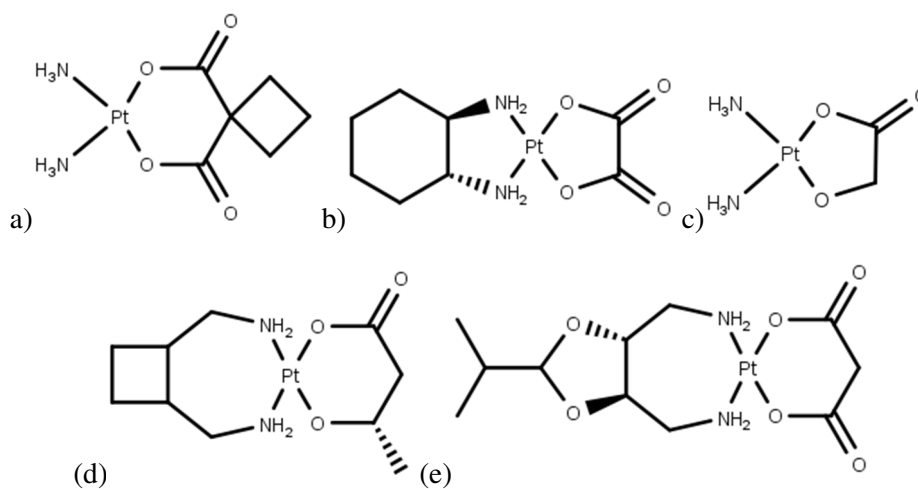Figure 4. Structures of clinically used platinum anticancer drugs: (a) carboplatin, (b) oxaliplatin, (c) nedaplatin, (d) lobaplatin, (e) heptaplatin.

1.2.1 Structure, reactivity and synthesis of cisplatin and transplatin

Platinum-based compounds encompass several intriguing structural features. First of all, the planarity of cisplatin and other metal complexes was explained by Alfred Werner in

1893 by means of his now well-known coordination theory of complex compounds, for which he was awarded the Nobel Prize in 1913 [24].

Secondly, it was the study of kinetics of substitution reactions in square planar platinum complexes which led I. I. Chernyaev to a discovery of what he called trans-influence in 1926: the rate of substitution in square or octahedral metal complexes is more affected by the opposite (= trans) ligand than by the neighbor (= cis) ones [25]. Trans-effect, i.e., the destabilization of the ligand in the trans-position, decreases in the series of ligands approximately as follows: C_2H_4, CN^-, CO, NO, H^- > CH_3^-, $C_6H_5^-$, $SC(NH_2)_2$, NO_2^-, SCN^-, I^- > Br^-, Cl^-, pyr > NH_3, H_2O, OH^-, F^- [26].

In the beginning the origin and mechanism was explained by an electrostatic model, specifically the polarization between the central metal and the ligands [27]. A later, rather elegant model by Dewar and Chatt & Duncanson was shown to work only with π-acceptor ligands [28]. Eventually a concerted action of σ-donation and π-back donation was identified as the causal mechanism: the trans-effect can be viewed as a competition of the ligands in the trans direction to donate the electron density into the same orbital on the metal [29] and into the σ* orbital of the metal-leaving group bond [30].

Two phenomena can be distinguished in the trans-effect: (1) kinetic, meaning influence on the rate of substitution which may include the transition state stabilization by π-back-donation; (2) thermodynamic (or structural trans effect or trans influence), influencing M–trans ligand bond lengths and stabilities in the reactant structure.

The syntheses of cisplatin [31] and transplatin [32] are a nice illustration of the trans-effect. For both compounds, the reaction starts with four chlorine ligands bound to platinum – the $K_2[PtCl_4]$ complex. In the case of cisplatin synthesis, the chlorines are exchanged by iodines in the saturated solution of KI. A subsequent addition of ammonia then results in the formation of a yellow compound cis-$[PtI_2(NH_3)_2]$. In aqueous solution of $AgNO_3$ the two iodines precipitate as AgI and in the dissolved cis-$[Pt(H_2O)_2(NH_3)_2]$ complex the water ligands are replaced by chlorines reacting with KCl. To prepare transplatin, all four chlorines leave when applying ammonia and heat yielding $[Pt(NH_3)_4]^{2+}Cl_2$. After adding HCl the desired product trans-$[PtCl_2(NH_3)_2]$ precipitates as a yellow powder.

Trans-effect is also a basis for the Kurnakow test, a method for distinguishing cis/trans isomers of square planar complexes [33]. It uses thiourea $[SC(NH_2)_2]$ which subsequently displaces all four ligands in cisplatin (starting with chlorines) but only two chlorines in transplatin, forming a deep yellow solution of $\{Pt[SC(NH_2)_2]_4\}^{2+}Cl_2$ or a white precipitate $\{Pt[SC(NH_2)_2]_2(NH_3)_2\}^{2+}Cl_2$, respectively.

1.2.2   The mechanism of action of cisplatin

The mechanism by which cisplatin manifests its selective toxicity to tumor cells is rather complex. It includes either passive and/or active transport over the cell membrane, transfer to the nucleus, hydrolysis, formation of DNA adducts, and recognition by damage-response proteins [34]. Subsequent signal transduction pathways activated by these interactions lead to cell-cycle arrest, attempts to repair the DNA lesions, and apoptosis or necrosis [35].

Rosenberg et al. first tested platinum compounds [Pt(II) as well as Pt(IV) species] on sarcoma and leukemia tumors in mice with unexpectedly high regression rates [36]. They noted a narrow dose-response curve, which accounts for the need of precise dosing, and hypothesized on three possible modes of action: a) a high uptake into the tumor and long lifetime inside, b) a higher sensitivity of tumor tissue compared to normal cells, and c) a stimulation of the immune system of the host [37]. Following analyses in mammalian cells showed irreversible inhibitory effects of Pt compounds on DNA synthesis [38].

The dependency of cisplatin hydrolysis on chloride ions concentration is crucial for the mechanism of action inside the patient body – naturally high plasma chloride level (~100 mM) prevents the premature hydrolysis connected with a rise of toxicity. From the same reason already Cleare & Hoeschele in their early work stressed out the need of the use of saline instead of aqueous solutions for the drug administration [39]. Crossing the cell membrane happens either via passive diffusion or by active transport [40]. Relatively low chloride concentration in the cytoplasm (4–20 mM) then promotes the aquation of the molecule, which may proceed in two steps. Losing the first Cl^- cisplatin changes into the reactive positively charged species cis-$[PtCl(NH_3)_2(H_2O)]^+$ which is the active form of the drug interacting with DNA [41]. In diluted solution the monoaqua form can undergo a second aquation to form cis-$[Pt(NH_3)_2(H_2O)_2]^{2+}$ which shows about 100 times faster speed of binding to DNA than the monoaqua form. Taking into account the specific local DNA microenvironment that may substantially speed up the second aquation step, the actual active form of the drug which reacts with DNA is still a matter of debate [42].

Binding to nuclear DNA as a primary cellular target of cisplatin was confirmed by numerous works both in vitro and in vivo [32,43]. Several early studies noted the dependency of the process on the concentration of chloride anions in the solution and

concluded that the rate-limiting step is the hydrolysis of the molecule to cis-$[PtCl(NH_3)_2(H_2O)]^+$ [44]. After a thorough research, several specific sites of interaction with the DNA chain were confirmed, which include interstrand but mainly intrastrand crosslinks leading to the distortion and unwinding of the double helix [45].

Solving the exact mechanism of aquation and DNA binding of cisplatin with respect to transition states and intermediate structures was enabled by the advancement of computer-aided quantum chemical modeling. Several studies showed that the first and second Cl → H_2O substitution reactions proceed over pentacoordinated transition states, confirmed preferential dGpG sequence target on the DNA strand forming 1,2-GG intrastrand adducts and highlighted the important role of hydrogen bond formation through the whole process [46].

1.2.3 Comparison of cytostatic activity of cis and trans isomers

A clear difference between the effects of cis- vs. trans-diamminedichloroplatinum(II) was found in the pioneering work of Rosenberg et al. who found the trans isomer is inactive against cancer cells [16]. The same result was reported by Cleare & Hoeschele [39,47], who tested more than 60 platinum compounds and summarized their findings into four essential requirements for anticancer activity of Pt complexes: 1) neutral charge of the complex; 2) a pair of cis-leaving groups; 3) leaving groups should be bound with similar and adequate strength (too labile means too toxic, too tight means less active); 4) nonleaving, so called "carrier ligands" should be relatively inert and neutral (preferentially amine ligands). Cleare & Hoeschele suggested the importance of the nonleaving groups for the selectivity of the complexes.

There are several reasons for the lack of anticancer activity of trans-complexes: transplatin hydrolyses four times faster; it reacts with ammonia and glutathione approximately 30 and two times faster, respectively, than cisplatin [48]. Thus transplatin is a less specific drug with more prospective targets leading to its faster deactivation [49]. Moreover, the DNA crosslinking ability of transplatin is lessened by the easier displacement of the monoadducts by trans-labilizing nucleophiles (glutathione, thiourea). Due to steric reasons trans-platinum complexes form interstrand adducts with DNA. However, their formation is at least 10 times slower and are more easily repaired compared to intrastrand cross-links of cisplatin [50].

Still, the question of the inactivity of trans-isomers is far from being settled. Transplatin was shown to bind DNA similarly to cisplatin in many in vitro studies [47,49,51]. The cytotoxic potency of trans-platinum complexes with bulky carrier ligands (such as aromatic amines, iminoethers, cyclohexylamine, ramified aliphatic amines) is dramatically increased [52]. More importantly, some of the novel trans-platinum derivatives are endowed with *in vivo* antitumor selectivity, thus showing that even platinum complexes with *trans* geometry may have favorable toxicological and pharmacokinetic profiles [53].

1.2.4 *The toxicity and cross-resistance of platinum complexes*

Adverse side effects have been a major obstacle since the beginning of the use of platinum anticancer drugs. One of the known causes is the activity of proteins in blood plasma – one day after cisplatin administration, 65–98 % of the drug was found to be bound by proteins [54]. Thiol-containing plasma proteins are probably responsible for both deactivation and unwanted side effects [54b,54c,55].

Tumor cells can be intrinsically resistant to cisplatin (e.g. colon cancer, non-small-cell lung cancer) or acquire the non-responsiveness during the drug exposure over time [56]. Cellular resistance to cisplatin is caused by many processes: altered membrane transport leading to decreased cellular accumulation, inactivation of the drug by intracellular thiols (increased levels of glutathione or glutathione-S-transferase activity, increased levels of intracellular metallothioneins), decreased DNA binding/increased DNA repair or toleration to DNA damage [34,57].

Preparation of new anticancer compounds should aim for clinical advantages over cisplatin: lower toxicity, activity against cancers with intrinsic or acquired resistance, or ability to be administered orally [58]. Manipulation of the structure of the leaving group(s) appears to influence the tissue and intra-cellular distribution of the platinum coordination complexes, but it is unlikely to prevent the cross-resistance. It was hypothesized that the modification of the carrier ligands could lead to a different spectrum of DNA lesions and therefore may circumvent the problem of cross-resistance [47]. For example, carboplatin with its bidentate cyclobutanedicarboxylate leaving group is more stable than the two chloride groups of cisplatin, resulting in a lower reactivity and toxicity [59]. In the case of oxaliplatin the bulky 1,2-diaminocyclohexane carrier ligand forms platinum-DNA adducts, which are more effective in blocking DNA replication and elicit DNA repair mechanisms differently than cisplatin leading to an improved cytotoxic effect. In addition, the anticancer

effects of oxaliplatin are optimized when it is administered in combination with other anticancer agents (such as 5-fluorouracil, gemcitabine, cisplatin, or carboplatin), topoisomerase I inhibitors, and taxanes [60]. Another example, compound AMD473 (picoplatin, cis-[PtCl$_2$(NH$_3$)(2-methylpyridine)]) with steric hindrance due to the pyridine ring was designed primarily to be less susceptible to the inactivation by thiols [61]. Indeed, it was shown to be active in cisplatin-resistant cell lines, with no renal toxicity but with dose-limiting myelotoxicity in a mouse model [62].

Attention is also returning to some of the earliest tested platinum compounds, Pt(IV) complexes, which possess high activity, low toxicity due to higher stability of platinum complexes in this oxidation state, and the ability to be effective oral agents (e.g. satraplatin) [63]. Like cisplatin, they form mono- or bifunctional adducts with DNA [64]. According to experimental results, it is generally accepted that the anticancer activity of platinum(IV) compounds is exerted only after in vivo reduction to the corresponding Pt(II) molecules [64b]. Thus, bioactive moieties can be used as the axial ligands which after the release could be harnessed to target other cellular processes and boost up the antiproliferative effect or fight the unwanted side effects [65].

1.2.5 Recent computational chemistry contributions

The computational chemistry has grown to a fully respected field of chemistry which is able not only to reproduce and explain experimental results but also to pinpoint the precise reaction mechanisms of known proceses and substances, as well as to uncover new promising ones. It profits from the evergrowing hardware performance and the use of more effective and precise methods of theory. In pharmacology the molecular modeling is a standard tool for the pre-selection of the potential drug candidates making the drug development more effective, faster and cheaper.

First theoretical studies of reactions of biologicaly important platinum complexes emerged in the 80s and were carried out in vacuo using semiempirical methodology [66], but quickly the ab initio methodology with the relativistic pseudopotentials was adopted [67]. Kozelka et al. employed molecular modeling in the binding studies of cisplatin with oligonucleotides [68]. Gradually more computationaly demanding methods and bigger basis sets were used for the description of electronic & geometric structures [69].

Thanks to the methodology evolution the elusive transition state in the cisplatin hydrolysis reaction could be described first by Chval & Šíp, who confirmed the

pentacoordinated nature of the transition state [46a]. Soon the effect of the level of theory on the results was the target of numerous papers [70].

The precise mode of interaction of the cytotoxic compounds with the final target, which is often DNA, continues to be frequent goal of the studies until today [44b-d,71]. Nevertheless, other cellular interaction partners have been resolved as well (RNA, proteins [72]).

In the quest of searching for the new drugs to tackle the problem with intrinsic or acquired resistance, quantitative structure−activity relationship (QSAR) prediction models for the anticancer activity were put forward as early as in 1982 by Abdul-Ahad & Webb [73]. The idea of selecting a small number of predictors, which would forecast the cellular toxicity was followed 23 years later by Monti et al., who selected 4 predictors (out of 197) of cellular toxicity for 16 Pt complexes using semiempirical methodology [74]. Sarmah & Deka used DFT and MM modelling and proved the usefulness of these methods in the prediction of cytotoxicity [75], with many followers, pointing at various important parameters, such as solubility, lipophilicity, stability in plasma, redox potential, vibrational spectra, rate of aquation, type of ligands etc. [76].

Finaly, there are several recent studies searching for the trans-effect strength quantification. At first the relative strengths of ligands were quantified by the changes of electron occupations of 5d platinum atomic orbitals and the trans-effect is driven by the changes of the electron density [29]. Similar conclusion was suggested by Guégan et al. who correlated the changes of the trans-effect strengths in octahedral complexes by the differences in electrophilicity at given sites around the metal cation [77]. Pinter et al. explained the trans-effect as an increase of Pauli repulsion towards the trans ligand caused by the electron accumulation when a ligand with the high donation ability is present [30].

Metal octahedral complexes with chromium were studied by Tsipis [78], who quantified the kinetic part of trans-effect by intrinsic bond dissociation energy [79], whereas the ground-state part, trans-influence, by vibrational frequencies and bond lengths. He suggested a unified trans-philicity concept, combining both structural and kinetic part of trans-effect with δ ^{13}C NMR chemical shifts as the sole descriptor.

Yet another predictor of bond strengths and ligand lability in several square planar Pt complexes was studied by Ponce-Vargas et al. [80]. They recognized the metal-ligand bond strength as the most important quantificator of the rate of hydrolysis and used the intrinsic bond strength index (IBSI) [81], which is praised for its ability to deliver a bond strength intrinsic to the considered atom pair. It is based on the independent gradient model (IGM)

[82] and stemms from the electron density analysis. It can be further differentiated into two parts, IBSI$^\sigma$ and IBSI$^\pi$, reflecting the σ-donation and π-back-donation channels, respectively.

1.3 Lewis acid & base theory

1.3.1 Historical excursion

Gilbert Newton Lewis (1875–1946) is considered by many as the most influential scientist, who did not receive the Nobel Prize [83].

Building on the idea of an electron-pair bond [84], in a book *Valence and the structure of atoms and molecules* [85] and subsequent series of several papers [86], among other themes Lewis dealt with various theories of acids and bases. He tried to propose the most unifying theory: starting with then accepted Arrhenius theory of aqueous solutions [87], he offered a generalization of an acid or base being "*a substance which gives up or takes up hydrogen ions*" (proposed also by Brønsted and Lowry) [88]. But he didn't stop there and denounced the "modern cult of the proton" as well as the solvent-based model proposed by Franklin and Cady & Elsey [89]. Finally, he acknowledged the electronic structure as the solemn fundamental cause of the acid-base behavior [85]. The International Union of Pure and Applied Chemistry (IUPAC) currently defines Lewis acid as "*a molecular entity (and the corresponding chemical species) that is an electron-pair acceptor and therefore able to react with a Lewis base to form a Lewis adduct, by sharing the electron pair furnished by the Lewis base*". Inversely, Lewis base is "*a molecular entity (and the corresponding chemical species) able to provide a pair of electrons and thus capable of coordination to a Lewis acid, thereby producing a Lewis adduct*" [90].

Lewis supported his acid-base theory by showing experimentally that the acidic behavior was not confined to the proton alone, but was exhibited by electron-pair acceptors in general – particularly striking in this regard were the reactions between metal halides and organic amines in nonaqueous solvents [86a]. Although there have been some efforts (by Lewis and others) to further classify Lewis acids and bases as primary and secondary according to the speed of neutralizing reactions, or whether the involved chemical species needs to undergo some kind of internal activation or some auxiliary bonds need to be broken so the initial unstable complex dissociates into respective fragments [86b,91], the ascent of quantum mechanics did finally prove the universality of Lewis' theory.

Today, the Lewis acid-base theory-based studies involve solar cells and chemical batteries, heterogeneous catalysis, pollutant removal, hydrogen storage etc. Quite recently,

the Lewis acid-base nomenclature was enriched with so-called frustrated Lewis pairs – a situation where the formation of a dative bond is hindered sterically, offering a unique route to new reactivity [92].

1.3.2 *Lewis acidity/basicity of the metal center*

The central metal ion in metal coordination compounds is a textbook example of Lewis acid, accepting electron density from the lone-pairs of its ligands into its empty or partially occupied *d* orbitals. This is the prevailing effect responsible for the σ-bond formation which is called σ-donation. Coordination bonds may have also the π-character caused by π-(back-)donation. Strictly speaking, the metal acts as a Lewis base in π-(back-)donation but the transferred charge is much lower than in accompanying σ-donation. In square-planar complexes, the strength of these effects depends on the nature of the ligands and determines the kinetics (trans effect) and the mechanism of substitutions reactions. Ligand with strong σ-donation and π-back-donation ability promotes substitution reactions of the ligand trans to it and the reactions proceed by dissociative and associative mechanisms, respectively. Ligands with weak σ-donation and π-back-donation abilities induce the least reactivity of the trans ligand [29].

Already in the late 20s and 30s, Walter Hieber synthesized what was later confirmed as coordination complexes of iron and cobalt with carbonyls and hydrogen, and he noted that transition metal carbonyl complexes could act as proton acceptors, showing strong nucleophilicity [93]. Next, Wilkinson and Birmingham [94] confirmed this observation – they noted that their newly prepared compound, biscyclopentadienylrhenium hydride, is soluble in diluted acids, i.e. the central Re atom could act as a base and be protonated.

In the 60s, the interest in the Lewis acid−base chemistry with basic transition metals was sparked by the synthesis of the square-planar d^8 Vaska's complex, $[IrClCO(P(C_6H_5)_3)_2]$, which readily undergoes oxidative addition with a number of oxidants, acids and electrophiles (e.g. CO, SO_2, Cl_2, CH_3I, BF_3) generating an 18-electron octahedral Ir(III) species [95]. Hodali et al. reported the preparation of square-planar d^8 Pt(II) analog, with bidentate ligands l-thiomethyl-2-diphenylphosphinoethane and 1-thiomethyl-2-diphenylarsinomethane, and its reaction with BF_3 [96].

The basicity of square planar transition metal complexes can be manifested by inverse hydration – H-bond contacts with H_2O (or HCl) molecules via the non-classical M···H-O-H interaction, which is mediated by a charge transfer, as was shown experimentally as well as

computationally for e.g. platinum [97] and gold [98]. Lately, intramolecular stabilization with OH groups was found in numerous cases of transition metal catalysts, leading to the change of conformation and subsequently enantioselectivity or stereoselectivity of the catalytic process [99] – for example the catalysis by Pd [100], Rh and Ir [101], and ferrocenes [102].

2. Methodology

2.1 Theoretical background

The methods of quantum chemistry include wide range of models offering various degrees of precision of the results. Although the description of any chemical system is theoretically possible by means of the Schrödinger equation [103], the solution for more than one electron is analytically impossible forcing the use of numerical methods with the need of approximations.

Born and Oppenheimer showed that due to the difference in the mass of protons and electrons (~1800x), atomic nuclei motions are much slower with respect to the electrons and so the nuclear part of the Schrödinger equation can be neglected (Born-Oppenheimer approximation) [104] and only internuclear repulsion is added to the total energies.

In the first step N-electron Schrödinger equation is approximated by a set of N 1-electron equations. Every electron moves in the mean field of the other electrons. The set of 1-electron equations is solved iteratively minimizing the total energy of the system (Hartree-Fock (HF) or self-consistent field (SCF) method) [105]. The final form of the wave function is expressed as the Slater determinant of one-electron wave functions (spin-orbitals) which ensures its antisymmetry [106].

The approximation of molecular orbital by a linear combination of atomic orbitals (MO-LCAO) was put forward by Pauling [107] and Lenard-Jones [108]. The mathematical description of MO's uses a combination of orbital basis functions multiplied by coefficients, which are then varied to locate the energy minimum. Due to the calculations of two-electron integrals Gaussian-type basis functions are usually used [109], although they decay too quickly with increasing distance, which is overcome by the use of linear combination of several primitive Gaussians forming the so called contracted Gaussian type orbital (CGTO). Single basis function may be flexile enough for the core electrons but the valence orbitals are usually described by more than one basis function is used to reach a reasonable accuracy. It leads to the construction of the split-valence double-ξ (DZ), triple-ξ (TZ) etc. basis functions. Very popular are Pople's 6-31G DZ and 6-311G TZ basis functions [110].

To allow the polarization of an orbital when participating in the chemical bond formation or in the presence of another charged particle, polarization functions – basis functions with higher angular momentum (l+1) – can be added [111]. For the correct description of weak bonds, very electronegative atoms or anions, long-reaching diffuse functions (with small ξ exponents) are very important enabling the electron movement

further from the nucleus [112]. These functions are usually marked by the '+' sign in the basis set designation. Thus, 6-31+G(d,p) basis set contains one set of diffusion functions and one set of polarization 'd' functions on the main group of elements and one set of polarization 'p' functions on the hydrogen atoms.

For heavier elements (like Pt) the reduction of the basis set size is welcomed and relativistic effects become important for inner shell electrons. As the inner orbitals are not so important in the reactions/chemical bonding (frozen core approximation), their influence can be reduced into an effective core potential (ECP), i.e. the Coulomb potentials of the nucleus and core electrons are replaced by the pseudopotentials acting on the valence electrons whose basis sets are designed to reproduce relativistic all-electron behaviour.

Nowadays, the database system of basis sets and pseudopotentials is avialble for all the elements of the periodic table and it can be easily downloaded from the internet (https://www.basissetexchange.org/).

The facts that electrons move just in the mean field of the other electrons and the wave function is described by a single determinant leads to a large error since the electron correlation is missing. Part of the electron correlation can be included by means of Möller-Plesset perturbation theory up to n-th order (MPn methods) [113] or configuration interaction (CI) [114]. Currently, the coupled clusters (CC) method is considered as the most appropriate method, with which the chemical accuracy can be reached (less than 2 kcal/mol [115]. This method is based on the HF method and the multi-electron wavefunction is constructed using the exponential cluster operator. CC method was developed by Čížek and Paldus in the late sixties [116].

Density functional theory (DFT) is a relatively cheap alternative to the above-mentioned methods which include the correlation energy. It is based on Hohenberg-Kohn theorems [117]: The ground-state properties of the system are determined by the ground-state electron density which minimizes the energy functional. Except the Coulomb and external potentials, the energy functional contains also the exchange-correlation term (E_{xc}) describing many-partical interactions [118]. However, the exchange-correlation functional does not exist, therefore its form is only approximated, giving rise to different flavors of DFT methods.

In his life-long excitement in DFT, John Perdew famously compared the ever-growing precision of E_{xc} approximations to the biblical Jacob's ladder [119]. The lowest rung is occupied by local (spin) density approximation [117b,120], followed by generalized gradient

approximation (GGA) [121]. Meta-GGAs add the orbital kinetic energy density [122], hyper-GGAs (hybrid functionals) add the exact exchange information [123] and so on.

Hybrid functionals include a contribution of exchange energy from Hartree-Fock theory, the most popular still being the Becke's functional augmented by Lee-Yang-Parr correlation functional B3LYP [123a,124]. Various functionals were shown to be able to describe various chemical behavior and/or systems accordingly to the experimental values, but the search and development of more universal functionals still continues [125].

Many commonly used DFT functionals cannot describe the systems where the dispersion energy is dominant since it arises from non-local electron correlation. Probably the simplest way to solve this problem is the use of functionals with an empirical (C_6/R^6) pair-wise term for the dispersion energy [126]. To correct the behavior of the dispersion function in the short-range, an additional damping function can be applied [127].

To compare the reactivity of different parts of a molecule and to quantify the amount of transferred charge, it is practical to calculate atomic charges, although due to the continuous nature of the electron distribution, the atomic charges are not a physical observable. Several methods of partitioning the electron density into atomic contributions have been derived – for example based on wavefunctions [128], natural bond orbitals [129], fitting to the electrostatic potential [130], etc. The unpleasant problem of some of the methods is the basis set dependence of the results [131]. Natural population analysis (NPA) is based on the summation of the localized 1-center natural atomic orbitals populations and is less dependent on the basis set size.

The interaction energy between two fragments of the complex can be calculated as a difference in energy of the complex and the sum of the energies of the isolated fragments. If both fragments are fully optimized, then the interaction energy includes also their deformation energies. However, since basis functions of the whole complex are more flexible than the basis functions of both fragments, the stability of the complex is overestimated with respect to the two fragments and this artificial increase of stability is called the, basis set superposition error (BSSE) [132]. BSSE is larger for smaller basis sets and decreases with their extent. Most often BSSE is evaluated by the counterpoise correction method [133]. It uses 'ghost' atoms from the other fragment when the energy of the given part is calculated. The method was adapted also for continuum solvent calculations (see below): ghost atomic orbital functions were located inside the complex cavity [134].

The interaction/binding energy between two fragments can be decomposed by the extended transition state – natural orbital for chemical valence methodology (ETS-NOCV)

[135]. Based on the extended transition state theory the binding energy can be divided into the individual contributions of electrostatic, orbital, Pauli and deformation energies [136]:

$$\Delta E_{total} = \Delta E_{orb} + \Delta E_{Pauli} + \Delta E_{elstat} + \Delta E_{def}$$

The energy required to bring the separated fragments from their equilibrium geometry to the structure in the molecule is referred to as the deformation or preparation term, ΔE_{def}. The ΔE_{elstat} energy corresponds to the classical electrostatic interaction between the fragments. The repulsive Pauli interaction between occupied orbitals on the two fragments is described by the ΔE_{Pauli} term. Finally, ΔE_{orb} represents the stabilizing interactions between the occupied molecular orbitals of one fragment with the unoccupied molecular orbitals of the other fragment during the bond formation, as well as the mixing of occupied and virtual orbitals within the same fragment (intra-fragment polarization).

NOCV combines the concepts of bond-order, bond-orbitals, and charge rearrangement with the deformation density. It uses eigenfunctions of the deformation density matrix (NOCV) to describe the bond formation in molecules from atoms or fragments. Moreover, the related eigenvalues can be used as valence indices as well as a measure of the change in the electron density associated with the bond formation. The combination with the ETS method provides the means of the chemical bond analysis in terms of orbitals, describing the charge rearrangement and the corresponding energy contributions from these orbitals to the chemical bond [135]. These contributions are either stabilizing (if the orbital E_{orb} and/or electrostatic E_{elst} interactions dominates) or destabilizing (if higher Pauli repulsion E_{Pauli} and/or geometry deformation E_{def} prevails). ETS-NOCV is a suitable method for studying various types of chemical bonds: donor-acceptor [135a,137], covalent [1359a,138], and weak intra- and intermolecular interactions [139]. The method is also able to decompose the activation energies of reactions offering the explanation of the transition states (de)stabilization [140]. Among other chemical phenomena which were studied by ETS-NOCV methodology belong the sigma hole- and halogen-bonding [141].

As the theoretically studied reactions and other chemical processes usually take place in the solution (most often in water), it is necessary to take into account the effect of solvent. There are two main methods with varying degree of complexity and computing demands: 1) explicit solvation, where the water molecules are placed in the vicinity of the explored system (due to huge number of possible configurations it is used usually in molecular dynamics simulations); and 2) implicit (continuum) solvation models, where the solvent is treated as a polarizable continuous dielectric medium acting on a solute placed in a cavity.

In polarizable continuum models (PCM) [142] the solute cavity is created as a set of overlapping spheres centered at the respective atoms. Other spheres can be added to smooth the surface and/or mimic the solvent-excluding surface area. The solute's electric field polarizes the continuum which creates a charge distribution on the cavity surface. It further affects the electron density of the solute and this mutual influence is solved iteratively via a solvent self-consistent reaction field (SCRF) method [143].

Currently, computational chemistry offers a wide range of inexpensive methods for studying the properties of new drugs or chemical compounds. In pharmacology molecular modeling serves as the first selection tool and only the most promising candidates can be involved in the subsequent more demanding phases of pharmacological testing.

2.2   Computational details

Several different functionals were used – partly due to historical reasons to allow the comparison with previous results, and to check the effect of the functional on the precision of the results.

The proper choice of the method was crucial only in the paper OD1 to calculate properly the binding energies between MX and YZ_3 structures. OD2 and OD3 papers dealt with relative values being not sensitive to the chosen functional and thus, "traditional" B3LYP functional was chosen. Energies were always calculated with D3 empirical dispersion correction as recommended [144].

Pople's 6-31+G(d) basis set (BS) of the double-ξ quality for main group elements offers reasonable geometries for relatively low cost which was important when all structures along the large number of reactive pathways (including the transition state structures) had to be optimized (papers OD2 and OD3). In OD1 we could effort to use the very reliable 6-311++G(2d,2p) BS of the triple-ξ quality since we performed only geometry optimizations of the minima on the potential energy surface. Inner electrons of the metal atoms (Pt, Ir) were treated by pseudopotentials with relativistic corrections [145]. Outer electrons were described by the double-ξ quality MWB-60 BS augmented by the set of diffuse functions (with exponents $\alpha_s = 0.0075$, $\alpha_p = 0.013$, $\alpha_d = 0.025$) and one (with exponent $\alpha_f(Pt)= 0.98$ in OD2 and OD3) or two sets (with exponent $\alpha_f(Pt)= 0.466, 1.419$ in OD1) of polarization functions [146]. Polarization f functions shorten Pt-ligand bonds [46a]. Total energies and wave function properties were always evaluated with the MWB-60(2fg)/6-311++(2df,2pd) BS with additional g, f and d sets of functions on Pt, heavy main group element and H atoms,

respectively [146]. Ir was described by Stuttgart effective core potentials with the split-valence triple-ξ BS (def2-TZVPPD).

In the paper OD1 at first a selected model structure was treated by 17 various DFT methods and the results were compared with CCSD(T) method as the benchmark. M06-2X-D3 and B3PW91-GD3BJ methods were found to give the best/closest agreement and were used for the calculations. In the papers OD2 and OD3, no benchmarking was done, but the results of B3LYP-GD3BJ functional [123a,127b] were compared to M06-2X [147] and PBE0 [148] functionals.

All optimizations and energy evaluations were performed in the Gaussian 09 (rev. D.01) program [149].

All structures along the reaction pathways were located either as the local minima (reactants, products) or the saddle points of the first order (transition states) by the analysis of the Hessian matrix having correct number of negative eigenvalues: zero and one for the minima and transition state structures, respectively. A zero-point energy and thermal contributions to energetic properties were calculated using the canonical ensemble at standard gas phase conditions (T = 298.15 K; p = 101325 Pa). In OD2 and OD3 papers the energy of reactants and products was obtained by the Boltzmann averaging (at T = 298 K) over all possible conformers. Activation free energies were evaluated with respect to the lowest lying transition state structure. Both gas phase as well as solvent (water) environment effects were analyzed – the latter with the self-consistent reaction field method of integral equation formalism variant of polarizable continuum model (IEFPCM) [150].

Atomic charges were calculated by natural population analysis as implemented in NBO 3.1 and NBO 5.0 programs excluding p orbitals as valence for transition metals [151].

When calculating binding energies in vacuum, basis set superposition error (BSSE) was treated by the counterpoise correction [133]. BSSE corrections in the PCM regime were calculated with ghost atomic orbital functions localized inside the cavity having the same size as the whole complex [134]. The contribution of deformation energy was taken into account in the case of OD1 and OD3 papers (where in some cases the E_{def} exceeded 10 kcal/mol).

The binding energies between two fragments were decomposed by the ETS-NOCV methodology [135a] on selected optimized structures, as implemented in the Amsterdam Density Functional 2014.05 package (ADF) [152].

3. Results and discussion

Metal coordination compounds are textbook examples of Lewis acid-base interactions where the electron density flows from the lone pair of the ligand (Lewis base) into a free atomic orbital of the central metal ion (Lewis acid). The metal center in the square planar complexes forms four coordination bonds. These standard interactions and reactivity of the Pt(II) complexes are to large extent determined by the nature of the coordinating atom. Pt(II) drugs have to have a low reactivity ensured by the non-leaving ligands with low σ-donation and π-back-donation abilities. The non-leaving ligands rely on nitrogen as the coordinating atom and thus, we focused on pyridine and amine ligands as the representatives of aromatic and non-aromatic ligand environments, respectively. In OD2 and OD3 papers we studied how the substitution of these ligand in the trans- position with respect to the leaving group affects the complex reactivity.

To compare the influence of the ligand substitution on the strengths of trans- and cis-effects we analyzed also the kinetics of the hydrolysis reactions on the platinum complexes pyriplatin and cis-amminedichloropyridineplatinum and their derivatives based on the substituted pyridine (pyrX) ligand. The latter complex enabled us to analyze also the influence of the charge of the complex on the strengths of the above effects. All these results are summarized in the section 3.1.

However, at the same time the Pt(II) and Ir(I) metal centers may act as Lewis bases providing electron density from the doubly occupied $5dz^2$ atomic orbital. These interactions occur in the perpendicular direction to the complex and are responsible for the nonbonding interactions of the metal center called the inverse hydration [97] or intrinsic hydrogen bonding [153] which may also contribute to the stabilization of the Pt-DNA adducts [154]. A detailed description of these interactions with strong Lewis acids is shown in the OD1 contribution and summarized in the section 3.2.

3.1 Pt(II) center as the Lewis acid, binding properties and reactivity of its complexes.

Reactivity of square-planar complexes and stabilities of their bonds are governed by the trans effect. Pt(II)-complexes used in the antitumor treatment have to be relatively little reactive to have the time to reach DNA as its intracellular target. All currently used drugs have nonleaving ligands based on nitrogen as the metal binding atom. That is why we decided to study the influence of the molecular environment of the bound nitrogen on the reactivity and binding properties of the Pt(II)-complexes. We considered the nitrogen atom

in two molecular environments: (1) as a part of the aromatic system: in the pyridine ring and its derivatives (pyrX ligands); (2) a part of nonaromatic system: in the amine group and its derivatives (NH$_2$X ligands). To obtain easily comparable data the other three ligands were the same for both system: two amine NH$_3$ ligands in cis positions and the leaving Cl$^-$ ligand in the trans position being replaced by the solvent water molecule. Detailed analyses of these results were published in the papers OD2 and OD3 and are briefly summarized in the subsections 3.1.1 and 3.1.2. More recently we have studied also the kinetics of hydrolysis reactions on pyriplatin and cis-aminedichloropyridineplatinum. These unpublished results are shown in the subsections 3.1.3–4.

3.1.1 Tuning the reactivity of the Pt(II) complexes by the substitution(s) on the trans-coordinated either pyridine or amine ligands

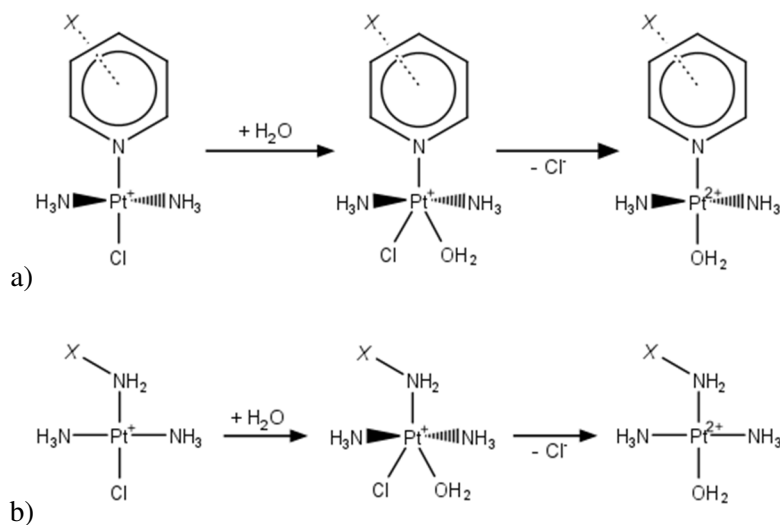The schematic representation of the structures along the reaction pathways is shown in Fig. 5.

Figure 5. Schematic representation of the two studied sets of reactions. Pt(II)-complex with a) aromatic (designated as trans-Pt-pyrX complexes), and b) non-aromatic (designated as trans-Pt-NH$_2$X complexes) ligand in the trans position with respect to the leaving Cl$^-$ ligand.

The dative character of the Pt–N bond can be clearly documented by the fact that the binding energies of the Pt–N, Pt–Cl and Pt–O bonds depended on the basicity of the pyrX ligand which was quantified by the energy of the 2p(N$_{pyrX}$) natural atomic orbital (NAO) oriented along the N$_{pyrX}$–C4 axis. Such a good correlation was enabled by a negligible π-back-donation from the Pt(II) center toward the ligands for all the bonds due to the positive charge of the complexes. The basicity of NH$_2$X ligands has lower predicting power due to

the possible presence of nonbonding X···cis-NH$_3$ interaction leading to variable and hardly predictable changes of electrostatic energy.

Several substituents X were used, some with electron-donating or electron-withdrawing capabilities: OH, Cl, F, Br, NO$_2$, NH$_2$, SH, CH$_3$, C≡CH, DMA (dimethylamine). Both pyrX and NH$_2$X ligands showed a comparable variability of the bond strengths due to substitution effects. However, substitutions of the pyrX ligand in the ortho position showed the highest variability with respect to the kinetics of the substitution reactions stabilizing some of the transition state structures by electrostatic interactions. This was caused by the coplanar orientation of the pyrX, leaving and entering ligands which enabled the *ortho*-pyr substituents with H-bond donor ability (o-NH$_2$, o-OH, o-SH) to interact with Cl⁻ leaving ligand stabilizing the TS structure and lowering the activation barrier of the aquation reaction. The o-NH$_2$-pyr pathway showed the fastest reaction rate (> 2000 times higher than the slowest m-CCH/p-NO$_2$).

We also studied the influence of the substitution effects on the stability of Pt–ligand bonds. Electron-donating substituents strengthened the Pt–pyr bond and weakened the Pt–Cl and Pt–w ones. Energy decomposition analysis showed that the changes of electrostatic energy were the main cause of the Pt–N$_{pyrX}$ bond strength variability. By similar reasoning, trans influence can be explained in the Pt-NH$_2$X system as well.

In the gas phase, the X's on the pyridine ring can be ordered according to their ability to promote the hydration reaction as follows: NH$_2$ > OH ≥ SH ~ CH$_3$ > DMA > H > F ≥ Cl ~ CCH ~ Br > NO$_2$.

The hydrolysis reaction Gibbs free energy profiles, together with the changes of structure (selected bond lengths), charges and binding energies during the five reaction steps for three trans-Pt-pyrX complexes (X = H, para-NH$_2$, para-NO$_2$) in both environments are depicted in Fig. 6. It shows several trends: 1) hydrolysis reactions were always endergonic; 2) the Pt–N$_{pyrX}$ bond gradually shortened in the course of reaction; 3) the electron-donating or withdrawing substituting groups had a clear effect on the Cl⁻ and pyrX BEs; 4) the negative charge was drained off the Pt atom, pyrX and H$_2$O ligands (totaling 0.4-0.5 *e*) and piled up on the Cl⁻; 5) water environment had a clear damping effect on the electrostatics.
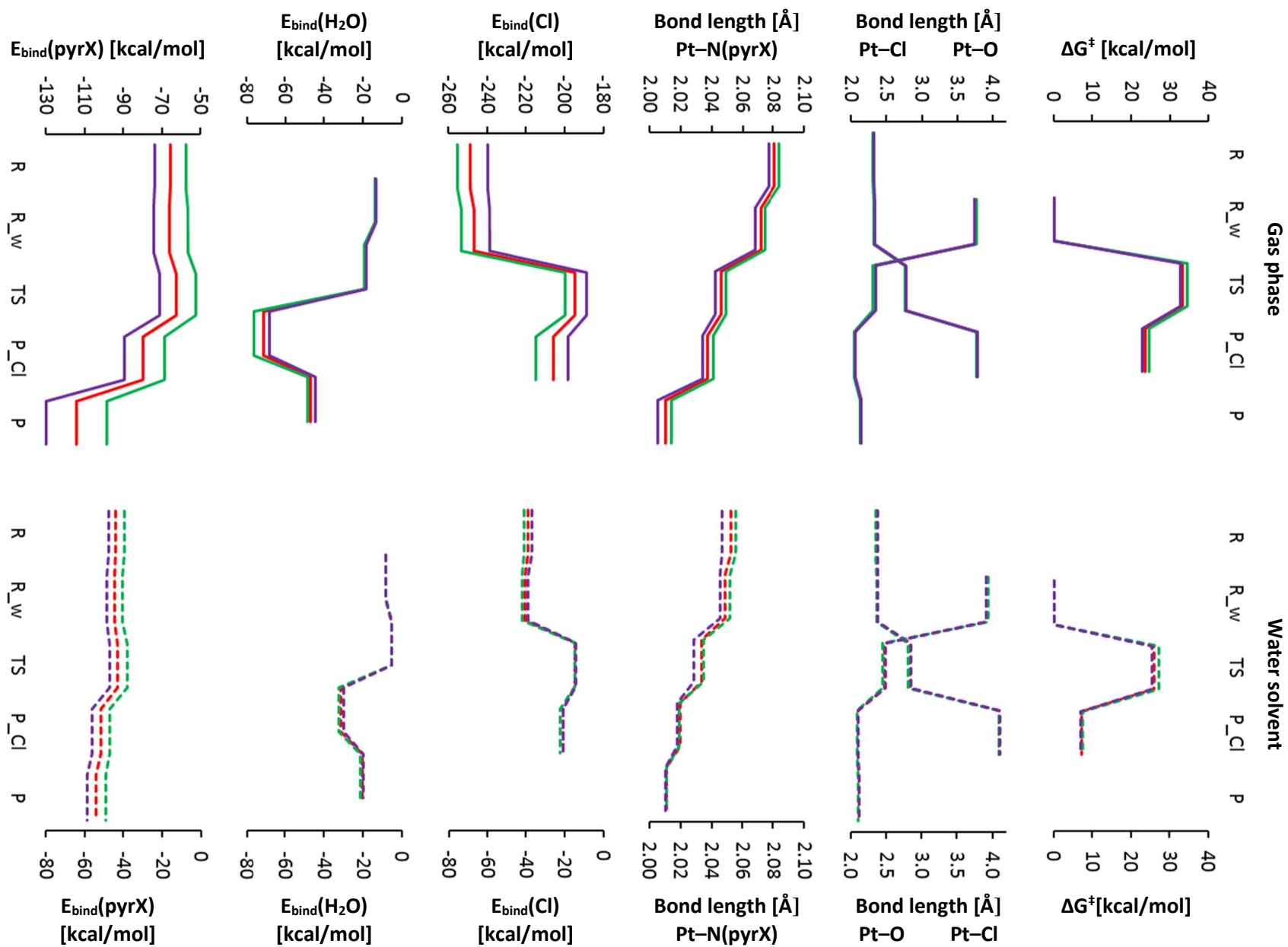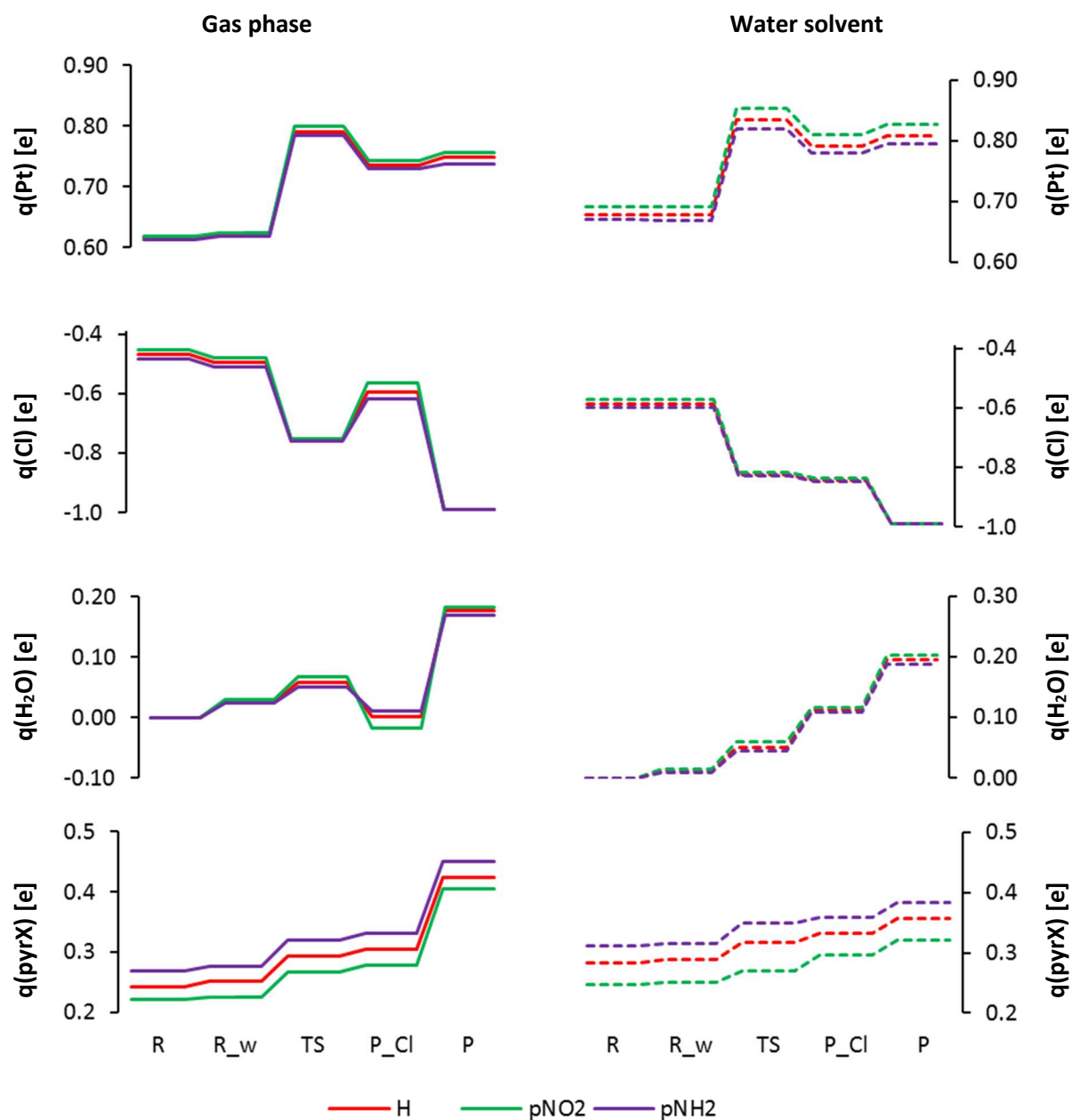
Figure 6. Gibbs free Energy profiles, bond lengths, binding energies, and charges of the three selected trans-Pt-pyrX complexes in the five reaction steps. **R** and **P** represent reactant and product structures with infinite separation of the metal complex from the entering water molecule and the leaving Cl⁻ ion, respectively, while in R_w and P_Cl structures these fragments interact by H-bonds. Solid lines, gas phase; dashed lines, water solvent.

In the case of the compounds with non-aromatic ligands, the effects of several nonleaving ligands present in pharmacologically active Pt drugs were studied: the cyclopropyl (CyP) and cyclohexyl (CyH) X substituents of the NH_2X ligands (present in JM11 and JM118, respectively [155,156]), and the bidentate 1,2-diaminocyclohexane (DACH) and 1,2-bis(aminomethyl)cyclobutane (BAMCB) ligands (present in oxaliplatin, Fig. 4b, and lobaplatin, Fig. 4d, respectively). The above-mentioned active drugs differ by

the nature of both nonleaving and leaving ligands and thus, it is impossible to extract just the influence of the nonleaving ligands from the kinetic data. We placed the nonleaving ligands into the complexes with the same ligand environment as shown in Fig. 7.
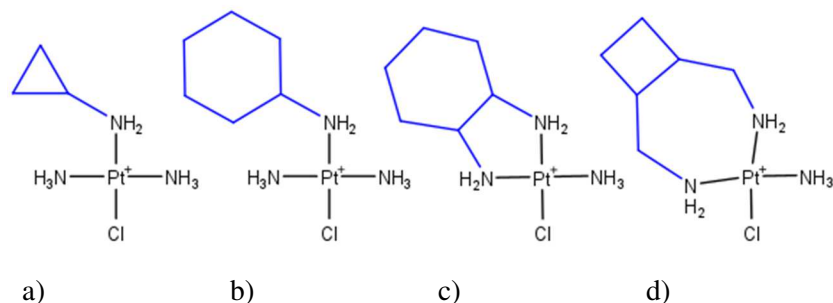

Figure 7. Structural representation of trans-Pt-NH$_2$X complexes substituted by the ligands that are present in anticancer Pt drugs (the carbohydrate substituents are shown in blue): a) cyclopropyl, b) cyclohexyl, c) bidentate 1,2-diaminocyclohexane, and d) 1,2-bis(aminomethyl)cyclobutane

A larger positive inductive +I effect is connected with the increase of the size of the saturated cycloalkyl substituents (in the row H < CH$_3$ < CyP < CyH). The enhancement of electron-donating ability leads to the increase of electron density on the Pt–NH$_2$X bond resulting in its strengthening and due to the trans effect the accompanying change is the weakening of the Pt–Cl and Pt–w bonds. BEs of the ligands as well as activation Gibbs free energies were logarithmically dependent on the number of hydrocarbon electrons.

The chelation (i.e., the formation of the bidentate DACH ligand from the monofunctional CyH one) leads to a slight decrease of the +I effect in the direction of the Pt–Cl bond compaired to CyH, but simultaneously it increases the +I effect along the other axis of the complex. For bifunctional Pt(II) drugs this may facilitate the second leaving group substitution.

In the water solvent, the reactivity of the complexes decreases in the order CyH ~ CyP > DACH ~ BAMCB > H. Our results should help to understand the differences in the biotransformation of the Pt(II) drugs based on these substituents.

3.1.2 *The effect of methodology*

For trans-Pt-pyrX complexes, the influence of the chosen B3LYP functional on the height of the activation barriers and Pt−ligand bond lengths was checked by utilizing two other functionals, M06-2X and PBE0 in the gas phase. In the solvent, these calculations were performed only with the M06-2X functional.

Very good correlation (R^2 > 0.94) was found for the Pt−ligand bond lengths (with B3LYP results being systematically longer). Reasonable correlation was found also for

activation Gibbs free energies which were systematically lower by 2.8 ± 0.5 kcal/mol and higher by 0.9 ± 0.4 kcal/mol for the M06-2X and PBE0-D3BJ functionals, respectively.

Comparison of the solvent results between B3LYP and M06-2X revealed a much smaller correlation in the case of Pt–Cl bond distance in the TS, and an almost nonexistent correlation of activation Gibbs free energies. Even though the typical electron-donating NH_2 and electron-withdrawing NO_2 substituents showed a similar effect on the activation barrier height (a lowering and an increase, respectively) in the para and ortho positions, other $\Delta(\Delta G^{\ddagger})$ differences are probably too small compared to the precision of our calculations.

3.1.3   *Hydrolysis of pyriplatin and its derivatives*

Pyriplatin ($[Pt(NH_3)_2(pyridine)Cl]^+$; designated as cis-Pt-pyrH; Fig. 8) is the cis-isomer of the trans-Pt-pyrH complex described above. It should help us to uncover the importance of the cis ligands for reactivity of Pt(II) complexes and reveal to what extent one can modify the reaction rates by the substitution of the ligand in the cis position.
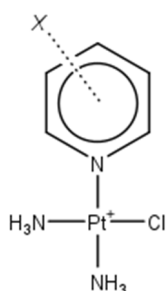
Figure 8. Structure of pyriplatin (*cis*-[PtCl(NH_3)_2(pyrX)]^+) (X = H) and its derivatives (X = CH_3, NO_2, NH_2)

Pyriplatin is a promising drug which forms monofunctional adducts with N7 atoms of guanine bases but still inhibiting DNA transcription probably due to steric hindrance, intercalation and/or H-bond formation [157]. It shows very promising results, significantly distinct from cisplatin and oxaliplatin, as was shown by the synergistic effect of pyriplatin and cisplatin when administered simultaneously [158].

We studied hydrolysis mechanism of this drug and its substituted derivatives. For the comparison purposes the same methodology as in the OD2 and OD3 papers was used. NH_2 and NO_2 substituents in the para position (designated as pNH_2 and pNO_2) were chosen as the representatives of electron donating and withdrawing groups, respectively. The influence of the substituent's position on the pyrX ligand was studied for the CH_3 substituent leading to pCH_3, mCH_3 and oCH_3 systems which correspond to the CH_3 substitution on the para-,

meta- and ortho- positions of the pyrX ligand, respectively. The main kinetic data are summarized in Table 1.

Table 1: Activation Gibbs free energies (in kcal/mol) for hydrolysis reactions of pyriplatin and its derivatives (cis-Pt-pyrX) in the gas phase ($\Delta G^{\ddagger}_{gas}$) and in the water solvent ($\Delta G^{\ddagger}_w$). Reaction Gibbs free energies (ΔG_{rw}) and kinetic constants (k_w) are shown only for water solvent. The data for the pyriplatin's trans isomer (trans-Pt-pyrX: see above and the paper OD2) are also shown for a comparison. Available theoretical $\Delta G^{\ddagger}_w$ value for pyriplatin hydrolysis [159] is shown in parenthesis. All energies are in kcal/mol. n.a. not available at present.

system / substituent (X)	$\Delta G^{\ddagger}_{gas}$	$\Delta G^{\ddagger}_w$	k_w [s⁻¹]	$\Delta G^{\ddagger}_{rw}$	$\Delta G^{\ddagger}_{gas}$	$\Delta G^{\ddagger}_w$	k_w [s⁻¹]	$\Delta G^{\ddagger}_{rw}$
	cis-Pt-pyrX				trans-Pt-pyrX			
H	31.9	26.1 (23.5)	4.49 x 10⁻⁷	7.2	33.2	25.9	6.92 x 10⁻⁷	7.2
pNH₂	31.2	24.1	1.35 x 10⁻⁵	7.6	32.6	25.4	1.59 x 10⁻	6.9
pNO₂	32.8	26.7	1.68 x 10⁻⁷	n.a.	34.3	27.2	7.34 x 10⁻	7.5
pCH₃	31.4	25.6	1.03 x 10⁻⁶	6.4	33.0	25.8	7.09 x 10⁻⁷	7.1
mCH₃	31.4	25.6	1.10 x 10⁻⁶	7.1	32.7	25.8	7.50 x 10⁻⁷	7.0
oCH₃	33.0	26.6	1.99 x 10⁻⁷	7.4	32.8	25.5	1.20 x 10⁻⁶	7.2

In the gas phase the presence of the pyrH ligand in the cis- position with respect to the leaving Cl⁻ ligand leads to a higher lability of the complex with respect to the hydrolysis reaction compared to the trans- isomer. It may look as a surprising result since the pyrH ligand has larger π-back-donation ability than the amine ligand. Therefore, the leaving Cl⁻ and entering water ligands should be stabilized better in the trans-Pt-pyrH-TS structure. However, this is not the case here since negligible π-back-donation was observed in trans-Pt-pyrX complexes due to the positive charge of the complex [OD2]. On the other hand, the cis-Pt-pyrH-TS structure is probably stabilized more effectively by electrostatic interactions since as the $\Delta(\Delta G^{\ddagger})$ gas phase difference of 1.3 kcal/mol for its favor fully diminished being inverted to -0.2 kcal/mol in the water solvent (Table 1).

The effect of para-X substituents on the rate of the hydrolysis is almost the same for the cis- and trans-Pt-pyrX complexes in the gas phase. The electron donating NH₂ ligand lowers $\Delta G^{\ddagger}$ value while electron withdrawing NO₂ has the opposite effect. The difference in the $\Delta G^{\ddagger}$ values ($\Delta(\Delta G^{\ddagger})$) between pNO₂ and pNH₂ is 1.6(1.7) kcal/mol for cis-(trans-)Pt-pyrX complexes which means that substituent effects are very similar and may influence the rate of the hydrolysis of these complexes by up 1–2 orders of magnitude in the gas phase. Fig. 9 brings a possible evidence of this phenomenon: $\Delta G^{\ddagger}$ values are to a large extent determined by the binding energies of the leaving Cl⁻ ligand and this ligand is bound in both

complexes by similar strength even through in cis-Pt-pyrX complexes it is able to donate more electrons to the complex. Note also a lower response of the transferred charge to the nature of the pyrX ligand (a corresponding line in Fig. 9 is steeper) which reflects the fact that the communication between the ligands occurs mainly in the trans- direction.
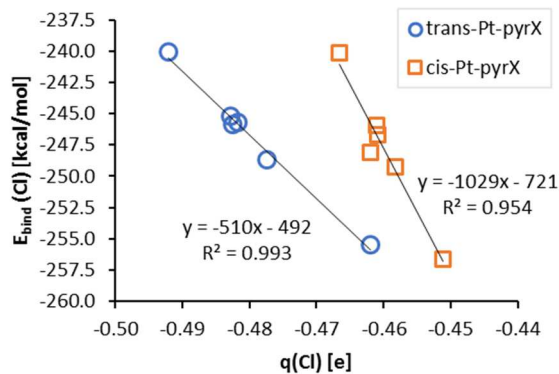

Figure 9: Dependence of the gas phase binding energies of the Cl$^-$ ligand on its NPA charges in cis-Pt-pyrX and trans-Pt-pyrX complexes.

The solvation lowered substantialy the activation Gibbs energies in all studied systems. However, the solvation increased the $\Delta(\Delta G^{\ddagger})$ difference between the pNO$_2$ and pNH$_2$ pathways up to 2.6 kcal/mol for cis-Pt-pyrX system which corresponds exactly to two orders of magnitude in the reaction rate. For the trans-Pt-pyrX system the $\Delta(\Delta G^{\ddagger})$ difference remained almost the same as in the gas phase (1.8 kcal/mol).

Meta- and para- positions of the CH$_3$ substituent showed exactly the same reactivity in agreement with the previous study od Dabbish et al. who studied the influence of the position of the CH$_2$Ph$_3$P$^+$ substituent in the pyrX ligand on the cis-Pt-pyrX system reactivity [159,160]. In our case the ortho-CH$_3$ substitution decelerated the hydrolysis by about one order of magnitude which is however exactly the opposite result to the influence of the ortho-CH$_2$Ph$_3$P$^+$ substituent in the cited study.

3.1.4 Hydrolysis of cis-amminedichloropyridineplatinum and its derivatives

Amminedichloropyridineplatinum *cis*-[PtCl$_2$(NH$_3$)pyr] is an interesting reference system since its ortho-CH$_3$ (2-picoline, picoplatin) and meta-CH$_3$ (3-picoline) derivatives were shown to have cytotoxic properties [161]. Picoplatin (ZD0473) already entered Phase II clinical trials in the treatment of lung and breast cancer [162]. These complexes are similar to cisplatin being neutral and having two leaving Cl$^-$ ligands in cis orientation (Fig. 10).
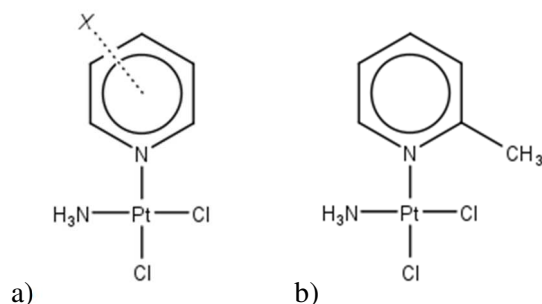
Figure 10. Structures of a) *cis*-[PtCl$_2$(NH$_3$)(pyrX)] complex (X = H) and its derivatives (X = CH$_3$, NO$_2$, NH$_2$), and b) picoplatin (*cis*-[PtCl$_2$(NH$_3$)(2-picoline)]) as the example of an anticancer derivative

We studied the influence of the substitution effects on the kinetics of the first activation step of the complex. Both Cl$^-$ ligands were considered as the possible leaving groups. As in case of pyriplatin it enabled us to evaluate and compare the influence of substitution effects of the ligands in the cis- and trans- positions with respect to the leaving on the reactivity but here for the system with neutral charge. The main kinetic data are summarized in Table 2.

Table 2: Activation Gibbs free energies for the first step of hydrolysis reactions of cis-amminedichloropyridineplatinum (X=H) and its derivatives substituted on the pyridine ring in the gas phase ($\Delta G^{\ddagger}_{gas}$) and in the water solvent ($\Delta G^{\ddagger}_{w}$). Reaction Gibbs free energies (ΔG_{rw}) and kinetic constants (k_w) are shown only for water solvent. The reaction may occur by the replacement of the Cl$^-$ ligand trans- and cis- position to the pyrX ligand (trans-Cl$^-$ and cis-Cl$^-$ pathway, respectively). Available theoretical [163] and experimental [164] results for the $\Delta G^{\ddagger}$ and k_w values, respectively, are shown in parenthesis. All energies are in kcal/mol.

	$\Delta G^{\ddagger}_{gas}$	$\Delta G^{\ddagger}_{w}$	k_w [s^{-1}]	ΔG_{rw}	$\Delta G^{\ddagger}_{gas}$	$\Delta G^{\ddagger}_{w}$	k_w [s^{-1}]	ΔG_{rw}
leaving ligand / substituent (X)	trans-Cl$^-$				cis-Cl$^-$			
H	26.0	24.6	6.02 x 10^{-6}	4.7	31.3	24.5	6.99 x 10^{-6}	6.4
pNH$_2$	25.7	23.6	3.14 x 10^{-5}	4.4	30.9	24.0	1.68 x 10^{-5}	5.8
pNO$_2$	25.8	24.7	4.80 x 10^{-6}	5.1	31.4	24.7	5.17 x 10^{-6}	7.0
pCH$_3$	25.9	24.3	9.28 x 10^{-6}	4.9	30.9	24.1	1.46 x 10^{-5}	6.2
mCH$_3$	25.8	24.1	1.28 x 10^{-5} (4.47 x 10^{-5})	4.9	31.1	24.1	1.24 x 10^{-5} (1.03 x 10^{-4})	6.1
oCH$_3$	25.7	24.5 (22.9)	7.28 x 10^{-6} (3.19 x 10^{-5})	5.1	32.4	25.5 (23.1)	1.29 x 10^{-6} (2.21 x 10^{-5})	5.3

Unlike the pyriplatin the preferred site for the nucleophilic attack to the cis-amminedichloropyridineplatinum is clearly the Cl$^-$ ligand in the trans- position to the pyrX ligand in the gas phase. To a large extent it has to be caused by electrostatic stabilization of the TS structure since no preferable site was detected in the water solvent. Moreover, there

is no intrinsic difference in the lability of the two Cl- ligands in the *cis*-[PtCl$_2$(NH$_3$)(pyrX)] complexes: the binding energies are almost exactly the same (Fig. 11 right panel) at the expense of the higher electron donation of the cis-Cl$^-$ ligand (Fig. 11 left panel, cf. Fig. 9).
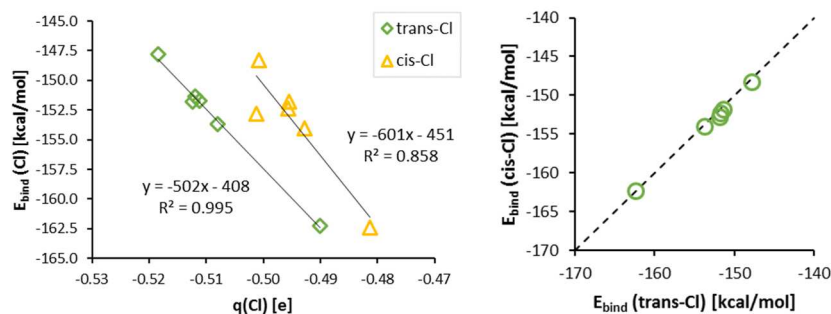
Figure 11: Dependence of the gas phase binding energies of the two Cl$^-$ ligand in *cis*-[PtCl$_2$(NH$_3$)(pyrX)] complexes on its NPA charges (left panel); mutual dependence of the binding energies of the two Cl$^-$ ligands (right panel).

In the solvent the difference of the trans- effect strengths of the amine and pyridine ligands is below the precision of our theoretical calculations. There is only a slight thermodynamic preference for the hydrolysis reaction on the trans-Cl$^-$ ligand being by 1.3 ± 0.6 kcal/mol less endergonic than the reaction on the cis-Cl$^-$.

Substitution effects on the pyrX ligand in the neutral cis-[PtCl$_2$NH$_3$(pyrX)] complex lead to small changes of the hydrolysis rates being only within one order of magnitude for both reactive Cl$^-$ centers in both the gas phase and the water solvent. It is a lower sensitivity of the reaction rates than in the positively charged cis/trans-[Pt(NH$_3$)$_2$Cl(pyrX)]$^+$ complexes discussed above. In the gas phase it can be at least partly explained by a lower donation ability (by ca. 20%) of the pyrX ligand towards neutral complexes compared to the positively charged ones. However, in the water solvent the NPA charges of the pyrX ligand are almost the same regardless of the charge of the complex. Clearly, further analyses are necessary to understand this phenomenon.

3.1.5 *Comparison of the results with other theoretical studies and experimental data*

Our calculated kinetic constants are in a very good agreement with the experimental data for 2- and 3-picoline complexes [164] differing by ca. one order of magnitude at most (Table 2).

Agreement with other theoretical studies is much worse since our ΔG‡ values are always higher. The highest difference of 2.6 kcal/mol is for pyriplatin (Table 1) for which

however no experimental data are available. For 2-picoline our results are closer to experimental values than the results of Sarmah & Deka [163].

Only crystal structures of 2-picoline and 3-picoline drugs are available [164]. Compared to the experimental structures our optimized bond lengths are systematically longer by a few hundredths of Å (Table 3) which probably reflects the use of the DZ-quality basis set for geometry optimizations.

Table 3: Comparison of the gas phase and water solvent optimized bond lengths of the 2-picoline and 3-picoline drugs with the experimental crystal structures [164].

compound	2-picoline			3-picoline		
	this work		exp.	this work		exp.
bond	gas phase	water solvent		gas phase	water solvent	
Pt–N$_1$	2.070	2.056	2.017	2.059	2.044	2.008
Pt–N$_2$	2.108	2.082	2.030	2.108	2.074	2.039
Pt–Cl$_1$	3.335	2.377	2.299	2.335	2.372	2.296
Pt–Cl$_2$	2.329	2.377	2.322	2.325	2.373	2.309

3.2 Pt(II) and Ir(I) metal centers as Lewis bases

In the paper OD1 we have shown that the metal center (Pt(II), Ir(I)) in the square planar complexes may behave also as a Lewis base center. Doubly occupied $5dz^2$ orbital which is oriented above and below the plane of the complex enables the formation of the dative bonds with electron deficient group 13 trihalides and trihydrides YZ_3 (Y = B, Al, Ga; Z = H, F, Cl, Br). These interactions lead to the formation of $MX_4 \cdot YZ_3$ adducts with the pentacoordinated square pyramidal conformation of ligands around the metal M atom (Figs. 12 & 13). These adducts are stabilized mainly by donor-acceptor M·Y bonds which can be basically described by the charge transfer from the $5d_{z^2}$ orbital of Pt(II) or Ir(I) to empty valence p_z orbital of Y (Fig. 14).

a)   b)
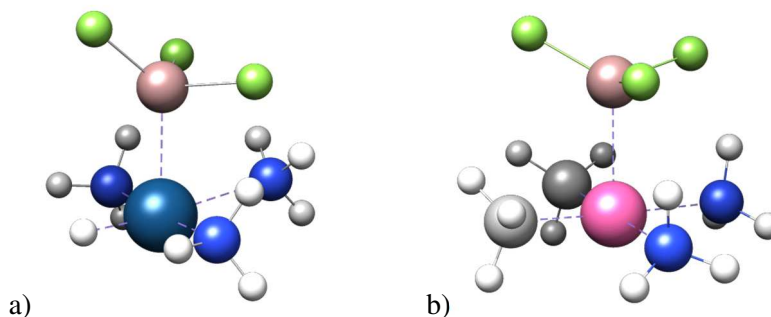
Figure 12. Example of the most stable $MX_4 \cdot YZ_3$ adducts: a) IrH(NH$_3$)$_3 \cdot$GaF$_3$; b) Pt(CH$_3$)$_2$(NH$_3$)$_2 \cdot$GaF$_3$.

Figure 13. Example of the most stable pincer $MX \cdot YZ_3$ adducts: a) $Ir(NNN)(CH_3) \cdot GaF_3$;
b) $Pt(NCN)(CH_3) \cdot GaF_3$.

Figure 14. Dependence of the binding energies on the absolute value of the transferred charge for
$IrX \cdot YZ_3$ adducts.
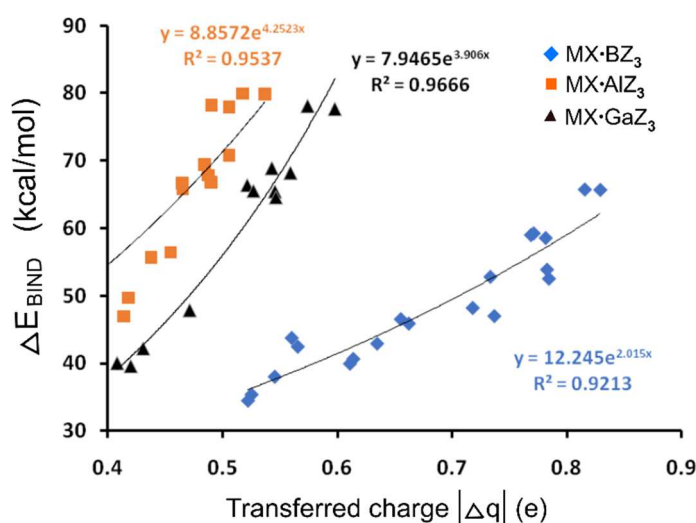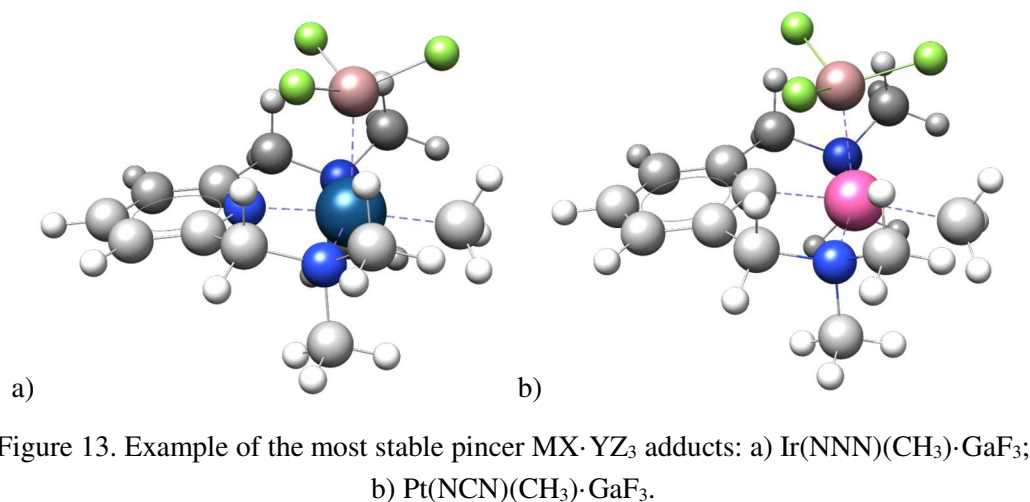
Binding energies of the adducts of the Ir(I) complexes reached up to ca. –85 kcal/mol and were by about 30 kcal/mol higher than those of the Pt(II). Ir(I) center is even a stronger Lewis base than ammonia with a higher interaction energy accompanied by the more important contribution of the charge transfer energy. The strongest Lewis acid was GaF_3, closely followed by AlF_3. The adduct formation led to pyramidalization of YZ_3 subunit and prolongation of Y-Z bonds. These structural changes were further enhanced by Pauli repulsion between Z atoms and the metal complex. The $M \cdot Y$ dative bonds had covalent (for Y=B) or charge-transfer (for Y= Al, Ga) character. However, despite their covalency the $M \cdot B$ bonds were weaker than their Al and Ga counterparts due to larger deformation energies of BZ_3 subunits.

4. Conclusions

In this work the Lewis acid/base properties of the metal Pt(II) and Ir(I) centers were studied by theoretical DFT calculations.

Kinetics of substitution reactions of square-planar complexes are strongly dependent on the electron donating/accepting abilities of the ligands. Here we focused on ligand substitution effects on the aromatic pyrX and non-aromatic NH_2X nonleaving ligands which enabled us to study the fine-tuning of the reactivity of Pt(II) complexes. The electron-donating and electron-withdrawing substituents X decrease and increase the activation free energy $\Delta G^{\ddagger}$, respectively. The influence of ligand substitution(s) on the changes of the activation free energy $\Delta(\Delta G^{\ddagger})$ were similar for Pt(II) complexes with pyrX and NH_2X ligands. The $\Delta(\Delta G^{\ddagger})$ variability due to substitution effects reached up to a value of 1.9 kcal/mol when taking all the substituents into consideration in the water solvent.

Surprisingly, quantitatively very similar changes of the reactivity of the Pt(II) complexes were achieved also by substitution of the pyrX ligand in the cis position with respect to the leaving ligand as shown by the comparisons of the reactivities of cis-Pt-pyrX / trans-Pt-pyrX complexes and the labilities of cis-Cl⁻ / trans-Cl⁻ ligands in *cis*-[PtCl$_2$(NH$_3$)(pyrX)] complexes. The latter Pt(II) complexes showed lower a sensitivity of the reaction rates with respect to the pyrX ligand modifications probably due to the neutral charge. We belive that our results improved understanding of the differences in the pharmacokinetics of the active Pt(II) anticancer compounds.

Metal's weak interactions are responsible for the recognition of the metal center in the environment and the metal center behaves as a Lewis base being the electron donor. The binding energy of these interactions depends strongly on the acidity of the interacting molecule. It is low for water but quite high for stronger Lewis acids like group 13 trihydrides and trihalides.

5. Literature

1. Ogburn, S. C. The Platinum Metals. *J Chem Educ* 1928, 5:1371−84; Bergsøe P. Metallurgy of Gold and Platinum among the Pre-Columbian Indians. *Nature* 1936, 137:29; Reichlen H. La métallurgie de l'or et du platine à Esmeraldas, Équateur. *J Soc Am N.S.* 1940, 32:293–5; Scott DA, Bray W. Ancient platinum technology in South America. *Platinum Metals Rev* 1980, 24:147–57.

2. Watson W, Brownrigg W. Several papers concerning a new semi-metal, called platina. *Phil Trans* 1750, 46:584–96; Dixon J. The Literary Life of William Brownrigg, M.D. F.R.S. Longman & Rees, London, 1801; Weeks ME. The discovery of the elements. VIII. The platinum metals. *J Chem Educ* 1932, 9:1017–34.

3. Juan J, de Ulloa A. *Relación histórica del viaje a la América Meridional*. Antonio Marín, Madrid, 1748; Juan G, de Ulloa A. *A voyage to South-America*. L. Davis and C. Reymers, London, 1758.

4. Moreno R. Antonio de Ulloa, 'Descubridor' del platino. In Losada M, Varela C (eds). *Actas del II Centenario de don Antonio de Ulloa*, Escuela de Estudios Hispano-Americanos C.S.I.C., Madrid, 1995, pp. 79–96; Lane K. Gone Platinum: Contraband and Chemistry in Eighteenth-Century Colombia. *Colonial Latin American Rev* 2011, 20:61–79.

5. McDonald D. The first platinum refiners. *Platinum Metals Rev* 1968, 12:142–8; Smith FJ. Standard kilogram weights. *Platinum Metals Rev* 1973, 17:66–8.

6. Bureau International des Poids et Mesures. *Comptes Rendus de la 1e Conférence générale des poids et mesures (1889)*. 1890. p. 34. Available from: <https://www.bipm.org/utils/common/pdf/CGPM/CGPM1.pdf>

7. Bureau International des Poids et Mesures. *Comptes Rendus de la 26e réunion de la Conférence générale des poids et mesures (novembre 2018)*. 2019. p. 210. Available from: https://www.bipm.org/utils/common/pdf/CGPM/CGPM26.pdf

8. Mudd GM, Jowitt SM, Werner TT. Global platinum group element resources, reserves and mining – A critical assessment. *Sci Total Environ* 2018, 622–3:614–25.

9. Global Burden of Disease Collaborative Network. Global Burden of Disease Study 2019 (GBD 2019) Results. Seattle, United States: Institute for Health Metrics and Evaluation (IHME), 2020. Available from: http://ghdx.healthdata.org/gbd-results-tool; Sung H, Ferlay J, Siegel RL, Laversanne M, Soerjomataram I, Jemal A, Bray F. Global cancer statistics 2020: GLOBOCAN estimates of incidence and mortality worldwide for 36 cancers in 185 countries. *CA Cancer J Clin* 2021. doi: 10.3322/caac.21660.

10. e.g. Rothschild BM, Witzke BJ, Hershkovitz I. Metastatic cancer in the Jurassic. *Lancet* 1999, 354:398; Czarnetzki A. Pathological changes in the morphology of the young paleolithic skeletal remains from Stetten (south-west Germany). *J Hum Evol* 9:15–17; Monge J, Kricun M, Radovčić J, Radovčić D, Mann A, et al. Fibrous dysplasia in a 120,000+ year old neandertal from Krapina, Croatia. *PLoS ONE* 2013, 8:e64539.

11. Virchow R. *Die Cellularpathologie in ihrer Begründung auf physiologische und pathologische Gewebelehre*. August Hirschwald, Berlin, 1859.

12. Grange JM, Stanford JL, Stanford CA. Campbell De Morgan's 'Observations on cancer', and their relevance today. *J R Soc Med* 2002, 95:296–299.

13. Boveri T. Concerning the origin of malignant tumours. (Transl. and annot. Harris H.) *J Cell Sci* 2008, 121 (Suppl. 1):1–84.

14. Peyrone M. Ueber die Einwirkung des Ammoniaks auf Platinchlorür. *Ann Chem Pharm* 1844, 51:1–29.

15. Rosenberg B, Van Camp L, Krigas T. Inhibition of cell division in Escherichia coli by electrolysis products from a platinum electrode. *Nature* 1965, 205:698–699.

16. Rosenberg B, Van Camp L, Grimley EB, Thomson AJ. The inhibition of growth or cell division in Escherichia coli by different ionic species of platinum(IV) complexes. *J Biol Chem* 1967, 242:1347–52.

17. Carpenter D. *Reputation and power: Organizational image and pharmaceutical regulation at the FDA*. Princeton University Press, Princeton, 2010.

18. e.g. Hayes D, Cvitkovic E, Golbey R, Scheiner E, Krakoff IH. Amelioration of renal toxicity of high dose cis-platinum diamminedichloride (CPDD) by mannitol-induced diuresis. *Proc Am Assoc Cancer Res* 1976, 17:169; Blachley JD, Hill JB. Renal and electrolyte disturbances associated with cisplatin. *Ann Intern Med* 1981, 95:628–32.

19. e.g. Cubeddu LX, Hoffmann IS, Fuenmayor NT, Finn AL. Efficacy of ondansetron (Gr38032F) and the role of serotonin in cisplatin-induced nausea and vomiting. *N Engl J Med* 1990, 322:810–6; Smith DB, Newlands ES, Rustin GJS, Begent RHJ, Howells N, McQuade B, Bagshawe KD. Comparison of ondansetron and ondansetron plus dexamethasone as antiemetik prophylaxis during cisplatin-containing chemotherapy. *Lancet* 1991, 338:487–90.

20. Galanski M, Jakupec MA, Keppler BK. Update of the Preclinical Situation of Anticancer Platinum Complexes: Novel Design Strategies and Innovative Analytical Approaches. *Curr Med Chem* 2005, 12:2075–94; Wheate NJ, Walker S, Craig GE, Oun R. The status of platinum anticancer drugs in the clinic and in clinical trials. *Dalton Trans* 2010, 39:8113–27.

21. Fuertes MA, Alonso C, Perez JM. Biochemical modulation of cisplatin mechanisms of action: enhancement of antitumor activity and circumvention of drug resistance. *Chem Rev* 2003, 103:645–62.

22. Weiss RB, Christian MC. New cisplatin analogues in development. A review. *Drugs* 1993, 46:360–77; Lebwohl D, Canetta R. Clinical development of platinum complexes in cancer therapy: a historical perspective and an update. *Eur J Cancer* 1998, 34:1522–34.

23. Apps MG, Choi EHY, Wheate NJ. The state-of-play and future of platinum drugs. *Endocr Relat Cancer* 2015, 22:R219–33.

24. Werner A. Beitrag zur Konstitution anorganischer. *Z Anorg Chem* 1893, 3:267–30.

25. Chernyaev II. Mononitrites of bivalent platinum. *Ann Inst Platine USSR* 1926, 4:243–76.

26. Langford CH, Gray HB. *Ligand substitution processes*. Benjamin, Inc.: New York, 1965.

27. Chernyaev II. *Ann Inst Platine USSR* 1927, 5:109; Grinberg AA. *Ann Inst Platine USSR* 1932, 10:58; Grinberg AA. *Acta Phys Chim* 1935, 3:573.

28. Dewar MJS. A review of π Complex Theory. *Bull Soc Chim Fr* 1951, 18:C71–9; Chatt J, Duncanson LA. Olefin co-ordination compounds. Part III. Infra-red spectra and structure: attempted preparation of acetylene complexes. *J Chem Soc* 1953, 2939–47.

29. Chval Z, Sip M, Burda JV. The trans effect in square-planar platinum(II) complexes – A density functional study. *J Comput Chem* 2008, 29:2370–81.

30. Pinter B, Van Spreyboeck V, Waroquier M, Geerlings P, De Proft F. *trans* effect and *trans* influence: importance of metal mediated ligand–ligand repulsion. *Phys Chem Chem Phys* 2013, 15:17354–65.

31. Dhara SC. A rapid method for the synthesis of cis-[PtCl$_2$(NH$_3$)$_2$]. *Indian J Chem* 1970, 8:193–4.

32. Reiset J. *Compt Rend* 1844, 18:1103; Peyrone M. *Ann Chem Pharm* 1846, 59:1; Kauffman GB, Cowan DO, Slusarczuk G, Kirschner S. cis- and trans-dichlorodiammineplatinum(II). *Inorg Synth* 1963, 7:239–45.

33. Kurnakow N. Ueber complexe Metallbasen; Erste Abhandlung. *J Prakt Chem* 1894, 50:481–507; Mellor DP. The stereochemistry of square complexes. *Chem Rev* 1943, 33:137–83; Kauffman GB. Nikolai Semenovich Kurnakov, the reaction (1893) and the man (1860–1941) a ninety-year retrospective view. *Polyhedron* 1983, 2:855–63.

34. Kasparkova J, Brabec V. Recognition of DNA interstrand cross-links of cisdiamminedichloroplatinum(II) and its trans isomer by DNA-binding proteins. *Biochemistry* 1995, 34:12379–87; Jamieson ER, Lippard SJ. Structure, recognition, and processing of cisplatin−DNA adducts. *Chem Rev* 1999, 99:2467–98; Jung Y, Lippard SJ. Direct cellular responses to platinum-induced DNA damage. *Chem Rev* 2007, 107:1387–407.

35. Siddik ZH. Cisplatin: mode of cytotoxic action and molecular basis of resistance. *Oncogene* 2003, 22:7265–79.

36. Rosenberg B, Van Camp L, Trosko JE, Mansour VH. Platinum compounds – A new class of potent antitumour agents. *Nature* 1969, 222:385–6.

37. Rosenberg B, Van Camp L. Successful regression of large solid sarcoma 180-tumors by platinum compounds. *Cancer Res* 1970, 30:1799–802.

38. Harder H, Rosenberg B. Inhibitory effects of anti–tumor platinum compounds on DNA, RNA and protein syntheses in mammalian cells in vitro. *Int J Cancer* 1970, 6:207–16.

39. Cleare MJ, Hoeschele JD. Anti-tumour platinum compounds. Relationship between structure and activity. *Platinum Met Rev* 1973, 17:2–13.

40. Gale GR, Morris CR, Atkins LM, Smith AB. Binding of an antitumor platinum compound to cells as influenced by physical factors and pharmacologically active agents. *Cancer Res* 1973, 33:813–8; Ishida S, Lee J, Thiele DJ, Herskowitz I. Uptake of the anticancer drug cisplatin

mediated by the copper transporter Ctr1 in yeast and mammals. *Proc Natl Acad Sci USA* 2002, 99:14298–302.

41. Bancroft DP, Lepre CA, Lippard SJ. Platinum-195 NMR kinetic and mechanistic studies of cis- and trans-diamminedichloroplatinum(II) binding to DNA. *J Am Chem Soc* 1990, 112:6860–71; Davies MS, Berners-Price SJ, Hambley TW. Rates of platination of AG and GA containing double-stranded oligonucleotides: Insights into why cisplatin binds to GG and AG but not GA sequences in DNA. *J Am Chem Soc* 1998, 120:11380–90; Davies MS, Berners-Price SJ, Hambley TW. Slowing of cisplatin aquation in the presence of DNA but not in the presence of phosphate: improved understanding of sequence selectivity and the roles of monoaquated and diaquated species in the binding of cisplatin to DNA. *Inorg Chem* 2000, 39:5603–13.

42. Legendre F, Bas V, Kozelka J, Chottard J-C. A complete kinetic study of GG versus AG platination suggests that the doubly aquated derivatives of cisplatin are the actual DNA binding species. *Chem Eur J* 2000, 6:2002–10; Kozelka J. Molecular origin of the sequence dependent kinetics of reactions between cisplatin derivatives and DNA. *Inorg Chim Acta* 2009, 362:651–68.

43. Howle JA, Gale GR. Cis-dichlorodiammineplatinum (II). Persistent and selective inhibition of deoxyribonucleic acid synthesis in vivo. *Biochem Pharmacol* 1970, 19:2757–62.

44. Horáček P, Drobník J. Interaction of cis-dichlorodiammineplatinum (II) with DNA. *Biochim Biophys Acta* 1971, 254:341–7; Bodenner DL, Dedon PC, Keng PC, Borch RF. *Cancer Res* 1986, 46:2745.

45. e.g. Roberts JJ, Pascoe JM. Cross-linking of complementary strands of DNA in mammalian cells by antitumour platinum compounds. *Nature* 1972, 235:282–4; Mansy S, Chu GYH, Duncan RE, Tobias RS. Heavy metal nucleotide interactions. 12. Competitive reactions in systems of four nucleotides with cis- or trans-diammineplatinum(II). Raman difference spectrophotometry of the relative nucleophilicity of guanosine, cytidine, adenosine, and uridine monophosphates and analogous DNA bases. *J Am Chem Soc* 1978, 100:607–16; Brabec V, Vrana O, Kleinwächter V, Kiss F. Modification of the DNA structure upon platinum binding. *Stud Biophys* 1984, 101:135–39; Pinto AL, Lippard SJ. Sequence-dependent termination of in vitro DNA synthesis by cis- and trans-diamminedichloroplatinum (II). *Proc Natl Acad Sci USA* 1985, 82:4616–9; Fichtinger-Schepman AMJ, van der Veer JL, den Hartog JHJ, Lohman PHM, Reedijk J. Adducts of the antitumor drug cis-diamminedichloroplatinum(II) with DNA: formation, identification, and quantitation. *Biochemistry* 1985, 24:707–13; Eastman A. Reevaluation of interaction of cis-dichloro(ethylenediamine)platinum(II) with DNA. *Biochemistry* 1986, 25:3912–5; Sherman SE, Gibson D, Wang AH-J, Lippard SJ. Crystal and molecular structure of cis-[Pt(NH3)2{d(pGpG)}], the principal adduct formed by cisdiamminedichloroplatinum(II) with DNA. *J Am Chem Soc* 1988, 110:7368–81; 37. Arpalahti J, Lippert B. Coordination of aquated cis-platinum(II) diamines to purine nucleosides. Kinetics of complex formation. *Inorg Chem* 1990, 29:104–10; Lemaire MA, Schwartz A, Rahmouni AR, Leng M. Interstrand cross-links are preferentially formed at the d(GC) sites in the reaction between cis-diamminedichloroplatinum (II) and DNA. *Proc Natl Acad Sci USA* 1991, 88:1982–5; Brabec V, Šíp M, Leng M. DNA conformational change produced by the site-specific

interstrand cross-link of trans-diamminedichloroplatinum(II). *Biochemistry* 1993, 32:11676–81; Huang H, Zhu L, Reid BR, Drobny GP, Hopkins PB. Solution structure of a cisplatin-induced DNA interstrand cross-link. *Science* 1995, 270:1842–5; Coste F, Malinge J-M, Serre L, Shepard W, Roth M, Leng M, Zelwer C. Crystal structure of a double-stranded DNA containing a cisplatin interstrand cross-link at 1.63 A resolution: hydration at the platinated site. *Nucleic Acids Res* 1999, 27:1837–46; Malinge J-M, Giraud-Panis M-J, Leng M. Interstrand cross-links of cisplatin induce striking distortions in DNA. *J Inorg Biochem* 1999, 77:23–9.

46. (a) Chval Z, Šíp M. Pentacoordinated transition states of cisplatin hydrolysis – ab initio study. *J Mol Struct THEOCHEM* 2000, 532:59–68; (b) Chval Z, Šíp M. Transition states of cisplatin binding to guanine and adenine: ab initio reactivity study. *Collect Czech Chem Commun* 2003, 68:1105–18; (c) Baik M-H, Friesner RA, Lippard SJ. Theoretical study of cisplatin binding to purine bases: why does cisplatin prefer guanine over adenine? *J Am Chem Soc* 2003, 125:14082–92; (d) Raber J, Zhu C, Eriksson LA. Theoretical study of cisplatin binding to DNA: the importance of initial complex stabilization. *J Phys Chem B* 2005, 109:11006–15.

47. Cleare MJ, Hoeschele JD. Studies on the anti-tumour activity of Group VIII transition metal complexes. Part I. Platinum(II) complexes. *Bioinorg Chem* 1973, 2:187–210.

48. Tucker MA, Colvin CB, Martin DS. Substitution reactions of trichloroammineplatinate(II) ion and the trans effect. *Inorg Chem* 1964, 3:1373–83; Colvin CB, Gunther RG, Hunter LD, McLean JA, Tucker MA, Martin DS Jr. Kinetics of ammonation of the chloro-ammine series of platinum(II) complexes. *Inorg Chim Acta* 1968, 2:487–9; Berners-Price SJ, Kuchel PW. Reaction of cis- and trans-[PtCl$_2$(NH$_3$)$_2$] with reduced glutathione inside human red blood cells, studied by ^{1}H and ^{15}N-{^{1}H} DEPT NMR. *J Inorg Biochem* 1990, 38:327–45.

49. Natile G, Coluccia M. Current status of trans-platinum compounds in cancer therapy. *Coord Chem Rev* 2001, 216–7:383–410.

50. Boudvillain M, Dalbiès R, Aussourd C, Leng M. Intrastrand cross-links are not formed in the reaction between transplatin and native DNA: relation with the clinical inefficency of transplatin. *Nucl Acids Res* 1995, 23:2381–8; Bernal-Méndez E, Boudvillain M, González-Vílchez F, Leng M. Chemical versatility of transplatin monofunctional adducts within multiple sitespecifically platinated DNA. *Biochemistry* 1997, 36:7281–7.

51. (a) Paquet F, Boudvillain M, Lancelot G, Leng M. NMR solution structure of a DNA dodecamer containing a transplatin interstrand GN7-CN3 cross-link. *Nucleic Acids Res* 1999, 27:4261–8; (b) Brabec V, Leng M. DNA interstrand cross-links of trans-diamminedichloroplatinum(II) are preferentially formed between guanine and complementary cytosine residues. *Proc Natl Acad Sci USA* 1993, 90:5345–9.

52. (a) van Beusichem M, Farrell N. Activation of the trans geometry in platinum antitumor complexes. Synthesis, characterization, and biological activity of complexes with the planar ligands pyridine, N-methylimidazole, thiazole, and quinoline. Crystal and molecular structure of trans-dichlorobis(thiazole)platinum(II). *Inorg Chem* 1992, 31:634–9; (b) Kelland LR, Barnard CFJ, Mellish KJ, Jones M, Goddard PM, Valenti M, Bryant A, Murrer BA, Harrap KR. A novel trans-platinum coordination complex possessing in vitro and in vivo antitumor activity. *Cancer Res* 1994, 54:5618–22; (c) Pérez JM, Montero EI, Solans X, Font-Bardia M, Fuertes

MA, Alonso C, Navarro-Ranninger C. X-ray structure of cytotoxic trans-[PtCl$_2$(dimethylamine)(isopropylamine)]: interstrand cross-link efficiency, DNA sequence specificity, and inhibition of the B–Z transition. *J Med Chem* 2000, 43:2411–8.

53. Heringova P, Woods J, Mackay FS, Kasparkova J, Sadler PJ, Brabec V. Transplatin is cytotoxic when photoactivated: enhanced formation of DNA cross-links. *J Med Chem* 2006, 49:7792–8; Aris SM, Farrell NP. Towards antitumor active trans-platinum compounds. *Eur J Inorg Chem* 2009, 2009:1293; Guerrero E, Miranda S, Lüttenberg S, Fröhlich N, Koenen J-M, Mohr F, Cerrada E, Laguna M, Mendía A. trans-Thionate Derivatives of Pt(II) and Pd(II) with Water-Soluble Phosphane PTA and DAPTA Ligands: Antiproliferative Activity against Human Ovarian Cancer Cell Lines. *Inorg Chem* 2013, 52:6635–47; Popova, EA, Serebryanskaya TV, Selivanov SI, Haukka M, Panikorovsky TL, Gurzhiy VV, Ott I, Trifonov RE, Kukushkin VY. Water-Soluble Platinum(II) Complexes Featuring 2-Alkyl-2*H*-tetrazol-5-ylacetic Acids: Synthesis, Characterization, and Antiproliferative Activity. *Eur J Inorg Chem* 2016, 4659–67; Orzechowska M, Fabijańska M, Ochocki J, Małecki M. Anticancer activity of a trans-platinum(II) complex of 3-aminoflavone to ovarian cancer cells. *Ginekol Pol* 2017, 88:68–74; Shaili E, Salassa L, Woods JA, Clarkson G, Sadler PJ, Farrer NJ. Platinum(iv) dihydroxido diazido N-(heterocyclic)imine complexes are potently photocytotoxic when irradiated with visible light. *Chem Sci* 2019, 10:8610–7; Alhoshani A, Seliman AAA, Osman Altoum A, Abuelizz HA, Ahmad S, Altaf M, Omer KH, Sohail M, Isab AA. Synthesis, X-ray structure and in vitro cytotoxicity of trans-diammineplatinum(II) complexes of selenones, trans-[Pt(NH$_3$)$_2$(selenone)$_2$](NO$_3$)$_2$. *Polyhedron* 2019,158:234–40; Icsel C, Yilmaz VT, Aygun M, Ulukaya E. Trans-Pd/Pt(II) saccharinate complexes with a phosphine ligand: Synthesis, cytotoxicity and structure-activity relationship. *Bioorg Med Chem Lett* 2020, 30:127077.

54. (a) DeConti RC, Toftness BR, Lange RC, Creasey WA. Clinical and pharmacological studies with cis-diamminedichloroplatinum (II). *Cancer Res* 1973, 33:1310–5; (b) Barnham KJ, Djuran MI, Murdoch PdS, Ranford JD, Sadler PJ. Ring-opened adducts of the anticancer drug carboplatin with sulfur amino acids. *Inorg Chem* 1996, 35:1065–72; (c) Ivanov AI, Christodoulou J, Parkinson JA, Barnham KJ, Tucker A, Woodrow J, Sadler PJ. Cisplatin binding sites on human albumin. *J Biol Chem* 1998, 273:14721–30.

55. Borch RF, Pleasants ME. Inhibition of cis-platinum nephrotoxicity by diethyldithiocarbamate rescue in a rat model. *Proc Natl Acad Sci USA* 1979, 76:6611–4.

56. Kelland LR. The Development of Orally Active Platinum Drugs. In Lippert B. (ed). *Cisplatin: Chemistry and biochemistry of a leading anticancer drug*. Verlag Helvetica Chimica Acta, Zurich; Wiley-VCH, Weinheim, Germany, 1999, pp 497–521; Andrews PA, Howell SB. Cellular pharmacology of cisplatin: perspectives on mechanisms of acquired resistance. *Cancer Cells* 1990, 2:35–43.

57. (a) Richon VM, Schulte N, Eastman A. Multiple mechanisms of resistance to cisdiamminedichloroplatinum (II) in murine leukemia L1210 cells. *Cancer Res* 1987, 47:2056–61; (b) Kelland LR. Preclinical perspectives on platinum resistance. *Drugs* 2000, 59 (Suppl.):1–8; Kartalou M, Essigmann JM. Mechanisms of resistance to cisplatin. *Mutat Res* 2001, 478:23–

43; (c) Ciarimboli G. Membrane transporters as mediators of cisplatin side-effects. *Anticancer Res* 2014, 34:547–50.

58. Weiss RB, Christian MC. New cisplatin analogues in development. *Drugs* 1993, 46:360–77.

59. Harrap KR. Preclinical studies identifying carboplatin as a viable cisplatin alternative. *Cancer Treat Rev* 1985, 12 (Suppl A):21–33; Calvert AH, Newell DR, Gumbrell LA, O'Reilly S, Burnell M, Boxall FE, Siddik ZH, Judson IR, Gore ME, Wiltshaw E. Carboplatin dosage: prospective evaluation of a simple formula based on renal function. *J Clin Oncol* 1989, 7:1748–56.

60. (a) Rixe O, Ortuzar W, Alvarez M, Parker R, Reed E, Paull K, Fojo T. Oxaliplatin, tetraplatin, cisplatin, and carboplatin: spectrum of activity in drug-resistant cell lines and in the cell lines of the National Cancer Institute's Anticancer Drug Screen panel. *Biochem Pharmacol* 1996, 52:1855–65; (b) Raymond E, Faivre S, Chaney S, Woynarowski J, Cvitkovic E. Cellular and molecular pharmacology of oxaliplatin. *Mol Cancer Ther* 2002, 1:227–35.

61. Holford I, Hartley J, Murrer B, Kelland L. In vitro evaluation of JM473, a novel sterically hindered platinum(II) complex. *Anal Oncol* 1996, 7 (Suppl. 1):36–8.

62. Raynaud FI, Boxall FE, Goddard PM, Valenti M, Jones M, Murrer BA, Abrams M, Kelland LR. cis-Amminedichloro(2-methylpyridine) platinum(II) (AMD473), a novel sterically hindered platinum complex: in vivo activity, toxicology, and pharmacokinetics in mice. *Clin Cancer Res* 1997, 3:2063–74; Beale P, Judson I, O'Donnell A, Trigo J, Rees C, Raynaud F, Turner A, Simmons L, Etterley L. A Phase I clinical and pharmacological study of cis-diamminedichloro(2-methylpyridine) platinum II (AMD473). *Br J Cancer* 2003, 88:1128–34; Tang CH, Parham C, Shocron E, McMahon G, Patel N. Picoplatin overcomes resistance to cell toxicity in small-cell lung cancer cells previously treated with cisplatin and carboplatin. *Cancer Chemother Pharmacol* 2011, 67:1389–400.

63. Hall MD, Hambley TW. Platinum(IV) antitumour compounds: their bioinorganic chemistry. *Coord Chem Rev* 2002, 232:49–67.

64. e.g. (a) van der Veer JL, Peters AR, Reedijk J. Reaction products from platinum(IV) amine compounds and 5'-GMP are mainly bis(5'-GMP) platinum (II) amine adducts. *J Inorg Biochem* 1986, 26:137–42; (b) Hall MD, Dillon CT, Zhang M, Beale P, Cai Z, Lai B, Stampfl APJ, Hambley TW. The cellular distribution and oxidation state of platinum(II) and platinum(IV) antitumour complexes in cancer cells. *J Biol Inorg Chem* 2003, 8:726–32; (c) Žák F, Turánek J, Kroutil A, Sova P, Mistr A, Poulová A, Mikolin P, Žák Z, Kašná A, Záluská D, Neča J, Šindlerová L, Kozubík A. Platinum(IV) complex with adamantylamine as nonleaving amine group: synthesis, characterization, and in vitro antitumor activity against a panel of cisplatinresistant cancer cell lines. *J Med Chem* 2004, 47:761–3.

65. e.g. Sinisi M, Gandin V, Saltarella T, Intini FP, Pacifico C, Marzano C, Natile G. Synthesis, characterization, and biological activity of platinum II, III, and IV pivaloamidine complexes. *J Biol Inorg Chem* 2014, 19, 1081–97; Hoffmeister BR, Hejl M, Jakupec MA, Galanski M, Keppler BK. Bis- and Tris(carboxylato)platinum(IV) Complexes with Mixed Am(m)ine Ligands in the *trans* Position Exhibiting Exceptionally High Cytotoxicity. *Eur J Inorg Chem*

2015, 1700–8; Gibson D. Multi-action Pt(IV) anticancer agents; do we understand how they work? *J Inorg Biochem* 2019, 191:77–84.

66. Lipinski J. Electronic Structure of Platinum(II). Antitumor Complexes and their Interactions with Nucleic Acid Bases I. *Inorg Chim Acta* 1988, 152:151–7; Lipinski J. Electronic Structure of Platinum(II). Antitumor Complexes and their Interactions with Nucleic Acid Bases. Part II. *J Mol Struct Theochem* 1989, 201:295–305.

67. Basch H, Krauss M, Stevens WJ, Cohen D. Electronic and Geometric Structures of Pt(NH$_3$)$_2^{2+}$, Pt(NH$_3$)$_2$Cl$_2$, Pt(NH$_3$)$_3$X, and Pt(NH$_3$)$_2$XY (X, Y = H$_2$O, OH$^-$). *Inorg Chem* 1985, 24(21):3313−7.

68. Kozelka J, Petsko GA, Lippard SJ, Quigley GJ. *J Am Chem Soc* 1985, 107(13):4079-81; Kozelka J, Chottard J-C. How does cisplatin alter DNA structure?: A molecular mechanics study on double-stranded oligonucleotides. *Biophys Chemistry* 1990, 35(2–3):165–78; Kozelka J, Savinelli R, Berthier G, Flament J-P, Lavery R. Force field for platinum binding to adenine. *J Comput Chem* 1993, 14(1):45–53; Elizondo-Riojas MA, Kozelka J. *J Mol Biol* 2001, 314:1227.

69. Carloni P, Andreoni W, Hutter J, Curioni A, Giannozzi P, Parrinello M. Structure and bonding in cisplatin and other Pt(II) complexes. *Chem Phys Lett* 1995, 234(1-3):50–6; Pavankumar PNV, Seetharamulu P, Yao S, Saxe JD, Reddy DG, Hausheer FH. Comprehensive Ab Initio Quantum Mechanical and Molecular Orbital (MO) Analysis of Cisplatin: Structure, Bonding, Charge Density, and Vibrational Frequencies. *J Comput Chem* 1999, 20:3888–91; Wysokińsky R, Michalska D. The Performance of Different Density Functional Methods in the Calculation of Molecular Structures and Vibrational Spectra of Platinum(II) Antitumor Drugs: Cisplatin and Carboplatin. *J Comput Chem* 2001, 22:901−12.

70. e.g. Zhang Y, Guo Z, You X-Z. Hydrolysis Theory for Cisplatin and its Analogs Based on Density Functional Studies. *J Am Chem Soc* 2001, 123:9378−87; Michalska D, Wysokiński R. The Prediction of Raman Spectra of Platinum(II) Anticancer Drugs by Density Functional Theory. *Chem Phys Lett* 2005, 403:211−7; Amado AM, Fiuza SM, Marques MPM, Batista de Carvalho LAE. Conformational and Vibrational Study of Platinum-(II) Anticancer Drugs: cis-Diamminedichloroplatinum(II) as a Case Study. *J Chem Phys* 2007, 127:185104/1−10; Fiuza SM, Amado AM, Marques MPM, Batista de Carvalho, LAE. Use of Effective Core Potential Calculations for the Conformational and Vibrational Study of Platinum(II) Anticancer Drugs. Cis-Diamminedichloroplatinum(II) as a Case Study. *J Phys Chem A* 2008, 112:3253−9; Dans PD, Crespo A, Estrin DA, Coitiño EL. Structural and Energetic Study of Cisplatin and Derivatives: Comparison of the Performance of Density Functional Theory Implementations. *J Chem Theory Comput* 2008, 4:740−50; de Berredo RC, Jorge FE. All-Electron Double Zeta Basis Sets for Platinum: Estimating Scalar Relativistic Effects on Platinum(II) Anticancer Drugs. *J Mol Struct THEOCHEM* 2010, 961:107−12.; Gao H, Xia F, Huang C, Lin K. Density functional theory calculations on the molecular structures and vibration spectra of platinum(II) antitumor drugs. *Spectrochim Acta Part A Mol Biomol Spectrosc* 2011, 78(4):1234–9; Paschoal D, Marcial BL, Lopes JF, De Almeida WB, Dos Santos HF. The Role of the Basis Set and the

Level of Quantum Mechanical Theory in the Prediction of the Structure and Reactivity of Cisplatin. *J Comput Chem* 2012, 33:2292–302.

71. e.g. Burda JV, Šponer J, Leszczynski J. The interactions of square platinum(II) complexes with guanine and adenine: A quantum-chemical ab initio study of metalated tautomeric forms. *J Biol Inorg Chem* 2000, 5(2):178–88; Pelmenschikov A, Zilberberg I, Leszczynski J, Famulari A, Sironi M, Raimondi M. Cis-[Pt(NH$_3$)$_2$]$^{2+}$ coordination to the N7 and O6 sites of a guanine-cytosine pair: Disruption of the Watson-Crick H-bonding pattern. Chem Phys Lett 1999, 314(5–6):496–500; Brabec V, Hrabina O, Kasparkova J. Cytotoxic platinum coordination compounds. *Coord Chem Rev* 2017, 351:2–31.

72. Mezencev R. Interactions of cisplatin with non-DNA targets and their influence on anticancer activity and drug toxicity: The complex world of the platinum complex. *Curr Cancer Drug Targets* 2014, 14(9):794–816; Alberti E, Zampakou M, Donghi D. *J Inorg Biochem* 2016, 163:278–291; Djuran MI, Lempers ELM, Reedijk J. Reactivity of chloro- and aqua(diethylenetriamine)platinum(II) ions with glutathione, S-methylglutathione, and guanosine 5'-monophosphate in relation to the antitumor activity and toxicity of platinum complexes. *Inorg Chem* 1991, 30(12):2648–52; Barnham KJ, Djuran MI, Murdoch PdS, Sadler PJ. Intermolecular displacement of S-bound L-methionine on platinum(II) by guanosine 5′-monophosphate: implications for the mechanism of action of anticancer drugs. *J Chem Soc Chem Commun* 1994, (6):721–2; Barnham KJ, Djuran MI, Murdoch PdS, Ranford JD, Sadler PJ. L-Methionine increases the rate of reaction of 5′-guanosine monophosphate with the anticancer drug cisplatin: mixed-ligand adducts and reversible methionine binding. *J Chem Soc Dalton Trans* 1995, (22):3721–6; Teuben JM, Reedijk J. Reaction of DNA oligonucleotides with [Pt(dien)GSMe]$^{2+}$ (GSMe =S-methylated glutathione) and *cis*-[Pt(NH$_3$)$_2$(GSMe)$_2$]$^{2+}$: evidence of oligonucleotide platination via sulfur-coordinated platinum intermediates. *J Biol Inorg Chem* 2000, 5(4):463–8; Peleg-Shulman T, Gibson D. Cisplatin−Protein Adducts Are Efficiently Removed by Glutathione but Not by 5'-Guanosine Monophosphate. *J Am Chem Soc* 2001, 123(13):3171–2; Kleine M, Wolters D, Sheldrick WS. *J Inorg Biochem* 2003, 97:354; cisPt+DNA+protein crosslinks=better action: Chválová K, Brabec V, Kašpárková J. Mechanism of the formation of DNA–protein cross-links by antitumor cisplatin. *Nucleic Acids Res* 2007, 35:1812–21.

73. Abdul-Ahad PG, Webb GA. Quantitative structure activity relationships for some antitumor platinum(II) complexes. *Int J Quantum Chem* 1982, 21: 1105–15.

74. Monti E, Gariboldi M, Maiocchi A, Marengo E, Cassino C, Gabano E, Osella D. Cytotoxicity of cis-platinum(II) conjugate models. The effect of chelating arms and leaving groups on cytotoxicity: a quantitative structure−activity relationship approach. *J Med Chem* 2005, 48:857−66.

75. Sarmah P, Deka RC. Solvent effect on the reactivity of *cis*-platinum (II) complexes: A density functional approach. *Int J Quantum Chem* 2008, 108:1400−9; Sarmah P, Deka RC. DFT-based QSAR and QSPR models of several cis-platinum complexes: solvent effect. *J Comput-Aided Mol Des* 2009, 23:343−54.

76. Galanski M, Jakupec MA, Keppler BK. Update of the preclinical situation of anticancer platinum complexes: novel design strategies and innovative analytical approaches. *Curr Med Chem* 2005, 12:2075−94; Hall MD, Mellor HR, Callaghan R, Hambley TW. Basis for design and development of platinum(IV) anticancer complexes. *J Med Chem* 2007, 50:3403−11; Varbanov HP, Jakupec MA, Roller A, Jensen F, Galanski M, Keppler BK. Theoretical Investigations and Density Functional Theory Based Quantitative Structure–Activity Relationships Model for Novel Cytotoxic Platinum(IV) Complexes. *J Medicin Chem* 2013, 56(1):330–44; Tsipis AC, Karapetsas IN. [195]Pt NMR parameters as strong descriptors in one-parameter QSAR models for platinum-based antitumor compounds. *Magn Reson Chem* 2017, 55:662–9; Süß, D., Huber, S.E. & Mauracher, A. Comparative study of electronic-structure methods for platinum-containing molecules: bond lengths and bond dissociation energies. *Eur Phys J D* 2019, 73:135; Sarmah P. DFT-based reactivity and QSPR studies of platinum (IV) anticancer drugs. *J Molec Graphics Model* 2020, 100:107682; Alvarado-Soto L, Ramirez-Tagle R. Relativistic Structure-Activity Relationship of Cisplatin(II) Complexes. *J Struct Chem* 2020, 61:688–93; Marques MPM, Valero R, Parker SF, Tomkinson J, Batista de Carvalho LAE. Polymorphism in Cisplatin Anticancer Drug. *J Phys Chem B* 2013, 117:6421–9.

77. Guégan F, Tognetti V, Joubert L, Chermette H, Luneau D, Morell C. Towards the first theoretical scale of the trans effect in octahedral complexes. *Phys Chem Chem Phys* 2015, 18(2):982–90; Tognetti V, Guégan F, Luneau D, Chermette H, Morell C, Joubert L. Structural effects in octahedral carbonyl complexes: an atoms-in-molecules study. *Theor Chem Acc* 2017, 136:85.

78. Tsispis AC. Building trans-philicity (trans-effect/trans-influence) ladders for octahedral complexes by using an NMR probe. *Dalton Trans* 2019, 48(5):1814–22.

79. Cremer D, Kraka E. Generalization of the Tolman electronic parameter: the metal–ligand electronic parameter and the intrinsic strength of the metal–ligand bond. *Dalton Trans* 2017, 46:8323–38.

80. Ponce-Vargas M, Klein J, Hénon E. Novel approach to accurately predict bond strength and ligand lability in platinum-based anticancer drugs. *Dalton Trans* 2020, 49(36):12632–42.

81. Klein J, Khartabil H, Boisson J-C, Contreras-García J, Piquemal J-P, Hénon E. New Way for Probing Bond Strength. *J Phys Chem A* 2020, 124(9):1850–60.

82. Lefebvre C, Rubez G, Khartabil H, Boisson J-C, Contreras-García J, Hénon E. Accurately extracting the signature of intermolecular interactions present in the NCI plot of the reduced density gradient versus electron density. *Phys Chem Chem Phys* 2017, 19(27):17928–36; Lefebvre C, Khartabil H, Boisson J-C, Contreras-García J, Piquemal J-P, Hénon E. The Independent Gradient Model: A New Approach for Probing Strong and Weak Interactions in Molecules from Wave Function Calculations. *ChemPhysChem* 2018, 19(6):724–35.

83. Lachman A. *Borderland of the Unknown: The Life Story of Gilbert Newton Lewis*. Pageant Press, New York, NY, 1955; Jolly WL. *From Retorts to Lasers: The Story of Chemistry at Berkeley*. College of Chemistry, University of California, Berkeley, 1987; Lewis ES. *A Biography of Distinguished Scientist Gilbert Newton Lewis*. Mellon Press, Lewiston, NY, 1998; Coffey P. *Cathedrals of Science: The Personalities and Rivalries that Made Modern Science*.

Oxford University Press, New York, NY, 2008; Laidler KJ. Lessons from the History of Chemistry. *Acc Chem Res* 1995, 28:187–92; Jensen WB. The Mystery of G. N. Lewis's Missing Nobel Prize. In: Strom ET, Mainz VV (eds). *The Posthumous Nobel Prize in Chemistry. Volume 1. Correcting the Errors and Oversights of the Nobel Prize Committee*. ACS Symposium Series, Vol. 1262, 2017. Chap. 6, pp. 107–20.

84. Lewis GN. The atom and the molecule. *J Am Chem Soc* 1916, 38:762–85.

85. Lewis GN. *Valence and the Structure of Atoms and Molecules.* The Chemical Catalog Co, New York, NY, 1923.

86. (a) Lewis GN. Acids and Bases. *J Franklin Inst* 1938, 226:293–313; (b) Lewis GN, Seaborg GT. Primary and Secondary Acids and Bases. *J Am Chem Soc* 1939, 61:1886–94.

87. Arrhenius S. *Recherches sur la conductibilité galvanique des électrolytes*. Doctoral dissertation. P.A. Norstedt, Stockholm, 1884.

88. Brønsted JN. Einige Bemerkungen über den Begriff der Säuren und Basen. *Recl Trav Chim Pays-Bas* 1923, 42:718–28; Lowry TM. The uniqueness of hydrogen. *J Chem Technol Biotechnol* 1923, 42: 43–7.

89. Franklin EC. Reactions in liquid ammonia. *J Am Chem Soc* 1905, 27:820–51; Franklin EC. Systems of acids, bases and salts. *J Am Chem Soc* 1924, 46:2137–51; Cady HP, Elsey HM. A general definition of acids, bases, and salts. *J Chem Educ* 1928, 5:1425–8.

90. Müller P. Glossary of terms used in physical organic chemistry (IUPAC Recommendations 1994). *Pure Appl Chem* 1994, 66:1077–1184.

91. Kolthoff IM. The Lewis and the Brönsted–Lowry Definitions of Acids and Bases. *J Phys Chem* 1944, 48:51–7; Bjerrum J. Die Entwicklungsgeschichte des Säure-Basenbegriffes und über die Zweckmäßigkeit der Einführung eines besonderen Antibasenbegriffes neben dem Säurebegriff. *Naturwissenschaften* 1951, 38:461–4; Bell RP. The use of the terms "acid" and "base". *Q Rev Chem Soc* 1947, 1:113–25.

92. McCahill JSJ, Welch GC, Stephan DW. Reactivity of 'frustrated Lewis pairs': three-component reactions of phosphines, a borane, and olefins. *Angew Chem Int Ed* 2007, 46:4968–71; Fontaine F-G, Stephan DW. On the concept of frustrated Lewis pairs. *Phil Trans R Soc A* 2017, 375:20170004.

93. Hieber W, Sonnekalb F. Reaktionen und Derivate des Eisencarbonyls. *Ber dtsch chem Ges* 1928, 61:558–65; Hieber W, Mühlbauer F, Ehmann EA. Derivate des Kobalt- und Nickelcarbonyls. *Ber dtsch chem Ges* 1932, 65:1090–101; Hieber W. Metal Carbonyls, Forty Years of Research. *Adv Organomet Chem* 1970, 8:1–28.

94. Wilkinson G, Birmingham JM. Biscyclopentadienylrhenium hydride – a new type of hydride. *J Am Chem Soc* 1955, 77:3421–2; Green MLH, Pratt L, Wilkinson G. Biscyclopentadienylrhenium hydride. *J Chem Soc* 1958, 3916–22.

95. Vaska L, DiLuzio JW. Carbonyl and hydrido-carbonyl complexes of iridium by reaction with alcohols. Hydrido complexes by reaction with acid. *J Am Chem Soc* 1961, 83:2784–5; Vaska

L, DiLuzio JW. Activation of Hydrogen by a Transition Metal Complex at Normal Conditions Leading to a Stable Molecular Dihydride. *J Am Chem Soc* 1962, 84:679–80.

96. Hodali HA. Five-Coordinated Boron Trifluoride Adducts of Platinum(II) Complexes. *J Chem Eng Data* 1987, 32:382−3.

97. Rizzato S, Bergès J, Mason SA, Albinati A, Kozelka J. Dispersion-Driven Hydrogen Bonding: Predicted Hydrogen Bond between Water and Platinum(II) Identified by Neutron Diffraction. *Angew Chem Int Ed* 2010, 49:7440−3; Bergès J, Fourré I, Pilmé J, Kozelka J. Quantum Chemical Topology Study of the Water-Platinum(II) Interaction. *Inorg Chem* 2013, 52:1217−27; Janjić GV, Milosavljević MD, Veljković DŽ, Zarić SD. Prediction of Strong O−H/M Hydrogen Bonding between Water and Square-Planar Ir and Rh Complexes. *Phys Chem Chem Phys* 2017, 19:8657−60; Aono S, Mori T, Sakaki S. 3D-RISM-MP2 Approach to Hydration Structure of Pt(II) and Pd(II) Complexes: Unusual H-Ahead Mode vs Usual O-Ahead One. *J Chem Theory Comput* 2016, 12:1189−206; Kroutil O, Předota M, Chval Z. Pt···H Nonclassical Interaction in Water-Dissolved Pt(II) Complexes: Coaction of Electronic Effects with Solvent-Assisted Stabilization. *Inorg Chem* 2016, 55:3252−64; (f) Hirakawa T, Bowler DR, Miyazaki T, Morikawa Y, Truflandier LA. Blue moon ensemble simulation of aquation free energy profiles applied to mono and bifunctional platinum anticancer drugs. *J Comput Chem* 2020, 41:1973–84.

98. Groenewald F, Raubenheimer HG, Dillen J, Esterhuysen C. Gold Setting the "Gold Standard" among Transition Metals as a Hydrogen Bond Acceptor − a Theoretical Investigation. *Dalton Trans* 2017, 46:4960−7; Groenewald F, Dillen J, Esterhuysen C. Ligand-Driven Formation of Halogen Bonds Involving Au(I) Complexes. *New J Chem* 2018, 42:10529−38.

99. Beletskaya IP, Nájera C, Yus M. Stereodivergent Catalysis. *Chem Rev* 2018, 118:5080–200.

100. Nordström K, Macedo E, Moberg C. Enantioselective Allylic Substitutions Catalyzed by [(Hydroxyalkyl)pyridinooxazoline]- and [(Alkoxyalkyl)pyridinooxazoline]palladium Complexes. *J Org Chem* 1997, 62:1604–9; Hallman K, Frölander A, Wondimagegn T, Svensson M, Moberg C. OH−Pd(0) Interaction as a Stabilizing Factor in Palladium-Catalyzed Allylic Alkylations. *Proc Natl Acad Sci USA* 2004, 101:5400−4; Frölander A, Lutsenko S, Privalov T, Moberg C. Conformational Preferences and Enantiodiscrimination of Phosphino-4-(1-hydroxyalkyl)oxazoline−Metal−Olefin Complexes Resulting from an OH−Metal Hydrogen Bond. *J Org Chem* 2005, 70:9882–91; Yang W, Liu C, Qiu J. In situ formation of N,O-bidentate ligand via the hydrogen bond for highly efficient Suzuki reaction of aryl chlorides. *Chem Commun* 2010, 46:2659–61; Fernandes RA, Kattanguru P, Bethi V. Stereoselective inversion of γ-vinyl-γ-butyrolactone under palladium catalysis: application to the synthesis of (+)-exo- and (+)-endo-brevicomins. *RSC Adv* 2014, 4:14507–12; Zeifman AA, Novikov FN, Stroylov VS, Stroganov OV, Svitanko IV, Chilov GG. An explicit account of solvation is essential for modeling Suzuki–Miyaura coupling in protic solvents. *Dalton Trans* 2015, 44:17795–9.

101. Frölander A, Moberg C. Ag+-Assisted Hydrosilylation: Complementary Behavior of Rh and Ir Catalysts (Reversal of Enantioselectivity). *Org Lett* 2007, 9:1371–4.

102. Yao L, Nie H, Zhang D, Wang L, Zhang L, Chen W, Li Z, Liu X, Zhang S. Chiral Ferrocenyl N,N Ligands with Intramolecular Hydrogen Bonds for Highly Enantioselective Allylic Alkylations. *ChemCatChem* 2018, 10:804.

103. Schrödinger E. Quantisierung als Eigenwertproblem (Erste Mitteilung). *Ann Phys* 1926, 384:361–76; Schrödinger E. Quantisierung als Eigenwertproblem (Zweite Mitteilung). *Ann Phys* 1926, 384:489–527; Schrödinger E. Quantisierung als Eigenwertproblem (Dritte Mitteilung). *Ann Phys* 1926, 385:437–90; Schrödinger E. Quantisierung als Eigenwertproblem (Vierte Mitteilung). *Ann Phys* 1926, 386:109–39.

104. Born M, Oppenheimer JR. Zur Quantentheorie der Molekeln. *Ann Phys* 1927, 389:457–84.

105. Hartree DR. The Wave Mechanics of an Atom with a Non-Coulomb Central Field. Part I. Theory and Methods. *Math Proc Cambridge Phil Soc* 1928, 24:89–110; Fock V. Näherungsmethode zur Lösung des quantenmechanischen Mehrkörperproblems. *Z Physik* 1930, 61:126–48; Slater JC. Note on Hartree's Method. *Phys Rev* 1930, 35:210–11.

106. Slater JC. The Theory of Complex Spectra. *Phys Rev* 1929, 34:1293–322.

107. Pauling L. The Application of the Quantum Mechanics to the Structure of the Hydrogen Molecule and Hydrogen Molecule-Ion and to Related Problems. *Chem Rev* 1928, 5:173–213.

108. Lennard-Jones JE. The electronic structure of some diatomic molecules. *Trans Faraday Soc* 1929, 25:668–86.

109. Boys SF. Electronic wave functions – I. A general method of calculation for the stationary states of any molecular system. *Proc R Soc Lond A* 1950, 200:542–54.

110. A series of „Self-Consistent Molecular Orbital Methods" papers, e.g.: Hehre WJ, Stewart RF, Pople JA. Self-Consistent Molecular-Orbital Methods. I. Use of Gaussian Expansions of Slater-Type Orbitals. *J Chem Phys* 1969, 51:2657–64; Hehre WJ, Ditchfield R, Pople JA. Self-Consistent Molecular Orbital Methods. XII. Further Extensions of Gaussian-Type Basis Sets for Use in Molecular-Orbital Studies of Organic Molecules. *J Chem Phys* 1972, 56:2257–61; Binkley JS, Pople JA, Hehre WJ. Self-Consistent Molecular Orbital Methods. 21. Small Split-Valence Basis Sets for First-Row Elements. *J Am Chem Soc* 1980, 102:939–47; Gordon MS, Binkley JS, Pople JA, Pietro WJ, Hehre WJ. Self-Consistent Molecular Orbital Methods. 22. Small Split-Valence Basis Sets for Second-Row Elements. *J Am Chem Soc* 1982, 104:2797–803.

111. Hariharan PC, Pople JA. The Influence of Polarization Functions on Molecular Orbital Hydrogenation Energies. *Theor Chim Acta* 1973, 28:213–22; Pietro WJ, Francl MM, Hehre WJ, DeFrees DJ, Pople JA, Binkley JS. Self-Consistent Molecular Orbital Methods. 24. Supplemental Small Split-Valence Basis Sets for Second-Row Elements. *J Am Chem Soc* 1982, 104:5039–48; Francl MM, Pietro WJ, Hehre WJ, Binkley JS, Gordon MS, DeFrees DJ, Pople JA. Self-consistent molecular orbital methods. XXIII. A polarization-type basis set for second-row elements. *J Chem Phys* 1982, 77:3654–65.

112. Clark T, Chandrasekhar J, Spitznagel GW, Schleyer PvR. Efficient diffuse function-augmented basis sets for Anion Calculations. III. The 3-21+G set for first-row elements, Li-F. *J Comput Chem* 1983, 4:294–301; Frisch MJ, Pople JA, Binkley JS. Self-consistent molecular orbital

methods. 25. Supplementary functions for Gaussian basis sets. *J Chem Phys* 1984, 80:3265–9; Del Bene JE. An *ab initio* molecular orbital study of the structures and energies of neutral and charged bimolecular complexes of NH_3 with the hydrides AH_n (A = N, O, F, P, S, and Cl). *J Comput Chem* 1989, 10: 603–15.

113. Møller C, Plesset MS. Note on an Approximation Treatment for Many-Electron Systems. *Phys Rev* 1934, 46:618–22; Pople JA, Binkley JS, Seeger R. Theoretical models incorporating electron correlation. *Int J Quant Chem* 1976, 10:1–19; Krishnan R, Pople JA. Approximate fourth-order perturbation theory of the electron correlation energy. *Int J Quantum Chem* 1978, 14:91–100; Kucharski SA, Bartlett RJ. Fifth-Order Many-Body Perturbation Theory and Its Relationship to Various Coupled-Cluster Approaches. *Advan Quantum Chem* 1986, 18:281–344.

114. Shavitt I. The Method of Configuration Interaction. In: Schaefer HF (ed). *Methods of Electronic Structure Theory*. Modern Theoretical Chemistry, vol 3. Springer, Boston, MA., 1977; Langhoff SR, Davidson ER. Configuration interaction calculations on the nitrogen molecule. *Int J Quantum Chem* 1974, 8:61–72; Pople JA, Seeger R, Krishnan R. Variational configuration interaction methods and comparison with perturbation theory. *Int J Quant Chem* 1977, 12:149–63.

115. Raghavachari K, Trucks GW, Pople JA, Head-Gordon M. A fifth-order perturbation comparison of electron correlation theories. *Chem Phys Lett* 1989, 157:479–83; Řezáč J, Hobza P. Describing Noncovalent Interactions beyond the Common Approximations: How Accurate Is the "Gold Standard," CCSD(T) at the Complete Basis Set Limit? *J Chem Theory Comput* 2013, 9:2151–5.

116. Čížek J. On the Correlation Problem in Atomic and Molecular Systems. Calculation of Wavefunction Components in Ursell-Type Expansion Using Quantum-Field Theoretical Methods. *J Chem Phys* 1966, 45:4256–66; Paldus J, Čížek J, Shavitt I. Correlation Problems in Atomic and Molecular Systems. IV. Extended Coupled-Pair Many-Electron Theory and Its Application to the BH_3 Molecule. *Phys Rev A* 1972, 5:50–67; Bartlett RJ. Many-Body Perturbation Theory and Coupled Cluster Theory for Electron Correlation in Molecules. *Ann Rev Phys Chem* 1981, 32:359–401; Scuseria GE, Schaefer III HF. A new implementation of the full CCSDT model for molecular electronic structure. *Chem Phys Lett* 1988, 152:382–6.

117. (a) Hohenberg P, Kohn W. Inhomogeneous electron gas. *Phys Rev B* 1964, 136:B864–71; (b) Kohn W, Sham LJ. Self-consistent equations including exchange and correlation effects. *Phys Rev* 1965, 140:A1133–8.

118. Kurth S, Perdew JP. Role of the exchange–correlation energy: Nature's glue. *Int J Quant Chem* 2000, 78:814–8.

119. Perdew JP, Schmidt K. Jacob's ladder of density functional approximations for the exchange-correlation energy. *AIP Conf Proc* 2001, 577:1–20.

120. von Barth U, Hedin L. A local exchange-correlation potential for the spin polarized case. *J Phys C: Solid State Phys* 1972, 5:1629–42; Vosko SH, Wilk L, Nusair M. Accurate spin-dependent electron liquid correlation energies for local spin density calculations: a critical analysis. *Can J*

Phys 1980, 58:1200–11; Perdew JP, Zunger A. Self-interaction correction to density-functional approximations for many-electron systems. *Phys Rev B* 1981, 23:5048–79.

121. Langreth DC, Mehl MJ. Beyond the local-density approximation in calculations of ground-state electronic-properties. *Phys Rev B* 1983, 28:1809–34; Langreth DC, Mehl MJ. Erratum: Beyond the local-density approximation in calculations of ground-state electronic-properties. *Phys Rev B* 1984, 29:2310; Perdew JP. Accurate density functional for the energy – real-space cutoff of the gradient expansion for the exchange hole. *Phys Rev Lett* 1985, 55:1665–8; Perdew JP. Erratum: Accurate density functional for the energy – real-space cutoff of the gradient expansion for the exchange hole. *Phys Rev Lett* 1985, 55:2370; Perdew JP, Yue W. Accurate and simple density functional for the electronic exchange energy: Generalized gradient approximation. *Phys Rev B* 1986, 33:8800–2; Perdew JP, Wang Y. Erratum: Accurate and simple density functional for the electronic exchange energy: Generalized gradient approximation. *Phys Rev B* 1989, 40:3399; Perdew JP. Density-functional approximation for the correlation energy of the inhomogeneous electron gas. *Phys Rev B* 1986, 33:8822–4; Perdew JP. Erratum: Density-functional approximation for the correlation energy of the inhomogeneous electron gas. *Phys Rev B* 1986, 34:7406; Becke AD. Density functional calculations of molecular bond energies. *J Chem Phys* 1986, 84:4524–9; Becke AD. Density-functional exchange-energy approximation with correct asymptotic behavior. *Phys Rev A* 1988, 38:3098–3100.

122. Becke AD, Roussel MR. Exchange holes in inhomogeneous systems: A coordinate-space model. *Phys Rev A* 1989, 39:3761–7; Perdew JP, Kurth S, Zupan A, Blaha P. Accurate Density Functional with Correct Formal Properties: A Step Beyond the Generalized Gradient Approximation. *Phys Rev Lett* 1999, 82:2544–7; Perdew JP, Kurth S, Zupan A, Blaha P. Erratum: Accurate Density Functional with Correct Formal Properties: A Step Beyond the Generalized Gradient Approximation. *Phys Rev Lett* 1999, 82:5179; Tao J, Perdew JP, Staroverov VN, Scuseria GE. Climbing the Density Functional Ladder: Nonempirical Meta–Generalized Gradient Approximation Designed for Molecules and Solids. *Phys Rev Lett* 2003, 91:146401; Perdew JP, Ruzsinszky A, Csonka GI, Constantin LA, Sun J. Workhorse Semilocal Density Functional for Condensed Matter Physics and Quantum Chemistry. *Phys Rev Lett* 2009, 103:026403; Perdew JP, Ruzsinszky A, Csonka GI, Constantin LA, Sun J. Erratum: Workhorse Semilocal Density Functional for Condensed Matter Physics and Quantum Chemistry. *Phys Rev Lett* 2011, 106:179902.

123. (a) Becke AD. Density-functional thermochemistry. III. The role of exact exchange. *J Chem Phys* 1993, 98:5648–52; Savin, A. On degeneracy, near–degenaracy and density functional theory. In Seminario JM (Ed.) *Recent Developments and Applications of Modern Density Functional Theory*. Elsevier, Amsterdam, 1996; p. 327; Vydrov OA, Scuseria GE. Assessment of a long-range corrected hybrid functional. *J Chem Phys* 2006, 125:234109.

124. Becke AD. A new mixing of Hartree–Fock and local density-functional theories. *J Chem Phys* 1993, 98:1372–7; Stephens PJ, Devlin FJ, Chabalowski CF, Frisch MJ. Ab Initio Calculation of Vibrational Absorption and Circular Dichroism Spectra Using Density Functional Force Fields. *J Phys Chem* 1994, 98:11623–7.

125. Mardirossian N, Head-Gordon M. Thirty years of density functional theory in computational chemistry: an overview and extensive assessment of 200 density functionals. *Mol Phys* 2017, 115:2315–72; Verma P, Truhlar DG. Status and challenges of density functional theory. *Trends Chem* 2020, 2:302–18.

126. Gianturco FA, Paesani F, Laranjeira MF, Vassilenko V, Cunha MA. Intermolecular forces from density functional theory. III. A multiproperty analysis for the Ar(^{1}S)-CO($^1\Sigma$) interaction. *J Chem Phys* 1999, 110:7832–45; Elstner M, Hobza P, Frauenheim T, Suhai S, Kaxiras E. Hydrogen bonding and stacking interactions of nucleic acid base pairs: A density-functional-theory based treatment. *J Chem Phys* 2001, 114:5149–55; Wu Q, Yang W. Empirical correction to density functional theory for van der Waals interactions. *J Chem Phys* 2002, 116:515–24; Grimme S, Antony J, Ehrlich S, Krieg H. A consistent and accurate ab initio parametrization of density functional dispersion correction (DFT-D) for the 94 elements H-Pu. *J Chem Phys* 2010, 132:154104.

127. (a) Becke AD, Johnson ER. Exchange-hole dipole moment and the dispersion interaction. *J Chem Phys* 2005, 122:154104; (b) Grimme S, Ehrlich S, Goerigk L. Effect of the Damping Function in Dispersion Corrected Density Functional Theory. *J Comput Chem* 2011, 32:1456–65; (c) Caldeweyher E, Ehlert S, Hansen A, Neugebauer H, Spicher S, Bannwarth C, Grimme S. A generally applicable atomic-charge dependent London dispersion correction. *J Chem Phys* 2019, 150:154122.

128. Mulliken RS. Criteria for the Construction of Good Self-Consistent-Field Molecular Orbital Wave Functions, and the Significance of LCAO-MO Population Analysis. *J Chem Phys* 1962, 36:3428–39.

129. Reed AE, Weinstock RB, Weinhold F. Natural population analysis. *J Chem Phys* 1985, 83:735–46; Reed AE, Curtiss LA, Weinhold F. *Chem Rev* 1988, 88:899–926.

130. Breneman CM, Wiberg KB. Determining atom-centered monopoles from molecular electrostatic potentials. The need for high sampling density in formamide conformational analysis. *J Comp Chem* 1990, 11:361–73.

131. e.g. Mulliken RS, Politzer P. Comparison of Two Atomic Charge Definitions, as Applied to the Hydrogen Fluoride Molecule. *J Chem Phys* 1971, 55:5135–6; Grier DD, Streitwieser A Jr. Electron density analysis of substituted carbonyl groups. *J Am Chem Soc* 1982, 104:3556–64; Wiberg KB, Rablen PR. Comparison of atomic charges derived via different procedures. *J Comput Chem* 1993, 14:1504–18; Martin F, Zipse H. Charge Distribution in the Water Molecule – A Comparison of Methods. *J Comp Chem* 2005, 26:97–105.

132. Durand P, Barthelat JC. A theoretical method to determine atomic pseudopotentials for electronic structure calculations of molecules and solids. *Theoret Chim Acta* 1975, 38:283–302; Andrae D, Häußermann U, Dolg M, Stoll H, Preuß H. Energy-adjusted *ab initio* pseudopotentials for the second and third row transition elements. *Theoret Chim Acta* 1990, 77:123–41; Bergner A, Dolg M, Küchle W, Stoll H, Preuß H. *Ab initio* energy-adjusted pseudopotentials for elements of groups 13–17. *Mol Phys* 1993, 80:1431–41.]

133. Boys SF, Bernardi F. The calculation of small molecular interactions by the differences of separate total energies. Some procedures with reduced errors. *Mol Phys* 1970, 19:553–66.

134. Zimmermann T, Chval Z, Burda JV. Cisplatin Interaction with Cysteine and Methionine in Aqueous Solution: Computational DFT/PCM Study. *J Phys Chem B* 2009, 113:3139–50.

135. (a) Mitoraj MP, Michalak A, Ziegler T. A Combined Charge and Energy Decomposition Scheme for Bond Analysis. *J Chem Theory Comput* 2009, 5:962−75; (b) Mitoraj MP, Zhu H, Michalak A, Ziegler T. On the origin of the trans-influence in square planar d^8-complexes: A theoretical study. *Int J Quantum Chem* 2009, 109:3379−86.

136. Ziegler T, Rauk A. On the calculation of bonding energies by the Hartree Fock Slater method. I. The transition state method. *Theor Chim Acta* 1977, 46:1–10; Ziegler T, Rauk A. A theoretical study of the ethylene-metal bond in complexes between Cu^+, Ag^+, Au^+, Pt^0, or Pt^{2+} and ethylene, based on the Hartree-Fock-Slater transition-state method. *Inorg Chem* 1979, 18:1558–65; Ziegler T, Rauk A. CO, CS, N_2, PF_3, and $CNCH_3$ as σ donors and π acceptors. A theoretical study by the Hartree-Fock-Slater transition-state method. *Inorg Chem* 1979, 18:1755–9.

137. Mitoraj M, Michalak A. Donor–Acceptor Properties of Ligands from the Natural Orbitals for Chemical Valence. *Organometallics* 2007, 26:6576–80; Mitoraj M, Michalak A. Natural orbitals for chemical valence as descriptors of chemical bonding in transition metal complexes. *J Mol Model* 2007, 13:347–55; Michalak A, Mitoraj M, Ziegler T. Bond Orbitals from Chemical Valence Theory. *J Phys Chem A* 2008, 112:1933–9; Broclawik E, Załucka J, Kozyra P, Mitoraj M, Datka J. New Insights into Charge Flow Processes and Their Impact on the Activation of Ethene and Ethyne by Cu(I) and Ag(I) Sites in MFI. *J Phys Chem C* 2010, 114:9808–16; Rejmak P, Mitoraj M, Broclawik E. Electronic view on ethene adsorption in Cu(i) exchanged zeolites. *Phys Chem Chem Phys* 2010, 12:2321–30; Srebro M, Mitoraj M. Role of Ancillary Ligands in a Description of Copper(I)−Bis(trimethylsilyl)acetylene bonding. A Theoretical Study. *Organometallics* 2009, 28:3650–5.

138. Mitoraj M, Michalak A. Applications of natural orbitals for chemical valence in a description of bonding in conjugated molecules. *J Mol Model* 2008, 14:681–7.

139. Kurzab R, Mitoraj MP, Michalak A, Ziegler T. Theoretical Analysis of the Resonance Assisted Hydrogen Bond Based on the Combined Extended Transition State Method and Natural Orbitals for Chemical Valence Scheme. *J Phys Chem A* 2010, 114:8581–90.

140. Mitoraj MP, Parafiniuk M, Srebro M, Handzlik M, Buczek A, Michalak A. Applications of the ETS-NOCV method in descriptions of chemical reactions. *J Mol Model* 2011, 17:2337–52; Díaz S, Brela MZ, Gutiérrez-Oliva S, Toro-Labbé A, Michalak A. ETS-NOCV Decomposition of the Reaction Force: The HCN/CNH Isomerization Reaction Assisted by Water. *J Comput Chem* 2017, 38:2076–87; Šebesta F, Brela MZ, Diaz S, Miranda S, Murray JS, Gutiérrez-Oliva S, Toro-Labbé A, Michalak A, Burda JV. The influence of the metal cations and microhydration on the reaction trajectory of the N3 ↔ O2 thymine proton transfer: Quantum mechanical study. *J Comput Chem* 2017, 38:2680–92; Talaba P, Brela MZ, Michalak A. ETS-NOCV decomposition of the reaction force for double-proton transfer in formamide-derived systems. *J Mol Model* 2018, 24:27.

141. Dyduch K, Mitoraj MP, Michalak A. ETS-NOCV description of σ-hole bonding. *J Mol Model* 2013, 19:2747–58; Mitoraj MP, Michalak A. Theoretical description of halogen bonding – an insight based on the natural orbitals for chemical valence combined with the extended-transition-state method (ETS-NOCV). *J Mol Model* 2013,19:4681–8.

142. Miertuš S, Scrocco E, Tomasi J. Electrostatic interaction of a solute with a continuum. A direct utilizaion of AB initio molecular potentials for the prevision of solvent effects. *Chem Phys* 1981, 55(1):117–29; Miertuš S, Tomasi J. Approximate evaluations of the electrostatic free energy and internal energy changes in solution processes. *Chem Phys* 1982, 65(2):239–45.

143. Cancès E, Mennucci B, Tomasi J. A new integral equation formalism for the polarizable continuum model: Theoretical background and applications to isotropic and anisotropic dielectrics. *J Chem Phys* 1997, 107:3032; Klamt A, Schuurmann G. COSMO: a new approach to dielectric screening in solvents with explicit expressions for the screening energy and its gradient. *J Chem Soc Perkin Trans 2* 1993, 799–805.

144. Kokoschka M, Galgonek J, Vondrasek J, Hobza P. Computational methods for the description of pharmacologically relevant platinum complexes – molecular structure and bond dissociation. *Phys Chem Chem Phys* 2016, 18:4051–62.

145. Andrae D, Häußermann U, Dolg M, Stoll H, Preuß H, Energy-Adjusted ab Initio Pseudopotentials for the Second and Third Row Transition Elements. *Theoret Chim Acta* 1990, 77:123−41; Bergner A, Dolg M, Küchle W, Stoll H, Preuß H. Ab Initio Energy-Adjusted Pseudopotentials for Elements of Groups 13−17. *Mol Phys* 1993, 80:1431–41.

146. Burda JV, Zeizinger M, Sponer J, Leszczynski J. Hydration of Cis- and Trans-Platin: A Pseudopotential Treatment in the Frame of a G3-Type Theory for Platinum Complexes. *J Chem Phys* 2000, 113:2224−32.

147. Zhao Y, Truhlar DG. The M06 suite of density functionals for main group thermochemistry, thermochemical kinetics, noncovalent interactions, excited states, and transition elements: two new functionals and systematic testing of four M06-class functionals and 12 other functionals. *Theor Chem Account* 2008, 120:215–41.

148. Adamo C, Barone V. Toward reliable density functional methods without adjustable parameters: The PBE0 model. *J Chem Phys* 1999, 110:6158–69.

149. Frisch MJ, Trucks GW, Schlegel HB, Scuseria GE, Robb MA, Cheeseman JR, Scalmani G, Barone V, Mennucci B, Petersson GA, Nakatsuji H, Caricato M, Li X, Hratchian HP, Izmaylov AF, Bloino J, Zheng G, Sonnenberg JL, Hada M, Ehara M, Toyota K, Fukuda R, Hasegawa J, Ishida M, Nakajima T, Honda Y, Kitao O, Nakai H, Vreven T, Montgomery JA Jr, Peralta JE, Ogliaro F, Bearpark M, Heyd JJ, Brothers E, Kudin KN, Staroverov VN, Kobayashi R, Normand J, Raghavachari K, Rendell A, Burant JC, Iyengar SS, Tomasi J, Cossi M, Rega N, Millam JM, Klene M, Knox JE, Cross JB, Bakken V, Adamo C, Jaramillo J, Gomperts R, Stratmann RE, Yazyev O, Austin AJ, Cammi R, Pomelli C, Ochterski JW, Martin RL, Morokuma K, Zakrzewski VG, Voth GA, Salvador P, Dannenberg JJ, Dapprich S, Daniels AD, Farkas Ö, Foresman JB, Ortiz JV, Cioslowski J, Fox DJ. *Gaussian 09, Revision D.01*. Gaussian, Inc., Wallingford CT, 2009.

150. Miertuš I, Scrocco E, Thomasi J. Electrostatic interaction of a solute with a continuum. A direct utilizaion of AB initio molecular potentials for the prevision of solvent effects. *Chem Phys* 1981, 55:117–29; Pascual-Ahuir JL, Silla E, Tuñon I. GEPOL: An improved description of molecular surfaces. III. A new algorithm for the computation of a solvent-excluding surface. *J Comput Chem* 1994, 15:1127–38; Tomasi J, Mennucci B, Cammi R. Quantum mechanical continuum solvation models. *Chem Rev* 2005, 105:2999–3093.

151. Glendening ED, Reed AE, Carpenter JE, Weinhold F. NBO 3.1. Theoretical Chemistry Institute and Department of Chemistry, University of Wisconsin: Madison, WI, 1990.

152. te Velde G, Bickelhaupt FM, Baerends EJ, Guerra CF, Van Gisbergen SJA, Snijders JG, Ziegler T. Chemistry with ADF. *J Comput Chem* 2001, 22:931–67.

153. Pérez-Bitrián A, Baya M, Casas JM, Martín A, Menjón B. Hydrogen bonding to metals as a probe for an inverted ligand field. *Dalton Trans* 2021, 50:5465–72.

154. Chval Z, Kabeláč M, Burda JV. Mechanism of the *cis*-[Pt(1*R*,2*R*-DACH)(H$_2$O)$_2$]$^{2+}$ Intrastrand Binding to the Double-Stranded (pGpG)·(CpC) Dinucleotide in Aqueous Solution: A Computational DFT Study. *Inorg Chem* 2013, 52:5801–13.

155. Connors TA, Jones M, Ross CJ, Braddock PD, Khokhar AR, Tobe ML. *Chem Biol Interact* 1972, 5:415–24; Harrap KR, Jones M, Wilkinson CR, Clink H McD, Sparrow S, Mitchley BCV, Clarke S, Veasey A. Antitumour, toxic and biochemical properties of cis-platin and eight other platinum complexes. In: Prestayko AW, Crooke ST, Carter SK (eds). *cis-Platin: Current status and new developments*. Academic Press, New York, 1980, pp 193-212; Thatcher N, Sharma H, Harrison R, Smith A, Zaki A, McAuliffe CA, Crowther D, Fox BW. Blood clearance of three radioactively labelled platinum complexes: cis-dichlorodiammine platinum II, cis, trans-dichlorodihydroxy-bis-(isopropylamine) platinum IV, and cis-dichloro-bis-cyclopropylamine platinum II, in patients with malignant disease. *Cancer Chemother Pharmacol* 1982, 9:13–6; Marzano C, Sbovata SM, Gandin V, Michelin RA, Venzo A, Bertani R, Seraglia R. Cytotoxicity of cis-platinum(II) cycloaliphatic amidine complexes: ring size and solvent effects on the biological activity. *J Inorg Biochem* 2009, 103:1113–9.

156. Poon GK, Mistry P, Raynaud FI, Harrap KR, Murrer BA, Barnard CFJ. Determination of metabolites of a novel platinum anticancer drug JM216 in human plasma ultrafiltrates. *J Pharm Biomed Anal* 1995, 13:1493–8; Raynaud FI, Mistry P, Donaghue A, Poon GK, Kelland LR, Barnard CFJ, Murrer BA, Harrap KR. Biotransformation of the platinum drug JM216 following oral administration to cancer patients. *Cancer Chemother Pharmacol* 1996, 38:155–62.

157. Hollis LS, Amundsen AR, Stern EW. Chemical and biological properties of a new series of *cis*-diammineplatinum(II) antitumor agents containing three nitrogen donors: *cis*-[Pt(NH$_3$)$_2$(N-donor)Cl]$^-$. *J Med Chem* 1989, 32:128–36; Lovejoy KS, Todd RC, Zhang S, McCormick MS, D'Aquino JA, Reardon JT, Sancar A, Giacomini KM, Lippard SJ. cis-Diammine(pyridine)chloroplatinum(II), a monofunctional platinum(II) antitumor agent: uptake, structure, function, and prospects. *Proc Natl Acad Sci USA* 2008, 105:8902–7; Veclani D, Tolazzi M, Cerón-Carrasco JP, Melchior A. Intercalation Ability of Novel Monofunctional Platinum Anticancer Drugs: A Key Step in Their Biological Action. *J Chem Inf Model* 2021, 61(9):4391–9.

158. Lovejoy KS, Serova M, Bieche I, Emami S, D'Incalci M, Broggini M, Erba E, Gespach C, Cvitkovic E, Faivre S, Raymond E, Lippard SJ. Spectrum of cellular responses to pyriplatin, a monofunctional cationic antineoplastic platinum(II) compound, in human cancer cells. *Mol Cancer Ther* 2011, 10:1709–19; McDevitt CE, Yglesias MV, Mroz AM, Sutton EC, Yang MC, Hendon CH, DeRose VJ. Monofunctional platinum(II) compounds and nucleolar stress: is phenanthriplatin unique? *J Biol Inorg Chem* 2019, 24:899–908.

159. Dabbish E, Russo N, Sicilia E. Rationalization of the Superior Anticancer Activity of Phenanthriplatin: An In-Depth Computational Exploration. *Chem–Eur J* 2020, 26:259–68.

160. Dabbish E, Ritacca AG, Mazzone G, Sicilia E. A comparative computational mechanistic study on derivatives of pyriplatin, modified with the –$CH_2Ph_3P^+$ group, as anticancer complexes targeting mitochondria. *Inorg Chim Acta* 2020, 512:119863.

161. Chen Y, Parkinson JA, Guo Z, Brown T, Sadler PJ. A New Platinum Anticancer Drug Forms a Highly Stereoselective Adduct with Duplex DNA. *Angew Chemie Int Ed* 1999, 38:2060–3.

162. Treat J, Schiller J, Quoix E, Mauer A, Edelman M, Modiano M, Bonomi P, Ramlau R, Lemarie E. ZD0473 treatment in lung cancer: an overview of the clinical trial results. *Eur J Cancer* 2002, 38(Suppl 8):S13–8; Gelmon KA, Vandenberg TA, Panasci L, Norris B, Crump M, Douglas L, Walsh W, Matthews SJ, Seymour LK. A phase II study of ZD0473 given as a short infusion every 3 weeks to patients with advanced or metastatic breast cancer: a National Cancer Institute of Canada Clinical Trials Group trial, IND 129. *Ann Oncol* 2003, 14(4):543–8; Hamilton G, Olszewski U. Picoplatin pharmacokinetics and chemotherapy of non-small cell lung cancer. *Expert Opin Drug Metab Toxicol* 2013, 9(10):1381–90; Tang CH, Parham C, Shocron E, McMahon G, Patel N. Picoplatin overcomes resistance to cell toxicity in small-cell lung cancer cells previously treated with cisplatin and carboplatin. *Cancer Chemother Pharmacol* 2011, 67:1389–1400.

163. Sarmah P, Deka RC. Hydrolysis and binding mechanism of AMD473 (cis-[$PtCl_2(NH_3)$(2-picoline)]) with guanine: A quantum mechanical study. *J Mol Struct THEOCHEM* 2010, 955:53–60.

164. Chen Y, Guo Z, Parsons S, Sadler PJ. Stereospecific and Kinetic Control over the Hydrolysis of a Sterically Hindered Platinum Picoline Anticancer Complex. *Chem–Eur J* 1998, 4:672–6; Chen Y, Guo Z, Parkinson JA, Sadler PJ. Kinetic control of reactions of a sterically hindered platinum picoline anticancer complex with guanosine 59-monophosphate and glutathione. *J Chem Soc, Dalton Trans* 1998, 3577–85.

Article OD1

Chval Z., Dvořáčková O., Chvalová D., Burda JV.

Square-Planar Pt(II) and Ir(I) Complexes as the Lewis Bases: Donor–Acceptor Adducts with Group 13 Trihalides and Trihydrides.

Abstract

The stability and properties of donor−acceptor adducts of square-planar Pt(II) and Ir(I) complexes (designated as PtX, IrX, or generally MX complexes) with trihydrides and trihalides of group 13 elements of general formula YZ_3 (Y = B, Al, Ga; Z = H, F, Cl, Br) were studied theoretically using DFT methodology in the gas phase. MX complexes were represented by wide range of the ligand environment which included model complexes $[Ir(NH_3)_3X]^0$ and cis-$[Pt(NH_3)_2X_2]^0$ (X = H, CH_3, F, Cl, Br) and isoelectronic complexes $[Ir(NNN)(CH_3)]^0$ and $[Pt(NCN)(CH_3)]^0$ with tridentate NNN and NCN pincer ligands. MX complexes acted as the Lewis bases donating electron density from the doubly occupied $5dz2$ atomic orbital of the metal M atom to the empty valence pz orbital of Y whose evidence was clearly provided by the natural atomic orbital (NAO) analysis. This charge transfer led to the formation of pentacoordinated square pyramidal MX·(YZ_3) adducts with M·Y dative bond. Binding energies were −44.7 and −75.2 kcal/mol for interaction of GaF_3 as the strongest acid with PtNCN and IrNNN pincer ligands complexes. Only M·B bonds had covalent character although MX·BZ_3 adducts were the least stable due to large values of Pauli repulsion and deformation energies. The highest degree of covalent character was found for adducts of BH_3 in all series of structures studied. Al and Ga adducts showed remarkably similar behavior with respect to geometry and binding energies.

Square-Planar Pt(II) and Ir(I) Complexes as the Lewis Bases: Donor–Acceptor Adducts with Group 13 Trihalides and Trihydrides

Zdeněk Chval,[*],[†] Olga Dvořáčková,[†],[‡] Daniela Chvalová,[§] and Jaroslav V. Burda[∥]

[†]Faculty of Health and Social Sciences, University of South Bohemia, J. Boreckého 27, 370 11 České Budějovice, Czech Republic
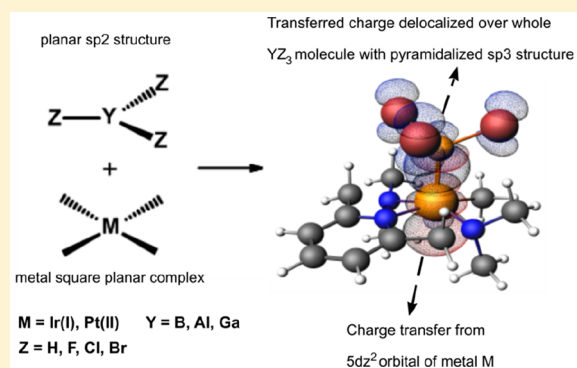
[‡]Faculty of Science, University of South Bohemia, Branišovská 1760, 370 05 České Budějovice, Czech Republic

[§]Biology Centre of the Czech Academy of Sciences, Institute of Entomology, Branišovská 31, 370 05 České Budějovice, Czech Republic

[∥]Faculty of Mathematics and Physics, Charles University, Ke Karlovu 3, Prague 2 121 16, Czech Republic

S *Supporting Information*

ABSTRACT: The stability and properties of donor–acceptor adducts of square-planar Pt(II) and Ir(I) complexes (designated as PtX, IrX, or generally MX complexes) with trihydrides and trihalides of group 13 elements of general formula YZ_3 (Y = B, Al, Ga; Z = H, F, Cl, Br) were studied theoretically using DFT methodology in the gas phase. MX complexes were represented by wide range of the ligand environment which included model complexes $[Ir(NH_3)_3X]^0$ and *cis*-$[Pt(NH_3)_2X_2]^0$ (X = H, CH_3, F, Cl, Br) and isoelectronic complexes $[Ir(NNN)(CH_3)]^0$ and $[Pt(NCN)(CH_3)]^0$ with tridentate NNN and NCN pincer ligands. MX complexes acted as the Lewis bases donating electron density from the doubly occupied $5d_{z^2}$ atomic orbital of the metal M atom to the empty valence p_z orbital of Y whose evidence was clearly provided by the natural atomic orbital (NAO) analysis. This charge transfer led to the formation of pentacoordinated square pyramidal $MX \cdot (YZ_3)$ adducts with M·Y dative bond. Binding energies were −44.7 and −75.2 kcal/mol for interaction of GaF_3 as the strongest acid with PtNCN and IrNNN pincer ligands complexes. Only M·B bonds had covalent character although $MX \cdot BZ_3$ adducts were the least stable due to large values of Pauli repulsion and deformation energies. The highest degree of covalent character was found for adducts of BH_3 in all series of structures studied. Al and Ga adducts showed remarkably similar behavior with respect to geometry and binding energies.

INTRODUCTION

Chemical and physical properties of group 13 trihalides and trihydrides including their interactions as Lewis acids with Lewis bases were subject of many previous studies.[1−19] Molecules with nitrogen as the interacting atom were mostly used as Lewis bases (e.g., NH_3,[1] N_2,[2] HCN,[3,4] RCN,[5] FCH_2CN, $Cl CH_2CN$,[6] piperidine).[7] Other systems included $SeMe_2$, $TeMe_2$(Me = methyl),[8] 9-fluorenone,[9] or unsaturated hydrocarbons.[10−12]

Metal coordination compounds are textbook examples of donor–acceptor bonds in which the central metal ion acts as a Lewis acid and the ligands as Lewis bases. Nevertheless, there is an increasing number of studies about complexes with at least one of the bonds being opposite in nature: a central metal ion as a Lewis base donates electron density to an acidic ligand. The basicity of metal complexes was revealed already in 1955 by Wilkinson and Birmingham who observed the protonation of di-π-cyclopentadienylrhenium hydride in acidic medium.[20] The formation of a donor–acceptor bond between the square-planar d^8 complex and BF_3 as a Lewis acid was first observed by Scott et al. for $[IrClCO(P(C_6H_5)_3)_2]$ complex.[21] The five

coordinated adducts of BF_3 with Pt(II)-complexes such as $[Pt(1\text{-thiomethyl-2-diphenylphosphinoethane})Cl_2]$, $[Pt(S-P)Cl_2]$ (S−P = 1-thiomethyl-2-diphenylarsinoethane) and $[Pt(S-P)I_2]$ were experimentally characterized 30 years ago.[22]

The basicity of the square planar complexes is manifested also in interactions with solvent water molecules. The nonclassical Pt(II)···HOH interaction (so-called inverse hydration)[23−26] is stabilized mainly by the charge transfer from the metal complex toward the water molecule.[27] Similarly, the nature of nonclassical Pt(II)···HCl interactions is based on the charge transfer.[28] Also, the Au(I) center was shown to be a hydrogen and halogen bond acceptor.[29,30] Au exhibits a stronger σ-donation ability than Ag and Cu group 11 metals.[31] Many examples of metal···H H-bonds from experimental studies were shown in the review of Martín.[32]

Currently, the main interest is focused on metal complexes acting as the Lewis bases on boron ambiphilic (bridged) ligands.[33,34] Besides the boron moiety, they contain a standard

ligand usually based on the nitrogen or phosphorus atoms which stabilize the M → B (M·B) dative bond. These systems offer interesting applications, e.g., in organic synthesis.[35] Another example is Pd···HO H-bond in Pd(0) olefin complexes of hydroxy-containing ligands which affected the stereochemistry and the rate of palladium-catalyzed allylic alkylations.[36] Very recently, the structure and catalytic activity of Pd(II)−In(III) and Pd(II)−Ga(III) acetate-bridged complexes was determined experimentally.[37] We may hypothesize that GaCl$_3$ interactions with cisplatin play some role also in vivo since GaCl$_3$ was proposed to improve efficacy and to lower toxicity of a combined anticancer treatment of cisplatin and etoposide.[38]

Studies dealing with interactions of metal complexes with free unbridged Lewis acids are still rare. Adducts of M(0) complexes were experimentally studied with GaCl$_3$ and with AlCl$_3$, BF$_3$ theoretically, by the groups of Braunschweig[39,40] and Sakaki,[41,42] respectively. The cage structures with the prepyramidalized boron center showed lower deformation energies which resulted in stronger interactions with Pt(0) complexes.[43] Strong bonding connected with large charge donation was observed for the T-shaped $[(PMe_3)_2M-EX_3]$ complexes (M = Ni, Pd, Pt; E = B, Al, Ga, In, Tl; X = H, F, Cl, Br, I) in the theoretical work of Frenking and co-workers.[44] The structure of $[Rh(CO)_4][Al_2Cl_7]$ and $[Rh(CO)_4][Ga_2Cl_7]$ adducts were determined by von Ahsen et al.[45]

Nonetheless, we have not found any experimental and/or theoretical work which would explain the nature of these interactions on wider range of structures for the metal complexes in the positive oxidation state of the metal center. In this contribution, we evaluated the Lewis basicity of the square planar complexes with isoelectronic Pt(II) and Ir(I) metal centers which differed in their ionization potential and the oxidation state. Both Ir(I) and Pt(II) complexes were studied with two distinct types of the ligand environment: 1) $[Ir(NH_3)_3X]^0$ and cis-$[Pt(NH_3)_2X_2]^0$ complexes (X = H, CH$_3$, F, Cl, Br); and 2) isoelectronic $[Ir(NNN)(CH_3)]^0$ and $[Pt(NCN)(CH_3)]^0$ complexes based on NNN and NCN tridentate pincer ligands, respectively (Scheme 1). Metal complexes will be abbreviated as PtX and IrX or generally as MX complexes (X = H, CH$_3$, F, Cl, Br, NCN, NNN).

Pincer ligands increase substantially the stability of metal complexes with respect to unwanted ligand substitution reactions. They also enable to fine-tune the electronic and steric properties of the metal center, thereby increasing the number of possible applications including catalysis.[46] Pt(II) complexes with NCN pincer ligand used in this study were recognized as building blocks in the construction of new (macromolecular) organometallic materials.[47]

MX interacted with Lewis acids which included trihalides and trihydrides of group 13 elements of general formula YZ$_3$(Y = B, Al, Ga; Z = H, F, Cl, Br). The use of neutral subsystems decreased the importance of electrostatic interactions which would be dominating for charged species in the gas phase. We will focus on the formation of the pentacoordinated (with respect to M) square pyramidal MX·YZ$_3$ adducts with Pt·Y and Ir·Y bonds (generally designated as M·Y bonds; Scheme 2A). The nature and stability of the M·Y dative bonds and corresponding electronic and structural changes in MX and YZ$_3$ species will be described and characterized.

Scheme 1. Structures of Metal Pt(II) and Ir(I) Complexes Used in This Study[a]

X = H , CH$_3$, F , Cl , Br
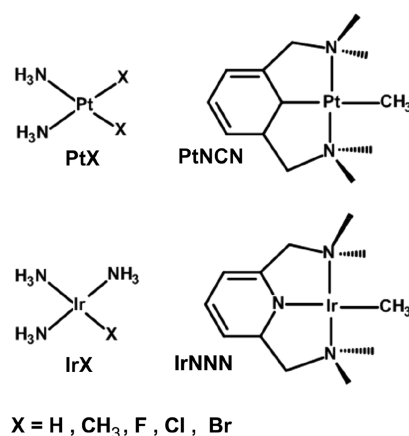
[a]Except for the metal's CH$_3$ and NH$_3$ ligands, the hydrogen atoms are not shown for clarity (amino groups in NCN and NNN ligands are methylated).

Scheme 2. Formation of the Dative M·Y Bond and Schematic Drawing of Charge Transfer[a]

Y = B, Al, Ga   Z = H, F, Cl, Br
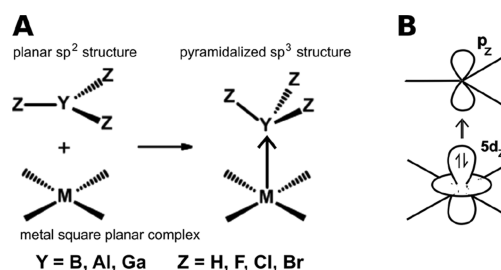
[a](A) Formation of the dative M·Y bond. Electron transfer to YZ$_3$ leads to the change of hybridization on atom Y and pyramidalization of YZ$_3$ (see below). (B) Schematic drawing of the charge transfer between the occupied 5d$_{z^2}$ NAO of MX and vacant p$_z$ NAO of YZ$_3$.

■ METHODS

All calculations were performed at the DFT level. To choose the most appropriate functional for structure optimizations and energy evaluations we performed test computations on the model cis-/trans-$[Pt(H_2O)_2F_2]$·BH$_3$ structures. All the considered functionals contained empirical dispersion corrections. The comparison of DFT geometries and energies with CCSD and CCSD(T) benchmark results is summarized in Tables S1 and S2, respectively. In combination with 6-311++G(d,p) basis set for the main group elements and Stuttgart quazirelativistic energy-averaged effective core potentials[48,49] with a pseudo-orbital basis set augmented by the set of diffuse (with exponents α_s = 0.0075, α_p = 0.013, α_d = 0.025) and one set of polarization (α_f(Pt)= 0.98) functions[50] for the Pt atom (MWB-60(f) basis set) the B3PW91-GD3BJ and M062X-D3 functionals gave the best agreement with CCSD reference structures (Table S1). We optimized all structures by both functionals and the differences in binding energies were never larger than 2 kcal/mol. Both functionals gave qualitatively the same results, but we decided to present M062X-D3 (M062X functional[51] combined with D3 Grimme dispersion[52]) optimized structures since this functional was already used with success for related systems.[41] However, the subsequent geometry optimizations were performed with larger basis set having two sets of polarization functions on each atom: MWB-60(2f) (α_f(Pt)= 0.466, 1.419)[50] for the Pt atom and 6-311++G(2d,2p) basis set for the main group elements. Analogously, Ir was described by Stuttgart effective core potentials with the split-valence def2-TZVPD basis set. This methodology is labeled as M062X-D3/BS1 in further text. The nature

of the obtained stationary points was always checked by the evaluation of the Hessian matrix. Contributions from the nuclear degrees of freedom to the energetic properties were calculated using the canonical ensemble of ideal gas at standard conditions (T = 298 K, p = 101.325 kPa).

The interaction energies ΔE_{INT} between MX and YZ$_3$ subsystems were calculated as

$$\Delta E_{INT} = E_{Adduct} - (E_{MX} + E_{YZ3}) + \Delta E_{BSSE} \qquad (1)$$

where E_{Adduct} is energy of whole adduct and E_{MX} and E_{YZ3} are energies of the MX metal complex and YZ$_3$ trihalide or trihydride, respectively. Geometries of both parts were taken from the optimized adduct. The basis set superposition errors ΔE_{BSSE} were calculated by the counterpoise method.[53]

The binding energies included deformation energies of both the metal complex (ΔE_{Def}^{MX}) and YZ$_3$ molecule (ΔE_{Def}^{YZ3}):

$$\Delta E_{Bind} = \Delta E_{INT} + \Delta E_{Def}^{MX} + \Delta E_{Def}^{YZ3} \qquad (2)$$

With respect to binding energies, the best agreement with reference CCSD(T) calculations was obtained for M062X-D3[51,52] and BLYP-D3BJ[54−56] functionals depending on whether or not ΔE_{BSSE} was included (Table S2). Energy profiles and wave function properties were determined at the M062X-D3/6-311++G(2df,2pd) single-point calculations. The use of BSSE corrected CCSD(T) energies as reference values may systematically underestimate the binding energies since BSSE of CCSD(T) was by few times larger (6.7 and 6.5 kcal/mol for cis and trans isomers, respectively) than those of any DFT method (respective values are 0.9 and 0.8 kcal/mol for M062X-D3). The Pt atom was augmented by the sets of diffuse and polarization functions in analogy to BS1 and by the extra set of polarization g-functions (α_g(Pt) = 1.208)[50] (MWB-60(2fg) basis set). Analogously, Ir was described by def2-TZVPPD basis set as taken from the Basis Set Exchange database.[57,58] These calculations are labeled as M062X-D3/BS2 in further text.

All optimizations and single-point calculations were carried out by the Gaussian 09 (G09) program package.[59] Atoms in molecules (AIM) topological analysis of the electron density at bond critical points (BCP's) was performed by the AIMAll program[60] and natural population analysis (NPA) partial charges were determined from the Natural Atomic Orbital (NAO) analysis by the NBO 3.1 program.[61]

Additional single-point calculations were conducted using the Amsterdam Density Functional 2017 package (ADF)[62] to determine the fragment energy decompositions according to the extended transition state theory[63] combined with natural orbitals for chemical valence (ETS-NOCV).[64,65] Gas-phase binding energies ΔE_{Bind} were decomposed to Pauli (ΔE_{Pauli}), electrostatic (ΔE_{elst}), orbital (ΔE_{orb}), and dispersion (ΔE_{disp}) energy contributions. In these calculations, scalar relativistic effects were treated within the Zeroth Order Regular Approximation (ZORA).[66] The BLYP-D3BJ functional (cf. above) was used in combination with the all-electron QZ4P (ZORA) basis set for all atoms.

RESULTS

Relative Stabilities of the Adducts with M·Y and X·Y Bonds. For PtNCN and IrNNN complexes, the adducts with the M·Y bonds represented the global minimum on the potential energy surface. The same was also true for the adducts of IrX (X = H, CH$_3$, Cl, Br), PtCH$_3$ and PtH (except PtH·BH$_3$). For some of the IrF·YZ$_3$ adducts and all the adducts of PtX (X = F, Cl, Br) complexes, the formation of the structure with the M·Y dative bond represented a local minimum since X·YZ$_3$ interactions (direct electron donation from halogen ligand to Y atom) were more advantageous. The differences in Gibbs free energies between adducts with M·Y and X·Y dative bonds are summarized in the Table S3. Although most of the higher energy M·Y adducts would be present only in negligible concentrations in the 1:1 reaction

mixture (based on Boltzmann equilibrium population) the structures with the M·Y bond may be present under the excess of YZ$_3$ as shown for the IrMeCl(PCy$_3$)$_2$(GaMe$_3$)(GaMe$_2$) complex.[67] Regardless the experimental availability we analyzed electronic properties of all 1:1 adducts with the M·Y bond to obtain data from a wider range of chemically distinct structures. They should be viewed as model systems that enabled us to provide a general description of physicochemical properties of the M·Y dative bonds.

Dative Character of the M·Y Bonds. Charge transfer interactions are often characterized by the energy difference between HOMO of the donor and LUMO of the acceptor. Within much more localized NAO's the formation of the M·Y bond can be simply viewed as the charge transfer from the doubly occupied 5d$_{z^2}$ NAO of M into the empty valence p$_z$ NAO of Y (Scheme 2B). The Figure 1 shows the dependence
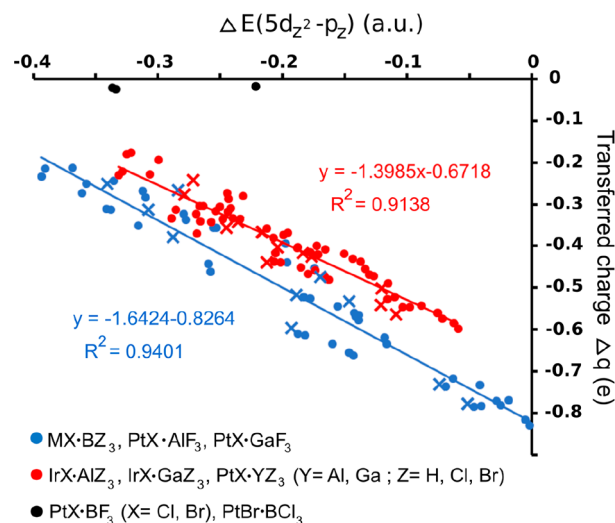

Figure 1. Dependence of the transferred charge Δq on the energy difference between occupied 5d$_{z^2}$ NAO of MX and vacant p$_z$ NAO of YZ$_3$ calculated at M062X-D3/BS2//M062X-D3/BS1 level. Both MX and YZ$_3$ were fully optimized as isolated structures. Points corresponding to adducts of MX complexes with pincer ligands and CH$_3$, H, F, Cl, and Br ligands are labeled by crosses (×) and circles (●), respectively. Three weakly bound adducts (black ●) were excluded from regression analyses.

of the transferred charge Δq on the energy difference between these two NAO's ($\Delta E(5d_{z^2}-p_z)$). Energies of both NAO's were evaluated for isolated fully optimized MX and YZ$_3$ molecules (Table S4) which should enable to predict the amount of Δq for any pair of MX and YZ$_3$ molecules. The values of Δq together with structural and electronic properties of M·Y bonds are shown in the Tables 1, 2, and S5 and S6 for adducts of PtNCN, IrNNN, and PtX and IrX (X = H, F, Cl, Br), respectively.

If we exclude three very weakly bound van der Waals structures (black points in Figure 1), then we obtain the regression line with the R^2 value of 0.797 (not shown in Figure 1). Such a good correlation suggests similar changes of electron density connected with the formation of the dative M·Y bond for all the systems studied. The role of the electrostatic field should be small at least at the initial stage since we consider two coplanar interacting species with the dipole moment of MX oriented perpendicularly with respect to the direction of the charge transfer. However, a substantial

Table 1. PtNCN·YZ$_3$ Adducts[a]

YZ$_3$	d(Pt−Y)	$\bar{\alpha}$	ρ(BCP)	$\nabla^2\rho$(BCP)	Δq
BH$_3$	2.279	101.1	0.064	−0.017	−0.378
BF$_3$	2.309	101.9	0.067	−0.058	−0.265
BCl$_3$	2.218	107.0	0.086	−0.100	−0.473
BBr$_3$	2.183	108.8	0.093	−0.115	−0.532
AlH$_3$	2.553	102.1	0.039	0.098	−0.277
AlF$_3$	2.434	104.8	0.051	0.142	−0.252
AlCl$_3$	2.446	108.5	0.052	0.129	−0.343
AlBr$_3$	2.450	109.9	0.052	0.125	−0.366
GaH$_3$	2.680	100.1	0.042	0.073	−0.243
GaF$_3$	2.468	107.8	0.068	0.104	−0.313
GaCl$_3$	2.502	109.7	0.065	0.086	−0.366
GaBr$_3$	2.526	111.3	0.063	0.074	−0.403

[a]Pt−Y bond lengths (d(Pt−Y), in Å); mean values of Pt−Y−Z angles ($\bar{\alpha}$, in deg); local topological properties of Pt·Y bonds calculated at the position of BCPs: the electron density (ρ(BCP)) and the Laplacian of electron density ($\nabla^2\rho$(BCP)); transferred charge (Δq, in e). The data were calculated at M062X-D3/BS2//M062X-D3/BS1 level.

Table 2. IrNNN·YZ$_3$ Adducts[a]

YZ$_3$	d(Ir−Y)	$\bar{\alpha}$	ρ(BCP)	$\nabla^2\rho$(BCP)	Δq
BH$_3$	2.189	105.2	0.088	−0.095	−0.596
BF$_3$	2.140	106.7	0.108	−0.186	−0.516
BCl$_3$	2.075	110.7	0.125	−0.190	−0.731
BBr$_3$	2.050	112.2	0.130	−0.200	−0.778
AlH$_3$	2.458	104.9	0.053	0.128	−0.417
AlF$_3$	2.385	107.2	0.063	0.155	−0.355
AlCl$_3$	2.367	110.5	0.066	0.162	−0.475
AlBr$_3$	2.360	111.5	0.067	0.165	−0.501
GaH$_3$	2.544	105.3	0.063	0.070	−0.426
GaF$_3$	2.413	110.1	0.082	0.093	−0.439
GaCl$_3$	2.419	112.0	0.082	0.080	−0.542
GaBr$_3$	2.418	112.8	0.083	0.077	−0.563

[a]Ir−Y bond lengths (d(Ir−Y), in Å); mean values of Ir−Y−Z angles ($\bar{\alpha}$ in deg); local topological properties of Ir·Y bonds calculated at the position of BCPs: the electron density (ρ(BCP)) and the Laplacian of electron density ($\nabla^2\rho$(BCP)); transferred charge (Δq, in e). The data were calculated at M062X-D3/BS2//M062X-D3/BS1 level.

improvement of the correlation between ΔE(5d$_{z^2}$−p$_z$) and Δq was achieved when the structures were divided into two sets with separate linear regression functions constructed for each of them (Figure 1). This reflected the Δq delocalization over the whole YZ$_3$ molecule and the dependence of Δq on Y−Z bond polarity and polarizability.[14] Delocalization of Δq occurred mostly via the occupation of the antibonding orbitals of Y−Z bonds BD*(Y−Z) which led to the elongation of those bonds (cf. below). Total population in the three BD*(Y−Z) orbitals ranged between 0.010 e (in PtCl·BH$_3$; cf. below) and 0.359 e (in PtBr·AlBr$_3$). It decreased systematically with decreasing atomic number of Z (Br > Cl > F > H) but no clear trends were found with respect to M, X, and Y.

The MX·BZ$_3$ and PtX·YF$_3$, (Y = Al, Ga)adducts belonged to the group with the higher |Δq| at a given value of ΔE(5d$_{z^2}$−p$_z$) (blue points in Figure 1) probably due to the M·B bond covalency and the polarity of Y−F bonds, respectively. For the MX·YZ$_3$ bonds (Y = Al, Ga; Z = H, Cl, Br) with charge-transfer character (see below), the ΔE(5d$_{z^2}$−p$_z$)/Δq dependence was impacted by neither M nor the X ligands. Since the transferred charge Δq originated from nonbonding 5d$_{z^2}$ NAO

of the M atom, the structures of the MX complexes were little affected by the M·Y bond formation.

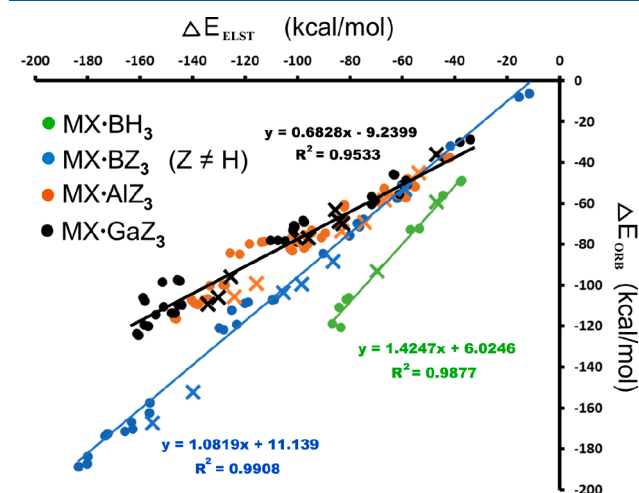The NOCV analysis showed that ΔE_{elst} term correlated with ΔE_{orb} for the adducts with the same M·Y bond (Figure 2). The

Figure 2. Correlation between ΔE_{orb} and ΔE_{elst} terms for the MX·YZ$_3$ adducts calculated at BLYP-D3BJ/QZ4P//M062X-D3/BS1 level. One regression line was constructed for adducts of both Al and Ga (black line). Points corresponding to the adducts of IrNNN and PtNCN are distinguished by crosses (×).

same effect was also observed for energy decomposition along the standard coordination Pt−OH$_2$ bond in square planar Pt(II) complexes[68] which could mean that it is a common descriptor of the donor−acceptor bonds at least in this type of complexes. A possible explanation at least for the systems in this study is that the NOCV analysis is performed for the interaction of distorted MX and YZ$_3$ subsystems as found in the final MX·YZ$_3$ adducts. The distortion of YZ$_3$ is dependent on the charge transfer (cf. below) which is the main contributor to ΔE_{orb} (cf. below), and at the same time, the pyramidalization of YZ$_3$ enhances substantially ΔE_{elst} inducing the dipole moment in this subsystem. Contrarily, the charge transfer and polarization effects are enhanced by increasing electrostatic fields between the interacting species. Thus, the $\Delta E_{elst}/\Delta E_{orb}$ ratio resulting from the mutual linear dependence of the two terms is probably the property of the specific interaction. When performed on a statistically relevant number of complexes, this analysis should enable to distinguish the structures with different nature of interaction and to group together similar systems.

Three groups of adducts were recognized according to the relative importance of ΔE_{orb} /ΔE_{elst} terms (Figure 2): (1) For MX·AlZ$_3$ and MX·GaZ$_3$ adducts, ΔE_{elst} reached the highest values at given value of ΔE_{orb} and ΔE_{elst} was the dominating stabilizing contribution for MX·AlZ$_3$ and MX·GaZ$_3$ inter-actions which reflected the charge-transfer character of M·Al and M·Ga bonds (see below). (2) For MX·BZ$_3$ adducts, the main stabilizing contribution came from ΔE_{orb}, and M·B bonds had covalent character. MX·BF$_3$ adducts were the exception, having slightly higher values of ΔE_{elst} due to polarity of B−F bonds but still belonging to this group of structures. (3) The relative importance of ΔE_{orb} with respect to ΔE_{elst} was further enhanced for MX·BH$_3$ adducts (Figure 2). Due to the nonpolarity of the B−H bonds and high energy of BD*(B−H) orbitals (population in these three orbitals reached the

maximum value of only 0.033 e in IrH·BH$_3$ and being below 0.024 e for all other adducts), the transferred charge Δq resided almost entirely on the B atom. As a result, the boron NPA charges changed from positive values to negative ones upon the adduct formation, while slight negative NPA charges of H atoms remained almost unchanged. Thus, BH$_3$ is the only YZ$_3$ structure in which Y−Z bond polarity was overturned, and the total dipole moment of the pyramidalized BH$_3$ subunit was oriented away from the MX complex. Qualitatively, the same results as described in the previous paragraph were obtained also for YZ$_3$ adducts with NH$_3$ and Pt(PMe$_3$)$_2$ (see below).

The dominant contribution to ΔE_{orb} (72 ± 7% and 76 ± 6% of its value for adducts of PtX and IrX, respectively) originated from the formation of the σ-donor−acceptor M·Y bond (Figure 3). It was formed by the overlap of the occupied 5d$_{z^2}$
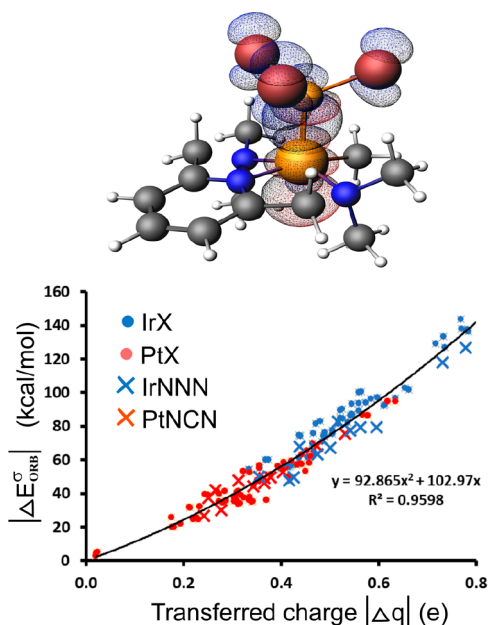

Figure 3. Top panel: contours of the most important deformation density contribution $|\Delta E^\sigma_{orb}|$, which corresponds to the charge transfer during the IrNNN·BBr$_3$ adduct formation ($|\Delta E^\sigma_{orb}|$ = −126.7 kcal/mol). The blue/red contours correspond to accumulation/depletion of electron density by ±0.002 a.u. Bottom panel: The correlation between absolute values of $|\Delta E^\sigma_{orb}|$ and $|\Delta q|$ for all studied adducts. $|\Delta E^\sigma_{orb}|$ and $|\Delta q|$ were calculated at BLYP-D3BJ/QZ4P//M062X-D3/BS1 and M062X-D3/BS2//M062X-D3/BS1 levels of theory, respectively.

orbital of the metal with empty valence p$_z$ orbital of Y, and the transferred charge is partly delocalized over whole YZ$_3$ molecule (cf. above). The absolute value of this contribution $|\Delta E^\sigma_{orb}|$ correlated very well with the absolute value of the transferred NBO charge using the second-order polynomial function for the joint data set of both PtX and IrX adducts (Figure 3). The zero intercept of this correlation may be interpreted by negligible contribution of other NOCV pairs to the charge transfer. For example, two π-orbital contributions accounted for 11 ± 4% of ΔE_{orb} having the same average values for Pt(II) and Ir(I) adducts. The same strengths of Y → M π-donation and M → Y π-back-donation can be expected based on previous results for M(PMe$_3$)-YZ$_3$ complexes (M = Ni(0), Pd(0), Pt(0)) which showed this charge cancellation for much higher π-orbital contributions (ranging between 12.7 and 29.8% of ΔE_{orb}).[44] Pt(II) as the metal in the higher

oxidation state is a weaker electron donor (Lewis base) than Ir(I) which is in agreement with relative energies of their 5d$_{z^2}$ orbitals (cf. above and Table S4).

Stability of the M−Y Dative Bonds. The data about deformation and binding energies together with binding enthalpies and Gibbs free energies are summarized in Tables 3 and 4 for adducts of PtNCN and IrNNN, respectively. The data for the other adducts (X = H, CH$_3$, F, Cl, Br) are shown in Tables S7 and S8 in the Supporting Information. Since PtNCN and IrNNN complexes are isoelectronic, ΔE_{disp} values were dependent mainly on the nature of Z having the values of −12.4 ± 1.2, −14.0 ± 1.7, −22.5 ± 0.5, and −25.2 ± 0.5 kcal/mol for the adducts of YH$_3$, YF$_3$, YCl$_3$ and YBr$_3$, respectively.

Binding energies of all optimized adducts as a function of the nature of MX and YZ$_3$ species are depicted in Figure 4. They range between −32.9 and −85.4 kcal/mol for the IrX·YZ$_3$ adducts. PtX complexes formed by about 30 kcal/mol weaker adducts with binding energies between −3.3 and −55.4 kcal/mol. For all MX complexes the most stable bonds were formed with GaF$_3$ as the strongest acid. Very stable adducts with both types of metal complexes gave also trihalides of Al and Ga, namely, AlF$_3$ and AlBr$_3$ closely followed by AlCl$_3$, GaCl$_3$, and GaBr$_3$. This is in agreement with the previous comparison of GaF$_3$ and GaCl$_3$ acidity.[14]

Boron formed the weakest adducts, the smallest ΔE_{Bind} difference with respect to Al and Ga analogues was found for trihydrides in all X ligand series. The adducts of Al and Ga trihydrides were much less stabilized than all the corresponding trihalides (YZ$_3$ where Y= Al, Ga; Z = F, Cl, Br). On the contrary, the adducts of BH$_3$ were always more stable than those of BF$_3$. Furthermore, stability of PtX·BH$_3$ adducts was comparable or even higher than those of BCl$_3$ and BBr$_3$(Figure 4). Comparing Al and Ga analogues, GaF$_3$ (Z = F) gave slightly more stable adducts than did AlF$_3$, but for Z = H, Cl, and Br, the trend was opposite.

The adduct formation was promoted by X ligands with a strong σ-donation ability such as H$^-$ and CH$_3^-$ which increased the energy of the 5dz^2 NAO as the main source of electrons for the M·Y dative bond (cf. above). For PtX and IrX complexes (X = CH$_3^-$, H$^-$, F$^-$, Cl$^-$, Br$^-$) the following order was obtained for the stability of the adducts with respect to X: CH$_3^- \sim$ H$^- >$ F$^- \geq$ Cl$^- \geq$ Br$^-$.

Figure 5 shows that $|\Delta E_{INT}|$ were roughly similar for all Y atoms, but B formed much shorter covalent bonds with M. The absolute values of interaction energy $|\Delta E_{INT}|$ can be estimated from the geometry of adducts although the dependence on the M−Y distance is exponential with a steep curve at short M−Y distances. Attempts to express the binding energies were less successful mainly for PtX·YZ$_3$ adducts which were very sensitive to relatively larger values of ΔE_{Def}^{YZ3} deformation energies.

Al and Ga formed similar adducts with almost the same $|\Delta E_{INT}|$ and M−Y distances. Both types of adducts could be extrapolated by just one common curve with the R^2 value of 0.883 instead the two curves shown in the Figure 5. Similar covalent radii of Al and Ga were explained by the transition series contraction (the higher nuclear charge of Ga is not fully screened by valence 3d electrons).[69] In our case, higher values of Pauli repulsion ΔE_{Pauli} of GaZ$_3$ adducts were almost exactly compensated by more negative sum of ($\Delta E_{orb} + \Delta E_{elst}$) terms compared to AlZ$_3$ adducts (see Tables 3, 4, S7, and S8).

Romm et al.[70] analyzed many different donor−acceptor molecular complexes based on organic donor molecules. Just

Table 3. PtNCN·YZ$_3$ Adducts[a]

YZ$_3$	ΔE_{Pauli}	ΔE_{elst}	ΔE_{orb}	ΔE_{disp}	ΔE_{def}^{YZ3}	ΔE_{def}^{PtNCN}	ΔE_{Bind}	ΔH^{298}	ΔG^{298}
BH$_3$	86.2	−47.1	−59.2	−10.9	8.4	1.8	−17.8	3.5[b]	9.1[b]
BF$_3$	94.2	−59.0	−53.1	−11.7	20.4	2.3	−10.0	−8.9	3.2
BCl$_3$	148.8	−86.4	−88.4	−22.0	31.4	6.9	−8.2	−6.8	6.2
BBr$_3$	168.9	−98.3	−99.6	−25.0	34.4	8.9	−9.2	−7.5	5.8
AlH$_3$	75.7	−53.8	−45.0	−13.5	7.3	2.2	−26.1	−6.2[b]	−0.2[b]
AlF$_3$	84.6	−66.9	−58.5	−15.3	16.0	2.5	−41.5	−39.5	−26.5
AlCl$_3$	105.0	−74.6	−69.3	−23.2	20.5	4.7	−34.4	−17.4[b]	−9.7[b]
AlBr$_3$	118.7	−83.1	−73.5	−25.8	22.1	5.7	−33.0	−17.6[b]	−9.7[b]
GaH$_3$	66.5	−47.1	−36.1	−13.2	5.1	1.9	−20.9	−5.3[b]	0.4[b]
GaF$_3$	107.4	−84.0	−68.8	−15.4	17.9	2.9	−44.7	−42.8	−29.9
GaCl$_3$	115.9	−82.7	−69.8	−22.9	19.6	4.4	−33.1	−18.6[b]	−10.7[b]
GaBr$_3$	136.8	−95.7	−76.8	−25.7	22.8	6.9	−30.1	−17.5[b]	−10.9[b]

[a]ETS-NOCV energy decomposition terms ΔE_{Pauli}, ΔE_{elst}, ΔE_{orb}, and ΔE_{disp} obtained at BLYP-D3BJ/QZ4P//M062X-D3/BS1 level. ΔE_{def}^{YZ3}, ΔE_{def}^{PtNCN}, ΔE_{Bind}, ΔH^{298}, and ΔG^{298} energy values calculated at M062X/BS2//M062X-D3/BS1 level. All values are in kcal/mol. [b]Calculated with respect to dimeric Y$_2$Z$_6$ structures.

Table 4. IrNNN·YZ$_3$ Adducts[a]

YZ$_3$	ΔE_{Pauli}	ΔE_{elst}	ΔE_{orb}	ΔE_{disp}	ΔE_{def}^{YZ3}	ΔE_{def}^{IrNNN}	ΔE_{Bind}	ΔH^{298}	ΔG^{298}
BH$_3$	121.7	−69.7	−93.1	−10.7	17.0	1.5	−37.1	−14.2[b]	−6.2[b]
BF$_3$	155.6	−105.4	−103.8	−11.9	44.3	2.8	−32.9	−29.8	−16.5
BCl$_3$	223.7	−139.8	−152.2	−21.8	53.0	7.8	−42.7	−39.3	−28.1
BBr$_3$	250.0	−155.2	−167.4	−24.7	54.7	9.9	−47.5	−43.9	−29.9
AlH$_3$	109.3	−83.5	−68.4	−13.1	13.5	2.0	−46.7	−25.4[b]	−18.5[b]
AlF$_3$	113.1	−100.9	−78.6	−14.7	23.8	2.9	−67.9	−64.3	−51.1
AlCl$_3$	146.2	−115.7	−99.1	−22.8	29.9	5.7	−66.2	−47.5[b]	−39.1[b]
AlBr$_3$	162.1	−124.2	−105.7	−25.4	30.6	6.8	−66.8	−50.0[b]	−41.5[b]
GaH$_3$	112.3	−85.6	−63.1	−13.0	12.0	2.2	−39.5	−22.7[b]	−16.1[b]
GaF$_3$	146.1	−125.3	−95.9	−14.9	26.2	2.5	−75.2	−71.4	−57.5
GaCl$_3$	167.2	−130.3	−106.0	−22.5	29.4	5.4	−66.5	−50.5[b]	−42.0[b]
GaBr$_3$	177.6	−134.1	−109.2	−24.8	30.0	5.9	−64.8	−50.5[b]	−42.9[b]

[a]ETS-NOCV energy decomposition terms ΔE_{Pauli}, ΔE_{elst}, ΔE_{orb}, and ΔE_{disp} obtained at BLYP-D3BJ/QZ4P//M062X-D3/BS1 level. ΔE_{def}^{YZ3}, ΔE_{def}^{IrNNN}, ΔE_{Bind}, ΔH^{298}, and ΔG^{298} energy values calculated at M062X -D3/BS2//M062X-D3/BS1 level. All values are in kcal/mol. [b]Calculated with respect to dimeric Y$_2$Z$_6$ structures.
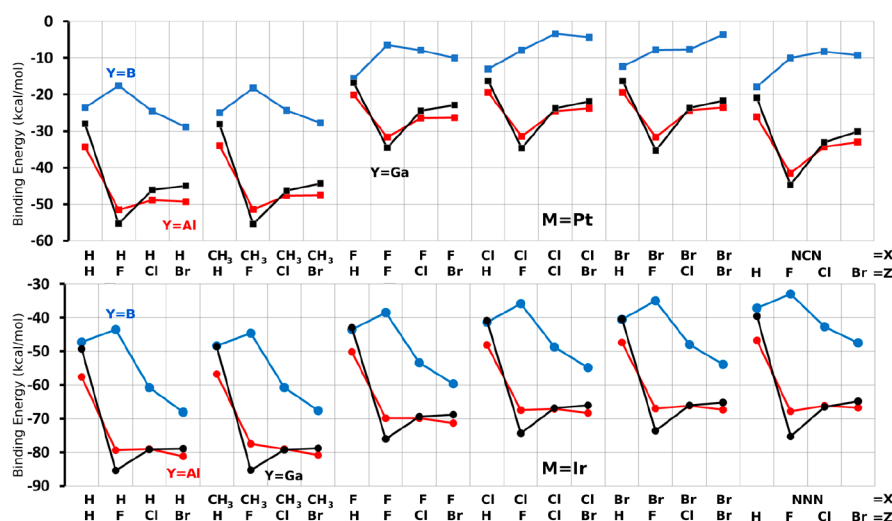

Figure 4. Dependence of binding energies of PtX (upper part) and IrX (lower part) with YZ$_3$ on the nature of X and Z. See Tables 3, 4, S7, and S8 for numeric values.

one hyperbolic curve was obtained for all these complexes when experimental enthalpies of formation were plotted against the difference between the distance of the donor–acceptor molecules and the scaled sum of covalent radii of interacting atoms.[70] Following this idea, the set of covalent atomic radii from ref 69 and the scaling factor 0.82 gave a reasonable dependence of our calculated interaction energies
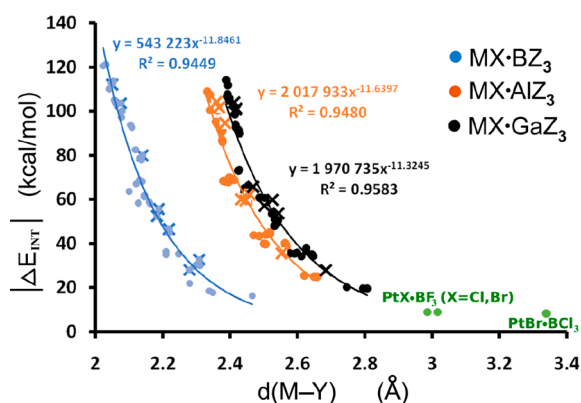
Figure 5. Exponential dependence of the absolute value of interaction energy $|\Delta E_{INT}|$ on the M−Y distance d(M−Y) calculated at M062X-D3/BS2//M062X-D3/BS1 level. Points corresponding to the adducts of IrNNN and PtNCN are distinguished by crosses (×). Three weakly bound adducts (green points) were excluded from regression analyses.

Figure 6. Total electron density difference isosurfaces calculated at M062X-D3/BS2//M062X-D3/BS1 level from IrH·BBr$_3$ (A) and IrH·AlBr$_3$ (B) adducts and from the isolated IrH and YBr$_3$ structures whose total electron densities were calculated at their deformed geometries as found in the adducts. Blue and red isosurfaces show electron accumulation (+0.005 a.u.) and depletion (−0.005 a.u.) regions, respectively.

of all adducts (including boron ones) on the modified M−Y distance (Figure S1).

The BZ$_3$ compounds were better electron acceptors compared to their AlZ$_3$ and GaZ$_3$ counterparts. However, the highly stabilizing ΔE_{orb} terms were compensated by larger values of destabilizing steric energy ($\Delta E_{Pauli} + \Delta E_{elst}$) for most of the BZ$_3$ adducts. Especially high values of ΔE_{Pauli} were found for adducts of BCl$_3$ and BBr$_3$ as the result of the large overlap of bulky occupied electron clouds of Cl and Br atoms with the MX complexes. Distances of Cl and Br atoms from the plane of MX complexes were smallest in the BZ$_3$ adducts since much shorter M·B and B−Z bonds (the shortest M·B bonds were detected for MX·BBr$_3$ adducts) could not be compensated by substantially bigger M-B-Z angles (Tables 1 and 2 and S5 and S6) comparing to Al and Ga complexes.

Lower binding energies of MX·BZ$_3$ adducts were caused by high BZ$_3$ deformation energies ΔE_{Def}^{BZ3} which had substantially larger values compared to their Al and Ga analogues. ΔE_{Def}^{BZ3} was facilitated by a higher charge transfer and in the same time it was enhanced by bigger Pauli repulsion ΔE_{Pauli} (cf. below). Larger deformation of BZ$_3$ decreased Pauli repulsion between the Z atoms and the MX complex at given M·B bond length.

M·Y Bond Covalency. AIM analysis showed that covalency of the M·Y bond depends on the nature of Y. The electron densities (ρ(BCP)) and the Laplacians of electron density ($\nabla^2\rho$(BCP)) calculated at BCPs of the M·Y bonds are depicted in Tables 1, 2 and S5, S6 for X = NNN, NCN and X = H, CH$_3$, F, Cl, Br, respectively. $\nabla^2\rho$(BCP) for the M·B bonds in most of the MX·BZ$_3$ adducts was negative proving an accumulation of the electron density between the M and B atoms and covalent nature of the M·B bonds (Figure 6A). However, $\nabla^2\rho$(BCP) was positive for M·Al and M·Ga bonds reflecting a depletion of electron density between the bonding atoms and an ionic character of these bonds with respect to the topology of electron density along the bond path (Figure 6B). We call these interactions as the charge-transfer bonds. Complementarily, the highest ρ(BCP) were found for M·B bonds with the order of BCP electron density: M·B > M·Ga > M·Al. The absolute values of $|\Delta E_{INT}|$ could be expressed as a power function of ρ(BCP) but depended on the nature of Y atom (Figure S2).

The M·Y bond length did not influence the character of M·Al bonds since their charge-transfer nature remained even at
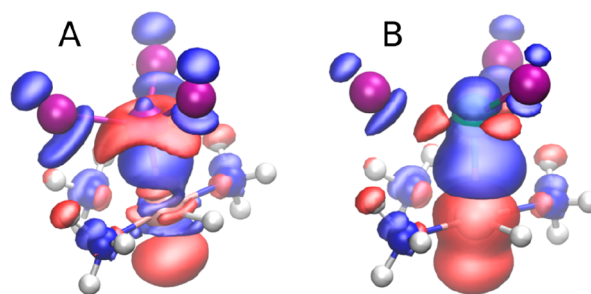
very short distances in our testing computations on the IrH·AlBr$_3$ adduct (see Table S9). However, the covalent character of the M·B bond was changed to the charge-transfer one only at very long M-B distances (≥ 3.0 Å) as found for the IrH·AlBr$_3$ complex (Table S9) and in optimized structures of weakly bound PtX·BF$_3$ (X = Cl, Br) and PtBr·BCl$_3$ adducts. IrH·BBr$_3$ and IrH·AlBr$_3$ were chosen for testing computations since they showed the highest ρ(BCP) of the M·Y bond from all covalent and charge-transfer adducts, respectively (Figure 6).

Structural and Electronic Changes in YZ$_3$. Geometrical changes of the fragments can be quantified by their deformation energies. ΔE_{Def}^{YZ3} deformation energies were by about one order of magnitude larger than corresponding ΔE_{Def}^{MX} values. Thus, MX·YZ$_3$ adduct formations led to substantial structural and electronic changes of the YZ$_3$ subsystem while the geometry of the MX complex remained almost unaffected. ΔE_{Def}^{YZ3} energies were roughly proportional to ΔE_{INT}. BZ$_3$ halides (Z= F, Cl, Br) showed a steeper dependence of ΔE_{Def}^{YZ3} on ΔE_{INT} than did AlZ$_3$ and GaZ$_3$ counterparts (Figure S3) which led to smaller binding energies (ΔE_{Bind}) of BZ$_3$ adducts (cf. above). Charge transfer Δq during the adduct formation was connected with the change of hybridization on the Y atom from sp^2 to sp^3 promoting the YZ$_3$ pyramidalization. The elongation of the Y−Z bonds was caused by delocalization of the transferred charge into antibonding BD*(Y−Z) orbitals (cf. above).

These structural changes are closely connected with the reduction of Pauli repulsion between Z atoms and the MX complex. Pauli repulsion was another driving force for YZ$_3$ distortion which enhanced the effect of the charge transfer. For example, the largest values of both transferred charge and Pauli repulsion were found for adducts of BBr$_3$ (cf. above). The optimized structure of isolated BBr$_3^-$ anion had by 0.124 Å longer B−Br bonds than the neutral BBr$_3$ molecule and its pyramidalization corresponded to the M−Y−Z bond angle of 106.7°. However, in the IrNNN·BBr$_3$ adduct the transferred charge of just −0.778 e (compared to −1e in BBr$_3^-$) led to the elongation of the B−Br bond by 0.177 Å and the increase of the Ir−B−Br angle to 113.8° (Table 2). In contrast, for YH$_3$ trihydrides much lower values of Pauli repulsion were determined, also being much less sensitive with respect to the nature of the Y atom compared to the adducts of corresponding trihalides. Thus, the adducts of BH$_3$ had only by a few kcal/mol higher ΔE_{Pauli} than the adducts of AlH$_3$ and GaH$_3$ which resulted in very similar deformation and binding
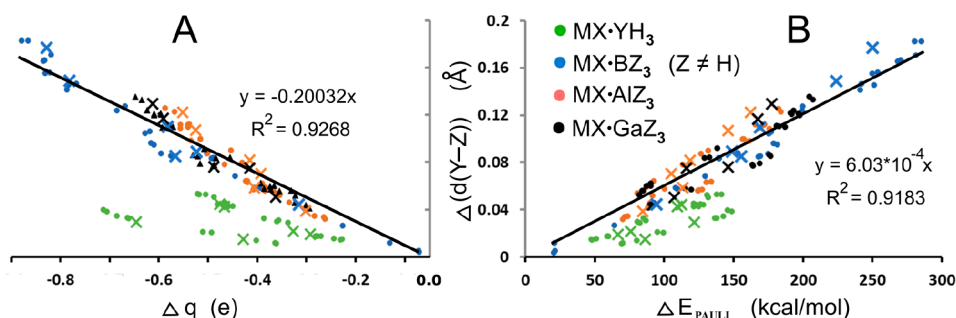
Figure 7. Dependency of the elongation of the Y−Z bonds (calculated from M062X-D3/BS1 optimized geometries) on Δq (panel A) and on ΔE_{Pauli} (panel B) for YZ_3 halides (Z = F, Cl, Br). The adducts of YH_3 hydrides (green points) are not included in either extrapolations. Points corresponding to the adducts of IrNNN and PtNCN are distinguished by crosses (×).

energies (cf. above). Figure 7 shows linear dependency of the Y−Z bond elongation on both Δq and ΔE_{Pauli} values. Very instructive straight regression lines with zero intercept could be obtained for all halides. However, Y−H bonds were much less elongated at given values of Δq and ΔE_{Pauli} (green points in Figure 7).

Comparison with $NH_3 \cdot YZ_3$ Adducts. Ammonia NH_3 is often used as a model compound representing a strong base.[1,71] Our results on $NH_3 \cdot YZ_3$ adducts are summarized in the Figure 8 and the Tables S10 and S11 and are in excellent agreement with previous experimental results.[1] $NH_3 \cdot YZ_3$
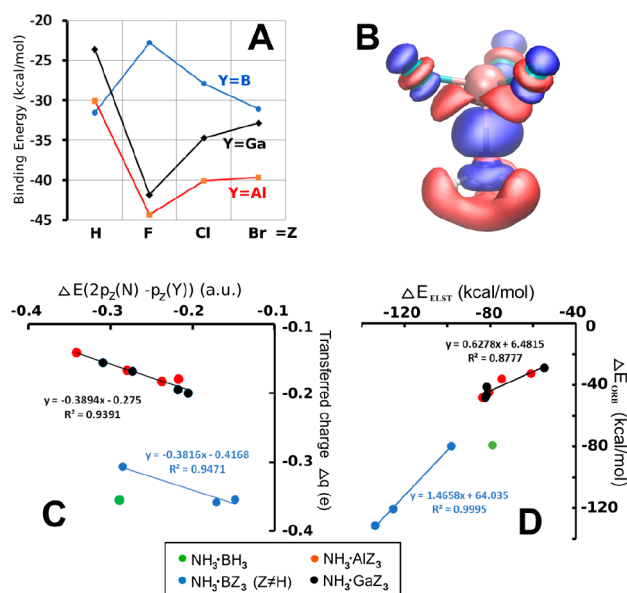

Figure 8. $NH_3 \cdot YZ_3$ adducts: (A) Dependence of binding energies on the nature of Z (cf. Figure 4). (B) Total electron density difference isosurfaces calculated from the $NH_3 \cdot AlF_3$ adduct and from the isolated NH_3 and AlF_3 structures whose total electron densities were calculated at their deformed geometries as found in the adducts (cf. Figure 6). Blue and red isosurfaces show electron accumulation (+0.0025 a.u.) and depletion (−0.0025 a.u.) regions, respectively. (C) Dependence of the transferred charge Δq on the energy difference between occupied $2p_z$ NAO of NH_3 and vacant p_z NAO of YZ_3. Both NH_3 and YZ_3 were fully optimized as isolated structures (cf. Figure 1). (D) Correlation of ΔE_{orb} and ΔE_{elst} terms for the $NH_3 \cdot YZ_3$ adducts. One regression line was constructed for adducts of both Al and Ga (black line) (cf. Figure 2). ΔE_{orb} and ΔE_{elst} terms were determined at BLYP-D3BJ/QZ4P//M062X-D3/BS1 level; the other properties were determined at M062X-D3/BS2//M062X-D3/BS1 level.

adducts were less stable than $IrX \cdot YZ_3$ but more stable than most $PtX \cdot YZ_3$ adducts (except those with X = H, CH_3 and Y = Al, Ga) (Figure 8A).

ΔE_{elst} is much more important contributor to ΔE_{Bind} in case of $NH_3 \cdot YZ_3$ adducts compared to $MX \cdot YZ_3$ due to permanent dipole moment of NH_3. Charge transfer (and ΔE_{orb}) is important only for $NH_3 \cdot BZ_3$ adducts. $NH_3 \cdot BH_3$ was the only adduct with larger value of ΔE_{orb} compared to ΔE_{elst} (Figure 8D). For Al and Ga adducts, the ΔE_{elst} term reached 2 times larger values than those of ΔE_{orb}, and the bonding between the two subunits clearly had electrostatic character. The most stable adduct was $NH_3 \cdot AlF_3$ since it was the only adduct studied with negative steric energy ($\Delta E_{Pauli} + \Delta E_{elst} < 0$). Much lower ΔE_{Pauli} term was a decisive factor of systematically higher stabilities of $NH_3 \cdot AlZ_3$ adducts compared to their Ga analogues since differences in ΔE_{elst} and ΔE_{orb} terms were much lower (cf. Figure 8D). All N·Y bonds (including N·B) had charge-transfer character ($\nabla^2 \rho(BCP) > 0$). The transferred charge was drained mainly from H atoms of NH_3 (Figure 8B) polarizing even more N−H bonds upon the adduct formation.

Comparison with $Pt(PMe_3)_2 \cdot YZ_3$ Adducts. $PtX \cdot YZ_3$ adducts showed surprisingly similar binding energies as the previously published $Pt(PMe_3)_2 \cdot YZ_3$ ones (Figure S4A).[44] Adducts of PtH and $PtCH_3$ complexes were slightly more stable by ca. −6.3 ± 4.2 kcal/mol while PtNCN and PtX (X = F, Cl, Br) complexes formed less stable adducts by 4.5 ± 3.1 kcal/mol and 11.8 ± 2.0 kcal/mol, respectively. Clearly such a good agreement in binding energies might be accidental considering differences in ligand environments and oxidation states of the platinum atom. However, ΔE_{Pauli}, ΔE_{elst}, and ΔE_{orb} terms, transferred charge and Pt−Y distances also correlated very well, and the lower the binding energy difference between corresponding Pt(II) and Pt(0) adducts, the better was an agreement in their numerical values. As a result similar properties of the systems were found: GaF_3 was the strongest base. Only adducts of boron (and especially BH_3) had prevailing covalent character, while adducts of Al and Ga were stabilized mainly by electrostatic energy (Figure S4B).

CONCLUSIONS

Detailed analyses of the adducts formation between the square planar MX complexes and YZ_3 trihydrides and trihalides of group 13 elements revealed that the main stabilization came from the donor−acceptor M·Y bond which could be basically described as a charge transfer from the $5d_{z^2}$ NAO of Pt(II) or Ir(I) to empty p_z NAO of Y. It led to pyramidalization of YZ_3 subunit and prolongation of Y−Z bonds. These structural

changes were further enhanced by Pauli repulsion between Z atoms and the MX complex.

The IrX complexes are stronger Lewis bases with by about 30 kcal/mol higher binding energies than the PtX ones. The strongest Lewis acid was GaF$_3$.

The M·Y dative bond has covalent (Y = B) or charge-transfer (Y= Al, Ga) character. However, despite the covalency the M·B bonds are weaker than their Al and Ga counterparts due to larger deformation energies of BZ$_3$ subunits.

Al and Ga adducts have considerably similar properties including the M·Y bond lengths and binding energies. Larger values of ΔE_{Pauli} for Ga adducts are compensated by more negative ($\Delta E_{orb} + \Delta E_{elst}$) sum of energies.

Neutral Pt(II) complexes with ligands showing strong σ-donation ability may probably form adducts of comparable strength as Pt(0) ones.

In the case of experimental synthesis of 1:1 PtX·YZ$_3$ adducts, an attention has to be paid to the choice of the ligands since ligands with free lone pairs (such as halogens, OH$^-$, CO, S(CH$_3$)$_2$) could be more advantageous targets for YZ$_3$ Lewis acids than the central Pt(II) atom.

The presented electronic (chemical) behavior of the MX·YZ$_3$ adducts is not dependent on the nature of X ligands or even on the metal M. Therefore, it might represent a general description of the formation of adducts between the square planar metal complexes and the group 13 hydrides and halides.

■ ASSOCIATED CONTENT

ⓈSupporting Information

The Supporting Information is available free of charge on the ACS Publications website at DOI: 10.1021/acs.inorg-chem.8b02765.

Comparison of bond lengths for *cis/trans*-[Pt-(H$_2$O)$_2$H$_2$]·BH$_3$ adducts optimized by CCSD/BS1 and various DFT/BS1 methods; comparison of binding energies for *cis/trans*-[Pt(H$_2$O)$_2$H$_2$]·BH$_3$ adducts calculated by CCSD(T)/BS2 and various DFT/BS2 methods; Gibbs free energy differences between adducts with M·Y and X·Y dative bonds; energies of 5d$_{z^2}$ and valence p$_z$ NAO's for isolated fully optimized MX and YZ$_3$ molecules; M—Y bond lengths, local topological properties of M·Y bonds calculated at the position of BCPs, mean values of M—Y—Z angles and transferred charge Δq for PtX·YZ$_3$ and IrX·YZ$_3$ adducts (X = CH$_3^-$, H$^-$, F$^-$, Cl$^-$, Br$^-$), respectively.ΔE_{Pauli}, ΔE_{elst}, ΔE_{orb}, ΔE_{disp}, ΔE_{Def}^{YZ3}, and ΔE_{Bind}, ΔH^{298} and ΔG^{298} energy values for the MX·YZ$_3$ adducts (X = CH$_3^-$, H$^-$, F$^-$, Cl$^-$, Br$^-$) are shown for M = Pt and Ir; local topological properties of M·Y bonds calculated at the position of BCPs are depicted for different Ir—Y distances in IrH·BBr$_3$ and IrH·AlBr$_3$ adducts; N—Y bond lengths, local topological properties of N·Y bonds calculated at the position of BCPs, mean values of N—Y—Z angles and transferred charge Δq for NH$_3$·YZ$_3$ adducts; ΔE_{Pauli}, ΔE_{elst}, ΔE_{orb}, ΔE_{disp}, ΔE_{Def}^{YZ3}, ΔE_{Bind}, ΔH^{298} and ΔG^{298} energy values for the NH3·YZ$_3$ adducts; exponential dependence of the absolute value of interaction energy $|\Delta E_{INT}|$ on the modified M—Y distance $[d(M-Y) - 0.82(r_M + r_Y)]$; dependence of ΔE_{INT} and ΔE_{Def}^{YZ3} on $\rho(BCP)$ and ΔE_{INT}; binding energies of Pt(PMe$_3$)$_2$·YZ$_3$ adducts and the linear correlation of ΔE_{orb} and ΔE_{elst}

terms in these adducts (data taken from the ref 44) (PDF)

Optimized Cartesian coordinates of all MX·YZ$_3$ and NH$_3$·YZ$_3$ adducts (TXT)

■ AUTHOR INFORMATION

Corresponding Author

*E-mail: chval@jcu.cz. Tel.: +420-389-037-612.

ORCID ⓘ

Zdeněk Chval: 0000-0003-1922-8390

Jaroslav V. Burda: 0000-0001-9909-8797

Notes

The authors declare no competing financial interest.

■ ACKNOWLEDGMENTS

■ REFERENCES

(1) Timoshkin, A. Y.; Suvorov, A. V.; Bettinger, H. F.; Schaefer, H. F. Role of the Terminal Atoms in the Donor−Acceptor Complexes MX3−D (M = Al, Ga, In; X = F, Cl, Br, I; D = YH3, YX3, X-; Y = N, P, As). *J. Am. Chem. Soc.* **1999**, *121* (24), 5687−5699.

(2) Smith, E. L.; Sadowsky, D.; Phillips, J. A.; Cramer, C. J.; Giesen, D. J. A Short Yet Very Weak Dative Bond: Structure, Bonding, and Energetic Properties of N2−BH3. *J. Phys. Chem. A* **2010**, *114* (7), 2628−2636.

(3) Grabowski, S. J. Boron and Other Triel Lewis Acid Centers: From Hypovalency to Hypervalency. *ChemPhysChem* **2014**, *15* (14), 2985−2993.

(4) Grabowski, S. J. π-Hole Bonds: Boron and Aluminum Lewis Acid Centers. *ChemPhysChem* **2015**, *16* (7), 1470−1479.

(5) Smith, E. L.; Sadowsky, D.; Cramer, C. J.; Phillips, J. A. Structure, Bonding, and Energetic Properties of Nitrile−Borane Complexes: RCN−BH3. *J. Phys. Chem. A* **2011**, *115* (10), 1955−1963.

(6) Buchberger, A. R.; Danforth, S. J.; Bloomgren, K. M.; Rohde, J. A.; Smith, E. L.; Gardener, C. C. A.; Phillips, J. A. Condensed-Phase Effects on the Structural Properties of FCH2CN−BF3 and ClCH2CN−BF3: A Matrix-Isolation and Computational Study. *J. Phys. Chem. B* **2013**, *117* (39), 11687−11696.

(7) Litvinenko, A. S.; Timoshkin, A. Y.; Schaefer, H. F. Thermodynamics of Thermal Decomposition of Group 13 Metal Trihalide Adducts with Piperidine: A Combined Theoretical and Experimental Study. *Polyhedron* **2006**, *25* (12), 2465−2470.

(8) Okio, C. K. Y. A.; Levason, W.; Monzittu, F. M.; Reid, G. Complexes of BX3 with EMe2 (X = F, Cl, Br, I; E = Se or Te): Synthesis, Multinuclear NMR Spectroscopic and Structural Studies. *J. Organomet. Chem.* **2017**, *848*, 232−238.

(9) Branch, C. S.; Bott, S. G.; Barron, A. R. Group 13 Trihalide Complexes of 9-Fluorenone: A Comparison of Methods for Assigning Relative Lewis Acidity. *J. Organomet. Chem.* **2003**, *666* (1−2), 23−34.

(10) Grabowski, S. J. Triel Bonds, π-Hole-π-Electrons Interactions in Complexes of Boron and Aluminium Trihalides and Trihydrides with Acetylene and Ethylene. *Molecules* **2015**, *20* (6), 11297−11316.

(11) Grabowski, S. J. Triel Bonds-Complexes of Boron and Aluminum Trihalides and Trihydrides with Benzene. *Struct. Chem.* **2017**, *28* (4), 1163−1171.

(12) Bauzá, A.; Frontera, A. Competition between Lone Pair-π, Halogen-π and Triel Bonding Interactions Involving BX3 (X = F, Cl, Br and I) Compounds: An Ab Initio Study. *Theor. Chem. Acc.* **2017**, *136* (3), 37.

(13) Cid, J.; Carbó, J. J.; Fernández, E. Disclosing the Structure/Activity Correlation in Trivalent Boron-Containing Compounds: A Tendency Map. *Chem. - Eur. J.* **2012**, *18* (40), 12794−12802.

(14) Ogawa, A.; Fujimoto, H. Lewis Acidity of Gallium Halides. *Inorg. Chem.* **2002**, *41* (19), 4888−4894.

(15) Sevastianova, T. N.; Bodensteiner, M.; Lisovenko, A. S.; Davydova, E. I.; Scheer, M.; Susliakova, T. V.; Krasnova, I. S.; Timoshkin, A. Y. Structural and Thermodynamic Properties of Molecular Complexes of Aluminum and Gallium Trihalides with Bifunctional Donor Pyrazine: Decisive Role of Lewis Acidity in 1D Polymer Formation. *Dalton Trans.* **2013**, *42* (32), 11589−11599.

(16) Bauzá, A.; Frontera, A. On the Versatility of BH2X (X = F, Cl, Br, and I) Compounds as Halogen-, Hydrogen-, and Triel-Bond Donors: An AbInitio Study. *ChemPhysChem* **2016**, *17* (20), 3181−3186.

(17) Timoshkin, A. Y.; Bodensteiner, M.; Sevastianova, T. N.; Lisovenko, A. S.; Davydova, E. I.; Scheer, M.; Graßl, C.; Butlak, A. V. Do Solid-State Structures Reflect Lewis Acidity Trends of Heavier Group 13 Trihalides? Experimental and Theoretical Case Study. *Inorg. Chem.* **2012**, *51* (21), 11602−11611.

(18) Timoshkin, A. Y.; Schaefer, H. F. Fascinating Transformations of Donor−Acceptor Complexes of Group 13 Metal (Al, Ga, In) Derivatives with Nitriles and Isonitriles: From Monomeric Cyanides to Rings and Cages. *J. Am. Chem. Soc.* **2003**, *125* (33), 9998−10011.

(19) Davydova, E. I.; Sevastianova, T. N.; Timoshkin, A. Y. Molecular Complexes of Group 13 Element Trihalides, Pentafluorophenyl Derivatives and Lewis Superacids. *Coord. Chem. Rev.* **2015**, *297-298*, 91−126.

(20) Wilkinson, G.; Birmingham, J. M. Biscyclopentadienylrhenium Hydride—A New Type of Hydride. *J. Am. Chem. Soc.* **1955**, *77* (12), 3421−3422.

(21) Scott, R. N.; Shriver, D. F.; Vaska, L. Lewis Acid Adducts of Planar Four-Coordinated D8 Complexes. Boron Trifluoride-Chlorocarbonylbis(Triphenylphosphine) Iridium and Related Systems. *J. Am. Chem. Soc.* **1968**, *90* (4), 1079−1080.

(22) Hodali, H. A. Five-Coordinated Boron Trifluoride Adducts of Platinum(II) Complexes. *J. Chem. Eng. Data* **1987**, *32* (3), 382−383.

(23) Rizzato, S.; Bergès, J.; Mason, S. A.; Albinati, A.; Kozelka, J. Dispersion-Driven Hydrogen Bonding: Predicted Hydrogen Bond between Water and Platinum(II) Identified by Neutron Diffraction. *Angew. Chem., Int. Ed.* **2010**, *49* (41), 7440−7443.

(24) Bergès, J.; Fourré, I.; Pilmé, J.; Kozelka, J. Quantum Chemical Topology Study of the Water-Platinum(II) Interaction. *Inorg. Chem.* **2013**, *52* (3), 1217−1227.

(25) Janjić, G. V.; Milosavljević, M. D.; Veljković, D. Ž.; Zarić, S. D. Prediction of Strong O−H/M Hydrogen Bonding between Water and Square-Planar Ir and Rh Complexes. *Phys. Chem. Chem. Phys.* **2017**, *19* (13), 8657−8660.

(26) Aono, S.; Mori, T.; Sakaki, S. 3D-RISM-MP2 Approach to Hydration Structure of Pt(II) and Pd(II) Complexes: Unusual H-Ahead Mode vs Usual O-Ahead One. *J. Chem. Theory Comput.* **2016**, *12* (3), 1189−1206.

(27) Kroutil, O.; Předota, M.; Chval, Z. Pt···H Nonclassical Interaction in Water-Dissolved Pt(II) Complexes: Coaction of Electronic Effects with Solvent-Assisted Stabilization. *Inorg. Chem.* **2016**, *55* (7), 3252−3264.

(28) Sánchez-de-Armas, R.; Ahlquist, M. S. G. On the Nature of Hydrogen Bonds to Platinum(II) − Which Interaction Can Predict Their Strength? *Phys. Chem. Chem. Phys.* **2015**, *17* (2), 812−816.

(29) Groenewald, F.; Raubenheimer, H. G.; Dillen, J.; Esterhuysen, C. Gold Setting the "Gold Standard" among Transition Metals as a Hydrogen Bond Acceptor − a Theoretical Investigation. *Dalton Trans.* **2017**, *46* (15), 4960−4967.

(30) Groenewald, F.; Dillen, J.; Esterhuysen, C. Ligand-Driven Formation of Halogen Bonds Involving Au(I) Complexes. *New J. Chem.* **2018**, *42* (13), 10529−10538.

(31) Kameo, H.; Kawamoto, T.; Bourissou, D.; Sakaki, S.; Nakazawa, H. Evaluation of the σ-Donation from Group 11 Metals (Cu, Ag, Au) to Silane, Germane, and Stannane Based on the Experimental/Theoretical Systematic Approach. *Organometallics* **2015**, *34* (8), 1440−1448.

(32) Martín, A. Hydrogen Bonds Involving Transition Metal Centers Acting As Proton Acceptors. *J. Chem. Educ.* **1999**, *76* (4), 578.

(33) Bontemps, S.; Gornitzka, H.; Bouhadir, G.; Miqueu, K.; Bourissou, D. Rhodium(I) Complexes of a PBP Ambiphilic Ligand: Evidence for a Metal→Borane Interaction. *Angew. Chem., Int. Ed.* **2006**, *45* (10), 1611−1614.

(34) Crossley, I. R.; Hill, A. F.; Willis, A. C. Formation of Metallaboratranes: The Missing Link. The First Iridaboratranes, [IrH(CO)(PPh3){κ3-B,S,S'-B(Mt)2R}](Ir→B) (Mt = Methimazolyl, R = Mt, H). *Organometallics* **2005**, *24* (6), 1062−1064.

(35) Bouhadir, G.; Bourissou, D. Complexes of Ambiphilic Ligands: Reactivity and Catalytic Applications. *Chem. Soc. Rev.* **2016**, *45* (4), 1065−1079.

(36) Hallman, K.; Frölander, A.; Wondimagegn, T.; Svensson, M.; Moberg, C. OH−Pd(0) Interaction as a Stabilizing Factor in Palladium-Catalyzed Allylic Alkylations. *Proc. Natl. Acad. Sci. U. S. A.* **2004**, *101* (15), 5400−5404.

(37) Stolarov, I. P.; Yakushev, I. A.; Churakov, A. V.; Cherkashina, N. V.; Smirnova, N. S.; Khramov, E. V.; Zubavichus, Y. V.; Khrustalev, V. N.; Markov, A. A.; Klyagina, A. P.; et al. Heterometallic Palladium(II)−Indium(III) and − Gallium(III) Acetate-Bridged Complexes: Synthesis, Structure, and Catalytic Performance in Homogeneous Alkyne and Alkene Hydrogenation. *Inorg. Chem.* **2018**, *57* (18), 11482−11491.

(38) Collery, P.; Morel, M.; Desoize, B.; Millart, H.; Perdu, D.; Prevost, A.; Vallerand, H.; Pechery, C.; Choisy, H.; Etienne, J. C. Combination Chemotherapy with Cisplatin, Etoposide and Gallium Chloride for Lung Cancer: Individual Adaptation of Doses. *Anticancer Res.* **1991**, *11* (4), 1529−1532.

(39) Braunschweig, H.; Gruss, K.; Radacki, K. Reactivity of Pt0 Complexes toward Gallium(III) Halides: Synthesis of a Platinum Gallane Complex and Oxidative Addition of Gallium Halides to Pt0. *Inorg. Chem.* **2008**, *47* (19), 8595−8597.

(40) Braunschweig, H.; Brunecker, C.; Dewhurst, R. D.; Schneider, C.; Wennemann, B. Lewis Acid Binding and Transfer as a Versatile Experimental Gauge of the Lewis Basicity of Fe0, Ru0, and Pt0 Complexes. *Chem. - Eur. J.* **2015**, *21* (52), 19195−19201.

(41) Tsukamoto, S.; Sakaki, S. Theoretical Study of Pt(PR3)2-(AlCl3) (R = H, Me, Ph, or Cy) Including an Unsupported Bond between Transition Metal and Non-Transition Metal Elements: Geometry, Bond Strength, and Prediction. *J. Phys. Chem. A* **2011**, *115* (30), 8520−8527.

(42) Guan, W.; Zeng, G.; Kameo, H.; Nakao, Y.; Sakaki, S. Cooperative Catalysis of Combined Systems of Transition Metal Complexes with Lewis Acids: Theoretical Understanding. *Chem. Rec.* **2016**, *16* (5), 2405−2425.

(43) Borthakur, B.; Das, S.; Phukan, A. K. Strategies toward Realization of Unsupported Transition Metal−Boron Donor−Acceptor Complexes: An Insight from Theory. *Chem. Commun.* **2018**, *54* (39), 4975−4978.

(44) Goedecke, C.; Hillebrecht, P.; Uhlemann, T.; Haunschild, R.; Frenking, G. The Dewar−Chatt−Duncanson Model Reversed — Bonding Analysis of Group-10 Complexes [(PMe3)2M−EX3] (M = Ni, Pd, Pt; E = B, Al, Ga, In, Tl; X = H, F, Cl, Br, I). *Can. J. Chem.* **2009**, *87* (10), 1470−1479.

(45) von Ahsen, B.; Bach, C.; Berkei, M.; Köckerling, M.; Willner, H.; Hägele, G.; Aubke, F. Cationic Carbonyl Complexes of Rhodium(I) and Rhodium(III): Syntheses, Vibrational Spectra, NMR Studies, and Molecular Structures of Tetrakis(Carbonyl)-Rhodium(I) Heptachlorodialuminate and -Gallate, [Rh(CO)4]-[Al2Cl7] and [Rh(CO)4][Ga2Cl7]. *Inorg. Chem.* **2003**, *42* (12), 3801−3814.

(46) Lawrence, M. A. W.; Green, K.-A.; Nelson, P. N.; Lorraine, S. C. Review: Pincer Ligands—Tunable, Versatile and Applicable. *Polyhedron* **2018**, *143*, 11−27.

(47) Slagt, M. Q.; Rodríguez, G.; Grutters, M. M. P.; Klein Gebbink, R. J. M.; Klopper, W.; Jenneskens, L. W.; Lutz, M.; Spek, A. L.; van Koten, G. Synthesis and Properties of Para-Substituted NCN-Pincer Palladium and Platinum Complexes. *Chem. - Eur. J.* **2004**, *10* (6), 1331−1344.

(48) Andrae, D.; Häußermann, U.; Dolg, M.; Stoll, H.; Preuß, H. Energy-Adjustedab Initio Pseudopotentials for the Second and Third Row Transition Elements. *Theor. Chem. Acc. Theory Comput. Model. Theor. Chim. Acta* **1990**, *77* (2), 123−141.

(49) Bergner, A.; Dolg, M.; Küchle, W.; Stoll, H.; Preuß, H. Ab Initio Energy-Adjusted Pseudopotentials for Elements of Groups 13− 17. *Mol. Phys.* **1993**, *80* (6), 1431−1441.

(50) Burda, J. V.; Zeizinger, M.; Sponer, J.; Leszczynski, J. Hydration of Cis- and Trans-Platin: A Pseudopotential Treatment in the Frame of a G3-Type Theory for Platinum Complexes. *J. Chem. Phys.* **2000**, *113* (6), 2224−2232.

(51) Zhao, Y.; Truhlar, D. G. The M06 Suite of Density Functionals for Main Group Thermochemistry, Thermochemical Kinetics, Noncovalent Interactions, Excited States, and Transition Elements: Two New Functionals and Systematic Testing of Four M06-Class Functionals and 12 Other Functionals. *Theor. Chem. Acc.* **2008**, *120* (1−3), 215−241.

(52) Grimme, S.; Antony, J.; Ehrlich, S.; Krieg, H. A Consistent and Accurate Ab Initio Parametrization of Density Functional Dispersion Correction (DFT-D) for the 94 Elements H-Pu. *J. Chem. Phys.* **2010**, *132* (15), 154104.

(53) Boys, S. F.; Bernardi, F. The Calculation of Small Molecular Interactions by the Differences of Separate Total Energies. Some Procedures with Reduced Errors. *Mol. Phys.* **1970**, *19* (4), 553−566.

(54) Becke, A. D. Density-Functional Exchange-Energy Approximation with Correct Asymptotic Behavior. *Phys. Rev. A: At., Mol., Opt. Phys.* **1988**, *38* (6), 3098.

(55) Lee, C.; Yang, W.; Parr, R. G. Development of the Colle-Salvetti Correlation-Energy Formula into a Functional of the Electron Density. *Phys. Rev. B: Condens. Matter Mater. Phys.* **1988**, *37* (2), 785.

(56) Grimme, S.; Ehrlich, S.; Goerigk, L. Effect of the Damping Function in Dispersion Corrected Density Functional Theory. *J. Comput. Chem.* **2011**, *32* (7), 1456−1465.

(57) Feller, D. The Role of Databases in Support of Computational Chemistry Calculations. *J. Comput. Chem.* **1996**, *17* (13), 1571−1586.

(58) Schuchardt, K. L.; Didier, B. T.; Elsethagen, T.; Sun, L.; Gurumoorthi, V.; Chase, J.; Li, J.; Windus, T. L. Basis Set Exchange: A Community Database for Computational Sciences. *J. Chem. Inf. Model.* **2007**, *47* (3), 1045−1052.

(59) Frisch, M. J.; Trucks, G. W.; Schlegel, H. B.; Scuseria, G. E.; Robb, M. A.; Cheeseman, J. R.; Scalmani, G.; Barone, V.; Mennucci, B.; Petersson, G. A.; Nakatsuji, H.; Caricato, M.; Li, X.; Hratchian, H. P.; Izmaylov, A. F.; Bloino, J.; Zheng, G.; Sonnenberg, J. L.; Hada, M.; Ehara, M.; Toyota, K.; Fukuda, R.; Hasegawa, J.; Ishida, M.; Nakajima, T.; Honda, Y.; Kitao, O.; Nakai, H.; Vreven, T.; Montgomery, J. A., Jr.; Peralta, J. E.; Ogliaro, F.; Bearpark, M.; Heyd, J. J.; Brothers, E.; Kudin, K. N.; Staroverov, V. N.; Kobayashi, R.; Normand, J.; Raghavachari, K.; Rendell, A.; Burant, J. C.; Iyengar, S. S.; Tomasi, J.; Cossi, M.; Rega, N.; Millam, J. M.; Klene, M.; Knox, J. E.; Cross, J. B.; Bakken, V.; Adamo, C.; Jaramillo, J.; Gomperts, R.; Stratmann, R. E.; Yazyev, O.; Austin, A. J.; Cammi, R.; Pomelli, C.; Ochterski, J. W.; Martin, R. L.; Morokuma, K.; Zakrzewski, V. G.; Voth, G. A.; Salvador, P.; Dannenberg, J. J.; Dapprich, S.; Daniels, A. D.; Farkas, O.; Foresman, J. B.; Ortiz, J. V.; Cioslowski, J.; Fox, D. J. *Gaussian 09*, revision D.01; Gaussian, Inc.: Wallingford, CT, 2009.

(60) Keith, T. A. *AIMAll*, version 10.11.24; TK Gristmill Software: Overland Park, KS, 2010. aim.tkgristmill.com

(61) Glendening, E. D.; Reed, A. E.; Carpenter, J. E.; Weinhold, F. *NBO* 3.1; Theoretical Chemistry Institute and Department of Chemistry, University of Wisconsin: Madison, WI, 1990.

(62) *ADF2017*; SCM, Theoretical Chemistry, Vrije Universiteit, Amsterdam, The Netherlands, 2017.

(63) Ziegler, T.; Rauk, A. Calculation of Bonding Energies by Hartree-Fock Slater Method.1. Transition-State Method. *Theor. Chim. Acta* **1977**, *46* (1), 1−10.

(64) Mitoraj, M.; Michalak, A.; Ziegler, T. A Combined Charge and Energy Decomposition Scheme for Bond Analysis. *J. Chem. Theory Comput.* **2009**, *5* (4), 962−975.

(65) Mitoraj, M. P.; Zhu, H.; Michalak, A.; Ziegler, T. On the Origin of the Trans-Influence in Square Planar D8-Complexes: A Theoretical Study. *Int. J. Quantum Chem.* **2009**, *109* (14), 3379−3386.

(66) van Lenthe, E.; van Leeuwen, R.; Baerends, E. J.; Snijders, J. G. Relativistic Regular Two-Component Hamiltonians. *Int. J. Quantum Chem.* **1996**, *57* (3), 281−293.

(67) Durango-García, C. J.; Jiménez-Halla, J. O. C.; López-Cardoso, M.; Montiel-Palma, V.; Muñoz-Hernández, M. A.; Merino, G. On the Nature of the Transition Metal−Main Group Metal Bond: Synthesis and Theoretical Calculations on Iridium Gallyl Complexes. *Dalton Trans.* **2010**, *39* (44), 10588−10589.

(68) Chval, Z.; Sip, M.; Burda, J. V. The Trans Effect in Square-Planar Platinum(II) Complexes—A Density Functional Study. *J. Comput. Chem.* **2008**, *29* (14), 2370−2381.

(69) Cordero, B.; Gómez, V.; Platero-Prats, A. E.; Revés, M.; Echeverría, J.; Cremades, E.; Barragán, F.; Alvarez, S. Covalent Radii Revisited. *Dalton Trans.* **2008**, *0* (21), 2832−2838.

(70) Romm, I. P.; Noskov, Y. G.; Malkov, A. A. The Strength and Length of Donor-Acceptor Bonds in Molecular Complexes. *Russ. Chem. Bull.* **2007**, *56* (10), 1935−1944.

(71) Bessac, F.; Frenking, G. Why Is BCl3 a Stronger Lewis Acid with Respect to Strong Bases than BF3? *Inorg. Chem.* **2003**, *42* (24), 7990−7994.

Article OD2

Dvořáčková O., Chval Z.

Tuning the Reactivity and Bonding Properties of Metal Square-Planar Complexes by the Substitution(s) on the Trans-Coordinated Pyridine Ring.

Correction to "Tuning the Reactivity and Bonding Properties of Metal Square-Planar Complexes by the Substitution(s) on the Trans-Coordinated Pyridine Ring".

Abstract

The kinetics of the hydration reaction on trans-$[Pt(NH_3)_2(pyrX)Cl]^+$ (pyr = pyridine) complexes (X = OH, Cl, F, Br, NO_2, NH_2, SH, CH3, C≡CH, and DMA) was studied by density functional theory calculations in the gas phase and in water solution described by the implicit polarizable continuum model method. All possible positions ortho, meta, and para of the substituent X in the pyridine ring were considered. The substitution of the pyr ligand by electron-donating X's led to the strengthening of the Pt−N1(pyrX) (Pt−N_{pyrX}) bond and the weakening of the trans Pt−Cl or Pt−Ow bonds. The electron-withdrawing X's have exactly the opposite effect. The strengths of these bonds can be predicted from the basicity of sigma electrons on the N_{pyrX} atom determined on the isolated pyrX ligand. As the pyrX ring was oriented perpendicularly with respect to the plane of the complex, the nature of the X···Cl electrostatic interaction was the decisive factor for the transition-state (TS) stabilization which resulted in the highest selectivity of ortho-substituted systems with respect to the reaction rate. Because of a smaller size of X's, the steric effects influenced less importantly the values of activation Gibbs energies $\Delta G^{\ddagger}$ but caused geometry changes such as the elongation of the Pt−N_{pyrX} bonds. Substitution in the meta position led to the highest $\Delta G^{\ddagger}$ values for most of the X's. The changes of $\Delta G^{\ddagger}$ because of electronic effects were the same in the gas phase and the water solvent. However, as the water solvent dampened electrostatic interactions, 2200 and 150 times differences in the reaction rate were observed between the most and the least reactive mono-substituted complexes in the gas phase and

the water solvent, respectively. An additional NO_2 substitution of the pyr-NO_2 ligand further decelerated the rate of the hydration reaction, but on the other hand, the poly-NH_2 complexes were no more reactive than the fastest o-NH_2 system. In the gas phase, the poly-X complexes showed the additivity of the substituent effects with respect to the Pt–ligand bond strengths and the ligand charges.

The Supporting Information is available free of charge at https://pubs.acs.org/doi/10.1021/acsomega.0c01161.

Article

Tuning the Reactivity and Bonding Properties of Metal Square-Planar Complexes by the Substitution(s) on the Trans-Coordinated Pyridine Ring

Olga Dvořáčková and Zdeněk Chval*
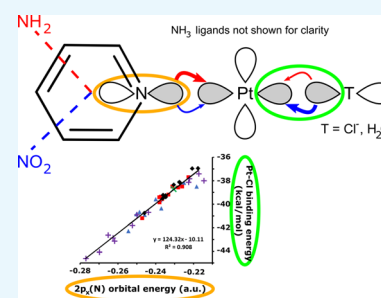
Read Online

ACCESS | Metrics & More | Article Recommendations | SI Supporting Information

ABSTRACT: The kinetics of the hydration reaction on *trans*-[Pt(NH$_3$)$_2$(pyrX)Cl]$^+$ (pyr = pyridine) complexes (X = OH$^-$, Cl$^-$, F$^-$, Br$^-$, NO$_2^-$, NH$_2$, SH$^-$, CH$_3$, C≡CH, and DMA) was studied by density functional theory calculations in the gas phase and in water solution described by the implicit polarizable continuum model method. All possible positions ortho, meta, and para of the substituent X in the pyridine ring were considered. The substitution of the pyr ligand by electron-donating X's led to the strengthening of the Pt−N1(pyrX) (Pt−N$_{pyrX}$) bond and the weakening of the trans Pt−Cl or Pt−O$_w$ bonds. The electron-withdrawing X's have exactly the opposite effect. The strengths of these bonds can be predicted from the basicity of sigma electrons on the N$_{pyrX}$ atom determined on the isolated pyrX ligand. As the pyrX ring was oriented perpendicularly with respect to the plane of the complex, the nature of the X···Cl electrostatic interaction was the decisive factor for the transition-state (TS) stabilization which resulted in the highest selectivity of ortho-substituted systems with respect to the reaction rate. Because of a smaller size of X's, the steric effects influenced less importantly the values of activation Gibbs energies $\Delta G^\ddagger$ but caused geometry changes such as the elongation of the Pt−N$_{pyrX}$ bonds. Substitution in the meta position led to the highest $\Delta G^\ddagger$ values for most of the X's. The changes of $\Delta G^\ddagger$ because of electronic effects were the same in the gas phase and the water solvent. However, as the water solvent dampened electrostatic interactions, 2200 and 150 times differences in the reaction rate were observed between the most and the least reactive mono-substituted complexes in the gas phase and the water solvent, respectively. An additional NO$_2$ substitution of the pyrNO$_2$ ligand further decelerated the rate of the hydration reaction, but on the other hand, the poly-NH$_2$ complexes were no more reactive than the fastest *o*-NH$_2$ system. In the gas phase, the poly-X complexes showed the additivity of the substituent effects with respect to the Pt−ligand bond strengths and the ligand charges.

INTRODUCTION

Platinum anticancer complexes are administered in their inactive neutral form as prodrugs, and at least one hydrolysis step is needed for their activation. The activated drug reacts rapidly with DNA or proteins, and the hydrolysis step is the rate-determining step of the whole process. Because platinum binding to proteins is probably responsible for the side effects of the drug,[1] the activation should not be too fast to enable the drug to reach the nuclei of the malignant cells. Thus, the rate of hydrolysis is one of the important factors which should be considered for new drug development.

The reactivity of square-planar Pt(II)-complexes is driven by the trans effect; that is, the stability of the ligand is strongly influenced by the ligand in the trans position.[2−9] It is a kinetic phenomenon whose origin lies in reactant destabilization and/or the transition state (TS) stabilization. The reactant destabilization is manifested itself by the Pt−trans ligand bond elongation, and it is sometimes called the trans influence.[10] The trans effect can be explained by different σ-donation and π-back-donation abilities of the ligands[6] and depends on the nature of the coordinating atom and its hardness.[7] However, the chemistry of currently used drugs[11] is

rather limited because only slowly hydrolyzing compounds are needed, considering the length of the delivery route. Thus, the non-leaving groups are always bound to the central Pt(II) by a nitrogen atom and are either two ammines or a diammine with an attached carbohydrate residue. The non-leaving group influence interactions with the proteins affecting cellular uptake of the drug and the repair of DNA-drug lesions.[12] The influence of the leaving groups on the biotransformation kinetics of the drug is less clear but two chlorine atoms in the first-generation drug cisplatin were displaced by bidentate groups (e.g. cyclobutanedicarboxylate or oxalate group) bound by the oxygen atom to the platinum central atom in the second- and third-generation drugs. The mechanism of hydrolysis of bidentate groups is still not well understood,

and it is not clear in which form these drugs react with DNA.[13−15]

The substitution effects were explored on Pt(II)-complexes with different *N,N,N*-tridentate and *N,N*-bidentate ligands which mainly differ in π-back-donation ability. Strong π-acceptor ligands increase the electrophilicity of the Pt(II) center increasing the rate of the substitution.[16−22]

Complexes with aromatic monodentate ligands having anticancer properties were also reported including those based on pyridine and its derivatives.[23−27] To minimize the inactivating interactions with thiols, a sterically hindered complex AMD 473 with 2-picoline (2-methylpyridine) ligand was synthesized.[28] The reactivity of Pt(II) complexes with 2- and 3-picoline as ligands was experimentally compared by Sadler and co-workers. The complex with 2-picoline showed a 45 times slower hydration reaction of the Cl⁻ ligand in the trans position which was attributed to the steric effect of the methyl group on the pyridine ring.[29] Hydrolysis of AMD 473 and its binding to guanine were studied also theoretically.[30−32] The influence of the substitution in the para position of the pyridine ring on the spin densities and NMR spectra was studied for analogues of the Ru(III) complex NAMI.[33]
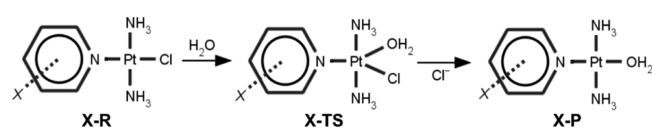
Monofunctional Pt complexes, which offer unique ways of transmembrane transport and DNA interactions, form another promising group of anticancer drugs. Pyriplatin and phenanthriplatin contain three non-leaving ligands: two ammines with pyridine and phenanthridine, respectively.[23,34] Despite rather negligible DNA structure deformation, the inhibition of transcription was seen in vitro as well as in vivo.[35,36] The antineoplastic effect of phenanthriplatin was discovered by Lippard and co-workers.[37,38] Very recently, the importance of stacking interactions for the binding of phenanthriplatin to DNA was shown in studies of Veclani at al. and Almaqwashi et al.[39,40]

The replacement of chloride ligands by water ligands in cisplatin and its derivatives was a subject of many previous studies[41−46] and was recently reviewed by Ahmad[47] and by Kozelka.[48]

The substitution on the pyr ring affects the electron density on the coordinating atom through the inductive and resonance effects. In this study, we explored how the substitutions on the aromatic non-leaving group in the trans position influence the reactivity of the Pt(II)-complexes. We used *trans*-[Pt-(NH₃)₂(pyrX)Cl]⁺ (pyrX = pyridine with the X substituent) complexes (X = OH⁻, Cl⁻, F⁻, Br⁻, NO₂⁻, NH₂, SH⁻, CH₃, C≡CH, DMA = dimethylamine) as the model compounds. We studied how the stability of Pt−pyrX, Pt−Cl, and Pt−w (w = water) bonds and the kinetics of the hydration reaction are affected by the nature and the position of the X in the pyrX ligand (Scheme 1).

All possible positions ortho, meta, and para of the X in the pyr ring were considered. X was represented by electron-

donating (NH₂, OH, and SH) and electron-withdrawing (C≡CH, and NO₂) groups as well as by halides (F, Cl, and Br) with mixed (resonance) donating and (inductive) withdrawal effects.

Because of a large number of optimized reaction pathways, only results for X = NH₂ and X = NO₂ as the main representatives of electron-donating and electron-withdrawing groups, respectively, together with reference non-substituted X = H structures are shown in most tables in the text. Complete versions of the respective tables can be found in the Supporting Information.

Finally, the metal complexes with poly-substituted pyrX (poly-X) ligands were considered. The reasons were threefold: (1) to evaluate more generally the limits for $\Delta G^{\ddagger}$ values due to substituent effects; (2) to test the additivity of substituent effects with respect to the bond strengths, bond lengths, NPA ligand charges, and $\Delta G^{\ddagger}$ values; and (3) to provide an independent set of structures for the validity testing of the $2p_x(N_{pyrX})$ natural atomic orbital (NAO) energy as the predictor of the Pt−ligand bond strengths and $\Delta G^{\ddagger}$ activation free energies (see below). We used NH₂ and NO₂ ligands as the representatives of electron-donating and electron-withdrawing groups, respectively. Furthermore, we used fluorine as the ligand with a small size and high electronegativity. Its derivatives may have interesting properties and found many applications mainly as agrochemicals and pharmaceuticals.[49] All poly-X ligands considered in this contribution are shown in Scheme 2.

Scheme 2. Poly-X Ligands Considered in This Study and Their Designation (X = F, NH₂, NO₂)
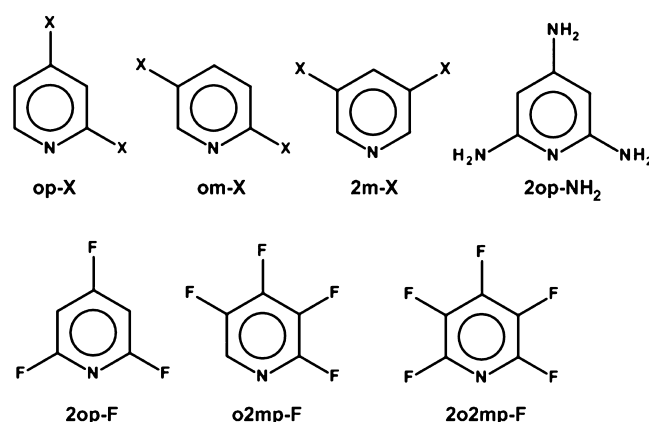
RESULTS AND DISCUSSION

Structure Labeling. The designation of the complexes with pyrX ligands reflects the position of the X on the pyr ring with respect to the N_{pyrX} atom: ortho (o-), meta (m-), and para (p-). Thus, reactant structures are denoted as **o-(m-, p-)X-R**. For corresponding transitions states and product structures, the letter 'R' is replaced by 'TS' and 'P', respectively. **X-R** and **X-P** structures represent isolated complexes without weakly bound H₂O and Cl⁻ ligands, respectively, and they were used for the evaluation of bonding properties and the electronic structure.

The same principle will be used for the complexes with the poly-X ligand for which **o-(m-, p-)X** will be replaced by the designation from Scheme 2.

Scheme 1. Reaction Mechanism of the Hydration Reactions Studied in This Contribution[a]

[a]All reaction pathways proceeded over pentacoordinated **X-TS** transition state structures.

Table 1. Gas Phase NPA Charges of the N_{pyrX} Atom ($q(N_{pyrX})$, in e) Calculated in the Isolated pyrX Ligands and in the X-R and X-P Complexes

X/position	PyrX			X-R			X-P		
	o-	m-	p-	o-	m-	p-	o-	m-	p-
H	−0.459			−0.503			−0.452		
DMA	−0.527	−0.444	−0.504	−0.530	−0.482	−0.553	−0.504	−0.423	−0.480
NH₂	−0.522	−0.443	−0.497	−0.551	−0.481	−0.547	−0.493	−0.426	−0.499
Br	−0.509	−0.476	−0.493	−0.535	−0.491	−0.510	−0.462	−0.439	−0.490
SH	−0.501	−0.443	−0.471	−0.537	−0.488	−0.522	−0.486	−0.436	−0.478
OH	−0.491	−0.442	−0.485	−0.564	−0.486	−0.530	−0.510	−0.433	−0.482
F	−0.486	−0.440	−0.470	−0.544	−0.489	−0.516	−0.502	−0.440	−0.467
Cl	−0.472	−0.442	−0.460	−0.531	−0.491	−0.510	−0.485	−0.441	−0.464
CH₃	−0.479	−0.456	−0.467	−0.514	−0.496	−0.511	−0.460	−0.444	−0.462
C≡CH	−0.437	−0.453	−0.453	−0.492	−0.498	−0.508	−0.445	−0.446	−0.464
NO₂	−0.420	−0.446	−0.430	−0.503	−0.497	−0.490	−0.467	−0.449	−0.445

Table 2. Pt−pyrX Interaction (X = H, NH₂, NO₂) in the Gas Phase Optimized X-R, X-TS, and X-P Structures: Pt−N_{pyrX} Bond Lengths (in Å); Total NPA Charges of the Pt Atom ($q(Pt)$) and pyrX Ligands ($q(pyrX)$) (in e); and ETS-NOCV Energy Decomposition Terms ΔE_{Pauli}, ΔE_{elst}, ΔE_{orb}, ΔE_{disp}, ΔE_{orb}^{σ}, and ΔE_{orb}^{π} Obtained at the BLYP-D3BJ/TZ2P//B3LYP/BS1 Level[a]

		Pt−N_{pyrX}	$q(Pt)$	$q(pyrX)$	ΔE_{Pauli}	ΔE_{elst}	ΔE_{orb}	ΔE_{disp}	ΔE_{orb}^{σ}	ΔE_{orb}^{π}	ΔE_{bind}
					X-R						
H		2.081	0.617	0.241	127.6	−122.5	−61.6	−7.2	−40.7	−11.6	−65.7
NH₂	o-	2.086	0.601	0.257	135.6	−129.9	−64.5	−9.0	−41.2	−10.9	−69.9
	m-	2.078	0.616	0.254	129.7	−127.4	−63.4	−7.4	−41.8	−10.3	−70.4
	p-	2.077	0.612	0.268	130.5	−131.0	−64.0	−7.3	−42.5	−12.1	−73.8
NO₂	o-	2.111	0.613	0.205	114.4	−103.3	−57.7	−10.2	−34.7	−11.6	−57.5
	m-	2.089	0.618	0.220	120.3	−108.0	−59.5	−7.3	−38.0	−10.4	−55.6
	p-	2.084	0.618	0.221	122.8	−109.6	−60.6	−7.2	−38.6	−12.7	−57.5
					X-TS						
H		2.046	0.791	0.294	174.2	−147.2	−78.6	−7.6	−53.4	−12.5	−62.7
NH₂	o-	2.050	0.770	0.312	192.7	−160.6	−85.9	−9.8	−57.4	−12.5	−67.1
	m-	2.044	0.789	0.304	176.9	−152.4	−80.8	−7.8	−54.8	−10.7	−67.5
	p-	2.043	0.784	0.319	177.0	−155.4	−81.5	−7.7	−55.7	−12.7	−71.1
NO₂	o-	2.072	0.799	0.243	159.6	−128.2	−73.2	−10.7	−45.6	−12.5	−54.5
	m-	2.053	0.797	0.269	166.8	−133.1	−75.8	−7.7	−49.8	−10.9	−52.5
	p-	2.050	0.799	0.268	169.6	−134.8	−77.1	−7.6	−50.5	−13.7	−52.4
					X-P						
H		2.011	0.749	0.424	147.3	−153.1	−101.7	−7.5	−64.2	−19.6	−114.3
NH₂	o-	2.016	0.736	0.439	152.7	−159.0	−105.1	−9.5	−63.9	−18.9	−120.4
	m-	2.007	0.745	0.437	151.0	−162.4	−105.8	−7.7	−66.0	−19.3	−123.7
	p-	2.005	0.738	0.450	152.6	−168.4	−107.5	−7.6	−66.8	−22.3	−130.0
NO₂	o-	2.038	0.780	0.369	131.8	−128.7	−97.0	−10.1	−55.2	−19.1	−102.7
	m-	2.016	0.757	0.404	139.4	−132.5	−100.1	−7.6	−61.4	−19.6	−99.3
	p-	2.014	0.757	0.404	141.0	−133.1	−100.1	−7.5	−61.5	−21.1	−98.6

[a]ΔE_{bind} energy values were calculated at the B3LYP-D3BJ/BS2//B3LYP/BS1 level. All energy values are in kcal/mol. The data for all X's are shown in Table S1.

The reaction energetics of the hydration reactions were determined by the supermolecular approach. Here, "_w" and "_Cl" suffixes in **o-(m-, p-)X-R_w** reactants and **o-(m-, p-)X-P_Cl** products represent entering water and leaving chloride anion, respectively, being associated to Pt-complexes by H-bonding.

Electronic Structure of the Isolated pyrX Ligands. The influence of substitution effects on the reactivity of aromatic systems was studied in many previous studies.[50−52] In the pyrX ring, the π-electrons are shifted in accordance with the mesomeric effect. For electron-donating NH₂ substituent, π-electron density is increased on atoms in the ortho and para positions with respect to NH₂ while the opposite is true for the electron-withdrawing X such as NO₂ (Figure S1). However, the σ-electrons are shifted independently and in fact contrarily with respect to π-electrons.[50] For p-NH₂, the density of σ-electrons is decreased on the N_{pyrX} atom while the opposite is true for p-NO₂ (Figure S1).

Looking at atomic NPA charges, the shifts of the σ-electrons are masked by quantitatively larger shifts of the π-electrons. Values of NPA charge of the N_{pyrX} atom ($q(N_{pyrX})$) in pyrX molecules are shown in Table 1. As expected, in the isolated pyrX molecule, $q(N_{pyrX})$ is increased in electron-donating groups in ortho or para positions. The electron-withdrawing NO₂ group lowers electron density in all ring atoms with the least effect for atoms in the meta position. Thus, $q(N_{pyrX})$ is almost independent on the nature of the X when being bound in the meta position.
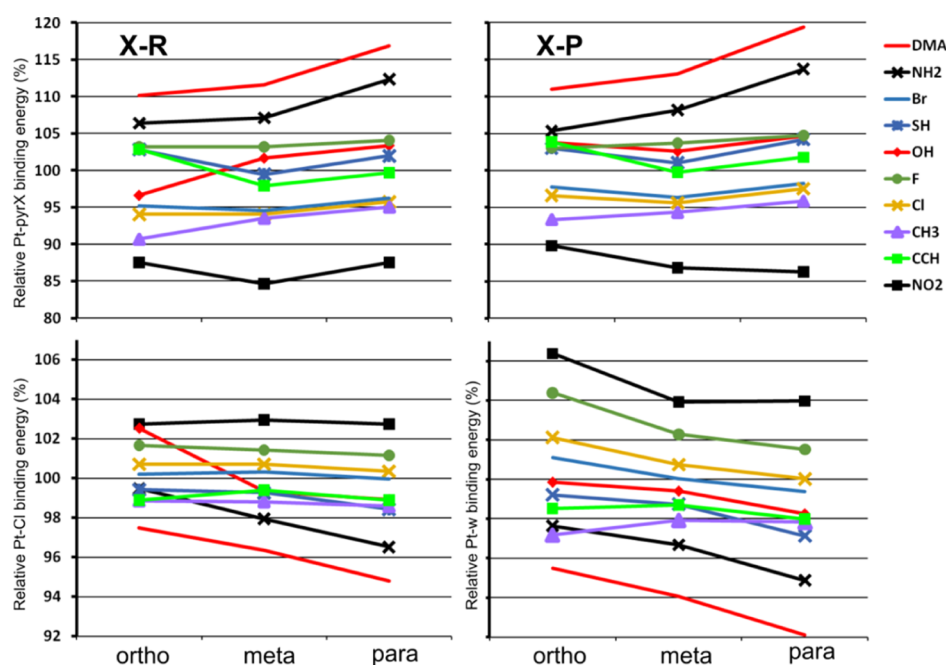
Figure 1. Relative Pt−pyrX (upper panels) and Pt−Cl and Pt−w (lower left and right panels, respectively) gas phase binding energies calculated with respect to the strength of the bonds in the non-substituted **H-R** and **H-P** complexes (set as 100%). The values of reference Pt−pyrH binding energies in **H-R** and **H-P** complexes are −65.7 and −114.3 kcal/mol, respectively (Table 2). Reference values for Pt−Cl and Pt−w bonds are −248.7 and −46.8 kcal/mol, respectively (Table 3).

Strength of the Pt−pyrX Bonds. The differences of $q(N_{pyrX})$ between the positional isomers in metallic **X-R** and **X-P** complexes were qualitatively similar to the isolated pyrX ligands (Table 1) and are discussed in more detail below. The Pt−pyrX bond was stabilized mainly by electrostatic energy ΔE_{elst} due to +e and +2 e total charges of metal complex fragments in **X-R** and **X-P** (Table 2 and Table S1), respectively. The binding was accompanied by the charge transfer and polarization effects whose extent strongly depended on the charge of the complex. As expected, the amount of transferred negative charge from pyrX toward the metal was much higher in doubly charged **X-P** products compared to **X-R** reactants. For X = H, the respective pyrH charges were 0.424 and 0.241 (Table 2). The amounts of ΔE_{orb} energy are about one-half (52 ± 2%) and two-thirds (69 ± 3%) of the values of ΔE_{elst} energy in **X-R** and **X-P**, respectively (cf. below).

Pt−pyrX interaction energies were almost two (1.77 ± 0.03) times higher for **X-P** than for **X-R**, and all stabilizing terms contributed to this difference (Table 2 and Table S1). The nature of the X on the pyrX ring influenced strongly the strength of the Pt−pyrX bond being weakened by electron-withdrawing X's and made stronger by electron-donating ones. The binding energies were usually larger for para-X complexes than for otho-X and meta-X ones (Figure 1). For **X-R**, the highest value of the binding energy was obtained for *p*-DMA-R (−76.8 kcal/mol) while the lowest for *m*-NO₂-R (−55.6 kcal/mol).

Electron-donating X's promoted higher charge transfer from the pyrX ligand to the Pt atom by up to 10% (Table 2 and Table S1) being caused by stronger σ-donation. Five most important ETS-NOCV deformation density contributions describing the formation of the Pt−N$_{pyrX}$ bond in **H-R**, **H-TS**, and **H-P** structures are shown in Figure S2. The σ-donation energy ΔE_{orb}^{σ} and π-donation energy $\Delta E_{orb}^{\pi\pi}$

contributions were the most stabilizing terms for all structures. The σ-donation energy ΔE_{orb}^{σ} contributions correlated well with total ΔE_{orb} energies for meta-X and para-X subsets (Figure 2B and Figure S3) accounting for 65.2 ± 0.8, 67.1 ± 0.9, and 61.7 ± 0.8% of their values for **X-R**, **X-TS**, and **X-P** structures, respectively.

For ortho-X's, the correlation was worse (Figure 2B and Figure S3), and relative importance of ΔE_{orb}^{σ} was slightly lower (by 2−3%) due to the existence of X···Pt and X···ligand nonbonding interactions in some structures (Figure S4). Similar information can be also seen from the dependence of Pt−pyrX binding energy on the transferred $q(pyrX)$ charge. The amount of the total transferred charge from the pyrX ligand to the metal complex correlated very well with the Pt−N$_{pyrX}$ bond strength for m-X and p-X subsets (Figure S5). For the o-X subset, the correlation was worse with a less steep slope compared to m-X and p-X subsets and R^2 values 0.807, 0.690, and 0.799 for **X-R**, **X-TS**, and **X-P** structures, respectively (Figure S5). It reflected the existence of additional charge transfer channels (nonbonding interactions of X with Pt or NH₃ ligands) besides the Pt−N$_{pyrX}$ bond (cf. Figure S4).

The dependence of ΔE_{bind}^{pyrX} on the Pt−N$_{pyrX}$ bond lengths was steeply linear for meta-X and para-X complexes (Figure 2A). The ortho-X complexes had clearly larger Pt−N$_{pyrX}$ bond lengths for given values of ΔE_{bind}^{pyrX}, and the correlation between the two variables was also linear for all o-X's including those not involved in any nonbonding interactions (*o*-CH₃) but with exception of *o*-DMA as the bulkiest X. *o*-DMA complexes showed a substantial Pt−N$_{pyrX}$ bond elongation at a large value of ΔE_{bind}^{pyrX} (Figure 2A and Figure S3). Thus, the steric hindrance should be responsible for the Pt−N$_{pyrX}$ bond elongation.

No clear trends were found for the π-bonding energy $\Delta E_{orb}^{\pi\pi}$ and $\Delta E_{orb}^{\pi\sigma}$ contributions which involve π and σ orbitals of the pyrX ring, respectively, as the main source of the transferred
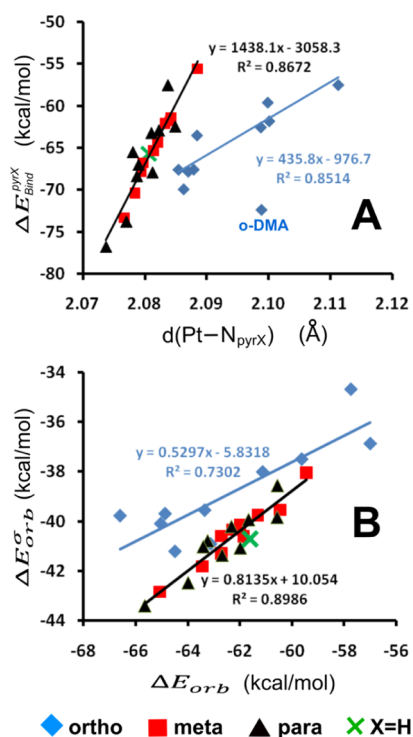
Figure 2. **X-R** structures: panel A: dependence of pyr-X ligand binding energies on the Pt−N$_{pyrX}$ bond lengths. The *o*-DMA point was not included in the regression analysis for the ortho-X subset (blue line). Panel B: dependence of the *σ*-donation energy ΔE^{σ}_{orb} contributions on total ΔE_{orb} energies. One regression line was constructed for both meta-X and para-X subsets in the two graphs (black lines). The graphs for **X-TS** and **X-P** structures are shown in Figure S3.

electrons (Figure S2). $\Delta E^{\pi\pi}_{orb}$ was always the second most stabilizing contribution, and it was enhanced slightly for the CCH and NO$_2$ X's with conjugated multiple bonds with respect to the pyr ring. This term was much more important than $\Delta E^{\pi\sigma}_{orb}$ which could be mixed with the *σ*-back-donation or nonbonding interaction contributions in some ortho-X systems (Figure S4). Note that the *π*-back-donation was not apparent in the NOCV analysis possibly due to the positive charge of the Pt(II) fragment. For example, the *π*-back-donation transferred charges of 0.005, 0.001, and 0.009 e were calculated by the charge decomposition analysis,[53] as provided by the Multiwfn program[54] for the Pt−N$_{pyrX}$ bonds in **H-R**, *p*-NH$_2$-R, and *p*-NO$_2$-R structures, respectively.

Despite the positive charge of pyrX ligands, the negative NPA charge on the N$_{pyrX}$ atom ($q(N_{pyrX})$) increased by about 10% (varying from 5.6% for *o*-NH$_2$-R up to 19.7% for *o*-NO$_2$-R, cf. Table 1) in **X-R** reactants and almost did not change in **X-P** products compared to the isolated pyrX ligand. It was caused by the polarization of the aromatic pyrX ligand upon binding with the positively charged metal complex. The transferred charge was drained from the CH and CX groups of the pyrX ligand roughly following the order para > meta > ortho (cf. ETS-NOCV deformation density contributions in Figure S2).

The changes of total electron densities with respect to the **H-R** structure caused by the H → X substitution are shown in Figure 3 for *p*-NH$_2$-R and *p*-NO$_2$-R structures. These differences reflected only pure electronic effects caused by the H → X substitution not considering accompanying
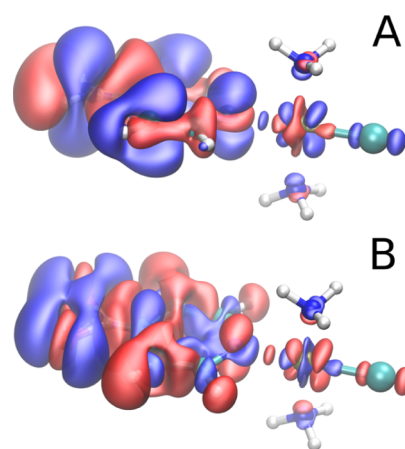

Figure 3. Electron density difference isosurfaces of *p*-NH$_2$-R (A) and *p*-NO$_2$-R (B) structures with respect to the reference **H-R** structure which show electron accumulation (blue: 0.0004 a.u.) and depletion (red: −0.0004 a.u.) regions caused by *p*-NH$_2$ (A) and *p*-NO$_2$ (B) substitution of the pyr ring. Electron densities were calculated on the **H-R** geometry for all atoms of respective complexes except the atoms of the X substituent whose positions were optimized.

changes of molecular structures. The shifts of electron density within the pyrX ligand were very similar to those in the isolated pyrX system (cf. Figure S1). With respect to the Pt(II) fragment, the substitution by the electron-donating NH$_2$ group led to exactly opposite changes of electron density compared to the electron-withdrawing NO$_2$ group (Figure 3). Thus, let us describe only the changes caused by the H → *p*-NH$_2$ substitution here: (1) the strengthening of the Pt−pyrX bond could be clearly documented by an increase of electron density roughly in the middle of this bond. (2) The electron density was increased in the p$_x$ orbital of the trans Cl$^-$ ligand (if the *x* axis is oriented along the Pt−Cl bond). It reflected the lower *σ*-donation and the weakening of the Pt−Cl bond (cf. below). (3) The changes of the total charge on the Pt atom ($q(Pt)$) were small for **X-R** structures (Table 2 and Table S1) due to compensating effects on the 5d NAO's: electron density was increased in 5d$_{xy}$ but decreased in 5d$_{x^2-y^2}$ orbital (Figure 3). However, for the water trans ligand as a weaker electrophile, the changes of $q(Pt)$ were larger and $q(Pt)$ was decreased/increased for electron-donating/withdrawing X's (Table 2 and Table S1).

We used also the concept of the activation strain model[55] and performed the fragment energy decomposition of the Pt−pyrX bond for the structures in Figure 3. For *p*-NH$_2$-R (*p*-NO$_2$-R), the Pauli, electrostatic, orbital, and dispersion energies were 130.5 (125.0), −130.9 (−111.4), −63.7 (−61.3), and −7.2 (−7.3) kcal/mol, respectively. A comparison of these values and also the ones for **H-R** (Table 2) confirmed the influence of X on the strength of the Pt−pyrX bond mainly through electrostatic energy which is in agreement with the analyses on fully optimized structures (cf. above).

Trans Influence: The Strength of the Pt−Cl and Pt−w Bonds. Trans influence is a thermodynamic phenomenon in which the binding of a more strongly bound ligand weakens the Pt−trans ligand bond which becomes elongated. Thus, the electron-withdrawing X's strengthened the Pt−trans ligand bond, and the opposite was true for electron-donating ones (Table 3 and Table S2). The influence of the X on the strengths of Pt−Cl and Pt−w bonds was roughly 8 and 14% of

Table 3. Interactions of Cl⁻ and Water Ligands with the Rest of the Complex in the Gas Phase Optimized X-R and X-P Structures (X = H, NH₂, NO₂), Respectively: Pt−Cl, Pt−O_w Bond Lengths (in Å); the Total NPA Charges of the Cl⁻ and Water Ligands (q(Cl), q(w)); and ETS-NOCV Energy Decomposition Terms ΔE_{Pauli}, ΔE_{elst}, ΔE_{orb}, ΔE_{disp}, ΔE_{orb}^{σ}, and ΔE_{orb}^{π} Obtained at the BLYP-D3BJ/TZ2P//B3LYP/BS1 Level[a,b]

X-R		Pt−Cl	q(Cl)	ΔE_{Pauli}	ΔE_{elst}	ΔE_{orb}	ΔE_{disp}	ΔE_{orb}^{σ}	ΔE_{orb}^{π}	ΔE_{bind}
H		2.315	−0.477	130.5	−283.4	−95.3	−3.0	−67.5	−9.8	−248.7
NH₂	o-	2.316	−0.482	130.4	−282.6	−94.4	−3.1	−67.0	−9.4	−247.4
	m-	2.317	−0.486	131.8	−278.3	−95.8	−3.0	−68.5	−9.7	−243.6
	p-	2.320	−0.492	128.4	−275.0	−92.5	−3.0	−65.2	−10.1	−240.0
NO₂	o-	2.301	−0.444	135.0	−289.8	−100.4	−2.8	−70.9	−10.4	−255.5
	m-	2.308	−0.460	135.2	−288.7	−100.7	−2.9	−72.4	−9.9	−256.0
	p-	2.309	−0.462	131.9	−289.8	−98.0	−3.0	−69.0	−10.7	−255.5
X-P		Pt−O_w	q(w)	ΔE_{Pauli}	ΔE_{elst}	ΔE_{orb}	ΔE_{disp}	ΔE_{orb}^{σ}	ΔE_{orb}^{π}	ΔE_{bind}
H		2.137	0.177	60.9	−64.4	−37.9	−3.0	−27.9	−5.9	−46.8
NH₂	o-	2.141	0.174	60.1	−63.2	−37.0	−3.0	−27.3	−5.7	−45.6
	m-	2.141	0.172	60.7	−63.4	−36.9	−3.0	−27.2	−5.7	−45.2
	p-	2.147	0.170	59.3	−62.3	−36.1	−2.9	−26.6	−5.5	−44.4
NO₂	o-	2.116	0.191	64.1	−67.6	−40.7	−3.1	−29.7	−6.5	−49.7
	m-	2.131	0.183	63.5	−66.2	−39.8	−3.0	−29.2	−6.2	−48.6
	p-	2.130	0.182	61.5	−65.6	−39.1	−3.0	−28.8	−6.2	−48.6

[a]All energy values are in kcal/mol. The data for all X's are shown in Table S2. [b]ΔE_{bind} energies were calculated at the B3LYP-D3BJ/BS2//B3LYP/BS1 level.

their relative value, respectively. These values were obtained from a comparison of binding energies of the strongest respective bond with the weakest one (Figure 1). Such low values reflected a rapid weakening of the electronic effects with increasing distance from the bound X because the relative change of the Pt−pyrX bond strength was more than 32%. This trend is visible in Figure 3 as the decrease of the isosurface volume with the increasing distance from the X group. However, the increase of electron density in the 3p$_x$ natural bond orbital (NBO) of the trans Cl⁻ ligand in the **p-NH₂-R** structure can be still clearly seen as the result of smaller electron donation from Cl⁻ toward the central Pt(II) atom forming a weaker Pt−Cl bond. Exactly the opposite was true for **p-NO₂-R**. Note that due to much larger absolute strength of the Pt−Cl bond, the changes of the absolute values of its binding energies (Table 3 and Table S2) are comparable with the binding energy changes of the Pt−pyrX bond (Table 2 and Table S1).

Prediction of the Pt−Ligand Bond Strengths. In previous studies, the strength of the Pt−ligand bonds was proportional to the properties such as the Pt−ligand bond lengths[6,56] (cf. Figure 2A and Figure S3), the linear combinations of electron densities at bond critical bonds,[56,57] or the populations in 5d orbitals of the Pt(II) atom.[5,6] These properties were calculated for the optimized structures of whole metal complexes.

However, our aim was to propose a predictor for the Pt−pyrX bond strength, which would be based just on the property of the isolated pyrX ligand as the putative reactant. First, we started with predictors typical for electrostatic energy such as the q(N$_{pyrX}$) atomic NPA charge, the total dipole moment of pyrX, and the projection of the dipole moment into the C4−N$_{pyrX}$ bond direction. These predictors worked well for para-X subset but completely failed for meta-X and ortho-X ones (Figure S6).

The minimum surface electrostatic potential calculated on the surface of the N atom of the amino groups enabled accurate estimation of their basicities and pK_b values.[58] Here, these calculations were performed on the surface of the N$_{pyrX}$

atom, and a very good prediction of the Pt−pyrX bond strength was obtained for meta and para subsets but not for some ortho-X's (o-DMA, o-NO₂, o-NH₂, o-OH, and o-F) (Figure S7) probably due to a strong interference of o-X and N$_{pyrX}$ local electrostatic fields.

The electron shifts caused by the H → X substitution in the isolated pyrX ring (see above and Figure S1) were accompanied by changes of the energies of NAO's on the N$_{pyrX}$ atom. The energy of the 2p$_x$(N$_{pyrX}$) NAO considering N$_{pyrX}$ and C4 atoms of the pyrX ring were oriented along the x axis (Figure 4I) reflected the origin of electrons which were involved in σ-donation as the decisive contributor to the formation of the Pt−pyrX dative bond (Figure 2B and Figure S3). Thus, the 2p$_x$(N$_{pyrX}$) NAO energy quantified σ-electron basicity of the pyrX ligand, and it was increased for electron-donating X substituents while the opposite was true for electron-withdrawing X's.

Differences in ΔE_{orb} contributions to ΔE_{bind}^{pyrX} were in the order of units of kcal/mol when systems with different X's were compared while differences in ΔE_{elst} could be by up to one order of magnitude higher (see Table 2 and Table S1). However, 2p$_x$(N$_{pyrX}$) NAO energy is still a good predictor of the Pt−pyrX bond strength because prevailing ΔE_{elst} is linearly correlated with ΔE_{orb} (see below and Figure S8), as it was already shown in our previous studies on similar systems.[6,59] Polarization and charge transfer effects as parts of ΔE_{orb} are strongly influenced by ΔE_{elst}.

The steric effect was quantified from the relation between complex stability and ligand basicity.[60] The graphs on panels A, B, E, F in Figure 4 have a similar meaning because 2p$_x$(N$_{pyrX}$) NAO energies and Pt−N$_{pyrX}$ binding energies can be expected to be related to ligand basicities and complex stabilities, respectively. Ortho-X substituents had mostly a stabilizing effect showing higher Pt−N$_{pyrX}$ bond strengths at a given value of 2p$_x$(N$_{pyrX}$) NAO energy compared to meta-X and para-X counterparts (see Figure 4A,B).

Because Pt−pyrX and Pt−trans ligand binding energies are dependent quantities due to the trans influence (see above), the 2p$_x$(N$_{pyrX}$) NAO energies calculated on the isolated pyrX
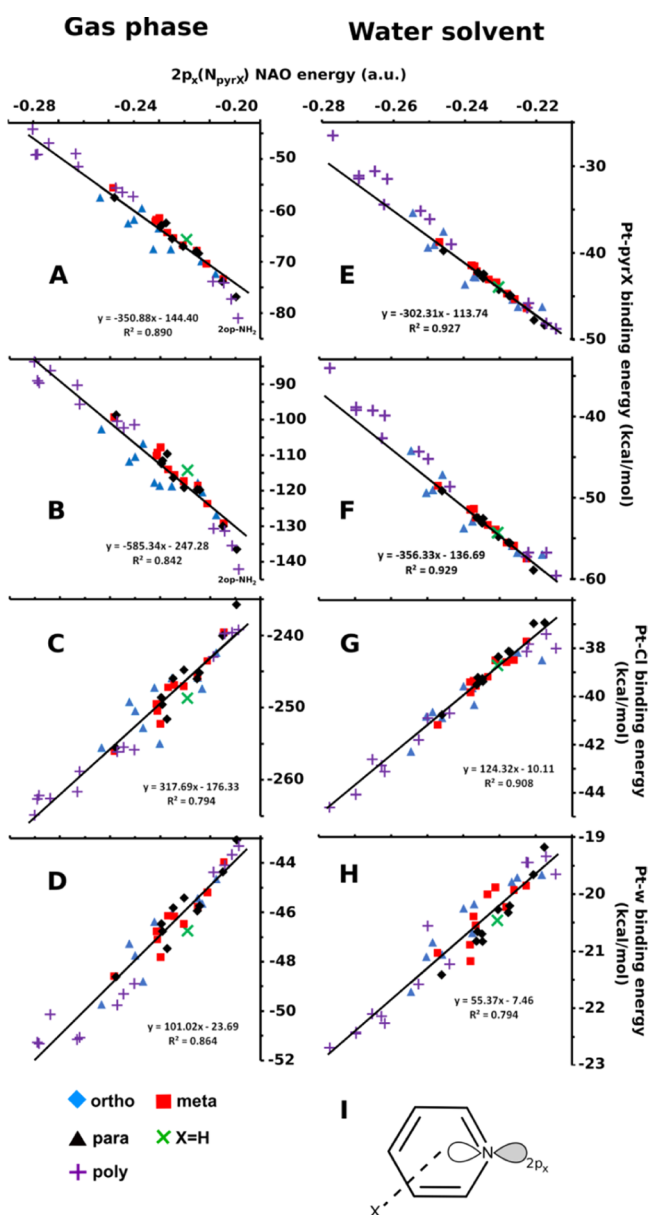
Figure 4. Dependence of the Pt−pyr(X) (panels A, B), Pt−Cl (panel C), and Pt−w (panel D) gas phase binding energies in **X-R** and **X-P** complexes (A, C and B, D panels, respectively) on the $2p_x(N_{pyrX})$ NAO energies calculated on the isolated pyrX ligands. Panels E, F, G, and H represent analogous results calculated in the water solvent. Points for the poly-X complexes were not included in the regression analyses (cf. below). Relative orientation of the $2p_x(N_{pyrX})$ orbital with respect to the isolated pyrX ligand (panel I). $2p_x(N_{pyrX})$ represents $2p(N_{pyrX})$ NAO orbital oriented along the C4−N_{pyrX} axis which is the direction of the pyrX nucleophilic attack to form the Pt−N_{pyrX} bond.

ligand could be used also for the Pt−trans ligand bond strength prediction. This predictor worked very well for the Pt−Cl bond strengths in **X-R** structures especially for para-X and meta-X subsets (cumulative $R^2 = 0.897$) but gave less satisfactory results for ortho-X ($R^2 = 0.604$) (Figure 4C). On the other hand, the Pt−w bond strengths in **X-P** structures could be well-predicted by this parameter regardless of the X position (cumulative $R^2 = 0.864$) (Figure 4D) probably due to much higher relative importance of the ΔE_{orb} contribution.

Note that the energy of the lone pair on the N_{pyrX} atom (LP(N_{pyrX}) NBO) gave slightly worse correlation with Pt−ligand binding energies than $2p_x(N_{pyrX})$ NAO energy (Figure S9) although both these parameters quantified a dative ability of the pyrX ligand. The reason may lie in the fact that LP(N_{pyrX}) NBO is an sp² hybrid NBO (Figure S9I) with a variable contribution of $2s(N_{pyrX})$ NAO which depended on the nature and the position of X and ranged from 27.9% (o-Cl) to 29.9% (p-DMA).

Trans Effect: The Binding Properties of the Transition State X-TS Structures and Kinetics of the Substitution Reactions. Pt−pyrX bonds in the **X-TS** structures were shortened by about 0.02−0.03 Å as observed for cisplatin in our previous study,[41] but contrary to our expectation, they were also weakened by about 4 ± 3% compared to **X-R** structures. It was caused by a large increase of ΔE_{Pauli} as the leaving Cl⁻ and entering water ligands lied in the plane of the pyrX ligand in most **X-TS** structures. This increase of ΔE_{Pauli} was not compensated by a rise of ΔE_{elst} and ΔE_{orb} terms (Table 2 and Table S1).

The influence of X on binding energies of ligands in **X-TS** is similar to **X-P** and **X-R** structures: Pt−N_{pyrX} bonds are stronger for electron-donating X's, while Pt−Cl and Pt−w interactions are more stabilized for electron-withdrawing X's (cf. above, Tables 4and 5and Tables S3 and S4).

Table 4. Pt−Cl and Pt−O$_w$ Bonds in the Gas Phase Optimized X-TS Structures (X = H, NH₂, NO₂): Pt−Cl, Pt−O$_w$ Bond Lengths (in Å); the Total NPA Charges of the Cl and Water Ligands (q(Cl), q(w); in e)^a

		Pt−Cl	Pt−O$_w$	q(Cl)	q(w)
H		2.770	2.327	−0.765	0.058
NH₂	o-	2.710	2.384	−0.761	0.064
	m-	2.768	2.344	−0.765	0.054
	p-	2.776	2.344	−0.768	0.051
NO₂	o-	2.752	2.302	−0.735	0.073
	m-	2.760	2.307	−0.758	0.068
	p-	2.759	2.309	−0.763	0.067

^{a}The data for all X's are shown in Table S3.

The substitution reaction proceeded by the associative interchange mechanism[6] which assumed a comparable importance of the leaving ligand (Cl⁻) destabilization in the reactant **X-R** structures and the **X-TS** transition state stabilization for the height of the activation barrier ($\Delta G^{\ddagger}$). Thus, $\Delta G^{\ddagger}$ values resulted from a complex event of the **X-TS** formation which should not be predictable by a single variable. However, TS stabilization was important only for **o-X-TS** structures (see below), and thus, we obtained a reasonable correlation between the $2p_x(N_{pyrX})$ NAO energy calculated on the isolated pyrX ligand (see above) and $\Delta G^{\ddagger}$ values for m-X and p-X reaction pathways (Figure 5). Only the points which corresponded to the stabilized **o-NH₂-TS**, **o-OH-TS**, and **o-SH-TS** structures (see below) were considerably outside the linear correlation.

Nucleophilicity of organic compounds was estimated by the Hirshfeld charges.[61] However, here the Hirshfeld charge on the Pt(II) center offered a slightly worse correlation with the $\Delta G^{\ddagger}$ energies for meta and para subsets ($R^2 = 0.596$) than $2p_x(N_{pyrX})$ NAO energies (Figure S11).

In accordance with the influence of X on the stability of the Pt−Cl bond (see above), the electron-donating X's tend to

Table 5. Gas Phase Optimized X-TS Structures (X = H, NH$_2$, NO$_2$): ETS-NOCV Energy Decomposition Terms ΔE_{Pauli}, ΔE_{elst}, ΔE_{orb}, ΔE_{disp}, and ΔE_{orb}^{σ} for the Interaction of the Joint (Cl + w) Fragment (Leaving and Entering Ligands) with the Rest of the Complex Were Obtained at the BLYP-D3BJ/TZ2P//B3LYP/BS1 Level[a,b]

		ΔE_{Pauli}	ΔE_{elst}	ΔE_{orb}	ΔE_{disp}	ΔE_{orb}^{σ}	ΔE_{bind}	$\Delta G^{\ddagger}$
H		88.0	−236.2	−69.8	−6.0	−37.7	−222.9	33.2
NH$_2$	o-	93.6	−243.6	−69.6	−6.8	−36.7	−225.3	29.9
	m-	87.3	−231.2	−68.5	−6.0	−37.5	−217.9	32.7
	p-	85.8	−227.4	−67.3	−6.0	−36.1	−214.2	32.6
NO$_2$	o-	91.4	−242.2	−74.0	−6.1	−39.8	−230.0	33.3
	m-	92.2	−241.8	−74.6	−6.1	−41.5	−230.4	34.4
	p-	90.8	−243.2	−73.2	−6.1	−39.4	−230.8	34.3

[a]All energy values are in kcal/mol. The data for all X's are shown in Table S4. [b]ΔE_{bind} energies of the (Cl + w) fragment and activation Gibbs energies $\Delta G^{\ddagger}$ were calculated at the B3LYP-D3BJ/BS2//B3LYP/BS1 level.
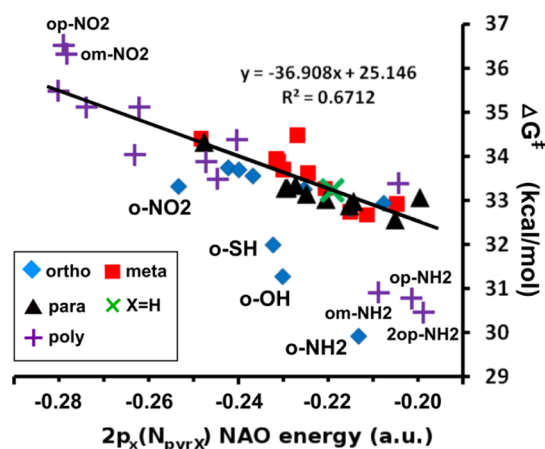

Figure 5. Dependence of the gas phase activation Gibbs free energies ($\Delta G^{\ddagger}$) on the energies of $2p_x(N_{pyrX})$ NAO's calculated on the isolated pyrX ligand (see Figure 4I). One regression line was constructed for m-X and p-X reaction paths while excluding all o-X and poly-X (see below) points.
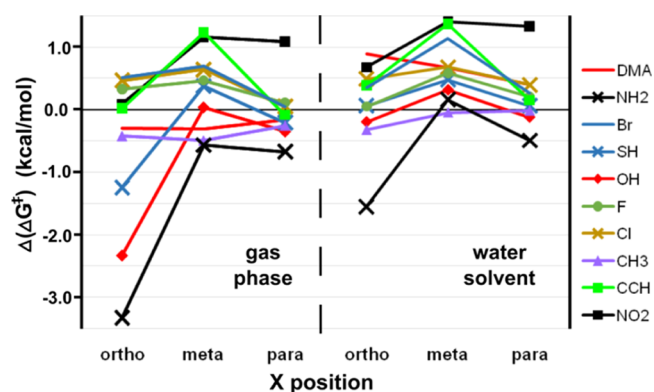

Figure 6. Dependence of the relative values of the activation Gibbs free energy barriers ($\Delta(\Delta G^{\ddagger})$) of the hydration reactions of the *trans*-[Pt(NH$_3$)$_2$(pyrX) Cl]$^+$ complexes on the nature and the position of the X in the gas phase and in the water solvent. $\Delta(\Delta G^{\ddagger})$ was calculated with respect to the reference values (33.2 and 25.7 kcal/mol in the gas and water solvent, respectively) determined for the X = H pathway. Absolute values of $\Delta G^{\ddagger}$ are shown in Table 5, Table S4 and Table 7, and Table S6 for the gas phase and the water solvent, respectively.

lower the activation $\Delta G^{\ddagger}$ energy while the opposite was true for electron-withdrawing X's (Figure 6). It was caused by much higher relative importance of the Pt−Cl bond destabilization compared to Pt−water ligand stabilization in **X-TS** structures.

In the ortho position, the electronic effects were probably stronger than in para and meta positions (cf. NPA charges in Table 1) but were hardly distinguishable from the structural (de)stabilizations (see below), giving together the widest range of $\Delta G^{\ddagger}$ values of 3.8 kcal/mol between the analyzed reaction profiles (Figure 6). For para-X's, the structural effects were negligible, and the $\Delta G^{\ddagger}$ range of 1.8 kcal/mol could be attributed purely to electronic effects.

The meta-X substitution always decreased the electron density on the N$_{pyrX}$ atom (Table 1), which led to the formation of electron-deficient Pt(II) complexes compared to ortho and para analogues. It may be responsible for the highest $\Delta G^{\ddagger}$ values and the least reactivity of meta substituted systems. Thus, the dependence of $\Delta G^{\ddagger}$ on the position of X in the order ortho−meta−para has usually the shape of inverted "V". The exceptions are DMA and CH$_3$ substituents, but they show very small $\Delta G^{\ddagger}$ differences of just tenths of kcal/mol between the three isomers' reaction pathways (Figure 6).

Considering both the nature and the position of X on the pyrX ligand, we obtained the total difference of 4.6 kcal/mol in the height of the reaction free energy barrier between the slowest reaction for *m*-CCH and the fastest one for *o*-NH$_2$. It

corresponds to ca. 2200-fold difference in the reaction rate at 298 K.

TS Structure (de)stabilizations. X-TS structures preserved all X⋯HNH$_2$ and X⋯Pt nonbonding interactions (Figure 7) which were established already in **X-R** structures, and thus, these interactions did not contribute importantly to the decrease of $\Delta G^{\ddagger}$ (cf. below the case of *o*-DMA pathway). However, for most **X-TS** structures, the entering water and leaving Cl$^-$ ligands are roughly coplanar with the pyrX ligand which means that the nucleophilic attack of the water ligand occurred in the plane of the pyrX ligand. Depending on the nature of X, it may dictate the direction of the water attack and stabilize/destabilize the TS structures through the electrostatic field of X. The most striking examples are *o*-NH$_2$, *o*-OH, and *o*-SH pathways, which showed the lowest activation energies (Figure 6) having the leaving Cl$^-$ ligand stabilized by internal HNH⋯Cl, OH⋯Cl, and SH⋯Cl contacts with distances 2.745 Å, 2.673 Å, and 2.560 Å in *o*-NH$_2$-TS, *o*-OH-TS, and *o*-SH-TS structures, respectively (Figure 7). NOCV analysis revealed neither any contribution of these contacts to the orbital energy nor any corresponding bond critical points were found by QTAIM analysis. Thus, these contacts had fully electrostatic nature (cf. ΔE_{elst} values in Table 5 and Table S4) but still led to the substantial lowering of the reaction free energy barrier of corresponding substitution reactions compared to meta- and
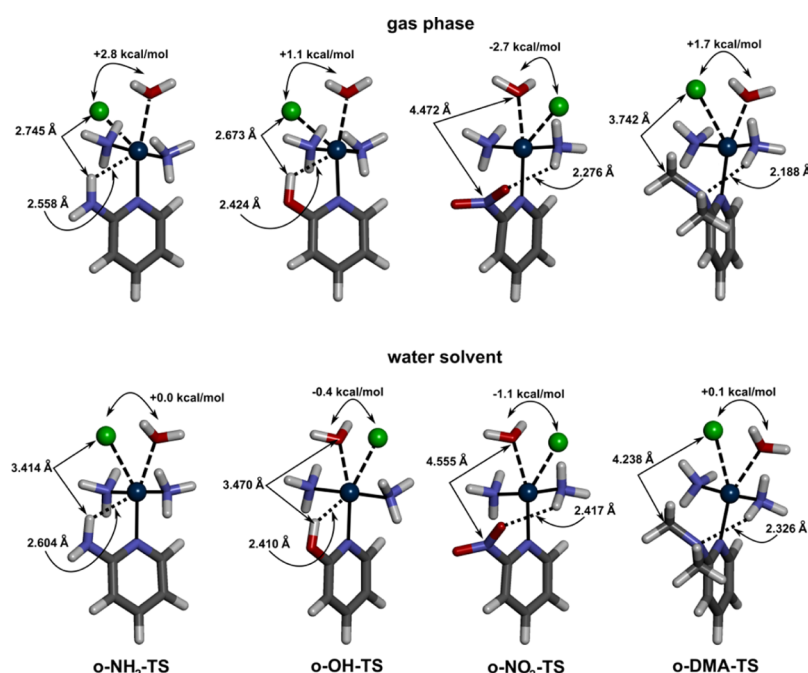
Figure 7. Energetically the most feasible structures of *o*-NH$_2$-TS, *o*-OH-TS, *o*-NO$_2$-TS, and *o*-DMA-TS in the gas phase (upper structures) and in the water solvent (lower structures) with depicted distances of the X···HNH$_2$, X···Pt nonbonding, and X···Cl (X···w) electrostatic interactions. The Gibbs energy conformational preferences ($\Delta(\Delta G^{\ddagger}_{conf})$) of the water nucleophilic attack from the semispace defined by the plane of the Pt complex and the position of the o-X group relative to the opposite direction are also shown (in kcal/mol). Pt−N$_{pyrX}$, Pt−Cl, and Pt−O$_w$ bond lengths are shown in Table 2, Table S1 and Table 4, and Table S3, respectively, for the gas phase optimized structures and in Table 7 and Table S6 for the water solvent ones.

Table 6. Bonding Interactions in X-R and X-P Structures (X = H, NH$_2$, NO$_2$) Optimized in the Water Solvent and Calculated by the B3LYP-D3BJ-PCM/BS2//B3LYP-PCM/BS1 Method: Pt−N$_{pyrX}$, Pt−Cl, and Pt−O$_w$ Bond Lengths (in Å); the Total NPA Charges of the pyrX, Cl, and Water Ligands (q(pyrX), q(Cl) and q(w), Respectively) (in e); ΔE_{bind} Energy Values are in kcal/mol^a

X-R		Pt−N$_{pyrX}$	q(pyrX)	ΔE_{bind}^{pyrX}	Pt−Cl	q(Cl)	ΔE_{bind}^{Cl}
H		2.052	0.284	−43.9	2.370	−0.597	−38.7
NH$_2$	o-	2.064	0.292	−46.2	2.363	−0.594	−38.2
	m-	2.051	0.289	−45.3	2.363	−0.599	−38.5
	p-	2.047	0.312	−47.7	2.378	−0.610	−37.0
NO$_2$	o-	2.084	0.231	−35.4	2.341	−0.560	−42.3
	m-	2.067	0.251	−38.8	2.353	−0.576	−41.2
	p-	2.056	0.247	−39.7	2.360	−0.580	−40.8
X-P		**Pt−N$_{pyrX}$**	**q(pyrX)**	**ΔE_{bind}^{pyrX}**	**Pt−O$_w$**	**q(w)**	**ΔE_{bind}^{w}**
H		2.011	0.356	−54.3	2.118	0.195	−20.5
NH$_2$	o-	2.021	0.371	−56.7	2.123	0.195	−19.7
	m-	2.008	0.364	−55.9	2.120	0.194	−19.9
	p-	2.010	0.383	−58.9	2.123	0.189	−19.7
NO$_2$	o-	2.034	0.306	−44.2	2.098	0.211	−21.7
	m-	2.014	0.327	−48.5	2.114	0.202	−21.0
	p-	2.011	0.322	−49.1	2.108	0.203	−21.4

^{a}The data for all X's are shown in Table S5.

para-analogues (Figure 6). The conformation of the entering water ligand in the TS structure then clearly referred to the favored direction of the nucleophilic attack on the Pt(II) center being from the opposite semispace with respect to *o*-NH$_2$, *o*-OH, and *o*-SH substituents (Figure 7).

On the other hand, *o*-NO$_2$, *o*-F, *o*-Cl, and *o*-Br groups made a nucleophilic attack more difficult because their contact with the entering water ligand was destabilizing due to unsuitable orientation of the water ligand in *o*-NO$_2$-TS (see Figure 7), *o*-F-TS, *o*-Cl-TS, and *o*-Br-TS structures, respectively; never-

theless, it was more advantageous than the contact with the leaving Cl$^-$ ligand (by 2.7, 1.9, 0.9, and 1.1 kcal/mol for *o*-NO$_2$, *o*-F, *o*-Cl, and *o*-Br reaction pathways, respectively). It is probably the main reason of their highest activation energies compared to other ortho-X's (Figure 6).

The steric hindrance manifested itself by the elongation of the Pt−N$_{pyrX}$ bond (see above). It also changed the conformation of the *o*-DMA-R, *o*-DMA-TS, and *o*-DMA-P structures which had deformed geometries with the twist angles of 56.3, 54.4 (Figure 7), and 58.9°, respectively,

Table 7. Activation Free Energies ($\Delta G^{\ddagger}$) and Bonding Interactions in X-TS Structures (X = H, NH$_2$, NO$_2$) Optimized in the Water Solvent and Calculated by the B3LYP-D3BJ-PCM/BS2//B3LYP-PCM/BS1 Method: Pt−N$_{pyrX}$, Pt−Cl, and Pt−O$_w$ Bond Lengths (in Å); Total NPA Charges of the pyrX, Cl and Water Ligands (q(pyrX), q(Cl) and q(w), Respectively) (in e); and ΔE_{bind} and $\Delta G^{\ddagger}$ Energy Values in kcal/mol[a]

X-TS		Pt−N$_{pyrX}$	q(pyrX)	ΔE_{bind}^{pyrX}	Pt−Cl	q(Cl)	Pt−O$_w$	q(w)	$\Delta E_{bind}^{(w+Cl)}$	$\Delta G^{\ddagger}$
H		2.034	0.318	−42.9	2.837	−0.837	2.476	0.050	−18.6	25.9
NH$_2$	o-	2.042	0.333	−45.0	2.806	−0.832	2.482	0.053	−18.5	24.3
	m-	2.032	0.327	−44.3	2.843	−0.841	2.469	0.050	−18.1	26.0
	p-	2.029	0.350	−47.0	2.846	−0.841	2.495	0.044	−17.3	25.4
NO$_2$	o-	2.074	0.252	−33.0	2.783	−0.821	2.431	0.067	−21.9	26.5
	m-	2.042	0.281	−37.2	2.822	−0.830	2.447	0.059	−20.2	27.3
	p-	2.035	0.272	−38.1	2.816	−0.828	2.448	0.059	−19.6	27.2

[a]The data for all X's are shown in Table S6.

between the pyrX plane and the plane of the complex defined by Pt and two N$_{NH_3}$ and N$_{pyrX}$ atoms. This deformation enabled unfavorable interactions to be avoided between the *o*-DMA substituent and the NH$_3$ ligands. However, similar deformation was found also for structures along *o*-F, *o*-Cl, and *o*-Br pathways, but here it enabled the formation of the attractive halogen X···HNH$_2$ H-bond. For the other structures, the twist angle between the two planes is close to 90° (Figure 7) but its influence on $\Delta G^{\ddagger}$ is unclear.

The steric hindrance should lead to an increase of $\Delta G^{\ddagger}$. *o*-DMA, *o*-CH$_3$, *o*-Br, *o*-Cl, and *o*-F pathways have elevated $\Delta G^{\ddagger}$ values which are within 0.1 kcal/mol compared to their meta counterparts. However, the differences in $\Delta G^{\ddagger}$ are too small to find a clear reason. For example, as the above described deformation is similar for all structures along the *o*-DMA pathway, it has little effect on $\Delta G^{\ddagger}$ as it can be manifested by the values of 7.2, 7.2, and 8.8 kcal/mol which represent the free energy destabilizations of *o*-DMA-R, *o*-DMA-TS, and *o*-DMA-P structures, respectively, with respect to their *p*-DMA isomeric counterparts. Note that $\Delta G^{\ddagger}$ is even by 0.1 kcal/mol lower for the *o*-DMA pathway than for the *p*-DMA one (Figure 6 and Table S4).

Solvent Effects. Water environment dampened the electrostatic forces which were the most contributive to the stabilization of the Pt−ligand bonds of our charged complexes in the gas phase (see above). Thus, binding energies of all Pt−ligand bonds were lowered in the water environment (Tables 6 and 7 and Tables S5 and S6). Similarly as in the gas phase, the Pt−ligand binding energies could be estimated from 2p$_x$(N$_{pyrX}$) NAO energies calculated for the isolated pyrX ligand immersed in the polarizable continuum model (PCM) water solvent (Figure 4E−H). The linear correlations are even slightly better here than in the gas phase probably due to a smaller relative importance of electrostatic interactions. Note also that the changes of electron density induced by X's are qualitatively the same as in the gas phase (cf. Figure 3 and Figure S10). Thus, the findings described above for the gas phase should be qualitatively valid also for the water phase.

The weakening of the Pt−ligand bonds did not automatically lead to their elongation because bond length changes were inversely related to the changes of the ligand → Pt transferred charge. The trend of the change (increase/decrease) of the charge transfer and polarization effects depended on the nature of the interaction and nature of the complex.

As expected, Pt−Cl was the most affected bond in the **X-R** structures being ca. six times weaker in the solvent than in the gas phase because the arising Cl$^-$ anion was stabilized by

hydration. The charge donation from the Cl$^-$ ligand was by 22 ± 0.8% lower in the water solvent which resulted in 0.047 ± 0.006 Å Pt−Cl bond elongation. The ligand environment was crucial for the behavior of the pyrX ligand: the charge transfer from pyrX is higher/lower by 14.1 ± 1.7%/17.3 ± 1.3% in the solvent, and Pt−N$_{pyrX}$ bond lengths were shortened/slightly elongated by 0.026 ± 0.003 Å/0.002 ± 0.002 Å in **R-X**/**P-X** structures. The Pt−N$_{pyrX}$ bond was always weakened: by 54 ± 1.5% in **P-X** structures and by 34.4 ± 2.0% in **R-X** ones. The Pt−w bonds in the water solvent-optimized **X-P** structures were shortened by 0.019 ± 0.004 Å compared to the gas phase. The transferred charge from the water ligand increased by 11.7 ± 0.8%, and the Pt−O$_w$ bond was weakened by 56 ± 0.7%. As the result, the NPA charge of the Pt center was by 10.2 ± 0.8 and 7.9 ± 0.8% more positive in the solvent than in the gas phase in **R-X** and **P-X** structures, respectively.

The activation Gibbs energies ($\Delta G^{\ddagger}$) were substantially reduced: by 6.9 ± 0.5 kcal/mol compared to the gas phase (Table 7 and Table S6). 2p$_x$(N$_{pyrX}$) NAO energies worked substantially worse as the predictor of $\Delta G^{\ddagger}$ values giving the R^2 value of 0.483 for meta and para subsets (cf. Figure 5). It could be caused by higher complexity of the reaction in the water solvent and/or by a lower precision of our calculations.

Despite a general weakening of the Pt−ligand coordination bonds, the relative values of the activation barriers for different X's were similar to the gas phase when driven by the electronic effects. Thus, the meta and para subsets gave almost the same maximum $\Delta(\Delta G^{\ddagger})$ differences of 1.5 and 1.8 kcal/mol (cf. with respective values of 1.8 and 1.8 kcal/mol for the gas phase, see Figure 6). However, the water environment caused substantial weakening of the electrostatic forces which lowered spatial preferences of the nucleophilic attack in the TS structures and the importance of the long-range X···Cl and X···w interactions therein (cf. $\Delta(\Delta G_{conf}^{\ddagger})$ differences in Figure 7). The weakening of HNH···Cl and HO···Cl stabilization interactions in *o*-NH$_2$-TS and *o*-OH-TS, respectively (cf. above), resulted in the decrease of $\Delta(\Delta G^{\ddagger})$ variance for the ortho subset to the value of 2.4 kcal/mol. Taken the results for all three subsets together, $\Delta(\Delta G^{\ddagger})$ between the fastest (*o*-NH$_2$) and the slowest (*m*-NO$_2$) reaction was 3.0 kcal/mol in the water solvent which corresponded to ca. 150 times change in the reaction rate at 298 K. It is by about one order of magnitude smaller value than for the gas phase.

Complexes with the Poly-X Ligand. The 2p$_x$(N$_{pyrX}$) NAO energies and the Pt−ligand bond strengths for poly-substituted complexes were compatible with the results for the mono-substituted ligand complexes (cf. above). The mean deviations of 2.5 ± 1.3, 4.0 ± 2.8, 1.3 ± 0.9, and 0.7 ± 0.3

kcal/mol from the linear functions derived for the mono-substituted complexes (Figure 4) were calculated for Pt—pyrX (in **X-R**), Pt—pyrX (in **X-P**), Pt—Cl, and Pt—w binding energies, respectively, in the gas phase. In the water solvent, the respective values were 1.4 ± 1.2, 1.9 ± 1.2, 0.4 ± 0.3, and 0.2 ± 0.2 kcal/mol. The highest deviation values of 6.3 and 11.2 kcal/mol were detected for Pt—pyrX bonds of the gas phase **2op-NH$_2$-R** and **2op-NH$_2$-P** structures, respectively (Figure 4). This underestimation of the binding energies was caused by the presence of two strong $H_2NH\cdots NH_2$ H-bonds (Figure S12) whose energies were not compensated by the elongation of the Pt—N$_{pyrX}$ bond (by about 0.01 Å) (cf. above and values in the Tables S9 and S10).

The gas phase $\Delta G^{\ddagger}$ free energy values could be also estimated from the $2p_x(N_{pyrX})$ NAO energies of the poly-substituted ligand complexes except for the **om-NH$_2$**, **op-NH$_2$**, and **2op-NH$_2$** pathways which involved o-NH$_2\cdots$Cl electrostatic stabilization of the TS structures (cf. above). For the other poly-X pathways, the mean deviation of the $\Delta G^{\ddagger}$ values from the linear function in Figure 5 was 0.5 ± 0.3 kcal/mol.

The additivity of the substituent effects on the pyr ring was already shown for proton affinities and gas phase basicities of the substituted pyridines[62] while electron shifts within the pyrX ring were non-additive.[63] In this contribution, the values (X_{poly}) of NPA charges, binding energies, and bond lengths of the poly-substituted complexes could be estimated by a simple additive approach based on eq 1

$$X_{poly} = X_H + \sum_i n_i \Delta x_i \qquad (1)$$

where the summation goes over all positions (i = ortho, meta, para); X_H is the value for the non-substituted complex ($X = H$); Δx_i is the measured changes of the monosubstituted complexes with respect to the non-substituted complex ($X = H$); and n_i is the number of substituents in the position i. The plots of calculated versus estimated values for the ligand binding energies are shown in Figure 8. Numerical values are shown in Tables S7–S12. In the gas phase, the absolute differences between calculated and estimated values were within the experimental error for the binding energies (≤ 2.5 kcal/mol), NPA charges (≤ 0.01 e), and bond lengths (≤ 0.01 Å). For poly-F and poly-NO$_2$ complexes, the relative errors were below 20% (Tables S7, S8, S11, and S12). For the most sterically hindered complexes with the **2op-NH$_2$** ligand, this error reached almost 50% for q(Cl) and q(w) NPA charges (Tables S9 and S10). However, for the **poly-NH$_2$** complexes, the additive approach failed to predict the subtle changes of Pt—ligand bond lengths. Note that the relative error of 30% was measured for the additivity of substituent effects on much simpler (de)protonation processes of substituted pyridines in the gas phase.[62]

In the water solvent, the additive approach worked less satisfactory especially for the weakest Pt—w interaction (Figure 8H and Tables S8, S10, and S12). Partly, it might be caused by a lower precision of PCM calculations.

For $\Delta G^{\ddagger}$ activation energies, the additive approach did not offer useable results due to high relative errors (Tables S7, S9, and S11). The largest errors were for **poly-NH$_2$** pathways (Figure S13). While any single NH$_2$ substitution of the non-substituted pyrH system led to the decrease of $\Delta G^{\ddagger}$ activation free energy (except **m-NH$_2$** in the water solvent), any additional NH$_2$ substitution of o-NH$_2$ led to the $\Delta G^{\ddagger}$ value increase (Table S9). The electron-withdrawing poly-F and
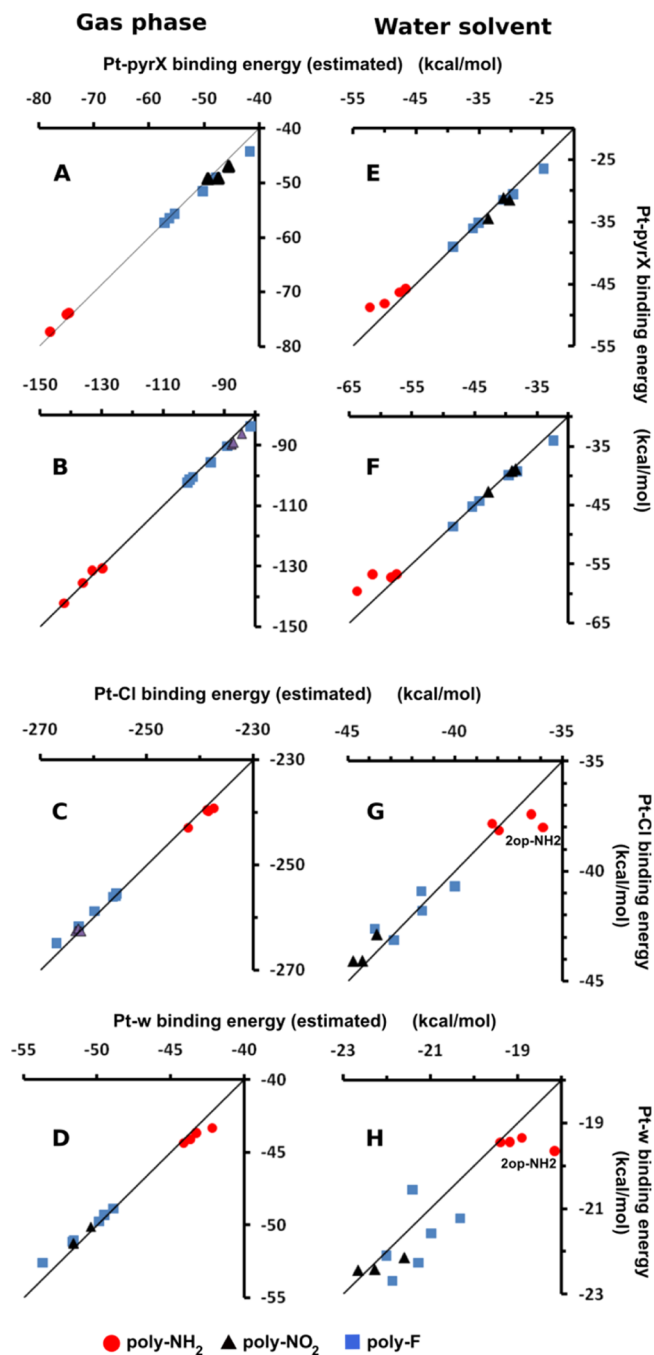

Figure 8. Plots of estimated vs calculated (eq 1) values of Pt—ligand binding energies for complexes with poly-substituted ligands in the gas phase (panels A–D) and the water solvent (panels E–H). Panels A, C, E, and G and B, D, F, and H correspond to poly-**X-R** and poly-**X-P** structures, respectively. The solid line represents equality of the two values.

poly-NO$_2$ systems worked more predictably and offered an increase of the $\Delta G^{\ddagger}$ values (with exception of the op-F system and in the water solvent of the om-F one, too) compared to mono-substituted systems. The $2m$-NO$_2$ and op-NO$_2$ pathways showed the highest $\Delta G^{\ddagger}$ values of 35.1 and 27.7 kcal/mol (Table S11), which are by 0.6 and 0.5 kcal/mol larger than the ones for the slowest hydration reactions of complexes with mono-functional pyrX ligands (Tables S4 and S6) in the gas phase and the water solvent, respectively. Thus, the $\Delta G^{\ddagger}$ value ranges (cf. above) increased up to 5.2 and 3.4 kcal/mol for the

gas phase and the water solvent, respectively, which corresponded to ca. 6400 and 320 times differences in the reaction rate at 298 K.

Reliability of Our Results. To obtain accurate absolute values of observables, one has to choose the appropriate combination of the density functional theory (DFT) functional, the solvation method, and the basis set.[64−66] In this contribution, we rely on the relative values which should be much less sensitive in this respect.

To check the influence of the B3LYP functional on the height of the activation barriers and Pt−ligand bond lengths, the **X-R_w** and **X-TS** structures were also optimized and energy of optimized structures was evaluated by M06-2X, PBE0 functionals[67] using BS1 and BS2 basis sets, respectively, in the gas phase (M062X/BS2//M062X/BS1, and PBE0-D3BJ/BS2//PBE0/BS1 calculations). In the solvent, these calculations were performed only with the M06-2X functional.

All M062X and PBE0 gas phase optimized Pt−ligand bond lengths correlated very well linearly with the B3LYP counterparts ($R^2 > 0.94$) and were systematically shorter with the exception of Pt−O distances in M06-2X optimized **X-TS** structures (Figures S14 and S15). Reasonable correlation was found also for activation Gibbs free energies which were systematically lower by 2.8 ± 0.5 kcal/mol and higher by 0.9 ± 0.4 kcal/mol for the M06-2X and PBE0-D3BJ functionals, respectively. Thus, for the gas phase, the relative changes of the variables studied in this paper should be not sensitive on the chosen functional.

For the M06-2X/PCM optimizations, the correlation was generally worse and not very satisfactory for Pt−Cl distances in **X-TS** structures ($R^2 = 0.430$) (Figure S16). No correlation was found for solvent phase activation energies. In agreement with the B3LYP results, the fastest reaction was detected for the o-NH$_2$ substitution (Figure S17), but for the other X's, the $\Delta(\Delta G^{\ddagger})$ differences are probably too small compared to the precision of our calculations. Thus, except of the $\Delta G^{\ddagger}$ values and the properties of the Pt−Cl bond in **X-TS** structures, the other relative changes of variables studied in this contribution and calculated in the water solvent should be described in our opinion satisfactorily and should be little dependent on the chosen functional.

Comparison with Experimental Data. We have not found experimental data about any of the complexes studied in this contribution. 2-Picoline and 3-picoline complexes are related compounds to o-**CH$_3$-R** and m-**CH$_3$-R**, respectively, but one of the ammine NH$_3$ groups is replaced by the chlorine Cl$^-$ ligand. We obtained slightly longer Pt−N$_{pyrX}$ (by 0.070 and 0.071 Å) and Pt−Cl bond lengths (by 0.019 and 0.007 Å) compared to the crystal structures of the 2- and 3-picoline complexes[29] (cf. Tables S1 and S2). In the crystal structure, the 3-picoline ligand is tilted by 48.9° while 2-picoline ligand is almost perpendicular (102.7°).[29,68] In o-**CH$_3$-R** and m-**CH$_3$-R**, both o-CH$_3$ and m-CH$_3$ ligands were perpendicular to the plane of the complex (90.0 and 87.7°). The difference for the 3-picoline complex has to be attributed to the Cl$^-$ ligand in the cis position because the gas phase mPW1PW1 DFT-optimized geometries of 2-picoline and 3-picoline complexes were in very good agreement with the crystal structures.[69]

According to our calculations, the rates of hydrolysis were the same for two related complexes: the experimental trans-[Pt(NH$_3$)(H$_2$O)(3-picoline)Cl]$^+$ complex[29] and m-**CH$_3$-R** which differed only by the nature of the group in the cis position (H$_2$O vs NH$_3$). However, in the water solvent, we did

not observe any steric hindrance of the o-CH$_3$ ligand (unlike the gas phase) and the kinetic constant for the o-CH$_3$ pathway was by two orders of magnitude higher compared to the trans-[Pt(NH$_3$)(H$_2$O)(2-picoline)Cl]$^+$ experimental analogue.[29]

The meta-X substitution of the pyrX ligand led to the slowest reaction for most X's in both the gas phase and the water solvent, which is in agreement with experimental evidence.[68,70]

■ CONCLUSIONS

Substitution of the pyridine ligand by electron-donating groups in the trans-[Pt(NH$_3$)$_2$(pyrX)Cl]$^+$ complexes led to the strengthening of the Pt−N$_{pyrX}$ bond and the weakening of the bonds in the trans direction (Pt−Cl and Pt−O$_w$ in **X-R** and **X-P** structures, respectively). The electron-withdrawing groups had exactly the opposite effect. In both the gas phase and the water solvent, the strengths of Pt−N$_{pyrX}$, Pt−Cl, and Pt−O$_w$ bonds in the **X-R** and **X-P** complexes were dependent on σ-electron basicity of the N$_{pyrX}$ atom which correlated linearly best with the energy of the 2p(N$_{pyrX}$) NAO oriented in the C4−N$_{pyrX}$ direction and calculated on the isolated pyrX ligand. These correlations were successfully validated on the complexes with the poly-substituted ligand.

The electron-donating/withdrawing groups tend to decrease/increase $\Delta G^{\ddagger}$ free activation energies. In the gas phase, the 2p(N$_{pyrX}$) NAO energy can be used also as a predictor for the estimation of $\Delta G^{\ddagger}$ of the meta-X and para-X reaction pathways with dominating influence of electronic effects.

Because of the perpendicular orientation of the pyrX ligand with respect to the metal complex plane, the substitution reactions occurred in the pyrX plane. The attractive X···Cl electrostatic interaction was established for o-X's with the H-bond donor ability (o-NH$_2$, o-OH, o-SH) which led to the **o-X-TS** structure stabilization and a substantial decrease of the $\Delta G^{\ddagger}$ values. The fastest reaction rate was observed for the o-NH$_2$ pathway. On the other hand, steric hindrance in **o-X-TS** structures led only to a moderate increase of $\Delta G^{\ddagger}$ probably due to a small size of X's considered in this study. Anyway, taken together the activation free $\Delta G^{\ddagger}$ energy of the hydration reactions can be most easily modified by the substitution of the pyridine ring in the ortho position giving the $\Delta G^{\ddagger}$ values range of 3.8 kcal/mol between the fastest o-NH$_2$ and slowest o-Br pathways (Table S4). Substitutions in the meta position led usually to the highest activation energies.

In the gas phase, the X's on the pyridine ring can be ordered according to their ability to promote the hydration reaction as follows: NH$_2$ > OH ≥ SH ≈ CH$_3$ > DMA > H > F ≥ Cl ≈ CCH ≈ Br > NO$_2$.

Water solvent weakens all coordination Pt−ligand bonds and lowers the activation free energies compared to the gas phase. Both shortenings and elongations of the bond lengths are possible being inversely related to the changes of the ligand → Pt transferred charge. The dampening of electrostatic interactions lowered the range of the $\Delta G^{\ddagger}$ values for the ortho subset to 2.4 kcal/mol. The ranges of $\Delta G^{\ddagger}$ for meta and para subsets being driven mainly by electronic effects remained almost unchanged with respect to the gas phase (ca. 1.8 kcal/mol).

Considering all three ortho, meta, and para positions (all mono-substituted systems), the ranges of $\Delta G^{\ddagger}$ values for all X's were 4.6 and 3.0 kcal/mol, which corresponded to ca. 2200

and 150 times differences in the reaction rate at 298 K in the gas phase and the water solvent, respectively.

The acceleration of the hydration reaction by an additional NH_2 substitution of the o-NH_2 ligand was not observed. On the other hand, a further slowdown of the Pt(II) complex reactivity with respect to the complexes with mono-substituted ligands was possible. The **2m-NO$_2$** and **op-NO$_2$** pathways increased the maximum value of $\Delta G^{\ddagger}$ by 0.6 and 0.5 kcal/mol in the gas phase and the water solvent, respectively. As the result, if poly-X complexes were considered, the ranges of possible $\Delta G^{\ddagger}$ values were increased up to 5.2 and 3.4 kcal/mol which corresponded to ca. 6400 and 320 times differences in the reaction rate at 298 K for the gas phase and the water solvent, respectively.

The additivity of substituent effects on poly-X complexes was shown with respect to the Pt–ligand bond strengths and the ligand NPA charges in the gas phase which had the relative errors below 30%.

■ COMPUTATIONAL METHODS

All geometries of the structures were optimized at the DFT level with the hybrid B3LYP functional[71] and 6-31+G(d) basis set for the first and second row elements. Heavier atoms were treated by Dresden–Stuttgart quasirelativistic energy-averaged effective pseudopotentials[72,73] with a pseudo-orbital basis set augmented by the set of diffuse (for Pt with exponents α_s = 0.0075, α_p = 0.013, α_d = 0.025; for Cl: α_s = 0.09, α_p = 0.0075) and polarization (α_f(Pt) = 0.98; α_d(Cl) = 0.618) functions.[74] These calculations are labeled as B3LYP/BS1 in further text. The nature of the obtained stationary points was always checked by the Hessian matrix evaluation. Thermal contributions to the energetic properties were calculated using the canonical ensemble at standard gas phase conditions (T = 298 K, p = 101.325 kPa).

The energy profiles and wave function properties were determined at the B3LYP-D3BJ/MWB-60(2fg)/6-311++G-(2df,2pd) single point calculations which combined the B3LYP functional with Grimme's DFT-D3 dispersion correction and Becke–Johnson damping[75] (labeled as D3BJ). The Pt atom was augmented by the set of diffuse functions in analogy to BS1 and by the set of polarization functions (α_f(Pt) = 1.419; 0.466, α_g(Pt) = 1.208)[74] (B3LYP-D3BJ/BS2 calculations). All possible rotamers were considered for the reactant and product structures, and the energy of the given minimum structure was obtained by Boltzmann averaging over all optimized rotamers at T = 298 K. For calculation of activation free energies ($\Delta G^{\ddagger}$), the lowest lying TS structure was considered. In calculations of binding energies ΔE_{bind}, the basis set superposition error (BSSE) was included by the counterpoise correction.[76] Deformation energies were not included.

Additional single-point calculations on selected optimized structures were conducted using the Amsterdam Density Functional 2014.05 package (ADF)[77] to calculate fragment energy decompositions according to the extended transition state theory[78] combined with natural orbitals for chemical valence (ETS-NOCV).[79,80] Gas phase interaction energies ΔE_{INT}^{gas} were decomposed to Pauli (ΔE_{Pauli}), electrostatic (ΔE_{elstat}), orbital (ΔE_{orb}), and dispersion (ΔE_{disp}) energy contributions

$$\Delta E_{INT}^{gas} = \Delta E_{Pauli} + \Delta E_{elstat} + \Delta E_{orb} + \Delta E_{disp} \quad (2)$$

In these calculations, scalar relativistic effects were treated within the zeroth order regular approximation (ZORA).[81] The BLYP-D3BJ functional was used with the all-electron TZ2P (ZORA) basis set for all atoms.

To include solvent effects, the above described B3LYP/BS1 optimizations and B3LYP-D3BJ/BS2 single point calculations were performed also in the water environment for all structures using IEFPCM (PCM) implicit solvent approach. BSSE corrections with the PCM regime were calculated with ghost atomic orbital functions localized inside the cavity having the same size as the whole complex.[82]

All optimizations and single point calculations were carried out by the Gaussian 09, revision D.01 (G09) program package.[83] Atoms in molecules (AIM) topological analysis of the electron density in bond critical points was performed on selected structures by the AIMAll program.[84] NBO analysis was carried out, and atomic charges based on NAO's (natural population analysis (NPA) charges) were determined by the NBO 3.1 program.[85] Wave function properties were analyzed by the Multiwfn 3.7 program.[54]

■ ASSOCIATED CONTENT

⑤ Supporting Information

The Supporting Information is available free of charge at https://pubs.acs.org/doi/10.1021/acsomega.0c01161.

Complete versions of Tables 2–7 with the data for all X's; electron density difference isosurfaces of p-**NH$_2$** and p-**NO$_2$** structures with respect to the reference pyrH structure; five most important ETS-NOCV deformation density contributions describing the formation of the Pt–N_{pyrX} bond in **H-R**, **H-TS**, and **H–P** structures; dependence of pyr-X ligand binding energies on the Pt–N_{pyrX} bond lengths and the dependence of the σ-donation energy ΔE_{orb}^{σ} contributions on total ΔE_{orb} energies for **X-TS** and **X-P** structures; ETS-NOCV deformation density contributions for the formation of the Pt–N_{pyrX} bond in **X-R** structures which involve contribution from Pt···H (o-NH$_2$-R, o-OH-R), Pt···S (o-SH-R) nonbonding interactions or NH$_3$···N (o-DMA-R), NH$_3$···O (o-NO$_2$-R) H-bond interactions; dependence of the Pt–pyrX binding energy on the transferred q(pyrX) charge for **X-R**, **X-TS**, and **X-P** structures; dependence of the gas phase Pt–pyrX binding energy on the NBO charge of the N_{pyrX} atom ($q(N_{pyrX})$), the total dipole moment of pyrX (p(pyrX)), and the projection of the dipole moment into C4–N_{pyrX} direction (p_x(pyrX)) for **X-R**, **X-TS**, and **X-P** structures; dependence of the gas phase Pt–pyrX binding energies for **X-R**, **X-TS**, and **X-P** structures on the minimum surface electrostatic potential calculated on the surface of the N_{pyrX} atom in the isolated pyrX ligand; correlation between ΔE_{elst} and ΔE_{orb} terms for the Pt–pyrX interaction in **X-R**, **X-TS**, and **X-P** structures; dependence of Pt–ligand binding energies on the LP(N_{pyrX}) NBO energy in the gas phase and the water solvent; electron density difference isosurfaces of p-**NH$_2$-R** and p-**NO$_2$-R** structures with respect to the reference **H-R** structure calculated in the water solvent; dependence of the gas-phase activation Gibbs free energies ($\Delta G^{\ddagger}$) on the Hirschfeld charges calculated on the Pt(II) atom; bonding energies, bond lengths, and ligand NPA charges in poly-**X-R** and poly-**X-P** structures (X = F, NH$_2$, NO$_2$) optimized in the gas

phase and water solvent, $\Delta G^{\ddagger}$ activation free energies, and estimated values of all these variables (eq 1) with absolute and relative errors; stabilizing H-bonds in the **2op-NH₂-R** and **2op-NH₂-P** structures; plots of calculated versus estimated (eq 1) values of $\Delta G^{\ddagger}$ activation free energies for complexes with poly-substituted ligands in the gas phase and the water solvent; correlations between B3LYP/BS1 and M06-2X/BS1 bond lengths for the **X-R_w** and **X-TS** structures and the correlations between B3LYP-D3BJ//BS2//B3LYP/BS1 and M06-2X/BS2//M06-2X/BS1 activation free energies in the gas phase and the water solvent; correlations between B3LYP/BS1 and PBE0/BS1 bond lengths for the **X-R_w**, **X-TS** structures and the correlations between B3LYP-D3BJ//BS2//B3LYP/BS1 and PBE0-D3BJ//BS2//PBE0/BS1 activation free energies in the gas phase; and dependence of the relative values M06-2X/BS2//M06-2X/BS1 calculated activation free energy barriers $(\Delta(\Delta G^{\ddagger}))$ of the hydration reactions of the *trans*-$[Pt(NH_3)_2(pyrX) Cl]^+$ complexes on the nature and the position of the X in the gas phase and in the water solvent (PDF)

Optimized Cartesian coordinates of all TS and the most stable minimum structures (XYZ)

■ AUTHOR INFORMATION

Corresponding Author
Zdeněk Chval − *Faculty of Health and Social Sciences, University of South Bohemia, 370 11 České Budějovice, Czech Republic;* orcid.org/0000-0003-1922-8390; Phone: +420-389-037-612; Email: chval@jcu.cz

Author
Olga Dvořáčková − *Faculty of Health and Social Sciences and Faculty of Science, University of South Bohemia, 370 11 České Budějovice, Czech Republic*

Complete contact information is available at:
https://pubs.acs.org/10.1021/acsomega.0c01161

Notes
The authors declare no competing financial interest.

■ ACKNOWLEDGMENTS

■ REFERENCES

(1) Reedijk, J.; Teuben, J. M. Platinum-Sulfur Interactions Involved in Antitumor Drugs, Rescue Agents, and Biomolecules. In *Cisplatin*; Lippert, B., Ed.; Verlag Helvetica Chimica Acta, 1999; pp 339−362.

(2) Lin, Z.; Hall, M. B. Theoretical studies of inorganic and organometallic reaction mechanisms. 2. The trans effect in square-planar platinum(II) and rhodium(I) substitution reactions. *Inorg. Chem.* **1991**, *30*, 646−651.

(3) Wendt, O. F.; Elding, L. I. Trans Effect and Trans Influence of Triphenyl-Stibine and -Phosphine in Platinum(II) Complexes. A Comparative Mechanistic and Structural Study. *J. Chem. Soc., Dalton Trans.* **1997**, *24*, 4725−4732.

(4) Khoroshun, D. V.; Musaev, D. G.; Morokuma, K. Electronic Reorganization: Origin of Sigma Trans Promotion Effect. *J. Comput. Chem.* **2007**, *28*, 423−441.

(5) Zhu, J.; Lin, Z.; Marder, T. B. Trans Influence of Boryl Ligands and Comparison with C, Si, and Sn Ligands. *Inorg. Chem.* **2005**, *44*, 9384−9390.

(6) Chval, Z.; Sip, M.; Burda, J. V. The Trans Effect in Square-Planar Platinum(II) Complexes—A Density Functional Study. *J. Comput. Chem.* **2008**, *29*, 2370−2381.

(7) Kapoor, P. N.; Kakkar, R. Trans and Cis Influence in Square Planar Pt(II) Complexes: A Density Functional Study of [PtClX-(DmS)(2)] and Related Complexes. *J. Mol. Struct.: THEOCHEM* **2004**, *679*, 149−156.

(8) Pinter, B.; Van Speybroeck, V.; Waroquier, M.; Geerlings, P.; De Proft, F. Trans Effect and Trans Influence: Importance of Metal Mediated Ligand−Ligand Repulsion. *Phys. Chem. Chem. Phys.* **2013**, *15*, 17354.

(9) Tsipis, A. C. Trans-Philicity (Trans-Influence/Trans-Effect) Ladders for Square Planar Platinum(II) Complexes Constructed by 35Cl NMR Probe. *J. Comput. Chem.* **2019**, *40*, 2550−2562.

(10) Manojlovic-Muir, L. J.; Muir, K. W. The Trans-Influence of Ligands in Platinum(II) Complexes. The Significance of the Bond Length Data. *Inorg. Chim. Acta* **1974**, *10*, 47−49.

(11) Wheate, N. J.; Walker, S.; Craig, G. E.; Oun, R. The Status of Platinum Anticancer Drugs in the Clinic and in Clinical Trials. *Dalton Trans.* **2010**, *39*, 8113−8127.

(12) Malina, J.; Novakova, O.; Vojtiskova, M.; Natile, G.; Brabec, V. Conformation of DNA GG Intrastrand Cross-Link of Antitumor Oxaliplatin and Its Enantiomeric Analog. *Biophys. J.* **2007**, *93*, 3950−3962.

(13) Legendre, F.; Bas, V.; Kozelka, J.; Chottard, J.-C. A Complete Kinetic Study of GG versus AG Platination Suggests That the Doubly Aquated Derivatives of Cisplatin Are the Actual DNA Binding Species. *Chem.—Eur. J.* **2000**, *6*, 2002−2010.

(14) Kozelka, J. Molecular Origin of the Sequence-Dependent Kinetics of Reactions between Cisplatin Derivatives and DNA. *Inorg. Chim. Acta* **2009**, *362*, 651−668.

(15) Chval, Z.; Kabeláč, M.; Burda, J. V. Mechanism of the cis-[Pt(1R,2R-DACH)(H2O)2]2+ Intrastrand Binding to the Double-Stranded (pGpG)·(CpC) Dinucleotide in Aqueous Solution: A Computational DFT Study. *Inorg. Chem.* **2013**, *52*, 5801−5813.

(16) Summa, N.; Schiessl, W.; Puchta, R.; van Eikema Hommes, N.; van Eldik, R. Thermodynamic and Kinetic Studies on Reactions of Pt(II) Complexes with Biologically Relevant Nucleophiles. *Inorg. Chem.* **2006**, *45*, 2948−2959.

(17) Petrović, B.; Bugarčić, Ž. D.; Dees, A.; Ivanović-Burmazović, I.; Heinemann, F. W.; Puchta, R.; Steinmann, S. N.; Corminboeuf, C.; van Eldik, R. Role of π-Acceptor Effects in Controlling the Lability of Novel Monofunctional Pt(II) and Pd(II) Complexes: Crystal Structure of [Pt(Tripyridinedimethane)Cl]Cl. *Inorg. Chem.* **2012**, *51*, 1516−1529.

(18) Kinunda, G.; Jaganyi, D. Understanding the Electronic and π-Conjugation Roles of Quinoline on Ligand Substitution Reactions of Platinum(II) Complexes. *Transition Met. Chem.* **2014**, *39*, 451−459.

(19) Khusi, B. B.; Mambanda, A.; Jaganyi, D. The Role of Substituents in a Bidentate N,N-Chelating Ligand on the Substitution of Aqua Ligands from Mononuclear Pt(II) Complexes. *Transition Met. Chem.* **2016**, *41*, 191−203.

(20) Jaganyi, D.; Hofmann, A.; van Eldik, R. Controlling the Lability of Square-Planar PtII Complexes through Electronic Communication between π-Acceptor Ligands. *Angew. Chem., Int. Ed.* **2001**, *40*, 1680−1683.

(21) Ćoćić, D.; Jovanović, S.; Radisavljević, S.; Korzekwa, J.; Scheurer, A.; Puchta, R.; Baskić, D.; Todorović, D.; Popović, S.; Matić, S.; Petrović, B. New Monofunctional Platinum(II) and Palladium(II) Complexes: Studies of the Nucleophilic Substitution Reactions, DNA/BSA Interaction, and Cytotoxic Activity. *J. Inorg. Biochem.* **2018**, *189*, 91−102.

(22) Shaira, A.; Reddy, D.; Jaganyi, D. A Kinetic and Mechanistic Study into the Substitution Behaviour of Platinum(II) Polypyridyl Complexes with a Series of Azole Ligands. *Dalton Trans.* **2013**, *42*, 8426−8436.

(23) Lovejoy, K. S.; Todd, R. C.; Zhang, S.; McCormick, M. S.; D'Aquino, J. A.; Reardon, J. T.; Sancar, A.; Giacomini, K. M.; Lippard, S. J. Cis-Diammine(Pyridine)Chloroplatinum(II), a Monofunctional Platinum(II) Antitumor Agent: Uptake, Structure, Function, and Prospects. *Proc. Natl. Acad. Sci. U.S.A.* **2008**, *105*, 8902−8907.

(24) Icsel, C.; Yilmaz, V. T.; Golcu, A.; Ulukaya, E.; Buyukgungor, O. Synthesis, Crystal Structures, DNA Binding and Cytotoxicity of Two Novel Platinum(II) Complexes Containing 2-(Hydroxymethyl)-Pyridine and Pyridine-2-Carboxylate Ligands. *Bioorg. Med. Chem. Lett.* **2013**, *23*, 2117−2122.

(25) Munk, V. P.; Diakos, C. I.; Ellis, L. T.; Fenton, R. R.; Messerle, B. A.; Hambley, T. W. Investigations into the Interactions between DNA and Conformationally Constrained Pyridylamineplatinum(II) Analogues of AMD473. *Inorg. Chem.* **2003**, *42*, 3582−3590.

(26) Cerón-Carrasco, J. P.; Jacquemin, D. Tuning the Optical Properties of Phenanthriplatin: Towards New Photoactivatable Analogues. *ChemPhotoChem* **2017**, *1*, 504−512.

(27) Stehlikova, K.; Kasparkova, J.; Novakova, O.; Martinez, A.; Moreno, V.; Brabec, V. Recognition of DNA Modified by Trans-[PtCl2NH3(4-Hydroxymethylpyridine)] by Tumor Suppressor Protein P53 and Character of DNA Adducts of This Cytotoxic Complex. *FEBS J.* **2006**, *273*, 301−314.

(28) Raynaud, F. I.; Boxall, F. E.; Goddard, P. M.; Valenti, M.; Jones, M.; Murrer, B. A.; Abrams, M.; Kelland, L. R. Cis-Amminedichloro(2-Methylpyridine) Platinum(II) (AMD473), a Novel Sterically Hindered Platinum Complex: In Vivo Activity, Toxicology, and Pharmacokinetics in Mice. *Clin. Cancer Res.* **1997**, *3*, 2063−2074.

(29) Chen, Y.; Guo, Z.; Parsons, S.; Sadler, P. J. Stereospecific and Kinetic Control over the Hydrolysis of a Sterically Hindered Platinum Picoline Anticancer Complex. *Chem.—Eur. J.* **1998**, *4*, 672−676.

(30) Gao, Y.; Zhou, L. DNA Bindings of a Novel Anticancer Drug, Trans-[PtCl2(Isopropylamine)(3-Picoline)], and Kinetic Competition of Purine Bases with Protein Residues in the Bifunctional Substitutions: A Theoretical DFT Study. *Theor. Chem. Acc.* **2009**, *123*, 455−468.

(31) Banerjee, S.; Sengupta, P. S.; Mukherjee, A. K. A Detailed Theoretical DFT Study of the Hydrolysis Mechanism of Orally Active Anticancer Drug ZD0473. *Chem. Phys. Lett.* **2010**, *487*, 108−115.

(32) Sarmah, P.; Deka, R. C. Hydrolysis and Binding Mechanism of AMD473 (Cis-[PtCl2(NH3)(2-Picoline)]) with Guanine: A Quantum Mechanical Study. *J. Mol. Struct.: THEOCHEM* **2010**, *955*, 53−60.

(33) Novotný, J.; Sojka, M.; Komorovsky, S.; Nečas, M.; Marek, R. Interpreting the Paramagnetic NMR Spectra of Potential Ru(III) Metallodrugs: Synergy between Experiment and Relativistic DFT Calculations. *J. Am. Chem. Soc.* **2016**, *138*, 8432−8445.

(34) Lovejoy, K. S.; Serova, M.; Bieche, I.; Emami, S.; D'Incalci, M.; Broggini, M.; Erba, E.; Gespach, C.; Cvitkovic, E.; Faivre, S.; Raymond, E.; Lippard, S. J. Spectrum of Cellular Responses to Pyriplatin, a Monofunctional Cationic Antineoplastic Platinum(II) Compound, in Human Cancer Cells. *Mol. Cancer Ther.* **2011**, *10*, 1709−1719.

(35) Pinto, A. L.; Lippard, S. J. Sequence-Dependent Termination of in Vitro DNA Synthesis by Cis- and Trans-Diamminedichloroplatinum (II). *Proc. Natl. Acad. Sci. U.S.A.* **1985**, *82*, 4616.

(36) Hollis, L. S.; Amundsen, A. R.; Stern, E. W. Chemical and Biological Properties of a New Series of Cis-Diammineplatinum(II) Antitumor Agents Containing Three Nitrogen Donors: Cis-[Pt-(NH3)2(N-Donor) Cl]+. *J. Med. Chem.* **1989**, *32*, 128−136.

(37) Park, G. Y.; Wilson, J. J.; Song, Y.; Lippard, S. J. Phenanthriplatin, a Monofunctional DNA-Binding Platinum Anticancer Drug Candidate with Unusual Potency and Cellular Activity Profile. *Proc. Natl. Acad. Sci. U.S.A.* **2012**, *109*, 11987−11992.

(38) Gregory, M. T.; Park, G. Y.; Johnstone, T. C.; Lee, Y.-S.; Yang, W.; Lippard, S. J. Structural and Mechanistic Studies of Polymerase Bypass of Phenanthriplatin DNA Damage. *Proc. Natl. Acad. Sci. U.S.A.* **2014**, *111*, 9133−9138.

(39) Veclani, D.; Melchior, A.; Tolazzi, M.; Cerón-Carrasco, J. P. Using Theory To Reinterpret the Kinetics of Monofunctional

(40) Almaqwashi, A. A.; Zhou, W.; Naufer, M. N.; Riddell, I. A.; Yilmaz, Ö. H.; Lippard, S. J.; Williams, M. C. DNA Intercalation Facilitates Efficient DNA-Targeted Covalent Binding of Phenanthriplatin. *J. Am. Chem. Soc.* **2019**, *141*, 1537−1545.

(41) Chval, Z.; Sip, M. Pentacoordinated Transition States of Cisplatin Hydrolysis—Ab Initio Study. *J. Mol. Struct.: THEOCHEM* **2000**, *532*, 59−68.

(42) Zhang, Y.; Guo, Z.; You, X.-Z. Hydrolysis Theory for Cisplatin and Its Analogues Based on Density Functional Studies. *J. Am. Chem. Soc.* **2001**, *123*, 9378−9387.

(43) Costa, L. A. S.; Rocha, W. R.; De Almeida, W. B.; Dos Santos, H. F. The Hydrolysis Process of the Cis-Dichloro(Ethylenediamine)-Platinum(II): A Theoretical Study. *J. Chem. Phys.* **2003**, *118*, 10584−10592.

(44) Lau, J. K.-C.; Deubel, D. V. Hydrolysis of the Anticancer Drug Cisplatin: Pitfalls in the Interpretation of Quantum Chemical Calculations. *J. Chem. Theory Comput.* **2006**, *2*, 103−106.

(45) Burda, J. V.; Zeizinger, M.; Leszczynski, J. Hydration Process as an Activation of Trans- and Cisplatin Complexes in Anticancer Treatment. DFT and Ab Initio Computational Study of Thermodynamic and Kinetic Parameters. *J. Comput. Chem.* **2005**, *26*, 907−914.

(46) Zimmermann, T.; Leszczynski, J.; Burda, J. V. Activation of the Cisplatin and Transplatin Complexes in Solution with Constant PH and Concentration of Chloride Anions; Quantum Chemical Study. *J. Mol. Model.* **2011**, *17*, 2385−2393.

(47) Ahmad, S. Kinetic Aspects of Platinum Anticancer Agents. *Polyhedron* **2017**, *138*, 109−124.

(48) Kozelka, J. Hydrolysis of Chlorido Complexes of D8 Metals: Old Models, New Facts. *Inorg. Chim. Acta* **2019**, *495*, 118946.

(49) Grushin, V. V. The Organometallic Fluorine Chemistry of Palladium and Rhodium: Studies toward Aromatic Fluorination. *Acc. Chem. Res.* **2010**, *43*, 160−171.

(50) Mazurek, A.; Dobrowolski, J. C. Heteroatom Incorporation Effect in σ- and π-Electron Systems: The sEDA(II) and pEDA(II) Descriptors. *J. Org. Chem.* **2012**, *77*, 2608−2618.

(51) Siodła, T.; Ozimiński, W. P.; Hoffmann, M.; Koroniak, H.; Krygowski, T. M. Toward a Physical Interpretation of Substituent Effects: The Case of Fluorine and Trifluoromethyl Groups. *J. Org. Chem.* **2014**, *79*, 7321−7331.

(52) Stenlid, J. H.; Brinck, T. Nucleophilic Aromatic Substitution Reactions Described by the Local Electron Attachment Energy. *J. Org. Chem.* **2017**, *82*, 3072−3083.

(53) Dapprich, S.; Frenking, G. Investigation of Donor-Acceptor Interactions: A Charge Decomposition Analysis Using Fragment Molecular Orbitals. *J. Phys. Chem.* **1995**, *99*, 9352−9362.

(54) Lu, T.; Chen, F. Multiwfn: A Multifunctional Wavefunction Analyzer. *J. Comput. Chem.* **2012**, *33*, 580−592.

(55) Wolters, L. P.; Bickelhaupt, F. M. The Activation Strain Model and Molecular Orbital Theory. *Wiley Interdiscip. Rev.: Comput. Mol. Sci.* **2015**, *5*, 324−343.

(56) Sajith, P. K.; Suresh, C. H. Quantification of Mutual Trans Influence of Ligands in Pd(II) Complexes: A Combined Approach Using Isodesmic Reactions and AIM Analysis. *Dalton Trans.* **2009**, *39*, 815−822.

(57) Sajith, P. K.; Suresh, C. H. Bond Dissociation Energies of Ligands in Square Planar Pd(II) and Pt(II) Complexes: An Assessment Using Trans Influence. *J. Organomet. Chem.* **2011**, *696*, 2086−2092.

(58) Sandoval-Lira, J.; Mondragón-Solórzano, G.; Lugo-Fuentes, L. I.; Barroso-Flores, J. Accurate Estimation of PKb Values for Amino Groups from Surface Electrostatic Potential (VS,Min) Calculations: The Isoelectric Points of Amino Acids as a Case Study. *J. Chem. Inf. Model.* **2020**, *60*, 1445−1452.

(59) Chval, Z.; Dvořáčková, O.; Chvalová, D.; Burda, J. V. Square-Planar Pt(II) and Ir(I) Complexes as the Lewis Bases: Donor-Acceptor Adducts with Group 13 Trihalides and Trihydrides. *Inorg. Chem.* **2019**, *58*, 3616−3626.

(60) Kapinos, L. E.; Sigel, H. Acid−Base and Metal Ion Binding Properties of Pyridine-Type Ligands in Aqueous Solution.: Effect of Ortho Substituents and Interrelation between Complex Stability and Ligand Basicity. *Inorg. Chim. Acta* **2002**, *337*, 131−142.

(61) Wang, B.; Rong, C.; Chattaraj, P. K.; Liu, S. A Comparative Study to Predict Regioselectivity, Electrophilicity and Nucleophilicity with Fukui Function and Hirshfeld Charge. *Theor. Chem. Acc.* **2019**, *138*, 124.

(62) Ebrahimi, A.; Habibi-Khorasani, S. M.; Jahantab, M. Additivity of Substituent Effects on the Proton Affinity and Gas-Phase Basicity of Pyridines. *Comput. Theor. Chem.* **2011**, *966*, 31−37.

(63) Hęclik, K.; Dobrowolski, J. C. On the Nonadditivity of the Substituent Effect in Homo-Disubstituted Pyridines. *J. Phys. Org. Chem.* **2017**, *30*, No. e3656.

(64) Cerón-Carrasco, J. P.; Requena, A.; Jacquemin, D. Impact of DFT Functionals on the Predicted Magnesium−DNA Interaction: An ONIOM Study. *Theor. Chem. Acc.* **2012**, *131*, 1188.

(65) Dohm, S.; Hansen, A.; Steinmetz, M.; Grimme, S.; Checinski, M. P. Comprehensive Thermochemical Benchmark Set of Realistic Closed-Shell Metal Organic Reactions. *J. Chem. Theory Comput.* **2018**, *14*, 2596−2608.

(66) Gwee, E. S. H.; Seeger, Z. L.; Appadoo, D. R. T.; Wood, B. R.; Izgorodina, E. I. Influence of DFT Functionals and Solvation Models on the Prediction of Far-Infrared Spectra of Pt-Based Anticancer Drugs: Why Do Different Complexes Require Different Levels of Theory? *ACS Omega* **2019**, *4*, 5254−5269.

(67) Zhao, Y.; Truhlar, D. G. The M06 Suite of Density Functionals for Main Group Thermochemistry, Thermochemical Kinetics, Noncovalent Interactions, Excited States, and Transition Elements: Two New Functionals and Systematic Testing of Four M06-Class Functionals and 12 Other Functionals. *Theor. Chem. Acc.* **2008**, *120*, 215−241.

(68) McGowan, G.; Parsons, S.; Sadler, P. J. Contrasting Chemistry ofcis- andtrans-Platinum(II) Diamine Anticancer Compounds: Hydrolysis Studies of Picoline Complexes. *Inorg. Chem.* **2005**, *44*, 7459−7467.

(69) Michalska, D.; Wysokiński, R. Molecular Structure and Bonding in Platinum-Picoline Anticancer Complex: Density Functional Study. *Collect. Czech. Chem. Commun.* **2004**, *69*, 63−72.

(70) Martínez, A.; Lorenzo, J.; Prieto, M. J.; Font-Bardia, M.; Solans, X.; Avilés, F. X.; Moreno, V. Influence of the Position of Substituents in the Cytotoxic Activity of Trans Platinum Complexes with Hydroxymethyl Pyridines. *Bioorg. Med. Chem.* **2007**, *15*, 969−979.

(71) Becke, A. D. Density-functional thermochemistry. III. The role of exact exchange. *J. Chem. Phys.* **1993**, *98*, 5648.

(72) Andrae, D.; Häußermann, U.; Dolg, M.; Stoll, H.; Preuß, H. Energy-Adjustedab Initio Pseudopotentials for the Second and Third Row Transition Elements. *Theor. Chem. Acc. Theory Comput. Model. Theor. Chim. Acta* **1990**, *77*, 123−141.

(73) Bergner, A.; Dolg, M.; Küchle, W.; Stoll, H.; Preuß, H. Ab initio energy-adjusted pseudopotentials for elements of groups 13-17. *Mol. Phys.* **1993**, *80*, 1431−1441.

(74) Burda, J. V.; Zeizinger, M.; Šponer, J.; Leszczynski, J. Hydration of Cis- and Trans-Platin: A Pseudopotential Treatment in the Frame of a G3-Type Theory for Platinum Complexes. *J. Chem. Phys.* **2000**, *113*, 2224−2232.

(75) Grimme, S.; Ehrlich, S.; Goerigk, L. Effect of the Damping Function in Dispersion Corrected Density Functional Theory. *J. Comput. Chem.* **2011**, *32*, 1456−1465.

(76) Boys, S. F.; Bernardi, F. The Calculation of Small Molecular Interactions by the Differences of Separate Total Energies. Some Procedures with Reduced Errors. *Mol. Phys.* **1970**, *19*, 553−566.

(77) te Velde, G.; Bickelhaupt, F. M.; Baerends, E. J.; Guerra, C. F.; Van Gisbergen, S. J. A.; Snijders, J. G.; Ziegler, T. Chemistry with ADF. *J. Comput. Chem.* **2001**, *22*, 931−967.

(78) Ziegler, T.; Rauk, A. On the calculation of bonding energies by the Hartree Fock Slater method. *Theor. Chim. Acta* **1977**, *46*, 1−10.

(79) Mitoraj, M. P.; Michalak, A.; Ziegler, T. A Combined Charge and Energy Decomposition Scheme for Bond Analysis. *J. Chem. Theory Comput.* **2009**, *5*, 962−975.

(80) Mitoraj, M. P.; Zhu, H.; Michalak, A.; Ziegler, T. On the Origin of the Trans-Influence in Square Planar D8-Complexes: A Theoretical Study. *Int. J. Quantum Chem.* **2009**, *109*, 3379−3386.

(81) van Lenthe, E.; van Leeuwen, R.; Baerends, E. J.; Snijders, J. G. Relativistic Regular Two-Component Hamiltonians. *Int. J. Quantum Chem.* **1996**, *57*, 281−293.

(82) Zimmermann, T.; Chval, Z.; Burda, J. V. Cisplatin Interaction with Cysteine and Methionine in Aqueous Solution: Computational DFT/PCM Study. *J. Phys. Chem. B* **2009**, *113*, 3139−3150.

(83) Frisch, M. J.; Trucks, G. W.; Schlegel, H. B.; Scuseria, G. E.; Robb, M. A.; Cheeseman, J. R.; Scalmani, G.; Barone, V.; Mennucci, B.; Petersson, G. A.; Nakatsuji, H.; Caricato, M.; Li, X.; Hratchian, H. P.; Izmaylov, A. F.; Bloino, J.; Zheng, G.; Sonnenberg, J. L.; Hada, M.; Ehara, M.; Toyota, K.; Fukuda, R.; Hasegawa, J.; Ishida, M.; Nakajima, T.; Honda, Y.; Kitao, O.; Nakai, H.; Vreven, T.; Montgomery, J. A., Jr.; Peralta, J. E.; Ogliaro, F.; Bearpark, M.; Heyd, J. J.; Brothers, E.; Kudin, K. N.; Staroverov, V. N.; Kobayashi, R.; Normand, J.; Raghavachari, K.; Rendell, A.; Burant, J. C.; Iyengar, S. S.; Tomasi, J.; Cossi, M.; Rega, N.; Millam, J. M.; Klene, M.; Knox, J. E.; Cross, J. B.; Bakken, V.; Adamo, C.; Jaramillo, J.; Gomperts, R.; Stratmann, R. E.; Yazyev, O.; Austin, A. J.; Cammi, R.; Pomelli, C.; Ochterski, J. W.; Martin, R. L.; Morokuma, K.; Zakrzewski, V. G.; Voth, G. A.; Salvador, P.; Dannenberg, J. J.; Dapprich, S.; Daniels, A. D.; Farkas, Ö.; Foresman, J. B.; Ortiz, J. V.; Cioslowski, J.; Fox, D. J. *Gaussian 09*, Revision D.01; Gaussian, Inc.: Wallingford CT, 2009.

(84) Keith, T. A. *AIMAll*, Version 10.11.24, (aim.tkgristmill.com), 2010.

(85) Glendening, E. D.; Reed, A. E.; Carpenter, J. E.; Weinhold, F. *NBO 3.1*.

Correction to "Tuning the Reactivity and Bonding Properties of Metal Square-Planar Complexes by the Substitution(s) on the Trans-Coordinated Pyridine Ring"

Olga Dvořáčková and Zdeněk Chval*

Cite This: *ACS Omega* 2020, 5, 15761−15761

Read Online

ACCESS | Metrics & More | Article Recommendations

In the Abstract and the Introduction of the paper we mistakenly assigned a negative charge to some of the substituents X although all pyrX ligands are neutral. Instead of ($X = OH^-$, Cl^-, F^-, Br^-, NO_2^-, NH_2, SH^-, CH_3, $C \equiv CH$, and DMA) the correct designations of the substituents X are ($X = OH$, Cl, F, Br, NO_2, NH_2, SH, CH_3, $C \equiv CH$, DMA) as provided in the rest of the paper. The authors deeply apologize for any confusion this may have caused to readers.

Article OD3

Dvořáčková O., Chval Z.

Tuning the Reactivity and Bonding Properties of the Pt(II) Complexes by the Substitution(s) on the Trans-Coordinated Non-Aromatic Amine Ligand.

Abstract

Kinetics of the hydration reaction and the bonding properties of the trans-$[Pt(NH_3)_2(NH_2X)Cl]^+$ complexes (X=H, CH$_3$, F, Cl, Br, NH$_2$, NO$_2$, OH, dimethylamine (DMA), cyclopropyl (CyP), cyclohexyl (CyH)) were studied theoretically by DFT methodology in the gas phase and the water solution. The electron-donating and electron-withdrawing X substituents lower and increase, respectively, the activation free energy ($\Delta G^{\ddagger}$) and Pt-trans ligand binding energies (BEs) to a similar extent as meta and para substituents of the pyridine ligand studied previously (ACS Omega, 2020, 5, 11768). For the saturated hydrocarbon X substituents (X=H, CH$_3$, CyP, CyH), the $\Delta G^{\ddagger}$ values and Pt-trans ligand BEs decrease with the logarithm of the X substituent size being best quantified by the number of electrons. The additivity of the substituent effects was studied on the NF3 ligand and worked well for ligand charges and Pt-trans ligand BEs. The influence of chelation was evaluated by the comparison of the CyH system and the complexes with the cyclohexanediamine (DACH) ligand. Finally, the effect of isomerization was studied on the complexes with the 1,2-bis(aminomethyl)cyclobutane (BAMCB) ligand. Thus, this study also evaluates the influence of the non-leaving ligands present in cisplatin, oxaliplatin, lobaplatin, JM118, and JM11 drugs on the reactivity of the Pt(II) complexes in the same ligand environment.

The Supporting Information is available free of charge at https://pubs.acs.org/doi/10.1021/acsomega.0c01161.

▌ Inorganic Chemistry

Tuning the Reactivity and Bonding Properties of the Pt(II) Complexes by the Substitution(s) on the Trans-Coordinated Non-Aromatic Amine Ligand

Olga Dvořáčková[a, b] and Zdeněk Chval*[a]

Kinetics of the hydration reaction and the bonding properties of the *trans*-[Pt(NH$_3$)$_2$(NH$_2$X)Cl]$^+$ complexes (X = H, CH$_3$, F, Cl, Br, NH$_2$, NO$_2$, OH, dimethylamine (DMA), cyclopropyl (CyP), cyclohexyl (CyH)) were studied theoretically by DFT methodology in the gas phase and the water solution. The electron-donating and electron-withdrawing X substituents lower and increase, respectively, the activation free energy (ΔG^+) and Pt-trans ligand binding energies (BEs) to a similar extent as meta and para substituents of the pyridine ligand studied previously (ACS Omega, 2020, 5, 11768). For the saturated hydrocarbon X substituents (X = H, CH$_3$, CyP, CyH), the ΔG^+ values and Pt-trans ligand BEs decrease with the logarithm of the X substituent size being best quantified by the number of electrons. The additivity of the substituent effects was studied on the NF$_3$ ligand and worked well for ligand charges and Pt–trans ligand BEs. The influence of chelation was evaluated by the comparison of the CyH system and the complexes with the cyclohexanediamine (DACH) ligand. Finally, the effect of isomerization was studied on the complexes with the 1,2-bis (aminomethyl)cyclobutane (BAMCB) ligand. Thus, this study also evaluates the influence of the non-leaving ligands present in cisplatin, oxaliplatin, lobaplatin, JM118, and JM11 drugs on the reactivity of the Pt(II) complexes in the same ligand environment.

Introduction

Hydrolysis is a key step in the biotransformation of platinum metal drugs. A hydrolyzed drug is able to attack many biological targets in the cell such as nucleic acids and proteins. While the binding to proteins is responsible for the side effects of the drugs, the DNA structure modification caused by the platinum drug binding enables a successful explanation of their anticancer effect.[1] To reach the DNA target inside the malignant cells, the speed of hydrolysis has to correspond to the speed of the drugs' metabolism.[2] If it is too fast, the drugs attack proteins increasing their side effects but if it is too slow the drug is eliminated from the body with no remedial effect. Thus, the rate of hydrolysis should be tuned to reach the optimal efficacy of the drug.

The replacement of chloride ions by water molecules in cisplatin and its derivatives was a subject of many previous studies[3–9] and reviewed by Ahmad.[10] The reactivity of the Pt(II)-drugs depends on the nature of both the leaving and non-leaving ligands. Two monofunctional chlorines in cisplatin are replaced by bidentate dicarboxylate derivatives in the second generation Pt(II) anticancer drugs. The influence of the nature of the leaving group(s) on the Pt(II) drug reactivity has been studied extensively.[11–16] In the third generation Pt(II) drugs the two amines are substituted by hydrocarbonamine groups mostly forming a divalent chelate. The effects of the non-leaving ligand(s) modifications have also been investigated but mostly on aromatic systems[17] and/or the interest has been focused on their antiproliferative and anticancer activities.[18–22] Kinetic aspects of non-aromatic non-leaving ligands have been explored less frequently[23–25] being often compared with the NH$_3$ groups in cisplatin.[26,27] However, it is hard to exactly compare the data about the influence of the ligands on the reactivity of Pt(II) complexes from different studies due to a diversity of experimental conditions and theoretical models. The possible roles of NH$_3$ ligands in Pt complexes were reviewed by Lippert's group,[28] but the impact of NH$_3$ modifications was not covered.

In our previous study, we evaluated the changes in reactivity and binding properties of the Pt(II) complex connected with the substitution(s) of the aromatic pyridine (pyrH) ring as the non-leaving ligand.[29] This contribution is focused on the influence of modifications of the non-aromatic non-leaving amine ligand. We show how the X substitutions on the NH$_3$ group in the trans position (denoted as NH$_2$H in the further text to be distinguished from the two NH$_3$ groups in the cis positions) with respect to the leaving chlorine group influence the reactivity and binding properties of the *trans*-[Pt-(NH$_3$)$_2$(NH$_2$X)Cl]$^+$ complexes.

The paper is organized as follows: Firstly, the effects of the amine NH$_2$H and aromatic pyrH[29] ligands were compared.

[a] O. Dvořáčková, Z. Chval
Faculty of Health and Social Sciences,
University of South Bohemia,
J. Boreckého 27, 370 11
České Budějovice, Czech Republic
E-mail: chval@jcu.cz

[b] O. Dvořáčková
Faculty of Science,
University of South Bohemia,
Branišovská 1760, 370 05
České Budějovice, Czech Republic

ChemistrySelect

Full Papers
doi.org/10.1002/slct.202100887

Chemistry Europe
European Chemical
Societies Publishing

Secondly, the substitutions by the same X's as in the cited study[29] (X = OH, Cl, F, Br, NO₂, NH₂, CH₃, DMA = dimethylamine) (will be referred to as 'elemental' X's in the further text) were studied separately for comparison purposes. Elemental X's included both electron-donating (NH₂, DMA), electron-withdrawing (NO₂, OH, F, Cl, Br) groups. We show how the stability of Pt–NH₂X, Pt–Cl, Pt–w (w = water) bonds and the kinetics of

Scheme 1. The associative interchange mechanism[30] of the hydration reactions studied in this contribution. All reaction pathways proceed over the pentacoordinated **X-TS** transition state (TS) structures.[3]

Scheme 2. The structural formulas of **CyP-R** (a), **CyH-R** (b), **DACH-R** (c), and **BAMCB**-R (d) complexes.

the hydration reaction are affected by the nature of X in the NH₂X ligand (Scheme 1).

Thirdly, the additivity of the substituent effects was tested on the NF₃ ligand as a representative of multisubstituted complexes.

Fourthly, the substituents present in the real anticancer compounds were also included considering the cyclopropyl (CyP) and cyclohexyl (CyH) derivatives of the amine ligand (Scheme 2) which are the non-leaving ligands in the JM11 and JM118 Pt(II) drugs, respectively. These complexes represent the alpha-carbon substituents of the primary amine groups and can be also viewed as ethylene and pentylene derivatives of the CH₃ substituent. They were also used as independent structures for the validity testing of our findings.
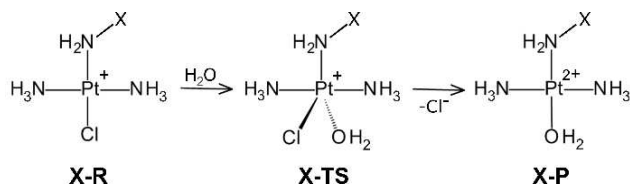
Fifthly, the system with the 1,2-diaminocyclohexane (DACH) ligand (Scheme 2) as the bidentate non-leaving group of oxaliplatin was studied to see the effect of chelation on the reactivity of the Pt(II) complex when compared with the CyH system.

Sixthly, the effect of isomerization was explored by the comparison of the systems with DACH and 1,2-bis (aminomethyl)cyclobutane (BAMCB) ligands. BAMCB is the non-leaving group of lobaplatin. Both DACH and BAMCB ligands were studied in the R,R configuration.

Results and discussion

Comparison of the influence of the NH₂H and pyrH ligands

In the gas phase, the Pt–NH₂H bond in the **H-R** and **H-P** structures was by 20% and 23% (i.e., by 13.5 and 25.9 kcal/mol) weaker (Tables 1 and S1), respectively than the Pt–pyrH bond analyzed in our previous study.[29] A similar decrease of relative values was calculated also for Pauli (by 19 and 18%), electrostatic (by 18 and 16%), and orbital (by 22 and 26%) energy decomposition terms in the two pairs of structures (Table S2). σ-donation was less affected (11% and 12% decrease), but dispersion and π-donation energies were
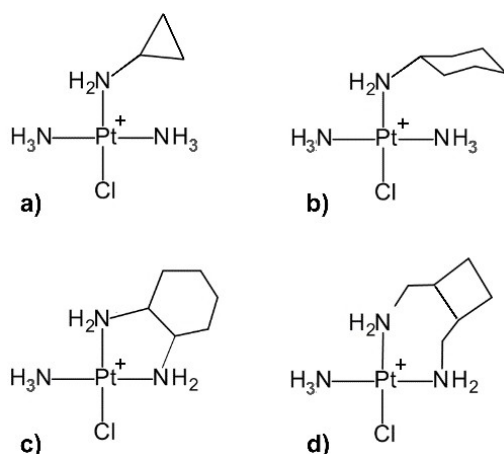
Table 1. Pt–ligand interactions in the optimized **X-R** structures: Pt–N$_{NH2X}$ and Pt–Cl bond lengths (in Å); ΔE_{Bind} energy values (in kcal/mol).[a,b]

X-R	gas phase				water solvent			
	Pt–N$_{NH2X}$	ΔE_{bind}^{NH2X}	Pt–Cl	ΔE_{bind}^{Cl}	Pt–N$_{NH2X}$	ΔE_{bind}^{NH2X}	Pt–Cl	ΔE_{bind}^{Cl}
H	2.132	−52.1	2.305	−266.8	2.086	−39.8	2.366	−39.7
Br	2.090	−48.6	2.301	−265.9	2.051	−34.5	2.350	−41.1
CH₃	2.129	−57.0	2.312	−259.7	2.088	−42.9	2.361	−38.0
Cl	2.112	−46.7	2.300	−269.0	2.082	−32.4	2.346	−43.0
DMA	2.122	−62.0	2.310	−253.6	2.089	−43.8	2.360	−38.4
F	2.084	−46.8	2.299	−274.0	2.042	−33.5	2.343	−42.5
NH₂	2.126	−57.5	2.305	−261.5	2.083	−41.9	2.358	−38.8
NO₂	2.137	−34.6	2.292	−276.1	2.126	−20.5	2.334	−44.9
OH	2.118	−50.8	2.302	−265.7	2.078	−36.8	2.355	−40.7
F₃	2.069	−25.4	2.279	−291.2	2.050	−11.7	2.320	−49.9
CyP	2.131	−57.8	2.314	−253.3	2.101	−41.4	2.364	−38.7
CyH	2.125	−63.0	2.318	−249.2	2.096	−45.3	2.366	−37.7
DACH	2.117	−134.2 [c]	2.312	−248.5	2.079	−85.2 [c]	2.367	−37.8
BAMCB	2.123	−133.1 [c]	2.317	−249.8	2.111	−77.9 [c]	2.363	−39.1

[a] The total NPA charges of the Pt atom and the NH₂X, Cl ligands are shown in Table S3. [b] Corresponding data for X–P structures are shown in Tables S1 and S4. [c] Bidentate bonding to the complex.

ChemistrySelect

Full Papers
doi.org/10.1002/slct.202100887

**Chemistry
Europe**
European Chemical
Societies Publishing

lowered substantially by about 50%. The π-donation energy decrease reflects the lower π(-back)-donation ability of NH$_2$H compared to the aromatic pyrH ligand.[31]

On the other hand, more favorable electrostatic energy is responsible for the Pt–Cl bond strength enhancement by about 7% (i.e., by 18.1 kcal/mol) when being in the trans position to the NH$_2$H ligand compared to pyrH in the **X-R** structures since the contributions of the other terms to the BE difference were by one order of magnitude lower (Table S2). The Pt–w bond in **X-P** structures was stronger when being in the trans position to the NH$_2$H ligand by 14% (6.7 kcal/mol) compared to pyrH due to more favorable electrostatic and orbital energies.

The water solvent reduced the differences in BEs compared to the gas phase. The Pt–NH$_2$H bond was weaker by 9 and 8% (by 4.0 and 4.3 kcal/mol) in the **H-R** and **H-P** structures (Tables 1 and S1), respectively, compared to the Pt–pyrH bond. The Pt–Cl and Pt–w bonds were stronger by 3 and 4% (by 1.0 and 0.7 kcal/mol) when being in the trans position to the NH$_2$H ligand in the respective structures.

In the gas phase and the water solvent, the activation free energies $\triangle G^{+}$ for the NH$_2$H system were 35.4 and 26.9 kcal/mol, which were by 2.2 and 1.0 kcal/mol, respectively, higher values than for the pyrH system.[29] It is probably caused by the higher stability of the Pt–Cl bond (cf. below).

Influence of the 'elemental' X substituents

Pt–ligand bond strength. The electron-donating and electron-withdrawing substituents make the Pt–NH$_2$X bond stronger and weaker, respectively, compared to parent X=H. The effect was strongest for X=DMA which showed by 23.2 and 25.0% (by 12.1 and 17.1 kcal/mol) stronger Pt–NH$_2$X bond in **DMA-R** and **DMA-P** structures than in the **H-R** and **H-P** ones, respectively (Tables 1, S1). The largest weakening of the Pt–NH$_2$X bond by 26.0 and 13.5% (13.6 and 11.9 kcal/mol) was in **NO$_2$-R** and **NO$_2$-P** structures, respectively. The above values are slightly larger for DMA but smaller for NO$_2$ when compared with the pyrX structures.[29]

Pt-trans ligand binding energies ΔE_{bind}^{Cl} and ΔE_{bind}^{w} show exactly the opposite trends than ΔE_{bind}^{NH2X} due to trans influence. However, the relative changes are smaller due to the weakening influence of the X substituent with increasing distance, which can be documented by the decreasing volume of the electron density difference isosurfaces in Figure 1. The largest weakening of the Pt–Cl/Pt–w bonds was observed for the **DMA-R/DMA-P** structures showing a relative decrease of 4.9/9.3% (13.2/5.0 kcal/mol) compared to the parent **H-R/H-P** structures. The most strengthened Pt–Cl/Pt–w bonds were found in the **NO$_2$-R/F-P** structures with corresponding changes of 3.5/4.5% (9.3/2.4 kcal/mol). The strengthening of the Pt–Cl bond in the **NO$_2$-R** structure compared to the **H-R** structure can be illustrated by a decrease of electron density in the 3p(Cl) orbital oriented along the bond which is the result of larger σ-donation from the Cl^{-} ligand. Exactly the opposite effect can be seen for **DMA-R** (Figure 1).

Generally, the NH$_2$X ligands gave a slightly larger range of Pt-trans ligand BE values by up to 2.5 kcal/mol (for the Pt–Cl bond in the gas phase) than the pyrX ligands.[29] The variation of the
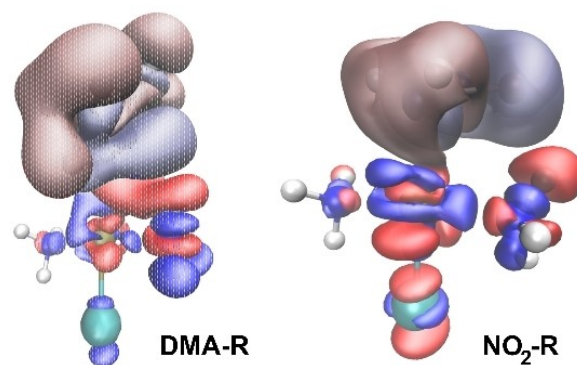

Figure 1. Electron density difference isosurfaces of **DMA-R** and **NO$_2$-R** structures calculated with respect to the reference **H-R** show electron accumulation and electron depletion regions (blue and red isosurfaces, respectively, at values ± 0.0005 a.u.) caused by DMA and NO$_2$ substitution of the NH$_2$H ligand. Electron densities were calculated on the optimized **DMA-R** and **NO$_2$-R** geometries and the reference **H-R** structures were obtained by the replacement of X substituents by the H atom whose position was optimized keeping other atoms fixed. The areas which are dominated by the atom additions/subtractions are depicted by the low contrast colors.

Pt–NH$_2$X bond BEs with respect to the Pt–pyrX ones was less predictable: even smaller by 3.8 kcal/mol for **X-P** structures in the gas phase but much larger in all other cases (by up to 8.2 kcal/mol for **X-R** structures in the water solvent).

BEs of the Pt–ligand bonds in the trans direction are inversely proportional due to trans influence. Their good mutual correlations in Figure 2 are caused by negligible π-back-donation of NH$_2$X, Cl^{-}, and water ligands in the positively charged complexes.
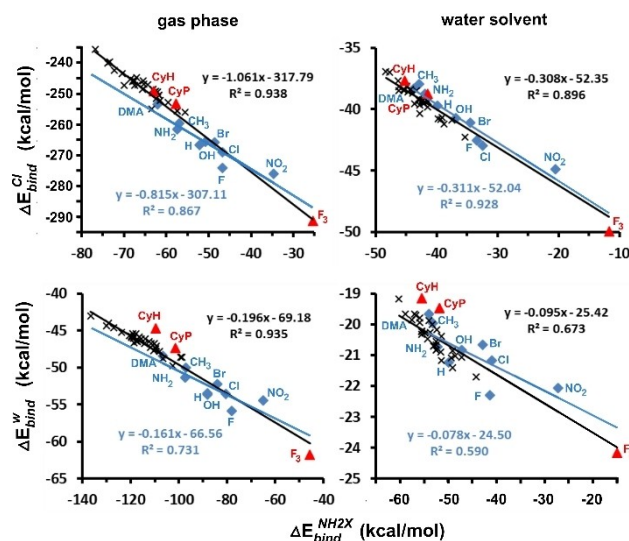

Figure 2. The mutual dependence of BEs of the ligands in the trans direction in the gas phase (left panels) and the water solvent (right panels): Pt–NH$_2$X (Pt–pyrX) vs. Pt–Cl and Pt–NH$_2$X (Pt–pyrX) vs. Pt–w dependencies are shown in the upper and lower panels for **X-R** and **X-P** structures, respectively. pyrX points are designated by black crosses. Black regression lines were constructed from both pyrX and NH$_2$X points while the blue ones just from NH$_2$X points. Red points were not included in the regression analyses.

ChemistrySelect

Full Papers
doi.org/10.1002/slct.202100887

Chemistry Europe
European Chemical
Societies Publishing

Since all Pt–ligand BEs depend directly proportionally on the transferred charge, the same relationship can be also observed for the ligand NPA charges (Figure S1). The correlation of BEs is even better when the results for the pyrX ligand are also included (Figure 2) since the data for the NH$_2$X ligand are more scattered due to the nonbonding X···cis-NH$_3$ interaction (cf. below). These findings are valid for both **X-R** and **X-P** complexes despite their different total charges and diverse strengths of the Pt–ligand bonds. The relative importance of orbital energy compared to the dominant electrostatic energy is much smaller for the Pt–Cl bond than for the Pt–w one, giving evidence of a different nature of the two bonds (Table S2).

Pt–ligand bond strength prediction from NH$_2$X properties. All atoms of the X substituents which bind to the N atom in the NH$_2$X ligand (N$_{NH2X}$ atom) have higher electronegativity than the hydrogen atom and thus the atomic charge of the N$_{NH2X}$ atom is less negative in all isolated substituted NH$_2$X ligands compared to the parent NH$_2$H. The change of the N$_{NH2X}$ atomic charge is roughly linear to the electronegativity difference (R^2 = 0.862). However, a much more important factor for the ligand donation ability is the energy of available electrons. For the pyrX ligands, we were able to predict the stability of the Pt–ligand bonds from the basicity of σ-electrons on the N$_{pyrX}$ atom determined on the isolated pyrX ligand. It was best evaluated by the energy of the 2p(N$_{pyrX}$) natural atomic orbital (NAO) oriented along the N$_{pyrX}$–C4 axis of the pyrX ligand.[29]

However, here all attempts to predict the gas phase BEs of the Pt–ligand bonds from the properties of the isolated NH$_2$X ligands were less successful with R^2 values below 0.9 (Table S5). More details are described in the Supporting Information. It was caused by the X···cis-NH$_3$ interaction which was established for most elemental X's and whose strength depended on the nature of X but without any relation to the dative properties of NH$_2$X. It led to a strong polarization of the cis-NH$_3$ group (Figure 1) accompanied by the charge transfer of up to 0.035e (for X = OH) from NH$_3$ to NH$_2$X. The nonspecific variability of the X···cis-NH$_3$ interaction could also be the reason why the orbital energies were not mutually dependent with the electrostatic ones for all

Pt–ligand bonds (cf. our previous studies[29,30,32]) except for the Pt–w bond in the **X-P** structures (Figure S2).

Water solvent dampens the electrostatic forces and the minimum value of the Average Local Ionization Energy (ALIE)[33] corresponding to the N$_{NH2X}$ atom works best as the predictor of the Pt–NH$_2$X and Pt–Cl BEs in the **X-R** and **X-P** complexes (Table S5, Figure S3 and see the Supporting Information for more details).

Note that BEs of the Pt–ligand bonds correlate with properties calculated for the whole Pt(II) complexes such as the ligand charges (cf. above), the Pt–ligand bond lengths,[30,34–36] the populations in 5d orbitals of the Pt(II) atom,[30,37] the linear combinations of electron densities at the bond critical points,[34,38] and the intrinsic bond strength indexes.[39]

Influence of elemental X's on the △G$^+$ values of the hydrolysis reaction. In the gas phase, the electron-donating DMA and electron-withdrawing F substituents lowered and increased the activation free energy barrier by up to 2.2 and 0.7 kcal/mol, respectively, compared to the parent NH$_2$H. In the solvent the respective values were 0.8 and 0.6 kcal/mol but this time for the CH$_3$ and Cl substituents (Table 2). The same trends were already observed for substituents on aromatic ligands,[29,40] but the NH$_2$X substitution offers a lower variability with respect to the reaction rate change than the pyrX one[29] (△(△G$^+$) ranges of values of 2.9 vs. 4.5 kcal/mol and 1.5 vs. 3.0 kcal/mol in the gas phase and the water solvent, respectively). It is caused not by electronic effects but by possible electrostatic stabilization of some TS structures due to the coplanar orientation of the pyrX, leaving and entering ligands.[29] If only meta and para substituents of pyrX are considered the NH$_2$X ligands show higher reaction rate variability in the gas phase (△(△G$^+$) ranges of values of 2.9 vs. 1.8 kcal/mol) but not in the water solvent (1.5 vs. 1.9 kcal/mol).

The △G$^+$ values roughly correlate with ΔE_{bind}^{Cl} in the **X-R** structures (Figures 3 and S4), which reflects a similar relative weakening of the coordination bonds for all X systems when moving from **X-R** towards **X-TS** structures. The ratio between BEs of the (Cl+w) fragment (the leaving and entering ligands considered together) ΔE_{bind}^{Cl+w} in the **X-TS** structures on the one

Table 2. Pt–ligand interactions in the optimized **X-TS** structures: Pt–Cl and Pt–O$_w$ bond lengths (in Å); ΔE_{bind}^{Cl+w} (BE of the joint (Cl+w) fragment (the leaving Cl$^-$ and entering water ligands) with the rest of the complex) and △G$^+$ energy values (in kcal/mol).[a]

X-TS	gas phase				water solvent			
	Pt–Cl	Pt–O$_w$	ΔE_{bind}^{Cl+w}	△G$^+$	Pt–Cl	Pt–O$_w$	ΔE_{bind}^{Cl+w}	△G$^+$
H	2.795	2.280	−240.3	35.4	2.835	2.453	−20.0	26.9
Br	2.782	2.242	−241.2	34.9	2.777	2.379	−22.4	26.8
CH$_3$	2.788	2.302	−234.3	34.4	2.832	2.482	−17.8	26.1
Cl	2.816	2.226	−243.8	35.4	2.755	2.383	−22.5	27.5
DMA	2.773	2.298	−228.9	33.2	2.829	2.457	−18.4	26.4
F	2.806	2.232	−249.3	36.1	2.743	2.373	−23.2	27.4
NH$_2$	2.775	2.279	−236.3	34.2	2.806	2.455	−19.5	26.6
NO$_2$	2.810	2.207	−249.5	35.5	2.793	2.362	−24.7	27.3
OH	2.745	2.284	−243.7	34.0	2.801	2.448	−20.9	26.5
F$_3$	2.859	2.145	−264.9	38.0	2.802	2.254	−31.5	27.4
CyP	2.802	2.305	−227.5	34.0	2.847	2.483	−18.3	25.8
CyH	2.792	2.330	−224.3	33.2	2.842	2.492	−18.8	25.7
DACH	2.777	2.320	−223.4	33.2	2.829	2.472	−18.9	26.1
BAMCB	2.786	2.342	−225.4	32.1	2.831	2.477	−18.7	26.2

[a] The total NPA charges of the Pt atom and the NH$_2$X, Cl$^-$, and w ligands are shown in Table S6.
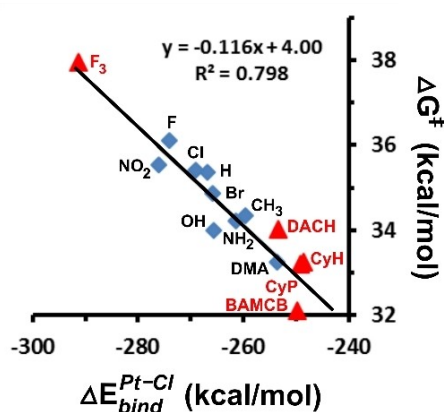
ChemistrySelect

Full Papers
doi.org/10.1002/slct.202100887

**Chemistry
Europe**
European Chemical
Societies Publishing

Figure 3. Dependence of the gas phase activation Gibbs free energy ($\Delta G^{\ddagger}$) on the Pt–Cl BE (ΔE_{bind}^{Cl}) in the **X-R** structures. Red points are not used for the regression analysis but serve as the reference.

side (Table 2) and ΔE_{bind}^{Cl} in the **X-R** structures on the other side (Table 1) was 0.905 ± 0.005 and 0.53 ± 0.04 in the gas phase and the water solvent, respectively. When the data for the para- and meta-pyrX substituents from our previous study were also included, the $\Delta E_{bind}^{Cl}/\Delta G^{\ddagger}$ relationship improved in the gas phase ($R^2 = 0.813$) but not in the solvent ($R^2 = 0.226$). Solvent data also failed to predict the $\Delta G^{\ddagger}$ values for CyP, CyH, and especially for the NF$_3$ ligand (Figure S4), while in the gas phase their values were forecasted with a good precision of 0.4 ± 0.2 kcal/mol (Figure 3). The water solvent $\Delta G^{\ddagger}$ values of hydrocarbon X's correlate very well with the number of X's electrons (see below).

Additivity of the substituent effects

The additivity of the substituent effects was tested on the NF$_3$ ligand whose results were compared against NH$_2$F and NH$_2$H systems. The estimated values (X_{NF3}^{est}) of NPA charges, BEs, and bond lengths were calculated by a simple additive approach based on the Equation $X_{NF3}^{est} = X_H + 3(X_F - X_H)$, where X_F and X_H are the values for the complexes with X=F and X=H, respectively. Absolute errors represent the difference $|X_{NF3} - X_{NF3}^{est}|$ and the relative errors were determined from the ratio $|X_{NF3} - X_{NF3}^{est}|^*100\%/|X_{NF3}^{est} - X_H|$, where X_{NF3} are the calculated values for the complexes with the NF$_3$ ligand (Tables 1, 2, S1, S3, S4, S6). Good additivities with relative errors below 30% were observed for q(NF$_3$), q(Cl), and q(w) ligand charges and Pt–Cl and Pt–w BEs. This finding is very similar to the pyrX system, but here the additivity works for the water solvent too. Pt–NF$_3$ BEs could be reproduced much less satisfactorily with relative errors of up to 69%.

Absolute errors of Pt–Cl and Pt–w bond lengths were ≤ 0.03 Å, but the changes of the bond lengths due to substitution effects were low, which when taken together resulted in high relative errors up to 98%. Activation Gibbs free energy values were estimated with absolute errors of 0.4 and 0.9 kcal/mol, which corresponded to relative errors of 16 and 64% in the gas phase and the water solvent, respectively.

Hydrocarbon substituents

The total electron density difference between the **CyH-R** and **CH$_3$-R** structures, which reflects the electronic changes caused by the CH$_3$→CyH substitution, is shown in Figure 4. Although the accompanying changes of the molecular geometry are not considered in Figure 4, a clear enhancement of electron-donating properties (a larger positive inductive +I effect) of the CyH substituent compared to CH$_3$ is documented by the increase of electron density in the center of the Pt–NH$_2$X bond leading to its strengthening. Furthermore, an increase of electron density in the 3p(Cl) orbital oriented along the Pt–Cl bond (Figure 4) is the result of lower σ-donation from the Cl$^-$ ligand, which led to the weakening of the Pt–Cl bond (cf. Figures 4 and 1A). Thus, the Pt–NH$_2$X and Pt–Cl/Pt–w bonds are strengthened and weakened, respectively, in the **CyH-R/CyH-P** structures.

The inductive substituent effects weaken rapidly with the distance and they show saturation with increasing alkyl chain length.[41] For our small hydrocarbon X's, the Pt–ligand BEs depend logarithmically on the size of X which can be best quantified by the number of X electrons (Figure S5).

No clear trends were found for the Pt–ligand bond lengths except the Pt–Cl/Pt–w bonds in the gas phase optimized **X-R/X-P** structures which are elongated for heavier hydrocarbon X's. Most importantly, in both the gas phase and the water solvent the logarithmic dependence also exists for the $\Delta G^{\ddagger}$ values, which decrease with the increased size of the X substituent as the result of the enhanced +I effect (Figure 5). Although no simple structure-activity relationships could be found for Pt(II) drugs,[42] it is interesting to mention that the increasing cytotoxic activity with a rising number of carbons in the linker was observed for Pt(II) hydrocarbondiamine complexes.[18] Note that the elongation of the chain length of the alkylamine group in the cis position with respect to the
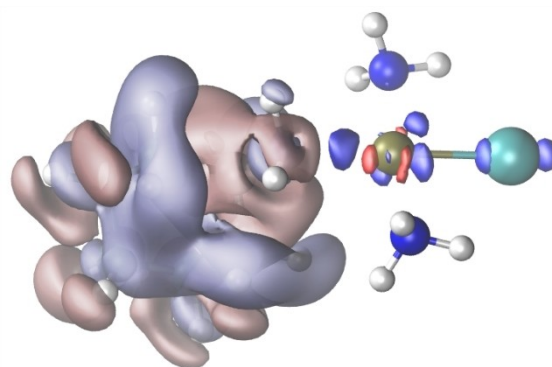

Figure 4. Electron density difference isosurfaces of the **CyH-R** structure calculated with respect to the reference **CH$_3$-R** structure show electron accumulation and electron depletion regions (blue and red isosurfaces, respectively, at values ± 0.0005 a.u.) caused by the CyH replacement of the CH$_3$ substituent. Electron densities were calculated on the optimized **CyH-R** geometry. The reference **CH$_3$-R** structure was obtained by the replacement of the CyH substituent by the CH$_3$ one and its partial optimization keeping all other atoms fixed. The areas which are dominated by atom additions/ subtractions are depicted by the low contrast colors.
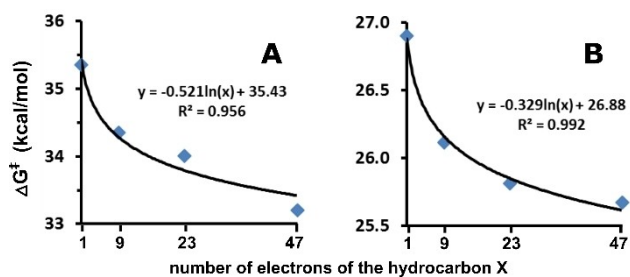
ChemistrySelect

Full Papers
doi.org/10.1002/slct.202100887

Chemistry
Europe
European Chemical
Societies Publishing

Figure 5. Logarithmic dependence of activation free energy ($\Delta G^{\ddagger}$) on the number of electrons of the saturated hydrocarbon X's in the gas phase (panel A) and water solvent (panel B). 1, 9, 23, and 47 electrons correspond to X = H, CH3, CyP, and CyH, respectively.

leaving ligand had a negligible effect on the electronic structure of the complex but decreased the rate of substitution reactions due to increased steric hindrance.[43]

Influence of chelation

The chelation of the CyH substituent forming the bidentate DACH ligand leads to a slight decrease of the +I effect along the Pt–Cl axis of the complex. The increase of $\Delta G^{\ddagger}$ values by 0.05 and 0.40 kcal/mol was observed after the chelation in the gas phase and the water solvent, respectively (Table 2). In the **DACH-R** structure, the Pt–Cl BE was lowered by 0.7 kcal/mol and increased by 0.1 kcal/mol compared to **CyH-R** (Table 1) which corresponded to relative changes of 0.3 and 0.4 % in the gas phase and the water solvent, respectively. The gas phase Pt–Cl bond weakening did not correspond to the supposed decrease of the +I effect but the relative change was small. The weakening of the +I effect had a higher impact on the Pt–w bond in the **DACH-P/CyH-P** structures, increasing the bond stability by 2.8 and 0.6 kcal/mol after the chelation (Table S1) which corresponded to relative changes of 5.7 and 3.4 % in the gas phase and water solvent, respectively.
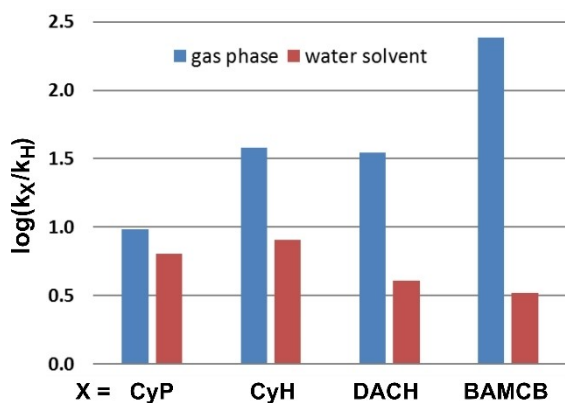

Figure 6. Relative rate constants of the systems with non-leaving ligands present in the biologically active drugs JM11 (CyP), JM118 (CyH), oxaliplatin (DACH), and lobaplatin (BAMCB) calculated with respect to the reference cisplatin's amine ligand (X=H) at 298 K.

Although both electrostatic and orbital energies contributed to the difference in Pt–w BEs, the decisive stabilization resulted from the Pauli energy decrease upon the chelation (Table S2).

As expected, the chelation increases the donation ability of the involved amine group and weakens the bond of the other amine ligand trans to it. BE of the *trans*-amine ligand was lowered by 2.7 and 3.1 kcal/mol in the gas phase **DACH-R** and **DACH-P** structures compared to **CyH-R** and **CyH-P**, respectively (4.4 % relative change in both cases). In the water solvent, the respective values were 1.2 and 1.1 kcal/mol (3.0 and 2.7 % relative changes).

Chelation can be important for difunctional Pt(II) drugs, making the two leaving sites equivalent and accelerating the second leaving ligand substitution due to an increase of the +I effect in its direction.

Effect of isomerization

The slightly stronger Pt–Cl bond (by 0.5 %, 1.3 kcal/mol) was detected in the gas phase optimized **BAMCB-R** structure compared to the isomeric **DACH-R** one (Table 1) due to more favorable ΔE^{Cl}_{elst} (by 1.6 %, 4.4 kcal/mol, Table S2) even though the lower σ-donation (by 1.2 %, 0.006e) from the Cl⁻ ligand led to the elongation of this bond by 0.005 Å (Tables S3, 1). Similar reasoning can explain a higher stabilization of the **BAMCB-TS** structure resulting in the lower $\Delta G^{\ddagger}$ value by 1.1 kcal/mol compared to the DACH system (Table 2).

In water solvent, the differences in electrostatics are almost diminished. However, the Pt–Cl bond was still stronger in the **BAMCB-R** structure (by 3.4 %, 1,3 kcal/mol, Table 1), but this time due to larger σ-donation from the Cl⁻ ligand (by 1.7 %, 0.01e, Table S3). More importantly, the basic characteristics of the **BAMCB-TS** and **DACH-TS** structures were almost the same in the water solvent and this was also valid for the $\Delta G^{\ddagger}$ values (Tables 2, S6).

Conclusions

The X substituents can be divided into three groups: 1) electron-donating X's (DMA, NH_2, CH_3, CyP, CyH) which increase electron donation from NH_2X ligands and thus strengthen and weaken the Pt–NH_2X and Pt–Cl bonds, respectively, and lower reactivity of the Pt-complex; 2) electron withdrawing X's (NO_2, F, Cl) have exactly the opposite effects compared to the previous group; and 3) substituents with electron-withdrawing ability but whose influence on the properties of the complex was not always predictable (OH, Br).

The Pt–ligand gas phase BEs of the Pt(II) complexes could be predicted from the properties of the pure NH_2X ligand with lower precision than for the pyrX ligands due to the presence of the nonbonding interaction between some X's and one of the *cis*-NH_3 groups. In the water solvent, the Pt–NH_2X and Pt–Cl BEs correlate well with the minimum values of ALIE(N_{NH2X}).

For the elemental substituents, the NH_2X ligand offers a slightly higher variability (by about 10–20 %) of Pt–trans ligand BEs than the pyrX one. The range of $\Delta G^{\ddagger}$ values for the NH_2X

system is comparable only with the meta and para subsystems of pyrX.

The electron-donating ability of saturated hydrocarbon X substituents (X=H, CH$_3$, CyP, CyH) increases with their size. Activation free energy (ΔG$^{\neq}$) and Pt–Cl, Pt–w BEs are decreased with the logarithm of the number of hydrocarbon X electrons.

The chelation decreases the +I effect of the hydrocarbon X along the N$_{NH2X}$–Pt–Cl axis but simultaneously it increases the +I effect along the other axis of the complex. For difunctional Pt(II) drugs this may facilitate the second leaving group substitution.

The additivity of the substituent effects was tested on the NF$_3$ ligand. It works well for the ligand charges and Pt–Cl, Pt–w BEs in both the gas phase and water solvent.

The influence of the non-leaving ligands present in the anticancer Pt(II) drugs on the reactivity and bonding properties of the Pt(II) complexes was studied in the same ligand environment. In the water solvent, the reactivity of complexes with the non-leaving ligands found in cisplatin (X=H), JM11 (X=CyP), JM118 (X=CyH), oxaliplatin (DACH), and lobaplatin (BAMCB) decreases in the order CyH~CyP>DACH~BAMCB>H (Figure 6). It should help to understand the differences in the biotransformation of these drugs. A similar study that would also quantify the influence of the leaving ligands present in active Pt(II) drugs is welcome.

Supporting Information Summary

Supporting Information contains computational methods, a detailed description of the Pt–ligand bond strength prediction from NH$_2$X properties, Figures S1–S5, Tables S1–S6, references, optimized Cartesian coordinates of all TS structures and the most stable minima of other structures.

Conflict of Interest

The authors declare no conflict of interest.

[1] U.-M. Ohndorf, M. A. Rould, Q. He, C. O. Pabo, S. J. Lippard, *Nature* **1999**, *399*, 708–712.
[2] M. J. Cleare, J. D. Hoeschele, *Bioinorg. Chem.* **1973**, *2*, 187–210.
[3] Z. Chval, M. Sip, *J. Mol. Struct.* **2000**, *532*, 59–68.
[4] L. A. S. Costa, W. R. Rocha, W. B. De Almeida, H. F. Dos Santos, *J. Chem. Phys.* **2003**, *118*, 10584–10592.
[5] J. K. C. Lau, D. V. Deubel, *J. Chem. Theory Comput.* **2006**, *2*, 103–106.
[6] J. V. Burda, M. Zeizinger, J. Leszczynski, *J. Comput. Chem.* **2005**, *26*, 907–914.
[7] T. Zimmermann, J. Leszczynski, J. V. Burda, *J. Mol. Model.* **2011**, *17*, 2385–2393.
[8] X. Feifan, C. Pieter, V. B. Jan, *J. Mass Spectrom.* **2017**, *52*, 434–441.
[9] T. Hirakawa, D. R. Bowler, T. Miyazaki, Y. Morikawa, L. A. Truflandier, *J. Comput. Chem.* **2020**, *41*, 1973–1984.
[10] S. Ahmad, *Polyhedron* **2017**, *138*, 109–124.
[11] N. Summa, T. Soldatović, L. Dahlenburg, Ž. D. Bugarčić, R. van Eldik, *J. Biol. Inorg. Chem.* **2007**, *12*, 461–475.
[12] M. Pavelka, M. F. A. Lucas, N. Russo, *Chem. Eur. J.* **2007**, *13*, 10108–10116.
[13] M. Alberto, M. Lucas, M. Pavelka, N. Russo, *J. Phys. Chem. B* **2009**, *113*, 14473–14479.
[14] V. P. Reddy, B. S. Mukherjee, I. Mitra, S. Mahata, W. Linert, S. Ch. Moi, *Chem. Phys. Lett.* **2016**, *663*, 115–122.
[15] R. Yin, S. Gou, X. Liu, L. Lou, *J. Inorg. Biochem.* **2011**, *105*, 1095–1101.
[16] J. Zhao, D. Wang, G. Xu, S. Gou, *J. Inorg. Biochem.* **2017**, *175*, 20–28.
[17] W. P. Asman, D. Jaganyi, *Int. J. Chem. Kinet.* **2017**, *49*, 545–561.
[18] H. Nowatari, Y. Kuroda, H. Hayami, K. Okamoto, H. Ekimoto, K. Takahashi, *Chem. Pharm. Bull.* **1989**, *37*, 2406–2409.
[19] R. Guddneppanavar, J. R. Choudhury, A. R. Kheradi, B. D. Steen, G. Saluta, G. L. Kucera, C. S. Day, U. Bierbach, *J. Med. Chem.* **2007**, *50*, 2259–2263.
[20] M. E. Graziotto, M. C. Akerfeldt, A. P. Gunn, K. Yang, M. V. Somerville, N. V. Coleman, B. R. Roberts, T. W. Hambley, E. J. New *J. Inorg. Biochem.* **2017**, *177*, 328–334.
[21] L. Biancalana, L. K. Batchelor, P. J. Dyson, S. Zacchini, S. Schoch, G. Pampaloni, F. Marchetti, *New J. Chem.* **2018**, *42*, 17453–17463.
[22] P. Papadia, V. Gandin, A. Barbanente, A. G. Ruello, C. Marzano, K. Micoli, J. D. Hoeschele, G. Natile, N. Margiotta, *RSC Adv.* **2019**, *9*, 32448–32452.
[23] N. Summa, W. Schiessl, R. Puchta, N. van Eikema Hommes, R. van Eldik, *Inorg. Chem.* **2006**, *45*, 2948–2959.
[24] G. Berger, L. Fusaro, M. Luhmer, J. Czapla-Masztafiak, E. Lipiec, J. Szlachetko, Y. Kayser, D. L. A. Fernandes, J. Sá, F. Dufrasne, S. Bombard, *J. Biol. Inorg. Chem.* **2015**, *20*, 841–853.
[25] M. A. Olusegun, D. Reddy, D. Jaganyi, *New J. Chem.* **2020**, *44*, 5138–5146.
[26] C. B. Zhu, J. Raber, L. A. Eriksson, *J. Phys. Chem. B* **2005**, *109*, 12195–12205.
[27] A. Melchior, E. Sánchez Marcos, R. R. Pappalardo, J. M. Martínez, *Theor. Chem. Acc.* **2011**. *128*, 627–638.
[28] P. J. S. Miguel, L. Roitzsch, P. Yin, P. M. Lax, L. Holland, O. Krizanovic, M. Lutterbeck, M. Schürmann, E. C. Fuscha, B. Lippert, *Dalton Trans.* **2009**, *48*, 10774–10786.
[29] O. Dvořáčková, Z. Chval, *ACS Omega* **2020**, *5*, 11768–11783.
[30] Z. Chval, M. Sip, J. V. Burda, *J. Comput. Chem.* **2008**, *29*, 2370–2381.
[31] B. Pitteri, M. Bortoluzzi, *Eur. J. Inorg. Chem.* **2007**, *28*, 4456–4461.
[32] Z. Chval, O. Dvořáčková, D. Chvalová, J. V. Burda, *Inorg. Chem.* **2019**, *58*, 3616–3626.
[33] P. Sjoberg, J. S. Murray, T. Brinck, P. Politzer, *Can. J. Chem.* **1990**, *68*, 1440–1443.
[34] P. K. Sajith, C. H. Suresh, *Dalton Trans.* **2009**, *39*, 815–822.
[35] M. P. Mitoraj, H. Zhu, A. Michalak, T. Ziegler, *Int. J. Quantum Chem.* **2009**, *109*, 3379–3386.
[36] B. Pinter, V. Van Speybroeck, M. Waroquier, P. Geerlings, F. De Proft, *Phys. Chem. Chem. Phys.* **2013**, *15*, 17354–17365.
[37] J. Zhu, Z. Y. Lin, T. B. Marder, *Inorg. Chem.* **2005**, *44*, 9384–9390.
[38] P. K. Sajith, C. H. Suresh, *J. Organomet. Chem.* **2011**, *696*, 2086–2092.
[39] M. Ponce-Vargas, J. Klein, E. Hénon, *Dalton Trans.* **2020**, *49*, 12632–12642.
[40] L. A. S. Costa, W. R. Rocha, W. B. De Almeida, H. F. Dos Santos, *J. Inorg. Biochem.* **2005**, *99*, 575–583.
[41] R. Tandon, T. A. Nigst, H. Zipse, *Eur. J. Org. Chem.* **2013**, 5423–5430.
[42] B. Montana, Á. M. Consuelo, *Curr. Med. Chem.* **2009**, *16*, 2235–2260.
[43] M. A. Olusegun, D. Reddy, D. Jaganyi, *Transition Met. Chem.* **2020**, *45*, 295–301.